

An Integrated Chip-based Device for Droplet-flow Polymerase Chain Reaction

Steven Poh Chuen Sim

Imperial College London

Department of Chemistry

Submitted for the degree of Doctor of Philosophy

First Submission: March 2016

Final Submission: June 2016

DECLARATION OF ORIGINALITY

I declare that this thesis is my original work. In instances where the work of others has been used, this has been properly acknowledged and referenced. None of this work has been previously submitted to satisfy any degree requirement at this or any other university.

Steven Sim

March 2016

COPYRIGHT DECLARATION

The copyright of this thesis rests with the author and is made available under a Creative Commons Attribution Non-Commercial No Derivatives licence. Researchers are free to copy, distribute or transmit the thesis on the condition that they attribute it, that they do not use it for commercial purposes and that they do not alter, transform or build upon it. For any reuse or redistribution, researchers must make clear to others the licence terms of this work.

ABSTRACT

The polymerase chain reaction (PCR) is an important *in-vitro* technique in molecular biology for amplifying trace quantities of deoxyribonucleic acid (DNA). PCR is carried out by mixing the DNA molecules to be amplified with primers, polymerase enzymes and deoxynucleotide triphosphates (dNTPs) in a suitable buffer solution. A conventional thermal-cycler is then used to cycle the PCR mixture between multiple temperatures for denaturation, annealing and extension. Bench-top thermal cyclers have large thermal masses and use large sample volumes, leading to overly long cycling times, excessive energy and material consumption, inhomogeneity in the reaction environment, and an inability to handle large numbers of small volume aliquots.

Microfluidic technologies overcome many of the limitations of bench-top thermal cyclers, providing a more controlled approach to PCR. Droplet-flow is one of the most promising microfluidic methods for carrying out PCR. The droplet-flow approach uses small water-in-oil droplets for compartmentalisation of the PCR reaction mixture, with each droplet behaving like an individual reaction chamber. By flowing the droplets over different temperatures for denaturation, annealing and extension, rapid thermal cycling can be achieved, greatly reducing the reaction time relative to bench-top thermal cyclers. The use of an oil phase to encapsulate the aqueous PCR mixture as droplets also prevent unwanted surface interactions and flow dispersion that can adversely affect the PCR yield.

Here we describe an integrated microfluidic device for carrying out droplet-flow PCR. Instead of using multiple temperature zones to thermally-cycle the flowing droplets, the device used an on-chip radial temperature gradient. The droplets passed through microchannels arranged in a spoke-like geometry, causing them to pass backwards and forwards along the radial temperature gradient and so undergo the repeated thermal cycling required for PCR. The device reported here builds on an earlier plastic microfluidic PCR device (by Schaerli *et al.*) in which the radial temperature gradient was generated using a bulky external heater and a thermoelectric cooler, together with heat sinks and fans. In the silicon- and glass-based device reported here, integrated heaters, temperature sensors and air gaps (for passive cooling) were used to generate the temperature gradient, leading to significant miniaturisation of the device. The dimensions of the complete device assembly were 6.0 cm x 5.0 cm x 2.0 cm compared to 25.0 cm x 25.0 cm x 25.0 cm for the device by Schaerli *et al.*

Despite the small size of the device, the achievable temperature gradient on the chip was sizeable. For instance, when the central heater was set to 92.0 °C, the temperature at the periphery was

~60.0 °C, corresponding to a temperature difference of ~32.0 °C – easily sufficient for PCR applications. Using chemical modification, the hydrophilic walls of the microchannel were rendered hydrophobic. An on-chip T-junction or flow-focusing junction was subsequently used to merge the oil and aqueous streams to generate the PCR-containing water-in-oil droplets.

A PCR recipe was optimised on a bench-top thermal cycle. With this recipe, droplet-flow PCR was conducted on the PCR device by flowing the generated droplets up and down the radial temperature gradient to induce thermal cycling. Gel electrophoresis analysis of the collected droplets from the device showed a 110 bp DNA band, confirming the ability of the integrated device to conduct droplet-flow PCR for the formation of the targeted PCR product. By varying the central temperature (between 96 and 85 °C) of the PCR device and the total volumetric flow rate (from 4.8 to 0.6 $\mu\text{L}/\text{min}$) of the droplets, the yield of the PCR product could be tuned. By serially diluting the concentration (from 10^4 to 0.01 pM) of the DNA molecules, it was found that the PCR device was able to amplify concentrations as low as 0.01 pM for detection by gel electrophoresis. When coupled to a laser-induced fluorescence detection system, the emission from the PCR mixture in the water-in-oil droplets could be successfully detected for each PCR cycle. The increase in the fluorescence over successive PCR cycles once again verified the feasibility of carrying out droplet-flow PCR on the integrated device.

ACKNOWLEDGEMENTS

I will like to express my gratitude and thanks to the following people:

- Prof. John deMello for his supervision, encouragements, and many insightful inputs to my work. I will like to thank the members of John's group for all the kind assistance.
- Prof. Andrew deMello for his supervision, inspirations, and many valuable ideas. I will like to thank the members of Andrew's groups at both ETH Zurich and Imperial College London for their help.
- Prof. Joshua Edel and his group for the use the confocal detection system.
- Prof. Tony Cass and his group for the use the gel imaging system.
- Dr. Chen Yu for her supervision at the Institute of Microelectronics (A*STAR, Singapore).
- Members of the Bio-electronics department at IME for the use of the bio-lab to carry out PCR experiments.
- Technicians and engineers of the various fabrication departments at IME for their expert advices on the fabrication of the PCR device.
- A*STAR Graduate Academy (A*STAR, Singapore) for the scholarship.
- My parents, family and friends for their love and support. I will like to remember my mother who is unfortunately now no longer around to see the completion of my work. I miss her very much.

LIST OF PUBLICATIONS AND CONFERENCES

International Conference on Materials for Advanced Technologies 2013;
Steven Poh Chuen Sim, Jack Sheng Kee, Yu Chen, Andrew deMello, John deMello;
Continuous-flow Droplet-based PCR in a Temperature Gradient Device

Advances in Microfluidics and Nanofluidics Asian-Pacific International Symposium 2011;
Steven Poh Chuen Sim, Tae Goo Kang, Yu Chen and Andrew deMello;
Thermal Simulation of Radial PCR Device with Air Gaps for Temperature Management

International Conference on Materials for Advanced Technologies 2011;
Steven Poh Chuen Sim, Tae Goo Kang, Yu Chen and Andrew deMello;
Thermal Characterization of a PCR device with a Temperature Gradient over a Radial Design

TABLE OF CONTENTS

Declaration of Originality	i
Abstract	ii
Acknowledgements	iv
List of Publications and Conferences	v
Table of Contents	vi
1 Introduction and Background	1
1.1 The Polymerase Chain Reaction.....	2
1.1.1 Thermal Cycling	3
1.1.2 Components in a PCR.....	5
1.1.3 PCR for Quantitative Analysis	10
1.1.4 End-point PCR.....	12
1.1.5 Real-Time PCR	12
1.1.6 Digital PCR.....	18
1.1.7 The Bench-top Thermal Cycler and its Limitations.....	21
1.2 Microfluidic Systems for PCR.....	22
1.2.1 Well-based PCR.....	24
1.2.2 Continuous-flow PCR	28
1.2.3 Continuous-flow Droplet-based PCR.....	30
1.2.4 Summary	33
1.3 Thesis Objectives.....	33
2 Design and Thermal Simulation of a Microfluidic Chip with Integrated Heating and Cooling Elements.....	34
2.1 Introduction	35
2.1.1 Continuous-flow PCR with Isothermal Temperature Zones.....	35
2.1.2 Continuous-flow PCR with Temperature Gradient	36
2.1.3 Issues with Temperature Gradient Devices	37
2.2 Radial PCR Device	38
2.2.1 The Original Design	38
2.2.2 Integrated Radial Temperature Device	40
2.3 Thermal Simulation.....	45
2.3.1 Building a Model and Generating a Solution	46
2.3.2 Varying Parameters for Simulation Studies	47
2.4 Results and Discussion.....	47
2.4.1 The Width of the Silicon Bridges.....	48

2.4.2	The Length of the Silicon Bridges	49
2.4.3	The Radius of the Central Heater	50
2.4.4	The Distance between the Heater and the Gaps	51
2.4.5	Prototype: Finalised Dimensions	52
2.5	Conclusions	53
3	Device Fabrication	55
3.1	Introduction	56
3.1.1	Hard Fabrication Methods	56
3.1.2	Soft Fabrication Methods	56
3.1.3	Selecting an Appropriate Substrate Material	57
3.1.4	The Original Radial PCR Device: SU-8 and PMMA	57
3.1.5	The New Radial PCR Device: Silicon and Glass	57
3.2	Device Fabrication	59
3.2.1	Preparations of Starting Wafers	60
3.2.2	Metal Thin-film Patterning	61
3.2.3	Protection of Metal Patterns and Thinning Wafers	63
3.2.4	Patterning of Fluidic Network	64
3.2.5	Exposing Metal Pads	65
3.2.6	Formation of Air Gaps	67
3.2.7	Capping with Glass Wafers	69
3.2.8	Variations to the Fabrication Process	70
3.3	Electrical Interface	71
3.4	Fluidic Interface	72
3.5	Discussion	73
3.6	Conclusions	76
4	Thermal and Fluidic Characterisation of the Radial PCR Device	78
4.1	Introduction	79
4.2	Thermal Characterisation	79
4.2.1	Calibration and Generation of Temperature Gradient	79
4.2.2	Employing the Radial Temperature Gradient for Continuous-flow PCR	85
4.2.3	Summary	88
4.3	Fluidic Characterisation	89
4.3.1	Surface Modification and Water-in-oil Droplet Generation	89
4.3.2	Summary	100
4.4	Conclusions	100
5	PCR Optimisation	101

5.1	Introduction	102
5.1.1	DNA Template.....	102
5.1.2	Primers	103
5.1.3	Probe.....	104
5.1.4	Polymerase.....	107
5.1.5	Buffer	107
5.1.6	Other Components	108
5.2	Experimental.....	108
5.2.1	Starting Recipe.....	108
5.2.2	Varying Concentration of the TaqMan Probe (P1)	111
5.2.3	Varying Concentration of the Primers (F2 and R2).....	112
5.2.4	Varying Concentration of the DNA Template	112
5.3	Results and Discussion.....	113
5.3.1	Starting Recipe.....	113
5.3.2	Variation of the Concentration of the TaqMan Probe (P1)	115
5.3.3	Variation of the Concentration of the Primers (F2 and R2).....	116
5.3.4	Variation of the Concentration of DNA Template	116
5.3.5	Optimised PCR Recipe for Droplet-based PCR.....	118
5.4	Conclusions.....	118
6	Chip-based Droplet PCR.....	119
6.1	Introduction	120
6.2	Chip-based Droplet PCR.....	120
6.2.1	Experimental	120
6.2.2	Results and Discussion.....	124
6.3	Effects of Varying the Central Temperature	126
6.3.1	Experimental	126
6.3.2	Results and Discussion.....	128
6.4	Effects of Varying the Total Flow Rate	132
6.4.1	Experimental	132
6.4.2	Results and Discussion.....	133
6.5	Effects of Varying the Concentration of DNA Template	135
6.5.1	Experimental	135
6.5.2	Results and Discussion.....	137
6.6	Conclusions.....	139
7	PCR Device with Fluorescence Detection System	140
7.1	Introduction	141

7.2	Measuring Emission Intensity of FITC-Containing Droplets.....	141
7.2.1	Detection of Droplets	142
7.3	Measuring Emission Intensity of the PCR Mixture (with TaqMan Probe) in Droplets	145
7.3.1	Injecting Bench-top PCR Samples into Microdevice as Droplets.....	145
7.3.2	Conducting Droplet-flow PCR with and without Temperature Gradient.....	148
7.3.3	Measuring Emission Intensity at Various Cycles on the PCR Microdevice	151
7.4	Conclusions.....	155
8	Conclusions and Further Works	156
8.1	Conclusions.....	157
8.2	Further Works.....	159
8.2.1	The Periphery Heater	159
8.2.2	Optimisation of TaqMan Probe or Selection of New Probe	159
8.2.3	Real-time PCR.....	160
8.2.4	Digital PCR.....	160
9	Appendix.....	162
9.1	Masks.....	163
9.1.1	Mask 1	163
9.1.2	Mask 2	164
9.1.3	Mask 3	165
9.1.4	Mask 4	166
9.1.5	Mask 2A	167
9.1.6	Mask 4A	168
9.2	Labview	169
9.3	PFPE-PEG Surfactant	170
9.4	Matlab	170
9.4.1	To Load Data (loaddata).....	170
9.4.2	To Analyse Data (dataanalysis)	171
10	References.....	175

Chapter 1

This chapter introduces the polymerase chain reaction (PCR), describes the various microfluidic approaches for conducting PCR, and highlights key studies that reported droplet-flow PCR in the literature.

1.1 THE POLYMERASE CHAIN REACTION

Deoxyribonucleic acid or DNA is called the “molecule of life” because it holds within its base sequence the information and instructions required for the proper development, maintenance and functioning of a living organism.¹⁻³ The base sequences comprising the genetic information in DNA are called genes. The regulation and expression of these genes play crucial roles in cell growth and division as well as in the production of bio-macromolecules such proteins, enzymes and antibodies.^{2,4} Due to its ubiquitous effect on life, the study of DNA is of great interest. For instance, by extracting the genetic information that is encoded within DNA, genetic diseases such as cancers can be better understood and potentially treated or prevented.^{2,4}

The polymerase chain reaction (PCR) is a technique that utilises a polymerase enzyme to amplify a specific target sequence of a DNA molecule *in-vitro*.⁵⁻⁸ The technique was first invented in 1985 by Kary Mullis.^{3,5,9-11} Since its conception and subsequent development, PCR has become one of the most important tools in molecular biology, with applications ranging from forensics to diagnostics, cloning and sequencing.^{3,7,11,12} Unsurprisingly, Mullis was awarded the 1993 Nobel Prize in Chemistry in recognition of the importance of PCR in molecular biology.¹¹

The beauty of PCR lies in the simple, rapid and *in-vitro* amplification process that generates millions to billions of copies of a particular DNA sequence from a single starting DNA template (**Figure 1.1**).^{5,7,8}

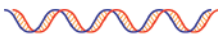

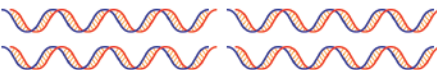
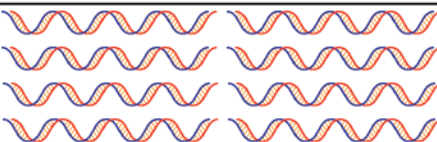
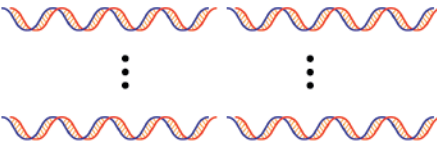
Number of Cycle	DNA Amplification	Number of Copy
0		1
1		2
2		4
3		8
36		~68 Billions

Figure 1.1. The amplification process of PCR showing the enrichment of a target sequence. In an ideal PCR reaction, the number of DNA strands doubles after each cycle. At the end of 36 cycles, approximately 68 billion copies of the target sequence result from a single starting DNA template.

PCR contrasts with the alternative *in-vivo* cell-based approach of DNA cloning, which is both time-consuming and laborious to perform.⁶ DNA cloning requires the attachment of a DNA sequence to a replicon, which must then be transferred to a host cell. The host cell is then grown in culture for cell division so that the original DNA sequence will be replicated in all daughter cells. Thereafter, the daughter cells are lysed and the target sequences are harvested from their DNA materials. PCR is substantially simpler than DNA cloning as it only involves the mixing of a DNA molecule with polymerase enzymes (and building blocks) in a buffer solution and the thermal cycling of this mixture between various temperatures.⁶ This simple amplification process allows DNA materials that are initially present in only trace concentrations to be rapidly harvested in ample quantities for further studies. The amplification process in PCR can be described by the following basic equations:¹³

$$N_c = N_0(E + 1)^C \quad (1.1)$$

$$\ln N_c = \ln N_0 + C[\ln(E + 1)] \quad (1.2)$$

Here C is the number of amplification cycles, E is the amplification efficiency equal to the fraction of DNA templates that are utilised to create new DNA strands in each round of PCR, N_c is the resulting number of PCR products after cycle C , and N_0 is the initial number of DNA templates. Based on these equations, it can be seen that amplification is exponential in the ideal case when $E = 1$ (**Figure 1.1 and 1.2**), with N_c doubling every cycle.¹³

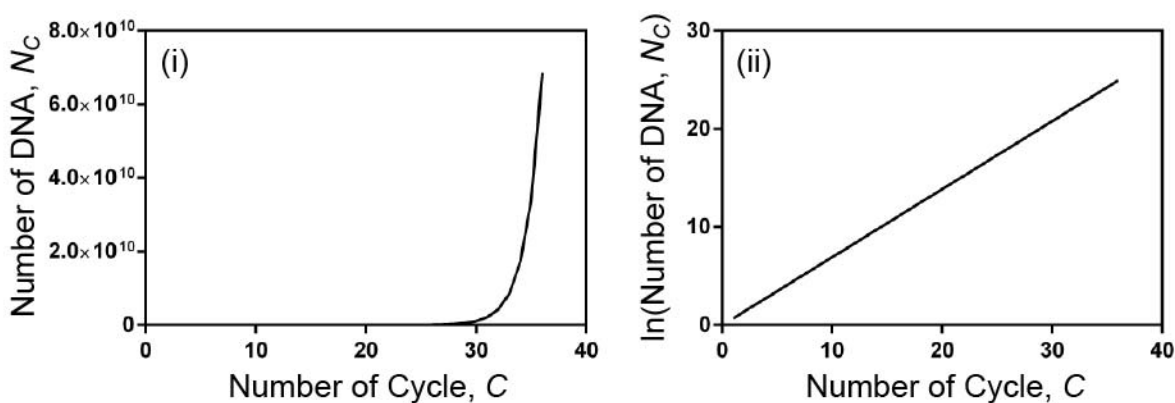


Figure 1.2. (i) The amplification process of PCR can be described as an exponential growth shown here for the ideal case where PCR efficiency (E) is 1 (**Equation 1.1**). (ii) Using a natural logarithmic Y-scale, the gradient of the straight line is $\ln(2)$ when $E = 1$ (**Equation 1.2**).

1.1.1 Thermal Cycling

A typical PCR protocol involves successively cycling a PCR mixture (**Section 1.1.2**) through three (or sometimes two) different temperatures to achieve the required steps (denaturation,

annealing, and extension) in PCR (**Figure 1.3**).^{6,14,15} During the denaturation step, the PCR sample is incubated at a high temperature between 92.0 °C and 98.0 °C to break the hydrogen bonds of double-stranded DNA templates (**Section 1.1.2.A**) to form single-stranded DNA. For the annealing step (at a temperature of ~55.0 °C), DNA primers (**Section 1.1.2.B**) are hybridised to the single-stranded DNA molecules so that the required sequence on the templates can be targeted for amplification. Both the length and sequence of the primers determine the specificity of the PCR. For the extension step, the PCR mixture is incubated at a temperature (~72.0 °C) for the polymerase enzymes (**Section 1.1.2.D**) in the PCR mixture to elongate the 3' end of the hybridised primers by incorporating basic monomer units called deoxynucleotide triphosphates (dNTPs) (**Section 1.1.2.C**) to synthesise new DNA strands that are complementary to the DNA templates.

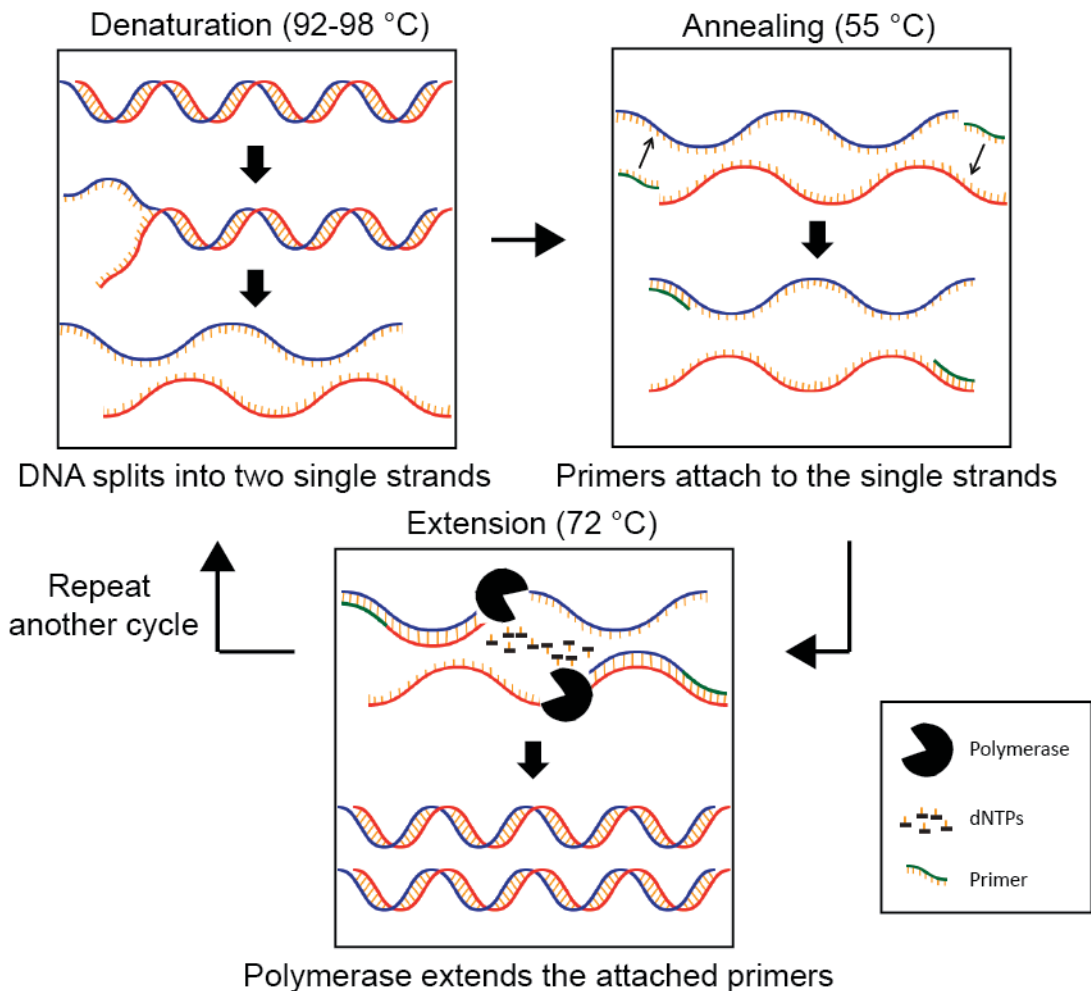


Figure 1.3. A typical thermal-cycling protocol for PCR. The PCR mixture undergoes stages of denaturation, annealing and extension in each cycle. The cycle is then repeated between 20-40 times to enrich the DNA target.

After the end of the first cycle, a single starting template will result in two copies assuming a PCR efficiency of 100 %. These two copies will consequently act as templates for the second cycle. After multiple cycles (typically, 20 to 40 cycles are used), substantial amplification of the target

DNA sequence in the PCR sample can be achieved (**Figure 1.2**). The resulting enriched sample can then be used for further studies or analyses.

1.1.2 Components in a PCR

A. DNA Template

DNA has a double-helical structure (**Figure 1.4**) which is made up of two single strands held together by hydrogen bonds.^{16,17}

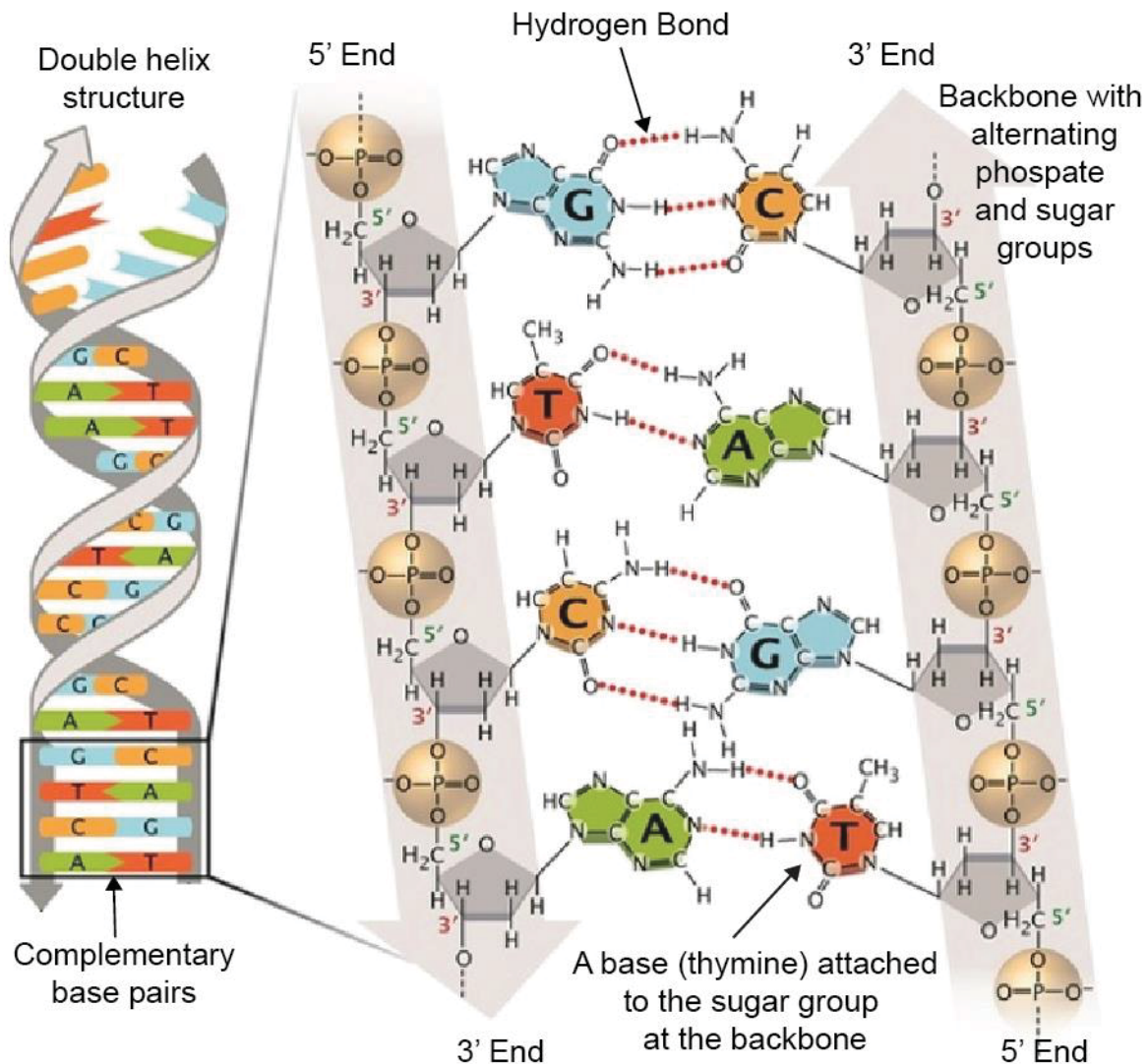


Figure 1.4. The structure of DNA.¹⁷ Two hydrogen bonds connect thymine (T) to adenine (A), while three hydrogen bonds connect guanine (G) to cytosine (C). The sugar-phosphate backbone of the two strands run anti-parallel to each other to form a double helix structure where the bases are always complementary (A-T, G-C).

Each individual strand consists of a backbone made of alternating phosphate and deoxyribose (sugar) groups that are held together by phosphodiester bonds. Within the backbone, each deoxyribose sugar group is bonded to one of four chemical bases – adenine (A), cytosine (C),

guanine (G) and thymine (T). The two single strands twist about each other so that adenine always forms two hydrogen bonds with thymine while guanine always forms three hydrogen bonds with cytosine. The result of this twisting is a double helical structure in which the bases on one strand are always complementary to the bases on the other strand.¹⁷ The sequence of the bases along the backbone of the DNA encodes the genetic information.^{2,4} PCR works by targeting a specific part of the sequence for amplification to get multiple copies.

B. DNA Primer

A DNA primer is a short single-stranded DNA molecule between 15 and 30 bases that serves as a starting point for the creation of new DNA strands.^{10,14,15} Primers are designed to be complementary to a specific sequence-location within the DNA template.

DNA primers determine the efficiency and the specificity of PCR.^{14,15} The efficiency of PCR can be defined as the fraction of DNA templates that are utilised to create new DNA strands during each cycle of PCR (**Equation 1.1**). A PCR with high efficiency will involve most (if not all) of the available templates for annealing by the primers for amplification. The specificity of PCR is determined by the extent of the primers in annealing selectively onto the targeted sites of the DNA templates for the amplification of the target sequence.^{14,15} If the primers get attached onto non-intended sites, the result will be a non-specific amplification with the production of unwanted DNA sequences. As primers determine both the efficiency and specificity of PCR, several important factors should be taken into consideration when designing them.

One important factor that affects PCR efficiency and specificity is the melting temperature (T_m). The melting temperature is defined as the temperature at which half of the primers are hybridised, with the remaining half being free.¹⁴ The melting temperature can be expressed as:¹⁴

$$T_m = \frac{\Delta H}{(\Delta S + R \ln[c])} - 273.15 + 16.6 \log[M^+] \quad (1.3)$$

Here ΔH and ΔS are the respective total enthalpy and entropy of hybridisation, R is the gas constant, $[c]$ is the concentration of the primers, and $[M^+]$ is the total concentration of monovalent cations such as K^+ and Na^+ .

The melting temperature has a strong influence on the annealing temperature. The annealing temperature is defined as the temperature at which the primer binds to the DNA template to form a primer-template hybrid.^{8,18} The annealing temperature can be determined from the melting temperatures of the PCR product and the primers using the following equation below:^{8,18}

$$T_a = 0.3 \times T_{m(\text{primer})} + 0.7T_{m(\text{product})} - 14.7 \quad (1.4)$$

where $T_{m(\text{primer})}$ is the melting temperature of the primers, and $T_{m(\text{product})}$ is the melting temperature of the product. To achieve high efficiency, DNA primers are designed to have an annealing temperature (as derived from its melting temperature) that is slightly higher than the working temperature used for annealing.^{14,15} This ensures that hybridised template-primer are formed readily with minimal non-specific hybridisations for elongation by the polymerase enzymes to form new DNA strands. However, if the annealing temperature is too high relative to the working temperature, specificity can be adversely affected since primers may hybridise partially to non-intended sites, resulting in the amplification of non-specific PCR products.^{14,15,19,20} If the annealing temperature is lower than the working temperature, a lower PCR efficiency will result as fewer of the hybridised template-primer forms will be available for elongation by the polymerase to form new DNA strands.¹⁴

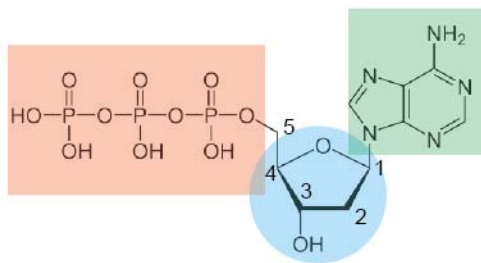
Another important factor that affects PCR efficiency and specificity is the ease with which primers are able to form hairpins²⁰ or primer-dimers¹⁹. A hairpin is formed when one end of a primer is complementary to its other end. As a result, both ends hybridise and form a loop that resembles a hairpin.²⁰ Primer-dimers are formed as a result of hybridisation of a primer pair due to the presence of complementary sequences.¹⁹ The formation of both hairpins and primer-dimers results in low PCR efficiency because these secondary structures prevent the annealing of the primers to the intended site in the DNA. Primer-dimers also affect the specificity of PCR because the amplification of primer-dimers occurs at the expense of the targeted sites. To achieve good PCR efficiency and specificity, primers should be designed to avoid the formation of hairpins or primer-dimer structures.

C. Deoxynucleotide triphosphate

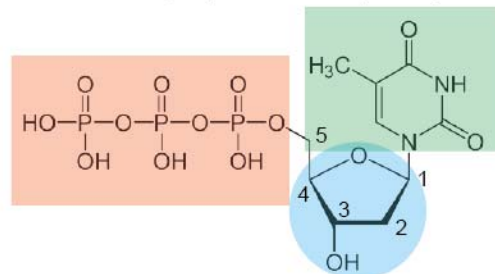
Deoxynucleotide triphosphate (dNTP) is the monomer or base unit of DNA.¹⁷ It consists of a phosphate group, a deoxyribose sugar group and a nitrogenous base group (**Figure 1.5**). Depending on the base type in the monomer, four different types of dNTPs are available: deoxyadenosine triphosphate (dATP), deoxycytidine triphosphate (dCTP), deoxyguanosine triphosphate (dGTP) and deoxythymidine triphosphate (dTTP).¹⁷ During polymerization, the phosphate group from one dNTP monomer adds to the third (3') carbon of the sugar group on another dNTP to form a phosphodiester bond. The alternating phosphate and sugar group then forms the backbone of the single-stranded DNA (**Figure 1.4**). The type of dNTP (dATP, dTTP,

dGTP or dCTP) to be used when making a new DNA strand during PCR is wholly dependent on the sequence of the DNA template for complementary pairing of the bases (A-T and G-C pairing).

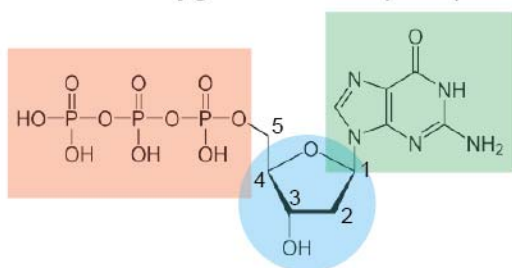
dATP: Deoxyadenosine Triphosphate



dTTP: Deoxythymidine Triphosphate



dGTP: Deoxyguanosine Triphosphate



dCTP: Deoxycytidine Triphosphate

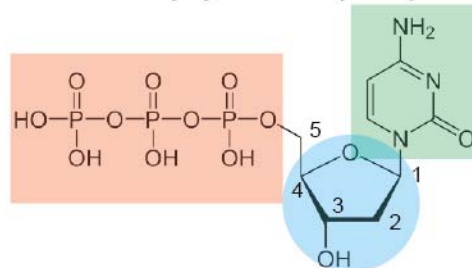


Figure 1.5. Four different types of deoxynucleotide triphosphates (dNTP).¹⁷ The monomer consists of a phosphate, deoxyribose sugar and base group. Depending on the base group (adenine (A), cytosine (C), guanine (G) or thymine(T)), the monomers are named deoxyadenosine triphosphate (dATP), deoxycytidine triphosphate (dCTP), deoxyguanosine triphosphate (dGTP) and deoxythymidine triphosphate (dTTP) respectively.

D. Polymerase Enzyme

The most important component in PCR is the polymerase enzyme; its main role being to synthesise new strands of DNA by incorporating dNTPs to elongate the DNA primers.^{5,6,10,21}

One of the first enzymes used in PCR was the DNA polymerase I, which was extracted from the bacterium *Escherichia coli* (*E. coli*).^{6,9,10} This enzyme is easily destroyed at high temperatures during the denaturation step of PCR (**Figure 1.3**). As a result, fresh enzymes must be added to the PCR mixture after each denaturation step so that active enzymes are always available in the next cycle for extension. The need to replenish the enzymes adds significantly to the complexity of the PCR reaction. DNA polymerase I has an optimal activity at 37 °C.^{6,22} At this low working temperature, PCR efficiency and specificity is low due to non-specific annealing of primers and the presence of secondary DNA structures.

With the introduction of thermostable polymerases²², the need to add fresh enzyme during each cycle was eliminated. Historically, the most popular thermostable polymerase enzyme has been *Taq* polymerase which is extracted from the bacterium *Thermus aquaticus*.^{10,22} *Taq* polymerase has a half-life of more than 2 hours at 92.5 °C and has an optimal activity at 80.0 °C.⁶ The long half-life at high temperature ensures that *Taq* polymerase remains stable throughout the PCR temperature cycles, removing the need to add fresh enzymes after each cycle and so simplifying the process. The higher working temperature for optimal activity compared to DNA polymerase I also promotes higher PCR efficiency and specificity.⁶ Annealing and extension are less likely to be impeded by secondary DNA structures at higher temperature and the more specific annealing of primers is also possible at higher working temperatures.

Processivity and fidelity are important considerations when choosing polymerase. Processivity is defined as the rate at which nucleotides are incorporated by the polymerase enzyme during the synthesis of a new strand and can also be interpreted as the extension rate (i.e. the rate at which the primers are elongated).²³ *Taq* polymerase has an extension rate of more than 35-100 nucleotides per second at 72.0 °C.²³ Based on this rate (median), a 15.0 s extension step at 72.0 °C is sufficient to generate a PCR product with 10³ base pairings. Fidelity is defined as the accuracy of the polymerase enzyme in incorporating the correct nucleotides based on complementary base-pairing during the extension step.^{21,24} A polymerase with low fidelity is more likely to make errors such as substitution and deletion of bases in the sequences of the new DNA strand during amplification. *Taq* polymerase has an error rate of 8.0 x 10⁻⁶ errors per base²¹, which is considered high due to its lack of 3'-5' exonuclease proofreading activity.²² By comparison, high fidelity thermostable polymerase such as *Pfu* (isolated from *Pyrococcus furiosus*) has an error rate of 1.3 x 10⁻⁶ errors per base.²¹

E. Buffer Solution and Additives

The buffer solution is the medium to which the above components are added to carry out PCR. The buffer solution for PCR controls the pH level to ensure the polymerase enzymes maintain optimal activity throughout the amplification process.^{6,15}

Salts such as magnesium chloride (MgCl₂) are also present in the buffer solution to maintain the ionic strength of the solution and so regulate PCR activity. MgCl₂ is an important component in the buffer solution because free magnesium ions (Mg²⁺) are a crucial co-factor for DNA polymerases.^{15,25,26} Insufficient Mg²⁺ due to an overly high concentration of dNTP or chelating agents may render the polymerase inactive and cause the PCR to fail. On the other hand, too much Mg²⁺ may increase the error rate of the polymerase enzyme and may also increase non-specific

amplification. Therefore, the concentration of $MgCl_2$ should be empirically optimized to attain the best PCR efficiency and specificity.^{15,26}

Besides salts, there are other additives in the buffer solutions which are used to improve the efficiency and/or specificity of the PCR process.²⁷ Common additives include dimethyl sulfoxide (DMSO)²⁸⁻³⁰, N,N,N-trimethylglycine (betaine)²⁹⁻³¹, formamide^{28,29}, glycerol^{28,29}, non-ionic detergents²⁷, and bovine serum albumin (BSA)³². Betaine and DMSO are known to facilitate double strand separation during denaturation.³⁰ DMSO disrupts the hydrogen bonds between the bases, while betaine lowers the energy required for denaturation. These additives also prevent the formation of unwanted secondary structures in DNA (which can lower PCR efficiency or cause the polymerase to stop working altogether). In circumstances where PCR amplification produces low yield or specificity, betaine and/or DMSO can be added at varying concentrations to determine their effectiveness. Formamide is thought to increase the specificity of primer annealing and therefore its addition can sometimes increase the efficiency of PCR.²⁹ Glycerol is added to reduce the formation of DNA secondary structure so that PCR efficiency can be improved.²⁸ Non-ionic detergents such as Tween-20 and Triton X-100 are added to neutralize traces of strong ionic detergents such as sodium dodecyl sulphate (SDS) which would otherwise inhibit the polymerase enzymes.²⁷ BSA is thought to be a general stabilizing agent to improve the stability of polymerase enzymes and so prevent the adsorption of polymerase onto the container walls which would lower PCR efficiency.^{32,33}

1.1.3 PCR for Quantitative Analysis

One of the most important applications of PCR is the quantification of initial DNA templates.³⁴⁻³⁶ In theory, PCR can be used for quantitative analysis because the reaction ideally doubles the amount of DNA every cycle. Given ideal behaviour, the final amount of product is related to the starting number of template by a well-defined relationship (**Equation 1.1 and 1.2**).¹³ However, in practice, substantial deviations from ideal behaviour can occur as a result of PCR efficiency dropping over successive amplification cycles.^{37,38} This drop in PCR efficiency must be considered when using PCR as a quantitative tool. The PCR process can be divided into three distinct phases (**Figure 1.6**) to illustrate the drop off in PCR efficiency.³⁷⁻³⁹

The first phase is described as the exponential stage.^{37,38} Here, the number of DNA primers is in large excess compared to the number of DNA templates. As a result, most (if not all) the templates hybridise with the primers during annealing. The hybridised template-primer species then undergo elongation during extension to form new strands. Under these conditions, the efficiency

of PCR is 100 % and the number of PCR product doubles with every cycle (**Equation 1.1**) resulting in an exponential enrichment of the target sequence. This stage should be precise and reproducible between replicates.

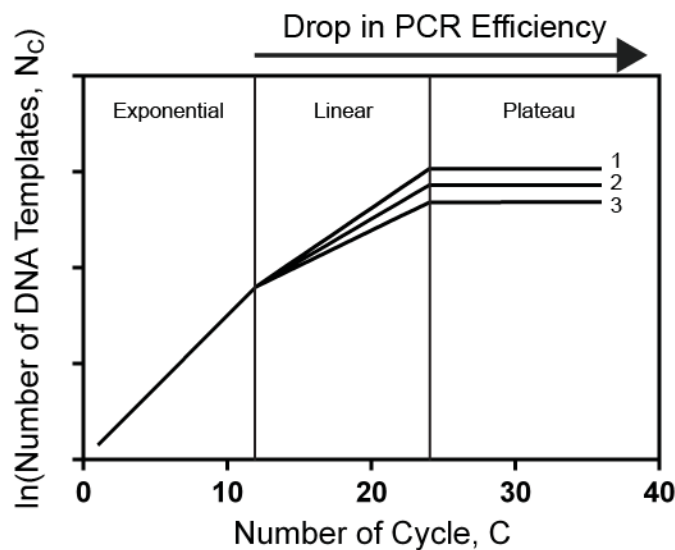


Figure 1.6. An illustrative plot showing the three phases of PCR which are observed over successive amplification cycles. The first phase is the (ideal) exponential stage where the PCR efficiency is 100 %, resulting in a doubling of PCR products in each cycle. For the three replicates depicted in the diagram, this phase is reproducible and precise. The second stage is known as the linear stage when the PCR efficiency starts to drop due to the number of primers decreasing while the number of DNA templates increases. The third stage is the plateau where the primers have exhausted. Little or no amplification takes place in the last stage. The three replicates have highly variable outcomes in both the linear and plateau stage.

The second phase is known as the linear stage.^{37,38} By this stage, a large number of primers have been consumed during the initial cycles and they are in continuous decline. At the same time, the amount of PCR product is increasing. Annealing of the primers to the single-stranded DNA templates is no longer favoured due to the increasing ratio of template-to-primer. As a result, fewer of the hybridised template-primers species are available for extension by the polymerase enzymes. In effect, the efficiency of PCR has dropped. The amount of PCR product is still increasing at this stage but no longer at an exponential rate. This stage has highly variable reaction kinetics and gives different outcomes for different replicates.

The last phase is the plateau stage.^{37,38} During this stage, the number of primers is nearly exhausted. As a result, little or no amplification takes place. The amount of PCR products remains roughly constant over subsequent cycles. In a similar fashion to the linear stage, this phase is also highly variable and differs substantially between replicates.

1.1.4 End-point PCR

Analyses of a PCR sample are most typically conducted after PCR is completed. However, quantitative information derived at this stage is usually unreliable because of the highly variable outcomes at the end-point (plateau stage, **Figure 1.6**).^{37,38,40} An example of an end-point analysis is capillary electrophoresis.⁴¹ Capillary electrophoresis is a method to separate DNA molecules based on their size and/or charge through a buffer-filled (or in the case of DNA, gel-filled) capillary using an electric field. After separation, the target DNA in the PCR mixture can be identified based on size discrimination. Such end-point analysis is only qualitative in nature; the analysis only confirms the presence of the PCR product. The amount of PCR products can be roughly estimated and compared between samples, but this approach is unreliable due to the highly inconsistent outcomes at the end-point.^{37,38,40} To overcome the limitation of end-point PCR for quantitative analysis, the PCR products can be measured during the exponential phase where quantitative analysis is most reliable, e.g. by removing a PCR aliquot at each successive cycle and measuring the product concentration on a cycle-by-cycle basis.^{34,37,42} In this way, the exponential phase can be identified and used for quantitative analysis. However, the requirement to physically sample a PCR reaction at multiple cycles makes such an approach unnecessarily time-consuming and laborious.

1.1.5 Real-Time PCR

Real-time PCR^{13,34,37,38,43-45} allows the continuous monitoring of PCR as it takes place. Such monitoring is done by exciting a PCR mixture (with fluorescent probes) with a light source and then determining the concentration of PCR product from the emission intensity. As the amount of PCR product increases with each cycle, the fluorescent signal increases proportionately.^{6,46-48} Measurements of the fluorescence without physically sampling and disturbing the PCR mixture allows the accumulation of PCR products to be monitored in a non-invasive fashion, allowing the exponential phase to be identified and used for quantitative analysis. In order to conduct real-time PCR, fluorescent indicators or probes must be added to the PCR mixture so that the concentration of PCR products can be monitored over time.⁶ The popular probes include intercalating dyes^{6,46-48}, hydrolysis probes^{6,34,49,50}, dual hybridisation probes^{6,48}, and molecular beacons^{6,51,52} as discussed below.

A. Intercalating Dyes

Examples of intercalating dyes include ethidium bromide and SYBR Green I.^{6,46-48} These dyes give a strong emission signal during excitation when they are bound to the double-stranded DNA

molecule, but give a low fluorescent signal when unbound (**Figure 1.7**). The low costs of intercalating dyes and their relative ease of use are the main advantages for use in real-time PCR. However, a major disadvantage of intercalating dyes is their non-specificity since they will bind with all double-stranded DNA. Hence the measured fluorescent signal may not always result primarily from the target DNA sequence, and in some cases may be dominated by the presence of other non-specific double-stranded DNA materials.

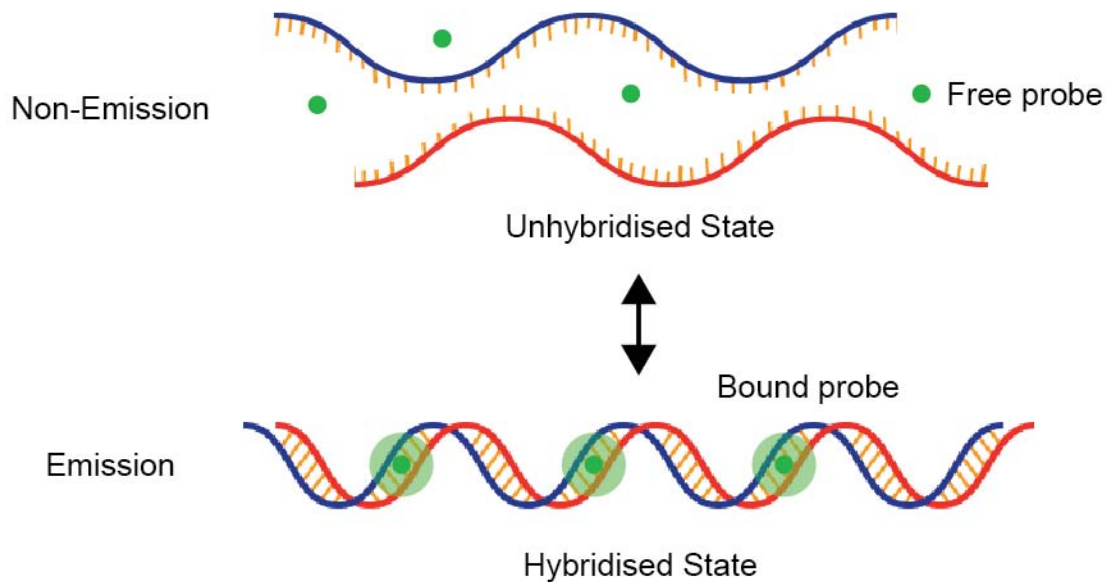


Figure 1.7. A diagram illustrating how an intercalating dye differentiates the unhybridised and hybridised state of DNA. The dye fluoresces strongly only when bound to a double-stranded DNA molecule.

B. Hydrolysis Probes or TaqMan Probe

Hydrolysis probes^{6,34,49,50}, also known as TaqMan probe, are another class of reporter, which can be used for real-time PCR. The hydrolysis probe is designed to include a complimentary strand to the PCR target sequence with a fluorophore covalently attached to the 5' end and a quencher molecule to the 3' end of the strand. Fluorescence from the fluorophore is normally quenched via fluorescence resonance energy transfer (FRET)^{53,54} due to the close proximity of the quencher molecule to the fluorophore (**Figure 1.8**).

During PCR, the hydrolysis probe hybridises with the single-stranded DNA template due to complementarity. During the extension step, the polymerase enzyme will extend the annealed primer by incorporating dNTPs. As the polymerase enzyme reaches the hydrolysis probe, the polymerase enzyme cleaves the bonded probe due to its 5'-3' exonuclease activity. (It is important to note that not all polymerase enzymes have the 5'-3' exonuclease activity). Upon breaking the hydrolysis probe, the fluorophore is released into solution. At this point, the fluorophore becomes fluorescent because it is no longer in close proximity with the quencher.⁴⁹

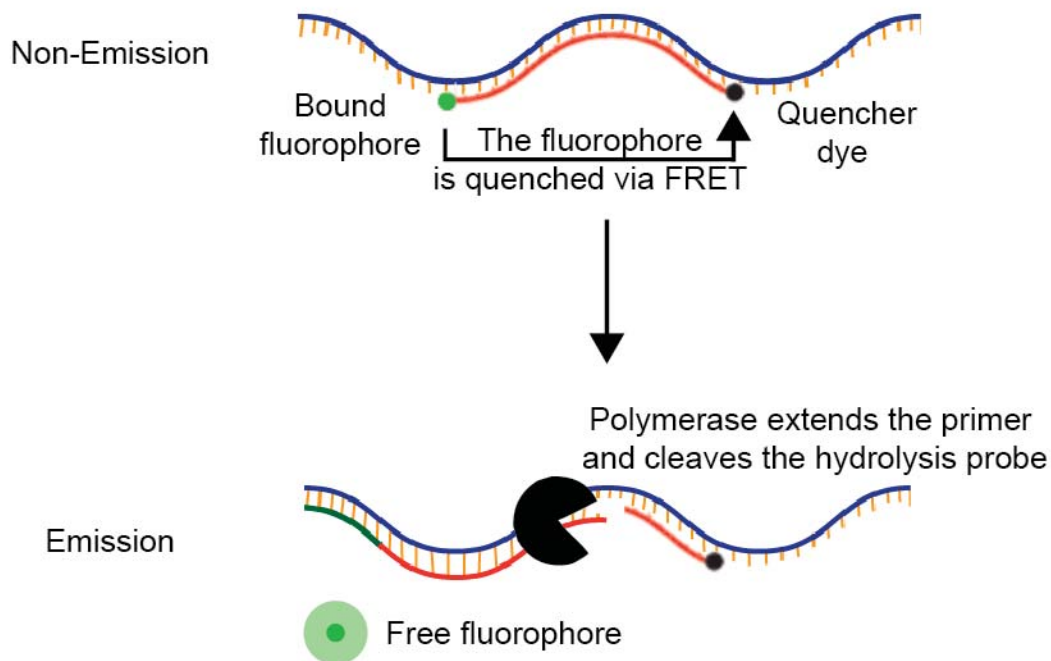


Figure 1.8. A diagram showing the working principle of a hydrolysis probe.⁴⁹ A fluorophore and a quencher dye are bound to each ends of a short DNA strand. Due to the close proximity of the fluorophore and the quencher dye, FRET takes place during excitation, and quenches the fluorophore emission intensity. Specificity is ensured by complementary base pairing between the probe and the DNA template. During extension, the attached probe is cleaved by the polymerase enzyme, releasing the fluorophore from the quencher and allowing it to emit.

The fluorescent signal is due to the increasing amount of free fluorophore released during the extension step in PCR. The hydrolysis probe is highly specific since it is complementary to the single-stranded DNA template; the resulting fluorescent signal is always derived from the synthesis of the target sequence. This removes any systematic bias that may come from the presence of other non-specific products. The specific, irreversible and cumulative nature of the signal generation by hydrolysis probes allows for the live monitoring of PCR. The exponential phase of PCR can then be easily identified and thus used for quantitative analysis.

Specificity is the main advantage of hydrolysis probe.⁴⁹ However, care must be taken when selecting the probe's hybridisation site on the target DNA sequence. If the probe has a lower annealing temperature than the working temperature, the annealing of the hydrolysis probe may not take place to a sufficient extent. A low signal may then result because only a minority of the probes are cleaved during amplification, releasing only a few fluorophores. If the probe has a higher annealing temperature than the working temperature, the annealing of the hydrolysis probe may not be specific. As a result, specificity may suffer because the fluorescent signal may now come from non-specific sites.

C. Dual Hybridisation Probes

Dual hybridisation probes^{6,48} consist of two oligonucleotides having sequences that are complementary to the target DNA. The probes are labelled with a pair of fluorophores that exhibit FRET.⁵⁴ One of the probes is labelled with a donor fluorophore at its 3' end while the other probe is labelled with an acceptor fluorophore at its 5' end (**Figure 1.9**).

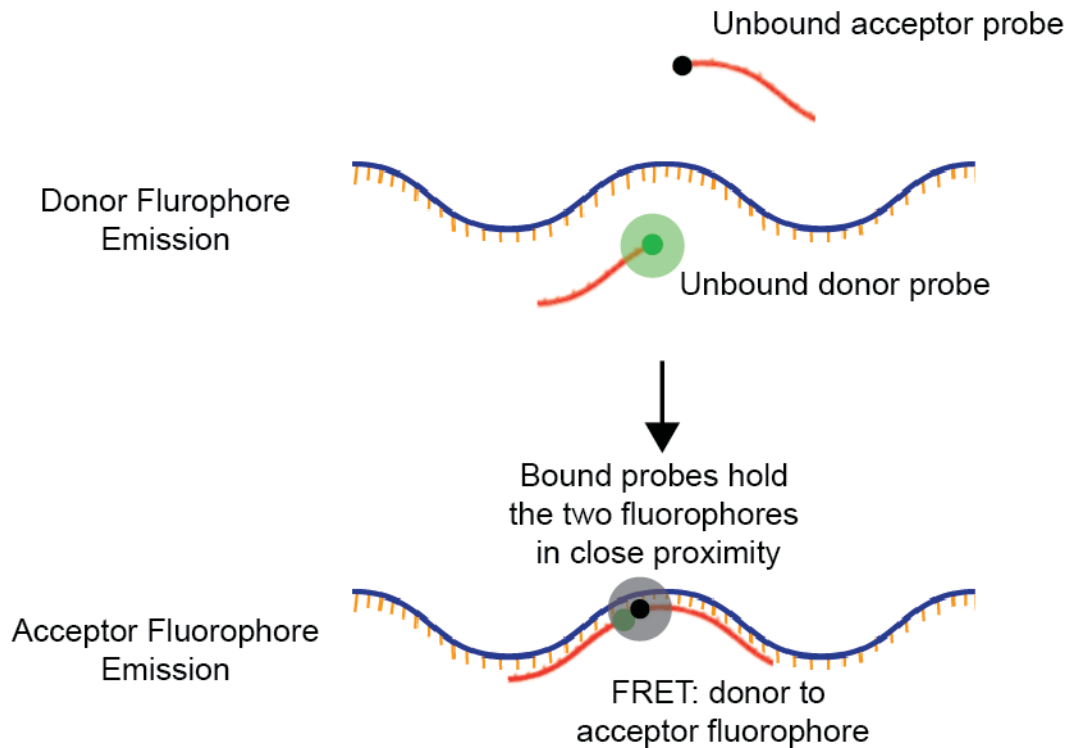


Figure 1.9. A diagram showing the working principle of dual hybridisation probes. Two short DNA strands are labelled with a donor and acceptor fluorophore respectively. Before binding to the DNA template, the donor fluorophore will emit when excited. When the two probes are bound to the DNA template, the donor and acceptor fluorophore are held close together, causing FRET to take place. Excitation at this point will result in the acceptor fluorophore emitting a fluorescence.

During hybridisation with the target DNA, the two probes are designed to bind close to each other so that the donor and the acceptor fluorophore are in close proximity with one another (**Figure 1.9**). Upon excitation of the donor fluorophore by a light source, FRET will occur resulting in emission by the acceptor fluorophore. Real-time PCR is conducted by monitoring the fluorescent signal from the acceptor fluorophore during the annealing step. The fluorescence intensity increases proportionally to the rising number of DNA targets that are generated over successive PCR cycles. In contrast to hydrolysis probes, the hybridisation probes are not required to be cleaved apart during the amplification so polymerase enzymes without 5'-3' exonuclease activity can be used. The fluorescent signal from hybridisation probes is reversible. Dual hybridisation probes are highly-specific probes because they are required to anneal to the DNA targets before the fluorescence signal can be measured.

D. Molecular Beacons

Molecular beacons^{6,51,52} are oligonucleotides that are labelled with a fluorophore and a quencher at the 5' and 3' ends. The 5' and the 3' ends have complementary sequences that cause the molecular beacon to undergo self-hybridisation at low temperature. Upon self-hybridisation, the molecular beacon forms a hairpin structure which consists of a stem and a loop. The stem is made up of the complementary ends coming together and the loop consists of sequences specific to the DNA target for PCR (**Figure 1.10**).

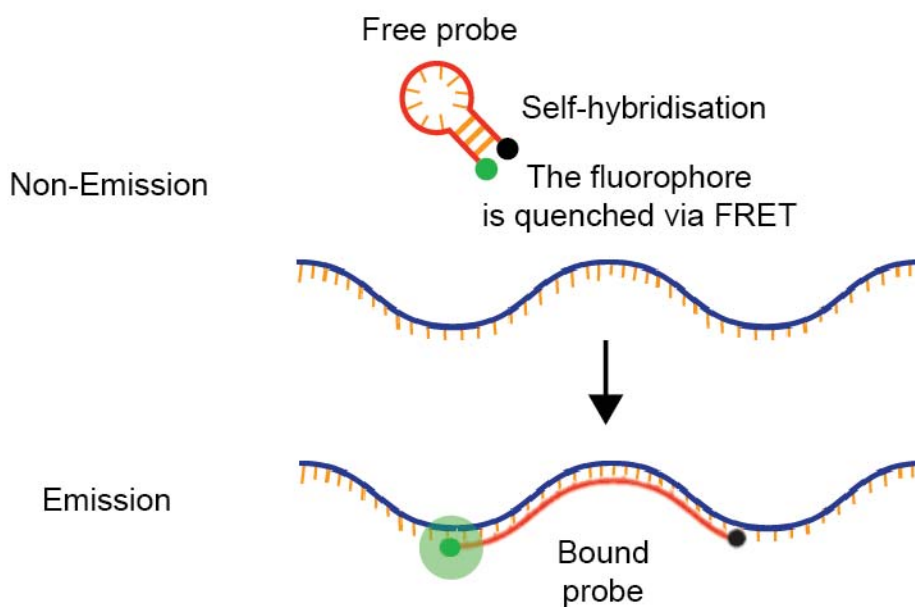


Figure 1.10. A cartoon illustrating the working principle of molecular beacon probes. In the probe's free state, it undergoes self-hybridisation to form a hairpin structure causing the fluorophore and quencher at the ends to be held close together. FRET takes place and the fluorescence from the fluorophore is quenched. When the probe binds to the DNA template, the hairpin structure is opened up. The fluorophore and the quencher are held apart, allowing the fluorophore to emit.

At low temperature, the two ends come together bringing the fluorophore and the quencher into close proximity, resulting in fluorescence quenching by FRET.⁵¹ At higher temperatures, the molecular beacon loses its hairpin structure and anneals to the DNA target based on the sequences in the loop. The resulting separation of the fluorophore and the quencher allows the fluorophore to emit under excitation, yielding a signal that is proportional to the number of DNA targets in the reaction.

The main advantage of molecular beacons is that they are highly specific.^{51,52} If the target sequence is not complementary with the sequence on the molecular beacon, hybridisation will not occur. Consequently, there will be no fluorescent signal. Similar to dual hybridisation probes, molecular beacons are not required to be cleaved apart so polymerase enzymes lacking 5'-3'

exonuclease activity can be used. The main disadvantage associated with molecular beacon lies in the difficulty of designing them. The complementary sequences at the 5' and 3' ends of the molecular beacon must be chosen carefully so that the stem can be opened up readily for specific annealing at the right temperature.

Quantitative real-time PCR is carried out by measuring the emission intensity every cycle.⁴⁸ The exponential phase, which provides the most reliable data for quantification, can be identified in retrospect by plotting the measured fluorescence against cycle number (C) (**Figure 1.11 (i)**). The threshold cycle (C_T), i.e. the cycle number at which the fluorescence surpasses the background level. From **Equation 1.2**, it follows that the threshold cycle is inversely dependent on the initial DNA template concentration, $\ln(N_0)$:

$$\ln N_0 = \ln N_{C_T} - C_T[\ln(E + 1)] \quad (1.5)$$

where E is the amplification efficiency, N_{C_T} is the number of template molecules after cycle C_T , and N_0 is the initial number of DNA templates. By measuring the C_T values of multiple standards with varying initial DNA template concentrations (N_0), a standard curve of $\ln(N_0)$ against C_T is obtained (**Figure 1.11(ii)**). Hence, by comparing the threshold cycle of a sample of unknown starting DNA concentration with the standard curve, the amount of template DNA can be quantified.¹³

Real-time PCR is an improvement over end-point PCR because it allows quantification of DNA.^{34,37,40,55} The use of fluorescence probes also provides higher sensitivity and specificity than end-point analyses. However, real-time PCR does have its limitations.^{36,56} One limitation is that the quantitation is achieved relative to standards, and matrix effects cannot easily be taken into account when using standards; internal constituents of the sample may affect the PCR efficiency, giving rise to behaviour that does not match the standard curve.^{56,57} Quantitation by real-time PCR assumes the PCR efficiency is the same for the prepared standards and the unknown samples which is seldom true in practice.¹³

Another limitation is that real-time PCR has a bias for amplifying common DNA strands over rare ones because rare DNA strands are present in very low number relative to the common ones in the mixture.⁵⁸⁻⁶¹ When targeting rare DNA strands that are present in very low concentration, quantitation is rarely reliable since conventional PCR is not sufficiently specific to ensure exclusive amplification of the rare DNA sequences against common ones.

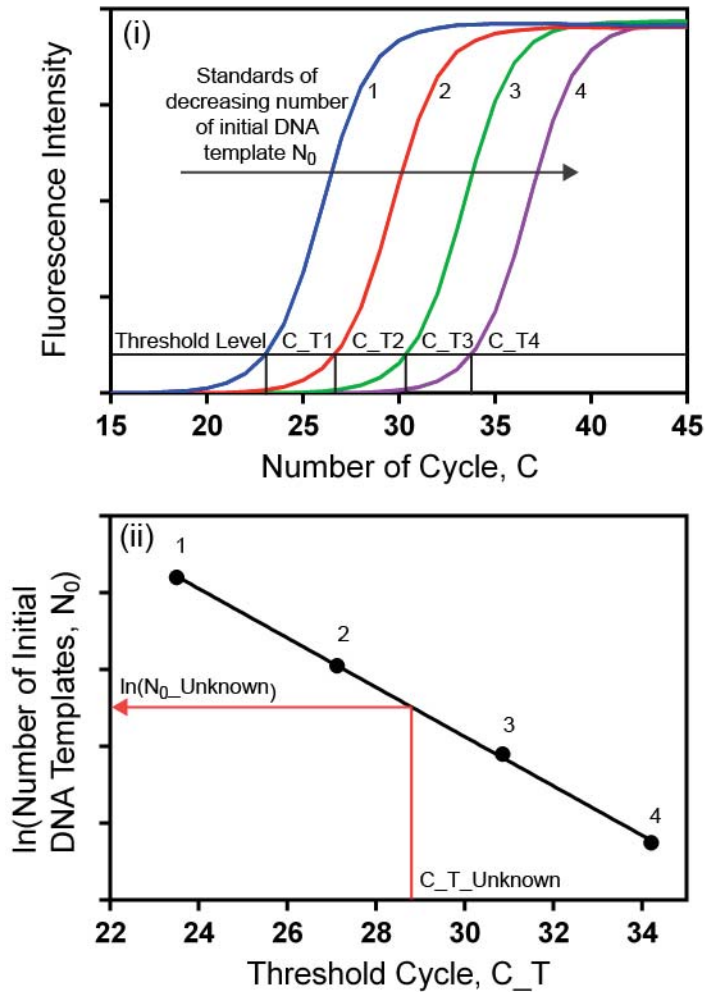


Figure 1.11. (i) A plot of measured fluorescence intensity against number of cycle (C) for four standards of varying known number of initial DNA template (N_0). The threshold cycle (C_T) for each standard is derived from the plot. (ii) A plot (calibration line) of the C_T values of the four standards against their corresponding $\ln(N_0)$ (**Equation 1.5**). By determining the C_T of an unknown sample and cross-referencing against the calibration line, the initial quantity of template molecules in the unknown sample can be determined.

1.1.6 Digital PCR

Digital PCR⁵⁹⁻⁶⁶ has been developed to enable absolute quantitation^{57,67,68} of DNA by allowing both rare and common sequences in a population to be amplified separately and analysed individually, and by allowing the analysis of complex mixtures without the use of relative standards. Given the benefits of absolute quantitation, digital PCR has been used for various clinical and diagnostic applications.^{60,69-76} In digital PCR (**Figure 1.12**), a pool of DNA templates undergoes limiting dilution.^{59,62} The diluted pool is then split up into many small volumes (cells) to ensure most cells do not contain DNA template, some cells have one DNA template, and a very low number of cells have two or more DNA templates.^{59,60,62} (This contrasts with conventional PCR which uses a single pool containing multiple templates.)

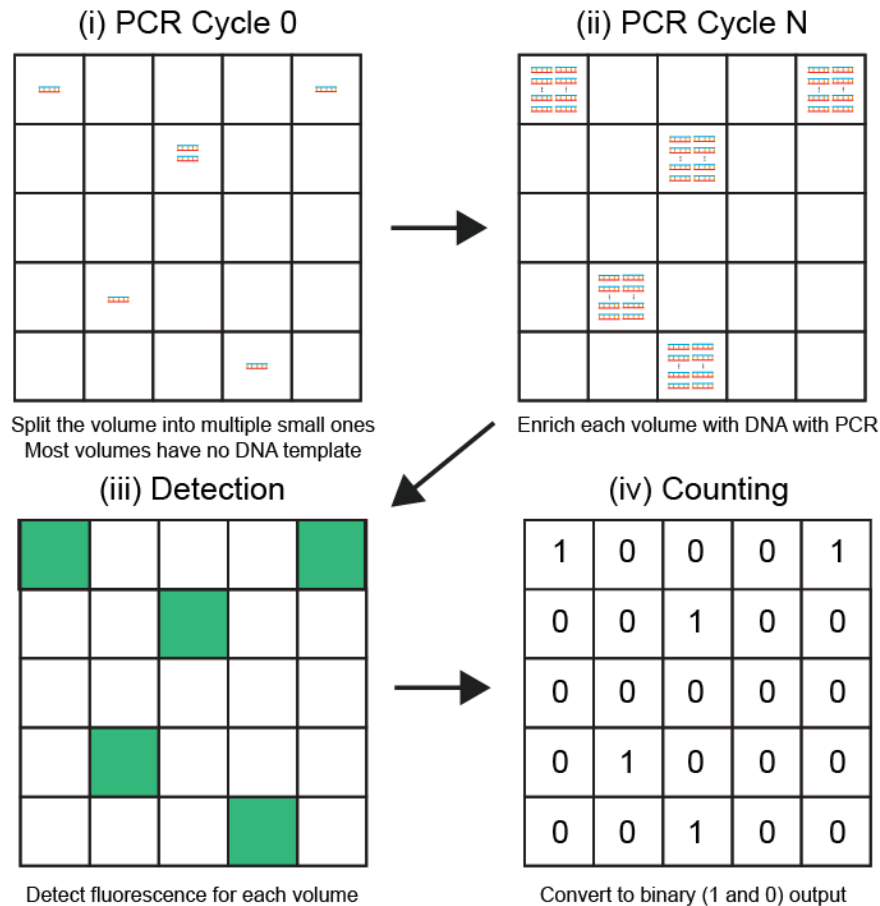


Figure 1.12. Digital PCR. (i) A pool of DNA template is diluted and split into small volumes (cells); most of these cells do not contain DNA template. (ii) After PCR, the cells with DNA templates are enriched with copies of the DNA templates (iii) Detection is carried out for each cell. Only those cells that initially contained DNA templates will fluoresce. (iv) The emitting cells are labelled as “1” and the non-emitting ones are labelled as “0”. By analysing the distribution of “0” and “1” in terms of Poisson statistics, absolute quantitation of the templates can be achieved.

The individual cells are then enriched with copies of the DNA template by thermal cycling, and the cells are subsequently probed for a target sequence by using one of the fluorescence probes described previously. Cells that contain the target DNA template will fluoresce, yielding a positive result (“1”) while those that contain none of the target DNA template will not fluoresce, yielding a negative result (“0”). This binary readout can be counted and analysed statistically to allow quantitation of the target sequence. The binary nature of the outcome has led to this form of quantitative PCR being known as digital PCR.^{59,60}

The probability of a small cell containing a certain number (0, 1, 2, or more) of DNA templates is governed by Poisson statistics.^{59,60} The probability (p) is described by:

$$p(x; \lambda) = \frac{e^{-\lambda} \lambda^x}{x!} \quad (1.6)$$

where λ is the mean number of templates molecules per cell, x is the number of DNA template (0, 1, 2, or more) in the cell.

When $x = 0$ (no template molecules in cell),

$$p(x = 0; \lambda) = e^{-\lambda} \quad (1.7)$$

When $x \geq 1$ (one or more template molecules in cell),

$$p(x \geq 1; \lambda) = 1 - e^{-\lambda} \quad (1.8)$$

By way of example, assuming a pool of 10^4 copies of DNA templates in $10.0 \mu\text{L}$, splitting this large cell into 10^4 small (1.0 nL) cells will result in a mean (λ) “occupancy” of 1 template molecule per cell. Based on **Equation 1.7**, the probability of having a negative “0” outcome (no template molecule in the cell) is 0.368. The probability of having a positive “1” outcome (one or more template molecules in the cell) is 0.632 (**Equation 1.8**). The probability of having a negative outcome increases as the mean number (λ) of template molecules per cell decreases (**Figure 1.13**).

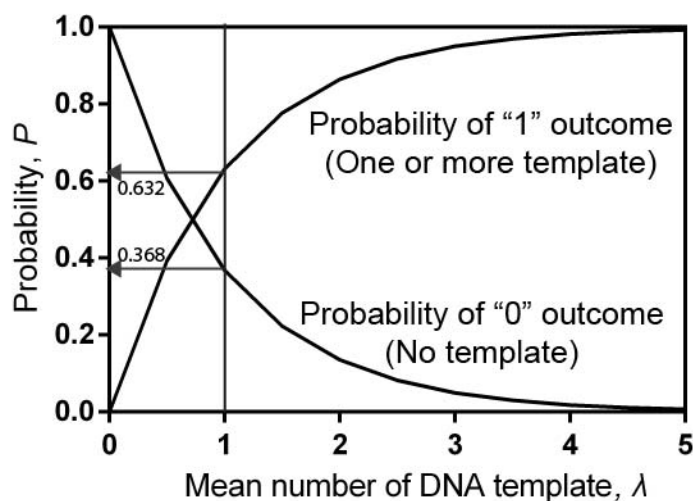


Figure 1.13. A plot showing how the probability of having positive and negative outcomes varies with the mean number (λ) of DNA template molecules.

In digital PCR experiments, the fraction of negative cells (i.e. those that yield a “0” outcome) is determined empirically. This value corresponds to the probability of having no DNA template (P) in the cell volume. Using **Equation 1.7**, the resulting mean number (λ) of DNA template molecules can be derived which in turn can be used to determine the concentration of DNA template molecules in the sample.

With digital PCR, multiple templates DNA molecules of substantially varying concentration can be quantified within a single sample.^{59,60} However, digital PCR, by its very nature, requires the

handling of large numbers of small (nanoliter to picoliter range) volume calls in order to arrive at a situation where most of the cells are “empty” of DNA template molecules and Poisson statistics may be readily applied.^{59,60} Unfortunately, dealing with large numbers of small volume cells is technically challenging, since thousands of DNA templates must be amplified separately and subsequently probed for their genetic content.

1.1.7 The Bench-top Thermal Cycler and its Limitations

End-point and real-time PCR are traditionally conducted on a bench-top thermal cycler. Although the conventional bench-top thermal cycler is one of the most common pieces of biochemical laboratory equipment, it has several limitations in relation to PCR, especially digital PCR.

A conventional bench-top thermal cycler works by thermally-cycling the PCR mixture through different temperatures for denaturation, annealing and extensions. To do this, the thermal cycler must heat up and cool down the entire sample chamber in addition to the PCR mixture, resulting in a large thermal mass that leads to unacceptably long heating and cooling times.⁷⁷⁻⁸⁰ Consequently, energy consumption is also high because of the long heating and cooling duration.^{78,79} If the thermal mass is reduced, PCR can be completed more quickly and with a lower energy consumption.

Conventional bench-top thermal cyclers work with large volumes (typically in the 10.0 to 25.0 μ L range), which leads to high reagent consumption. PCR can be a costly reaction because it uses multiple expensive reagents (**Section 1.1.2**) such as polymerase enzymes and primers.⁷⁸⁻⁸⁰ Reducing the consumption of these reagents can lower the cost of PCR. Aside from the high consumption of reagents, working with large volumes leads to an amplification bias for short DNA fragments.^{78,81} In a large PCR volume, the smaller fragments such as the dimer-primers are amplified preferably over the larger target sequence, leading to non-specific PCR products. As a result, the reaction yield is low. The PCR recipe and the PCR protocol must be carefully optimised to minimize such amplification bias when working with large volumes. More importantly, due to the large volume, a long time is required to reach a homogenous equilibrium temperature and substantial variations in temperature across the reaction volume typically exist, which can have a detrimental effect on the PCR efficiency.^{78,79} For instance, when the thermal cycler reaches the target temperature for annealing, less primers anneal for amplification in localised regions with higher temperatures, and non-specific annealing occurs in localised regions with lower temperatures. By reducing the working volume, the PCR reaction can occur at a more

homogenous temperature for each PCR step, allowing better controlled PCR amplification to be achieved.^{78,79}

On further issue relating to the use of a conventional bench-top thermal cycler is that PCR is carried out in a batch process. Other functions such as sample preparation and handling must be carried out separately and cannot easily be integrated into the thermal cycler.^{82,83} Without integration, automation is difficult to implement. Moreover, conventional bench-top thermal cyclers do not have the capability to handle large numbers of very small volume cell as required especially for digital PCR (nanoliter to picoliter cells are typically needed).^{59,60} To circumvent this limitation, adaptations such as the use of microtiter plates^{59,65} and emulsions^{57,84,85} have been used. The microtiter plate approach uses a large plate that contains a large array of small wells into which the PCR mixture may be loaded.⁵⁹ The whole plate is then thermally-cycled using a bench-top thermal cycler for PCR. The emulsion approach uses many water-in-oil droplets (either generated in bulk through mechanical agitation⁸⁶ or by using microfluidic tools⁸⁷⁻⁹⁵) that behave as independent reaction vessels. The droplets containing the PCR mixture can then be loaded into a typical plastic PCR tube for thermal-cycling on the bench-top thermal cycler. Although these adaptations allow conventional bench-top thermal cyclers to handle multiple samples and small volumes, many of the limitations mentioned above are unavoidable.

Due to the limitations of thermal cyclers, new approaches are needed to allow real-time and digital PCR to be carried out in a faster and more reliable manner. New approaches should ideally reduce the working volume of the PCR mixture so as to reduce cost, avoid amplification bias of small fragments, and more importantly allow a more homogenous reaction environment. They should also be amenable to integration and automation. Lastly, they should have the capability to handle large numbers of samples and very small volumes (nanoliter to picoliter), as required in digital PCR. As we describe below, one of the most promising approaches is based around the use of miniaturised reactors to reduce thermal mass and the working volume and to allow easier integration of additional functionality.

1.2 MICROFLUIDIC SYSTEMS FOR PCR

Microfluidics involves technologies that manipulate small volumes of fluids (typically in the microliter to picoliter range) using channels and wells with dimensions in the micrometer range (tens to hundreds of micrometers).⁹⁶⁻⁹⁸ Microfluidics is of significant current interest because it provides a means of miniaturising chemical processes, allowing for the manipulation of small volumes of samples or reagents.^{83,97,99} It also allows for rapid separation and analysis of products

with high sensitivity and resolution.^{83,97,99} Given these compelling advantages, microfluidics has attracted great attention in the fields of chemistry¹⁰⁰⁻¹⁰⁴ and biology¹⁰⁵⁻¹¹².

Molecular biology has greatly benefitted from the development and implementation of microfluidic technologies for PCR.^{77-80,113-115} Molecular biologists require PCR approaches that can handle, analyse and quantify nucleic acids with higher throughput, sensitivity and efficiency than achievable using conventional bench-top technologies.^{77-80,113-116} The ability to handle smaller sample volumes results in lower reagent consumption, while the small volumes result in fast mixing by diffusion.^{78,79} More importantly for PCR, the smaller system dimensions mean smaller thermal masses and thus faster heat transfer (due to large surface-area-to-volume ratios) so that thermal-cycling times may be drastically reduced.^{78,79} More homogenous reaction temperatures arise when working in small sample volumes, which in turn improves product yields.^{78,79} The adoption of microfluidic formats also allows the integration of multiple functions such as sample preparation, separation and detection within a single device.^{78,79,117,118} These advantages promise major improvements for both end-point and real-time PCR when compared to conventional bench-top thermal cyclers. It should also be noted that since microfluidic devices can handle picoliter sample volumes, the nanoliter to picoliter sample volumes required for digital PCR are easily accessible.^{77,80} Micro-wells, microchannels and even emulsion (water-in-oil) droplets can be used to handle such volumes.^{78,79} Digital PCR also requires the efficient handling of large number of individual samples.^{59,60} In this respect, large numbers of micro-wells have already been used to concurrently handle thousands of samples.⁷⁸ Moreover, emulsion droplets have been used to encapsulate PCR mixtures, where millions of droplets can be generated in a rapid and reproducible fashion.^{78,119}

The benefits of microfluidic tools in PCR were first recognised and demonstrated in the 1990s^{83,120}, and much work has followed since.^{77-80,113-115} Indeed, microfluidic PCR is a diverse and multidisciplinary field spanning materials science, device design, fabrication and integration, detection, and biological applications.⁷⁸⁻⁸⁰ The following sections do not aim to provide an exhaustive list of all works relating to microfluidic PCR, but rather highlight some of the more prominent developments of chip-based PCR, with a special focus on recent innovations that allow the handling of large numbers of small volume samples.

Two main approaches for performing chip-based PCR have been reported in the literature.⁷⁸⁻⁸⁰ The first approach is the well-based method, with the second is the continuous-flow method (**Figure 1.14**).

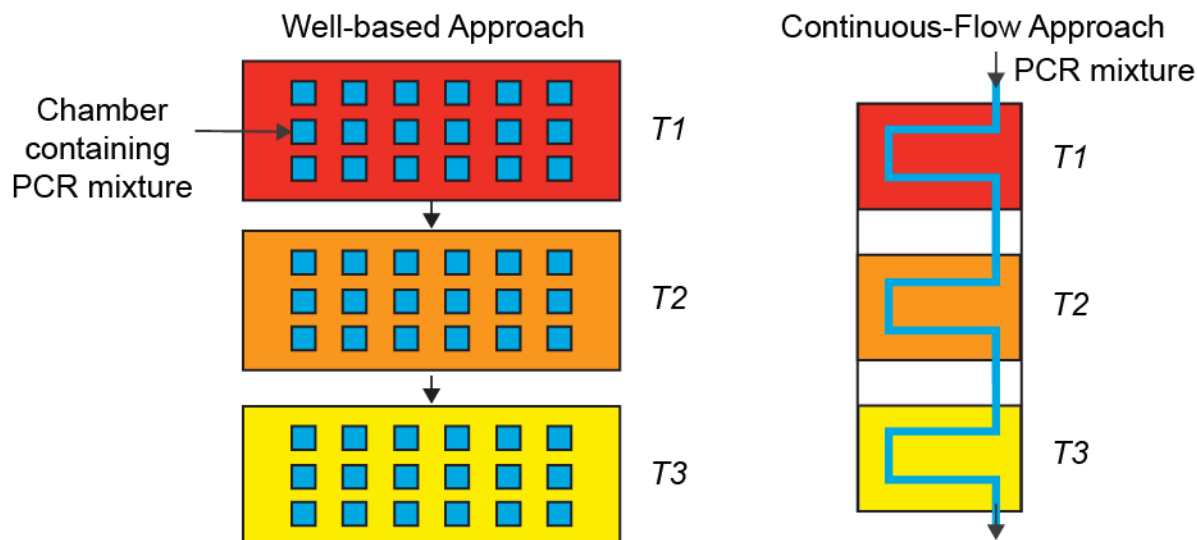


Figure 1.14. A cartoon showing the difference between well-based and continuous-flow approaches. In well-based approaches, samples and the entire chip are repeatedly heated and cooled to achieve temperature cycling from T1 to T2 and T3, while in the continuous-flow approaches, the sample passes sequentially through heated zones (held constant at T1, T2 and T3) to achieve the same temperature cycling effect.

In the well-based approach, the PCR mixture is injected into a reaction chamber in a chip-based device. The chip as well as the PCR mixture is then thermally-cycled through various temperatures.^{78,120} In the flow approach, the PCR mixture is flowed through a chip-based device over various temperature zones for thermal-cycling to conduct PCR.^{78,121} In continuous-flow methods, the time spent in the different temperature zones is varied by controlling the flow rate of the PCR mixture.

1.2.1 Well-based PCR

The first chip-based PCR device was well-based and presented by Alan Northrup and co-workers.^{120,122} The device was in essence a scaled-down version of a conventional bench-top cyclers. In this silicon-based device, a 50.0 μL micro-well was used as a PCR chamber. Through miniaturization and localization of heaters close to the reaction volume, four times faster amplification and lower energy consumption resulted when compared to a conventional thermal cyclers. This device provided the first experimental demonstration that fast and efficient PCR could be achieved by reducing the thermal mass of the sample and heater. The well-based approach has subsequently been widely investigated and further developed by other groups.^{79,123–125}

A major development in well-based PCR was the employment of multiple chambers in an array-format, allowing multiple PCR reactions to be carried out in parallel. The ability to handle a large number of PCR samples increases throughput and thus reduces analysis time. The current trend in using multiple chambers in well-based approaches is to further reduce the reaction volume (to the pL scale) and to pack as many chambers as possible per unit area.

An example of using multiple chambers within a chip-based platform is the highly-integrated silicon micro-chamber array developed by Matsubara *et al.* for DNA quantification and sequence detection.^{126,127} The reported device (**Figure 1.15**) consists of 1248 chambers; each holding 40 nL of PCR mixture. After thermally cycling the whole device, each chamber was probed using fluorescence. Based on this approach, the group demonstrated simultaneous amplification and detection of five different target sequences related to *Escherichia coli* on a single chip.

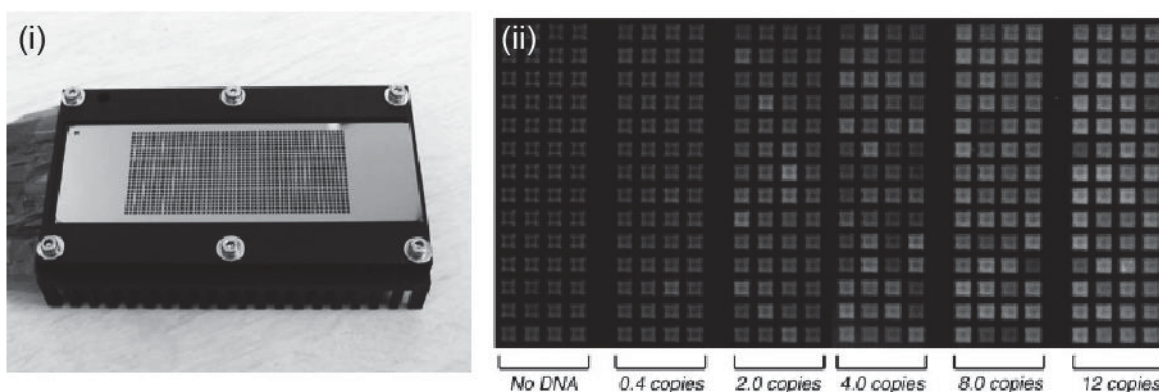


Figure 1.15. (i) A well-based PCR device reported by Matsubara *et al.* comprising an array of 1248 micro-chambers fabricated in silicon.¹²⁶ The chambers were used to hold PCR mixture and the whole device cycled through different temperatures for DNA amplification. (ii) Every chamber was then probed using fluorescence imaging.

Another example of a well-based device was reported by the Fluidigm Corporation, who successfully commercialised a microfluidic system for digital PCR.^{63,128–130} The device (**Figure 1.16(i)**) was able to test up to 48 samples, with each sample being partitioned into an array of 770 individual reaction chambers. Each chamber has a volume of 840 pL.

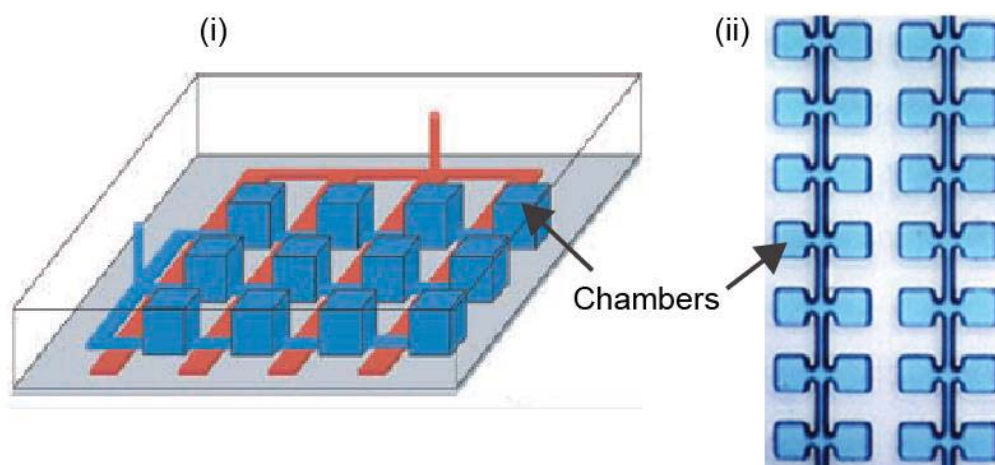


Figure 1.16. Schematic illustrating two different ways to create multiple chambers for PCR.^{128,131} (i) Multiple PCR chambers (in blue) are connected by channels to a single inlet. The PCR mixture is allowed to flow through the single inlet and fill up all the chambers. Upon filling, hydraulic pressure is applied to the control channel network (in red) to deflect a membrane between the red and blue channels. A deflectable membrane acts as a valve and traps the PCR mixture in the chambers. As a result, many independent reactors are created.¹²⁸ (ii) The chambers along the microchannel are filled via “dead-end” filling, and an oil phase used to seal each chamber.¹³¹

In a manner similar to that reported by Matsubara *et al.*^{126,127}, DNA amplification was achieved by thermally-cycling the whole chip. Digital PCR was achieved by counting the number of chambers that yielded positive fluorescence signals. The system was then used to investigate copy number variations and to carry out multi-gene analysis of individual environmental bacteria. An exceptionally elegant embodiment of the well-based approach is “megapixel digital PCR” (**Figure 1.16(ii)**), which used surface tension-based partitioning to generate 1 million reactors on a single microfluidic device.¹³¹

Other notable examples of such well-based systems are the spinning disk platform¹³² developed by Sundberg *et al.* and the “slip-chip” approach^{133–135} described by Shen and co-workers. In the spinning disk platform¹³², an inexpensive disk was fabricated with spiral channel that had 1000 nanoliter-sized wells lined up along the channel (**Figure 1.17(i)**).

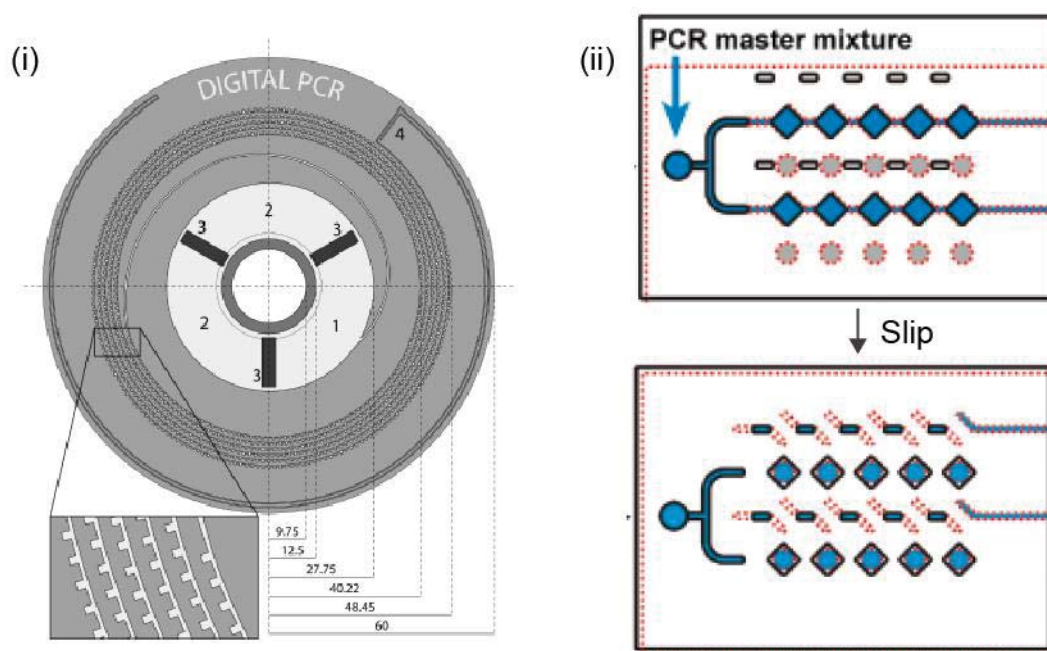


Figure 1.17. (i) Spinning disk PCR consisting of a loading reservoir and a spiral channel with wells facing outwards. Upon centrifugation, the PCR mixture in the loading reservoir fills up the channel and all the wells. Mineral oil is allowed to flow through the channel and trap the PCR mixture in the wells. Each well serves as an independent PCR chamber.¹³² (ii) The “slip-chip” approach. The rectangular and circular wells are fabricated on the top and bottom plate respectively. The circular wells are pre-loaded with primers and the rectangular wells are filled with PCR mixture. The top plate is slipped to align the rectangular and circular wells to mix the primers and the PCR mixture. The whole chip is then cycled over different temperatures.^{133–135}

By spinning the disk at high speed, PCR mixture was split into many small aliquots which were trapped in multiple wells. The whole disk was cycled over various temperatures for DNA amplification and each well was probed for positive PCR. In the “slip-chip” approach^{133–135}, 384 rectangular wells were fabricated on the top plate, while another 384 circular wells were fabricated on the bottom plate. The wells were pre-loaded with primers (**Figure 1.17(ii)**). Upon

filling up the rectangular wells with PCR mixture, the top plate was slipped downwards to align both top and bottom wells to mix PCR mixture with the pre-loaded primers. The whole chip was then cycled over different temperatures and wells assayed for amplification. It is interesting to note that the spinning and slip-chip approaches use fewer chambers than other well-based approaches (due to experimental limitations), but incorporate novel ways of handling small volumes of fluids.

As an alternative to the previous examples that used physical chambers on chip to handle the PCR mixture, emulsions (water-in-oil droplets) can be used as stationary reaction vessels or chambers for PCR.^{84,136-138} Beer *et al.* reported the use of water-in-oil droplets as independent chambers for PCR (**Figure 1.18(i)**).^{136,139} After formation of droplets on a chip-based device, the droplets were held stationary by a valve system^{140,141} and the whole chip thermally cycled. After PCR, the droplets were flowed downstream for optical interrogation. This approach is in essence a well-based approach as droplets act as stationary chambers, and the whole device is heated up and cooled down. Using such a system, the authors demonstrated digital PCR by amplifying the single templates in individual droplets. This system was also used for single-copy reverse-transcription PCR. In a similar manner, Hatch *et al.* generated 1-million droplets as PCR reaction vessels in an array¹⁴² on a PCR chip and conducted PCR by thermal-cycling the whole chip.¹⁴³ A wide-field fluorescence imaging system was used to survey the array for emitting and non-emitting droplets.

Instead of conducting PCR on-chip (as in the examples above), many researchers have generated droplets on-chip and collected these droplets for off-chip PCR.^{137,144-146} Commercial systems by Bio-Rad (California, USA)^{72,84,137,147,148} and other groups^{84,130,149} use such an approach. In the example by Bio-Rad (**Figure 1.18(ii)**)¹³⁷, a droplet generator cartridge is used to generate droplets and encapsulate PCR reagents. The generated droplets are then transferred to a 96-well PCR plate for thermal-cycling on a bench-top thermal cycler. Thereafter, droplets are introduced into another cartridge for fluorescence detection. A similar example was also reported by Kumaresan *et al.* (**Figure 1.18(iii)**).¹⁵⁰ The use of bench-top PCR cyclers to perform droplet-based PCR will inevitably face the issue of having large thermal masses, as discussed in **Section 1.1.7**.

It is evident that well-based PCR devices have several features that are ideal for performing high-efficiency reactions. The down-sizing of reaction volumes reduces thermal mass and shortens reaction time-scales. The use of multiple chambers increases throughput and allows PCR to be conducted in parallel. However, well-based formats are still inherently batch processes and this creates difficulties for integration which ultimately limits throughput. Space constraints also limit the maximum number of the chambers that can be fabricated onto a device, with any further

increase in size leading to an increase in thermal mass. Moreover, as surface-area-to-volume ratio increase, the increased surface-molecule interactions (between the wells and the components in PCR) becomes a major problem.^{78,79} These interactions normally lead to PCR inhibition or failure due to adsorption of polymerase enzymes and DNA to the surfaces of the micro-chambers, and also carry-over.

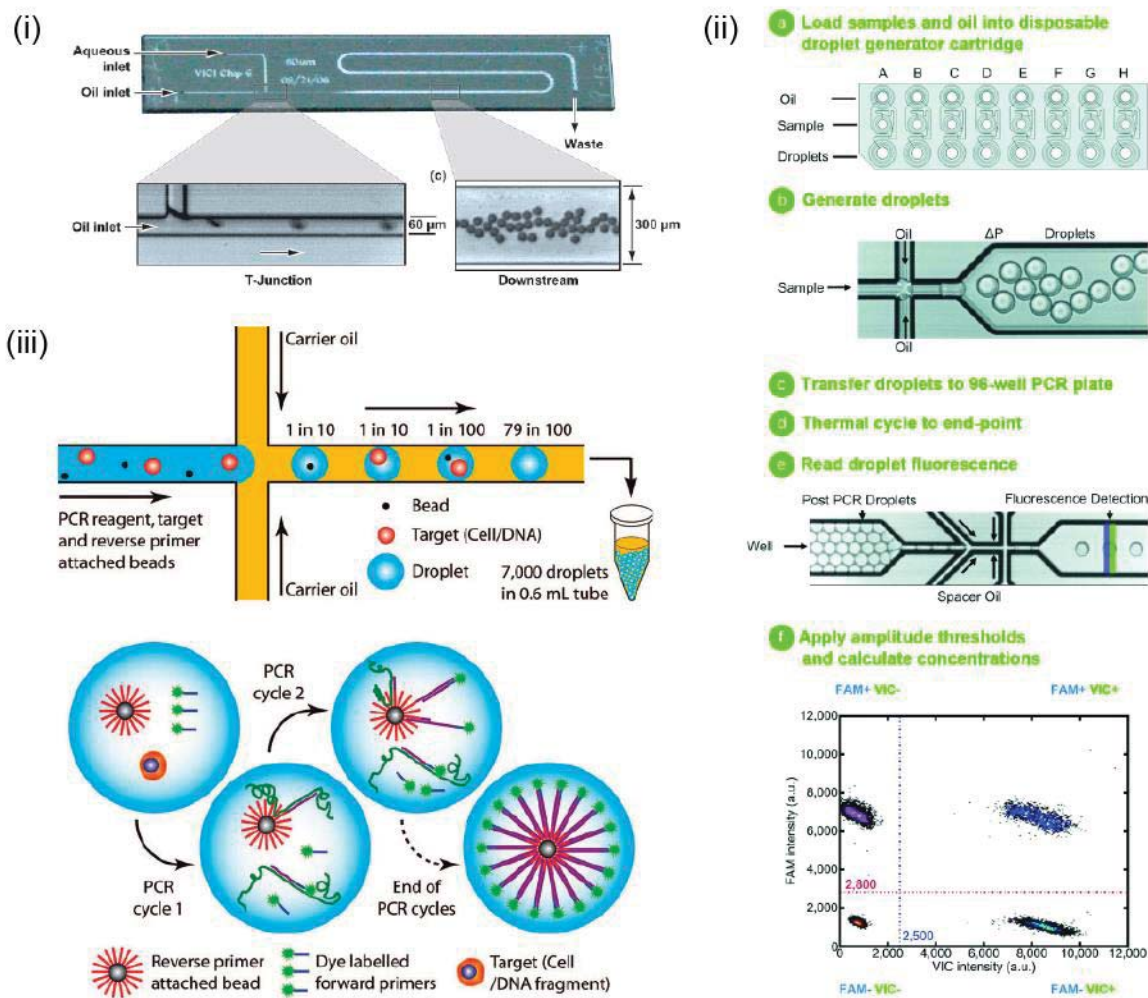


Figure 1.18. Three examples of using droplets as stationary PCR chambers.^{136,137,150} (i) Droplets containing DNA templates are formed using a T-junction at a rate of 1000 droplets per second. The flow of the droplets is stopped downstream, and thermal cycling of the whole chip carried out.¹³⁶ (ii) Flow-chart for conducting digital PCR in stationary droplets in a commercial system. In steps a and b, droplets are generated using a microfluidic cartridge. In steps c and d, the droplets containing the PCR mixture are transferred to a 96-well plate for thermal-cycling on the bench-top thermal cycler. In step e, the droplets are introduced to another microfluidic cartridge for fluorescence detection.¹³⁷ (iii) The droplet generator uses a flow-focusing junction to form monodisperse droplets for the encapsulation of single cells/DNA templates with primer functionalized beads. The droplets are collected for DNA amplification on a bench-top thermal cycler.¹⁵⁰

1.2.2 Continuous-flow PCR

Continuous-flow is an alternative format for conducting PCR on the microscale.^{78,79} Significantly, continuous-flow approaches involve the manipulation of smaller thermal masses because only

the PCR mixture is heated up and cooled down as the sample flows through various temperature zones.^{78,121} As a result, the technique allows for faster thermal-cycling and lower consumption of energy. Continuous-flow formats, unlike well-based approaches, are not batch processes and are consequently more amenable to integration.⁷⁸

The first chip-based continuous-flow PCR device was developed in 1998 by Kopp *et al.* (**Figure 1.19**).¹²¹ In this glass-based device, a 2.2 m microchannel (40.0 μm deep and 90.0 μm wide) was used to pass a flowing sample twenty times through three temperature zones (95.0 $^{\circ}\text{C}$, 60.0 $^{\circ}\text{C}$ and 77.0 $^{\circ}\text{C}$). As the PCR mixture flowed through the microchannel, thermal-cycling of the PCR mixture took place. The continuous-flow PCR device demonstrated a short PCR duration of 18.7 to 1.5 min depending on the flow rate (5.8 to 72.9 nL/s) that was used. Since this work, the approach has undergone further developments and improvements that include the use of integrated heaters and temperature sensors¹⁵¹, and coupling of the microfluidic device with appropriate detection systems¹⁵².

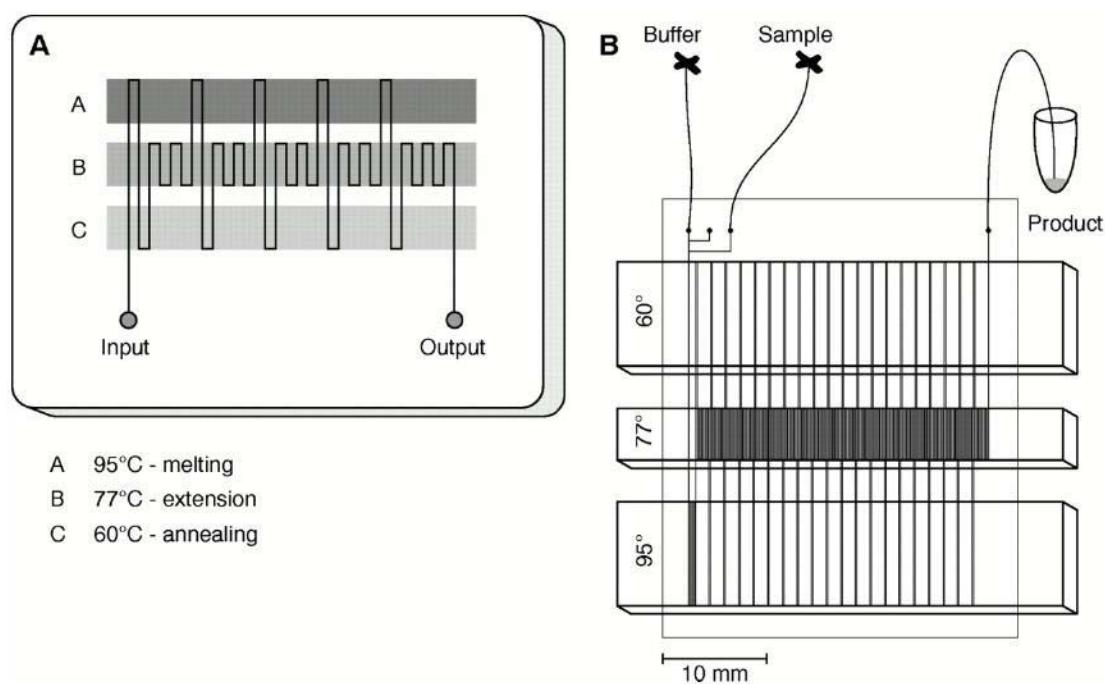


Figure 1.19. The first reported continuous-flow PCR device.¹²¹ The PCR mixture flows through three temperature zones (60, 77 and 96 $^{\circ}\text{C}$) on the chip for annealing, extension and denaturation.

Though the continuous-flow format has been widely investigated^{121,151-159}, it lacks the discrete compartmentalisation feature found in the well-based approach. As such, the continuous-flow format is unable to handle large numbers of samples. Running several continuous-flow devices in parallel may help to increase throughput, but such a setup, which requires multiple pumps and tubes, would be unacceptably complex. Moreover, the continuous-flow format has the same issue

of surface-molecule interactions found in well-based approaches.^{78,79} Continuous-flow formats also are hampered to some extent by the issue of velocity dispersion (due to parabolic flow profiles) of the fluid when the PCR mixture is pumped through the microchannel^{78,79}; the PCR mixture flowing near the surface drags against the wall and moves more slowly than reagent in the middle of the microchannel. As a result, the PCR mixture spends varying durations (or residence times) at different temperatures. This has a negative effect on both the efficiency and yield of PCR.

1.2.3 Continuous-flow Droplet-based PCR

To overcome the above issues with continuous-flow microfluidics PCR, the droplet-flow PCR has been developed.^{78,160-166} In the droplet-flow approach, two immiscible phases (specifically an aqueous PCR mixture and an oil phase) are pumped into the microchannel to form water-in-oil droplets (**Figure 1.20**).⁹²⁻⁹⁵ The reagents are then moved as aqueous droplets by the oil carrier fluid through the microchannel where PCR takes place. As such, the droplet-flow approach is also referred to as the segmented-phase flow method, while the continuous-flow approach is commonly known as a single-phase flow method.

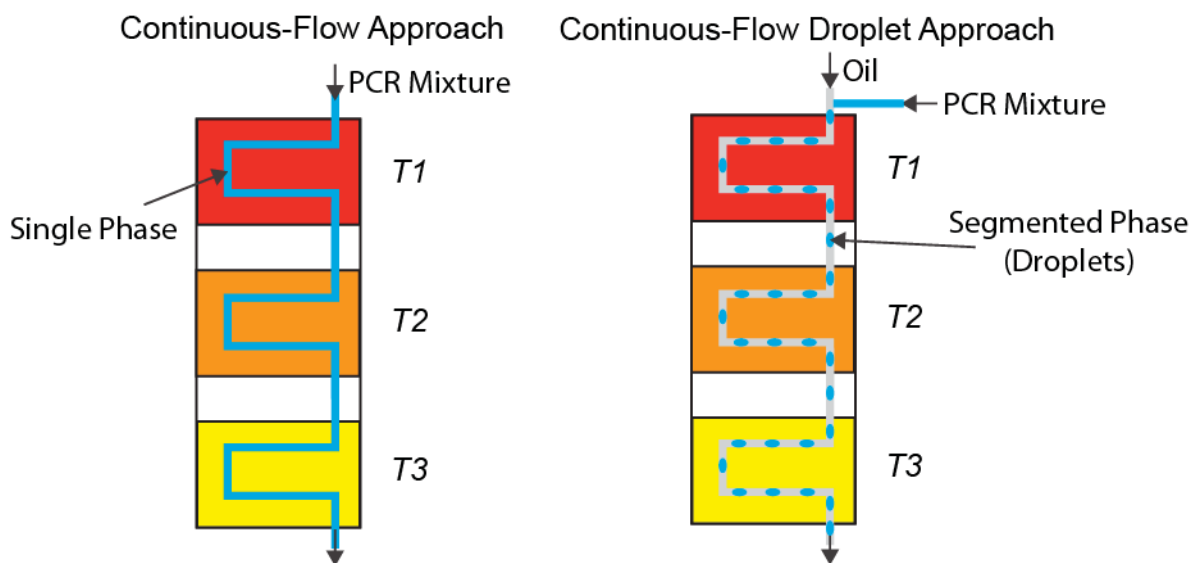


Figure 1.20. A schematic highlighting the differences between segmented-flow and continuous-flow PCR. The droplet-based approach is carried out by pumping two immiscible phases into the microchannel to form water-in-oil droplets

Droplet-based approaches allow compartmentalisation of the PCR mixture, with each microdroplets acting as independent reaction vessel.^{162-164,167} As microdroplets are formed and flowed through the microfluidic chip continuously, this approach can handle a large number of reaction vessels in high throughput.^{81,161,163,168}

Interactions between channel surfaces and PCR reagents are largely eliminated when using segmented flows. As the PCR mixture is encapsulated within droplets, it does not contact microchannel surfaces that are wetted by the oil phase, preventing PCR inhibition.⁷⁸ In addition, the parabolic flow profiles (characteristic of continuous-flows) are also eliminated when using flowing droplets and thus residence time distributions are removed.⁷⁸ It is further noted that many tools^{165,169,170} are available for droplet manipulations such as droplet mixing¹⁷¹, dilution¹⁷², merging¹⁷³⁻¹⁷⁷, splitting^{176,178-180}, sorting^{176,181}, and probing¹⁴⁶.

In contrast to Beer's method¹³⁶ (in which droplets were used for compartmentalisation but cycled in a stationary format), the examples below process droplets in a continuous fashion. Mohr *et al.* reported the use of a polycarbonate-based device (**Figure 1.21(i)**), in which large droplets (100 to 155 μm in diameter, ~ 5.0 nL) could be flowed through a microfluidic channel (500 μm wide and 400 μm deep) transiting temperature zones created by external heaters.¹⁶² A total of 32 cycles were performed with real-time fluorescence measurements being performed after each cycle. The droplet-based device was successful in amplifying a 60 bp DNA fragment.

Kiss *et al.* also reported a highly efficient and elegant strategy for droplet-based PCR (**Figure 1.21(ii)**).¹⁶³ 65 pL droplets were formed using a flow-focusing junction, and then shuttled between two temperature zones for denaturation and annealing. Fluorescent probes were included in the PCR mixture to enable the monitoring of the amplification process at different locations on the chip. The group demonstrated digital PCR by amplifying and detecting a 245 bp adenovirus at starting concentrations as low as 1 template molecule per 167 droplets. The number of droplets containing positive PCR reactions was found to agree closely with the Poisson statistics, confirming the device's suitability for digital PCR applications.

At the same time, Schaerli *et al.* also designed a continuous-flow polymer-based device for single-copy DNA PCR in microdroplets (**Figure 1.21 (iii)**).¹⁶⁴ In this work, monodisperse droplets containing PCR reagents were formed using a T-junction. They were then carried by an oil phase through a radial temperature gradient. The device was successful in completing 34 cycles within 17 minutes, demonstrating amplification of an 85 bp DNA template at four different starting concentrations.

In a simple sense, droplet-based PCR combines the best features of well-based and continuous-flow approaches. It utilises droplets for compartmentalisation much like the physical chambers in the well-based approach to permit the handling of many small volumes of PCR samples; yet unlike the well-based approach, droplet-based PCR is not limited by batch process and large

thermal masses. Throughput is also not limited by the size of the chip, and it is only dependent on the rate of droplet generation. Finally, whilst taking advantage of continuous-flow, droplet-based PCR is not plagued by issues such as surface-molecule interaction and dispersion.

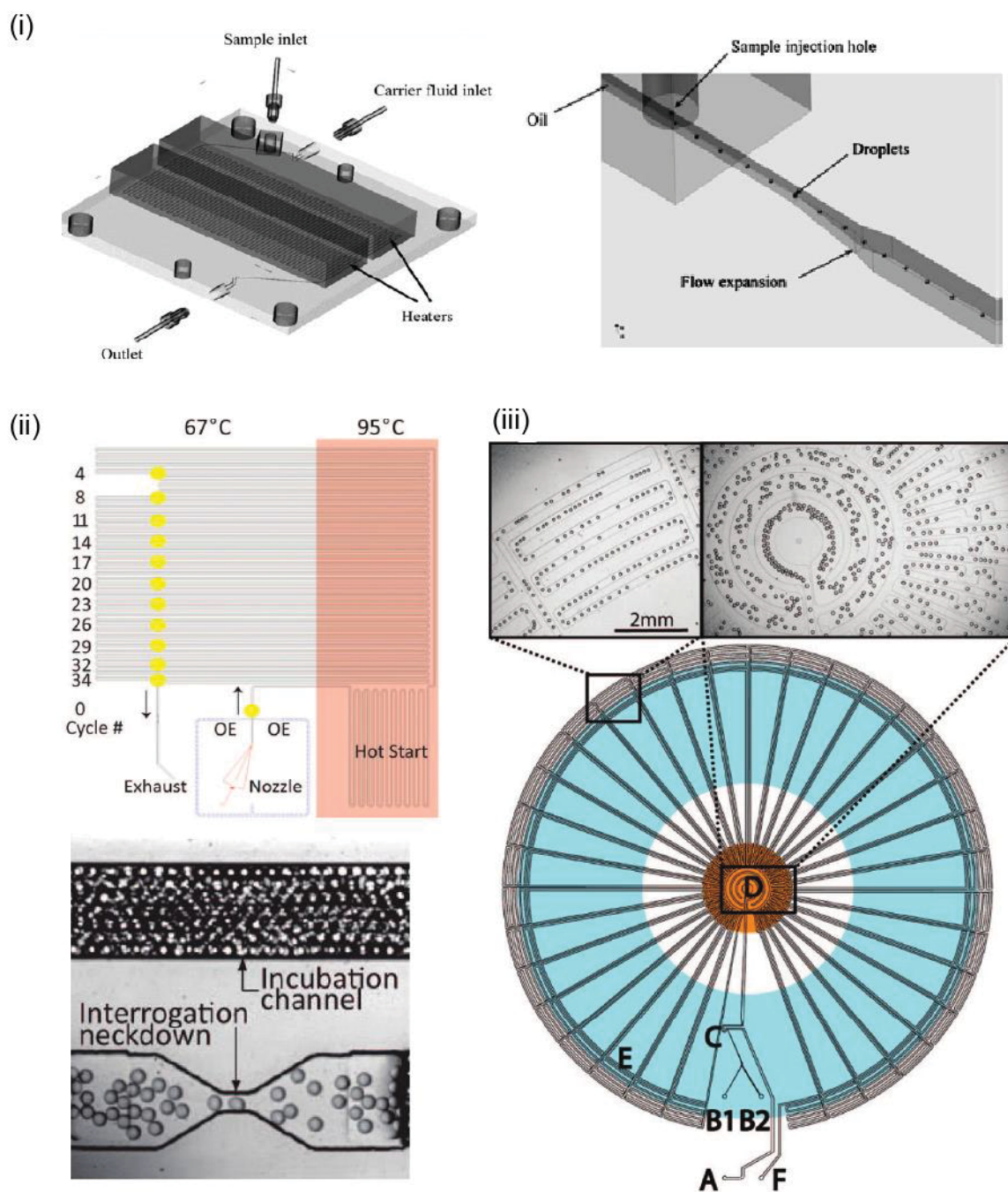


Figure 1.21. Three examples of segmented-flow PCR.¹⁶²⁻¹⁶⁴ (i) The polycarbonate-based device is used to generate the droplets for PCR.¹⁶² (ii) As the droplets containing the PCR mixture are formed, they flow into the hot start zone for activation of the polymerase. The droplets then alternate between two temperature zones (67.0 °C and 95.0 °C) for annealing and DNA denaturation respectively. The yellow dots define interrogation neckdowns (constrictions in the microchannel that allow only one droplet at a time through) where fluorescence detection is conducted.¹⁶³ (iii) Inlet A is used to inject the oil phase while inlets B1 and B2 are used to inject the aqueous phase (PCR mixture). Droplets are formed using a T-junction. After 34 cycles of PCR, the droplets flow out through F. A radial temperature gradient is used for PCR. The centre of the chip (D) is the hot zone for the DNA denaturation while the cooler periphery (E) is used for annealing and extension.¹⁶⁴

1.2.4 Summary

PCR remains one of the most important tools in molecular biology, and is primarily conducted using conventional bench-top thermal cyclers. As discussed, bench-top thermal cyclers have several limitations based around their large thermal masses and high consumption of reagent. More importantly, they are incapable of handling large number of small-volume samples (as required for digital PCR). Microfluidic technologies (both well-based and continuous-flow microfluidics) offer a far better platform for PCR by reducing thermal masses and reagent consumption. Moreover, the droplet-flow approach combines the best features of well-based and continuous-flow approaches. The droplet-flow approach uses droplets for compartmentalisation and is able to handle multiple, isolated small volumes without the limitations of large thermal masses, surface interactions and flow dispersion.

1.3 THESIS OBJECTIVES

In this thesis, the continuous-flow droplet-based approach is investigated and developed as a method for conducting PCR within a microfluidic environment. The primary objective is to develop an integrated silicon-based device for conducting PCR, with the potential to handle segmented flows. This work seeks to improve on the previously reported system described by Schaerli *et al.*¹⁶⁴, which used a radial temperature gradient to perform droplet-based PCR. The primary aim was to reduce the footprint of the original design through the use of integrated heaters, temperatures sensors and air-gaps (for passive cooling) to create temperature gradients for PCR.

A new silicon-based PCR device was designed and analysed using thermal simulation to determine the feasibility of creating a temperature gradient using integrated components. The optimum physical dimensions of the device were also determined using thermal simulation (**Chapter 2**). With the determined dimensions, the PCR device was fabricated with integrated heaters, temperature sensors and air-gaps (**Chapter 3**). Thermal and fluidic characterisations of the PCR device were conducted to validate the presence of a temperature gradient and establish its suitability for PCR, and to confirm the ability of the device to generate water-in-oil droplets (**Chapter 4**). Thereafter, a PCR application was selected and optimised for chip-based PCR (**Chapter 5**). Finally, continuous-flow droplet-based PCR was conducted on the fabricated PCR device (**Chapter 6**), and a fluorescence detection system was coupled with the device for real-time PCR (**Chapter 7**).

2 DESIGN AND THERMAL SIMULATION OF A MICROFLUIDIC CHIP WITH INTEGRATED HEATING AND COOLING ELEMENTS

Chapter 2

The first part of this chapter introduces the concept of using a temperature gradient on a chip to conduct continuous-flow PCR and describes a previously-reported polymer-based chip¹ that used a radial temperature gradient generated by external heaters. The previous design was modified here to allow for the inclusion of integrated heaters, temperature sensors, and air gaps so that the radial temperature gradient could be generated without the use of any external components. These modifications improved on the original design by allowing the use of highly thermally conductive silicon and glass as substrates in a smaller footprint format. Thermal simulation studies of the new design are presented in the last part of the chapter.

2.1 INTRODUCTION

The polymerase chain reaction (PCR) has become an established method for amplifying double-stranded DNA molecules.²⁻⁴ As described in the previous chapter, although it is usually carried out in conventional bench-top thermal cyclers, miniaturization of the process in continuous flow microfluidic devices makes it possible to reduce the cost and time needed to conduct DNA amplification.⁵⁻⁹

2.1.1 Continuous-flow PCR with Isothermal Temperature Zones

The first continuous-flow PCR device was first demonstrated by Kopp *et al.* in 1998.¹⁰ In their approach, the PCR mixture was flowed along a microchannel and passed repeatedly between three fixed temperature zones to achieve the required temperature cycling (**Figure 2.1**). Instead of heating and cooling the entire chip (as occurs in conventional thermal cycling), only the PCR mixture flowing along the microchannel was cycled between the various PCR temperatures. Since the thermal mass of materials for thermal-cycling was greatly reduced, a much faster thermal response could be achieved than with a conventional PCR cycler.

In order to achieve different temperature zones in continuous-flow PCR, thermally isolated areas with separate heaters were deployed on the micro-fabricated chips.¹⁰⁻¹³ Thermal isolation was achieved by using insulating features such as gaps and trenches. As sizeable air gaps and distances were needed to maintain these multiple isothermal areas, the footprints of such devices were typically relatively large.¹⁴

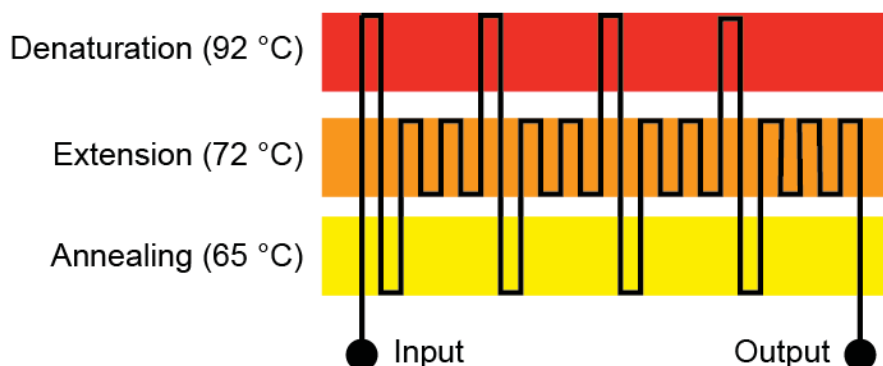


Figure 2.1. Schematic of the continuous-flow PCR format.¹⁰ The PCR mixture is pumped into the input and passes along the microchannel which alternates between three isothermal temperature zones for denaturation, extension and annealing. After alternating between these temperature zones the required number of times, PCR is completed and the mixture exits via the output.

2.1.2 Continuous-flow PCR with Temperature Gradient

To simplify the process of generating the required temperature zones, micro-fabricated PCR devices using a steady-state temperature gradient have been developed.^{1,14,15} With this approach, a continuous distribution of temperatures is maintained over a single zone, and the temperatures for PCR are mapped within this distribution for the PCR mixture to flow through for thermal-cycling. This contrasts with the isothermal temperature zones where multiples isolated zones are required (**Figure 2.2**). The use of a temperature gradient format allows the separate PCR steps to be carried out closer together, reducing the device footprint.¹⁴

A continuous-flow PCR device based on a temperature gradient was reported by Crews *et al.*¹⁴ in 2008. Similar to Kopp's work¹⁰, they used a serpentine channel in a glass device. Instead of three distinct temperature zones, a steady-state continuous temperature gradient was used. The temperature gradient was created using a heater strip at one end and a heat sink at the other. The device was used to carry out rapid continuous-flow thermal cycling and was successfully used to amplify 108 bp and 181 bp DNA targets.

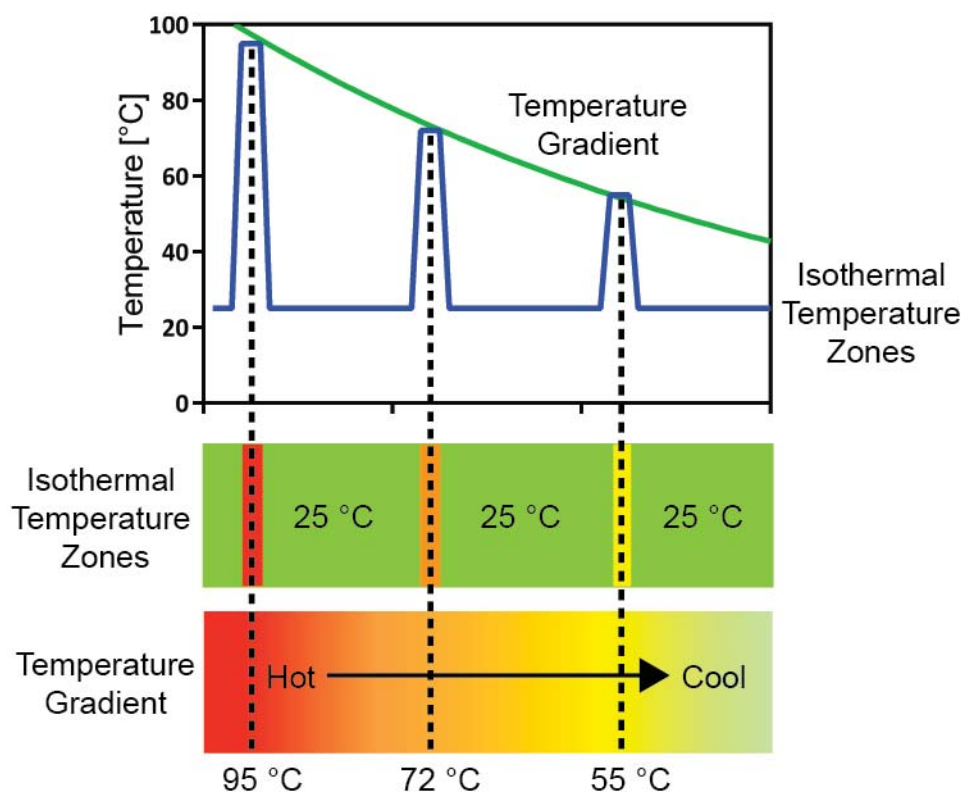


Figure 2.2. Two different approaches for generating the different temperatures needed for PCR in a continuous-flow device. In the first approach, three separate temperature zones are generated by thermally isolating and differentially heating different parts of the chip. In the second approach, the temperature zones are achieved by establishing a temperature gradient from left to right.

Schaerli *et al.* also reported a poly(methylmethacrylate) (PMMA) device which utilized a radial temperature gradient over microchannels arranged in a spoke-like geometry.¹ The centre of the device was heated by a hot metal rod, while the periphery was actively cooled by an annular thermoelectric cooler to generate a temperature gradient along the radius of the device. With this device, continuous-flow PCR of single-copy DNA in water-in-oil microdroplets was demonstrated.

An oscillatory-flow PMMA-based PCR device with a radial temperature gradient was also reported by Cheng *et al.*¹⁵ The PCR mixture was shuttled back and forth along the temperature gradient to achieve rapid temperature cycling. As PMMA has low thermal conductivity, the radial temperature gradient was formed and maintained passively by heating the central area of the device with a resistive heater.

2.1.3 Issues with Temperature Gradient Devices

As described above, temperature gradients have been successfully used by a number of groups^{1,14,15} for continuous-flow PCR. However, two issues should be noted. For systems employing active cooling^{1,14}, an external thermal conduit such as a heatsink or a thermo-electric cooling (TEC) module was needed to remove heat so that an adequate temperature gradient could be achieved. The external modules added considerable bulk to the devices. Furthermore, the use of TEC for active cooling increased power consumption. For systems without active cooling¹⁵, a material of low thermal conductivity such as PMMA was typically needed to achieve a wide enough temperature variation across the length of the device. With highly thermally conductive substrates such as silicon, only a small temperature difference (insufficient for PCR) could be established over the same length. The need to use a low thermal conductivity material for the formation of the temperature gradient restricted the substrate choice to plastics, which do not lend themselves well to high resolution, intricate micromachining or component integration and so limit the range of processes that can be carried out on-chip.^{7,8,16-18} Other substrates such as silicon and glass have desirable properties such as high thermal stability and inert surfaces for chip-based PCR.^{7,8} Moreover, silicon allows standard microfabrication techniques to be used for the integration of heaters and temperature sensors.^{7,16-18} However, glass and silicon have not previously been used for the generation of thermal gradient based PCR devices because of their high thermal conductivity.

With a view to create a much smaller thermal gradient based PCR device with fully integrated heating and temperature sensing, a number of modifications to the original device by Schaerli *et al.*¹ were made. To generate a sizeable radial temperature gradient, air-gaps were integrated into

the silicon-based PCR device. The use of these air gaps would promote passive cooling and avoid the need for external bulky heatsink and TEC assemblies. At the same time, the integration of air gaps could allow high thermal conductivity materials such as silicon and glass to be used as substrates for the fabrication of the PCR device, enabling standard micromachining techniques to be employed.^{7,8,16-18} Thermal simulation studies were conducted based on the new design to determine the optimum geometry and operating conditions to generate a suitable temperature gradient for PCR.

2.2 RADIAL PCR DEVICE

2.2.1 The Original Design

The original device (**Figure 2.3**) reported by Schaerli *et al.*¹ was fabricated by Epigem UK, using SU-8 (negative photoresist) films. Lithography was carried out on the SU-8 substrate to develop and form the channel network. The developed SU-8 substrate was then embedded in a poly(methylmethacrylate) (PMMA) matrix for structural support. The channel network was closed using thermal bonding. The inlets (A, B1, B2) and outlet (F) were interfaced to tubing by ferrule-based clamps. The final SU-8/PMMA PCR device was approximately 7.0 cm x 7.0 cm.

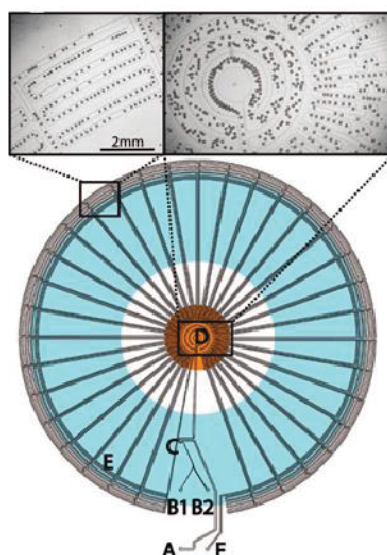


Figure 2.3. Schematic of a radial PCR device reported by Schaerli *et al.*¹ The device was made of SU-8 embedded in PMMA. The orange and blue areas indicate the position of the heated copper rod (diameter: 1.2 cm) and the Peltier module (inner diameter: 2.7 cm, outer diameter: 5.5 cm), respectively. These components created the required radial temperature gradient across the device. An oil inlet (A) joined with two aqueous inlet channels (B1 and B2) to form a T-junction (C) where water-in-oil droplets were formed. The aqueous droplets were carried by the oil carrier fluid through the inner circular channels (500 μm wide and 75 μm deep) in the hot central zone (D) for the initial denaturation of the DNA templates. The droplets were then carried by channels (200 μm wide and 75 μm deep channels) to the cool periphery (E) for primer annealing and template extension. The droplets then flowed back to the hot central zone (D) for denaturation to start a new cycle. In total, the droplets alternated between the hot central zone (D) and the cool periphery (E) for 34 cycles. The droplets were collected at the outlet (F) after passing all the way through the device.

As shown in **Figure 2.3**, their PCR device utilised a heater in the centre (orange area) and an annular Peltier module at the periphery (blue area) to create a radial temperature gradient between the hot central zone (D) and the cool periphery (E). PCR was carried out by passing the PCR mixture up and down the spoke-like microchannels of the chip (i.e. along the radial temperature gradient).

The central heater consisted of a 1.2 cm diameter copper rod with a 100 W cartridge heater that was controlled thermostatically by a thermocouple. The heater was supported on an aluminium heatsink which was in turn cooled by four thermoelectric heat pumps mounted on heat exchangers cooled by high-speed fans. The annular Peltier module (15 W, inner diameter of 2.7 cm and outer diameter of 5.5 cm) removed heat from the periphery of the PCR device. A heat sink was placed on the hot side of the Peltier module and was cooled by a high-speed fan. The heater and the Peltier module created a temperature gradient that could be adjusted by increasing the temperature of the copper rod and by varying the voltage across the Peltier module. The complete assembly comprising the heater, Peltier module and PCR device was approximately 25.0 cm x 25.0 cm x 25.0 cm.

To carry out droplet-based PCR on the device, different solutions were injected into the PCR device via inlets A, B1 and B2 (**Figure 2.3**) using syringe infusions pumps. For inlet A, light mineral oil with 3.0 % ABIL EM90 (cetyl PEG/PPG-10/1 dimethicone) non-ionic water-in-oil emulsifier was used. The inclusion of the surfactant was to promote droplet generation and to prevent coalescence of droplets at high temperatures. Two separate aqueous solutions were used for inlets B1 and B2. The first solution was a mixture of the polymerase enzyme, buffer solution and bovine serum albumin (BSA), and the second was a mixture containing the DNA template, primer pairs, deoxynucleotides (dNTPs), MgCl₂, buffer solution and BSA. These two solutions were combined and mixed after injection into the PCR device. The injection of these three solutions enabled the dynamic formation of monodisperse water-in-oil droplets at the T-junction (C). The typical droplet generation frequency was 15 Hz. The size of the droplets was tuneable from 40 to 150 µm (diameter) and was determined by the ratio of the aqueous to oil flow rate.

After generation, each of the water-in-oil droplets containing the PCR mixture was passed backwards and forwards along the temperature gradient of the PCR device. For the first cycle, the droplets flowed through circular channel (D) in the hot central zone for the initial denaturation of DNA templates (**Figure 2.3**). As the droplets flowed away from the central hot zone, the droplets moved along the radial temperature gradient towards the lower temperature at the periphery for the annealing of primers and the extension by the polymerase. The droplets were

allowed to loop seven times at the periphery (E) to increase the residence time for annealing and extension. After the end of the first cycle, the droplets flowed back into the hot central zone for the start of the second cycle. In total, the droplets were allowed to alternate between the hot central zone and the cool periphery 34 times to emulate a 34-cycle two-temperature PCR protocol. The residence times of the droplets at the hot zone (D) for DNA denaturation and the cool periphery (E) for primer annealing and template extension were determined by the total flow rate of the aqueous and oil fluids. The typical total flow rate used was 160 $\mu\text{L}/\text{h}$, resulting in a time of 29.0 s per cycle.

2.2.2 Integrated Radial Temperature Device

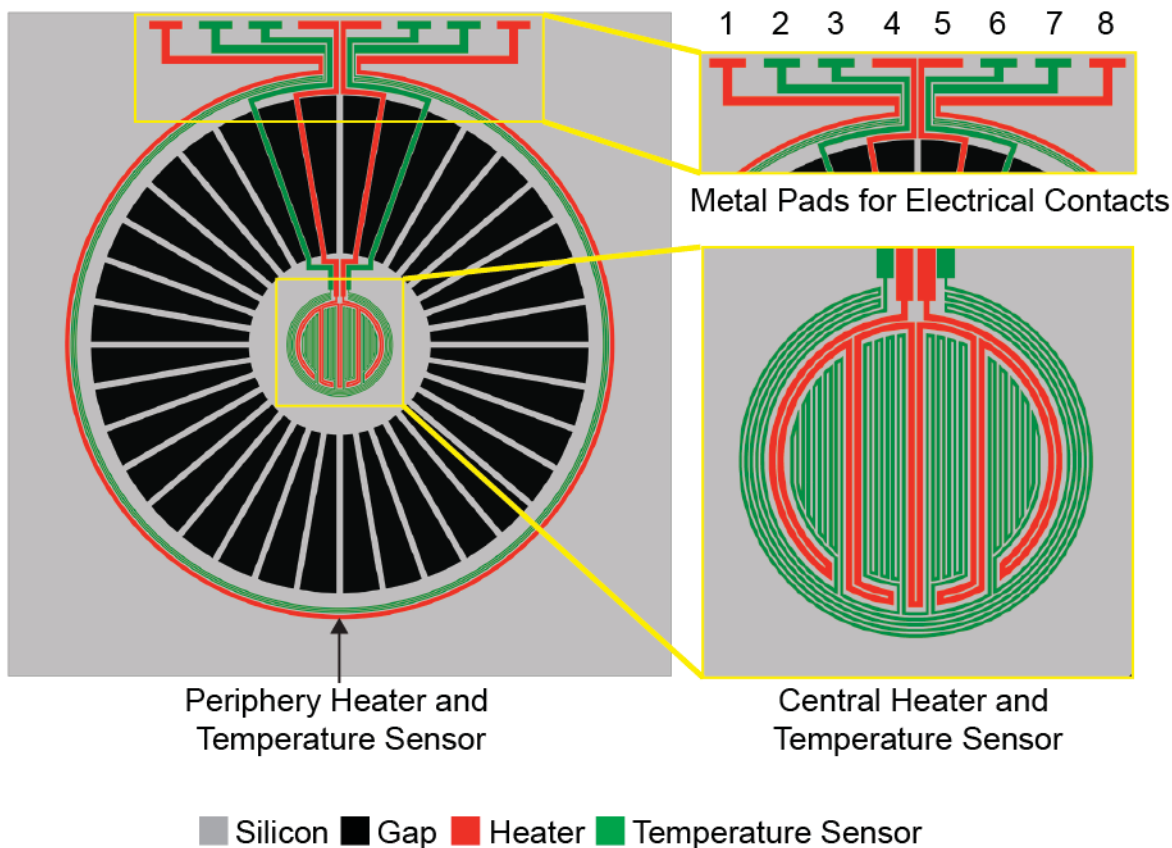
My new design used the same radial temperature gradient that was featured in the above PCR device¹. Although the microfluidic part of that device was relatively small, the overall assembly was large and cumbersome, preventing the setup from being coupled with a microscope and an optical detection system. The complete assembly including the heater and Peltier components was approximately 25.0 cm x 25.0 cm x 25.0 cm. A smaller overall footprint can be achieved by removing or miniaturising the various thermal components.

For the new design, I sought to integrate metal thin-film heaters and temperature sensors into the device (**Figure 2.4**). This modification was intended to save a substantial amount of space by removing the need for an external heater rod, heat sinks and fans. At the same time, the new design incorporated integrated gaps on the device for passive cooling so as to create the required temperature gradient (**Figure 2.4**). The use of passive cooling allowed the Peltier module to be eliminated so that the footprint of the assembly could be further reduced, while at the same time reducing power consumption.

The original PCR device¹ used a polymer-based design that was formed from SU-8 embedded in PMMA. The new design was fabricated from silicon and Pyrex glass. Metal thin-films which functioned as resistive heaters and temperature sensors were patterned on one side of the silicon (**Figure 2.4**), and trenches were created on the other side. Pyrex glass was used to cap the trenches to form the microfluidic channels (**Figure 2.5**). Silicon and glass were chosen for three reasons. The first reason was the ability to use well-established silicon/glass fabrication processes, which allowed for easy integration of metal thin-films under the channels.^{7,8,16-18} The second reason was the well-studied surface chemistries of silicon and glass⁷; both of which can be easily modified to promote water in oil droplet formation. The third reason was the high

thermal conductivity of silicon¹⁹ ($124 \text{ Wm}^{-1}\text{K}^{-1}$) and glass²⁰ ($1.25 \text{ Wm}^{-1}\text{K}^{-1}$), which allowed rapid heat transfer from the chip to the PCR mixture as required for fast PCR.^{7,8}

(i) Top Side (Silicon) of the PCR Device



(ii) The Radial Temperature Gradient

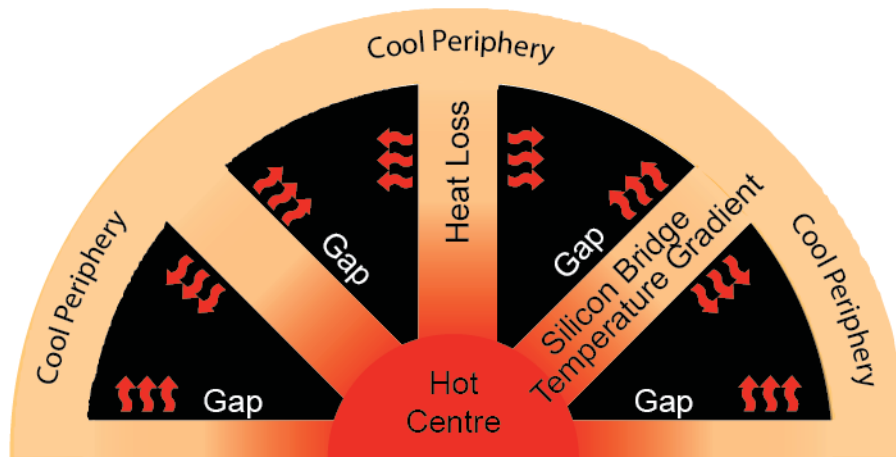


Figure 2.4. Schematic of new temperature gradient-based PCR device, incorporating on-chip heaters and temperature sensors. (i) The top side of the chip consists of metal thin-film resistive heaters (red) and temperature sensors (green). One heater (metal pads 4-5) and temperature sensor (metal pads 3-6) are positioned at the centre, and a second heater (metal pads 1-8) and temperature sensor (metal pads 2-3) are positioned at the periphery. (ii) The central heater is used to establish a high temperature and the periphery heater is used to establish a lower temperature. As a result, a temperature gradient is obtained from the hot central zone to the cool periphery via the silicon bridges. The integrated pie-shaped air gaps (black) are arranged around the device to promote heat loss along the silicon bridges in order to maintain a substantial temperature difference between the centre and periphery.

(i) Bottom Side (Glass) of the PCR Device

(ii) Flow Path of the Droplets

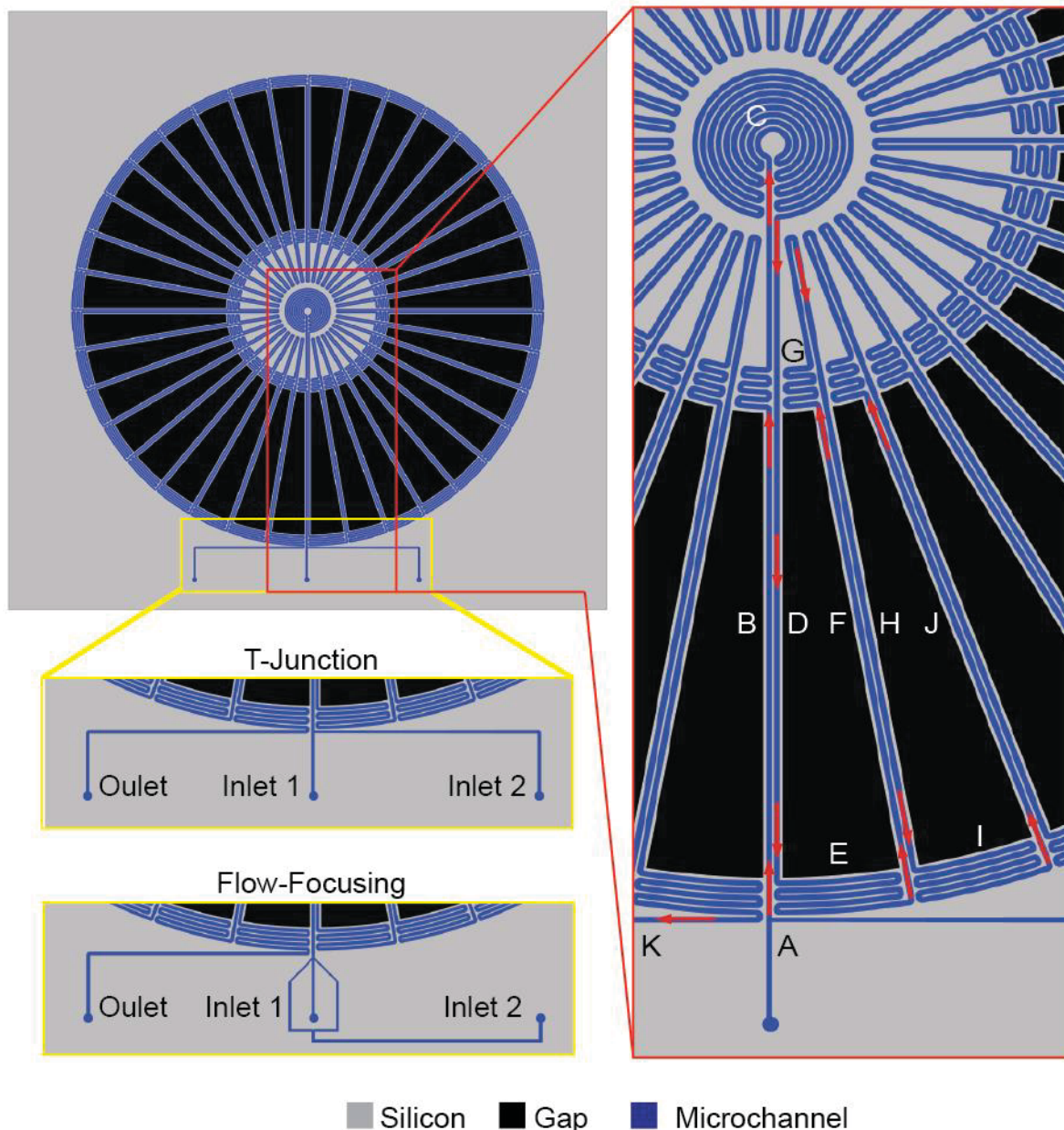


Figure 2.5. Schematic of the microfluidic channel network in the new temperature gradient-based PCR device. (i) The bottom side of the chip consists of a network of microfluidic channels (blue). The PCR mixture and oil carrier fluid are injected into the device via the inlets and are removed from the outlet. Droplets are generated with either a T-junction or a flow-focusing junction design. (ii) After generation (A), the droplets flow along the silicon bridge towards the hot central area (B to C) for the initial denaturation of DNA templates and heat-activation of the polymerase. The droplets then flow back along the bridge (D) to the cool periphery (E) for annealing and extension to complete the first cycle. For the second cycle, the droplets once again flow towards the hot central area (F to G) for denaturation and then back again to the cool periphery (H to I) for annealing and extension. The third cycle starts when the droplets flow along J towards the hot central zone again. The droplets alternate between the hot and cool area 36 times in an anti-clockwise manner, finally exiting at K.

Silicon and glass offer many advantages over plastics but their higher thermal conductivities compared to PMMA²¹ ($0.19 \text{ Wm}^{-1}\text{K}^{-1}$) makes it difficult to establish a sizeable steady-state temperature difference between the centre and periphery. Using a substrate of higher thermal conductivity typically leads to a smaller temperature difference. With the removal of active

cooling (by the Peltier module) in the new design, a conventional silicon/glass device built from a uniform substrate would need to be much larger than the PMMA device in order to achieve a sufficient temperature difference for PCR. This enlargement of the device was incompatible with my aim to reduce the device footprint. Integrated gaps in the silicon device were therefore proposed to promote heat loss on the PCR device and so allow a suitable temperature range to be achieved on a small footprint device.

To conduct PCR using the generated radial temperature gradient, microfluidic channels were fabricated on the bottom side of the silicon wafer (**Figure 2.5**). The channels were created with a width and depth of 100 μm . These small dimensions allowed the flowing PCR mixture in the microchannels to have a small thermal mass so that the mixture would respond rapidly and uniformly to temperature changes as it moved backwards and forwards along the temperature gradient of the device.

The PCR device was designed to provide a total of 36 cycles (**Figure 2.5**). Before the first cycle, the PCR mixture is dispersed in an immiscible oil-based carrier fluid using either a T-junction²² or a flow-focusing junction²³. The resulting water-in-oil droplets then flow into the heated central zone (B to C) to activate the hot-start polymerase and to begin the initial denaturation of the DNA templates. The time spent by the water-in-oil droplet at this hot-start zone is determined by the length of the microchannel and the flow rate. Given a total flow rate of 1.2 $\mu\text{L}/\text{min}$ (**Table 2.1**), the droplets would spend 30.0 s flowing through this hot-start zone (C). After this stage, the PCR mixture flows outwards (D to E) along the narrow silicon bridge and heat is lost to the environment, causing the temperature of the channel (and hence the droplets) to decrease. As the PCR mixture reaches the cool periphery (E) of the device, annealing and extension of the DNA primers takes place. The PCR mixture is allowed to loop four times on the periphery to ensure sufficient time (7.0 s with a total flow rate of 1.2 $\mu\text{L}/\text{min}$) for DNA extension before it flows back (F to G) to the central zone for denaturation (5.0 s) and the start of another PCR cycle. The PCR mixture may be probed with an online detector at each of the 36 cycles or be collected from the device for further analysis. The time spent by the droplet at each part of a cycle may be controlled by changing the flow rate.

Table 2.1. Durations of various PCR steps in a cycle on chip

Cycle	Length (μm)	Volume (μL)	Total Flow Rate ($\mu\text{L}/\text{min}$)	Duration (s)
Initial Denaturation and Hot-start Activation	60000	0.60	1.2	30.0
Denaturation	9930	0.10		5.0
Annealing and Extension	14000	0.14		7.0
Bridge	9500	0.10		5.0

To operate the PCR device, interfaces to the electrical and fluidic components were required (Figure 2.6).

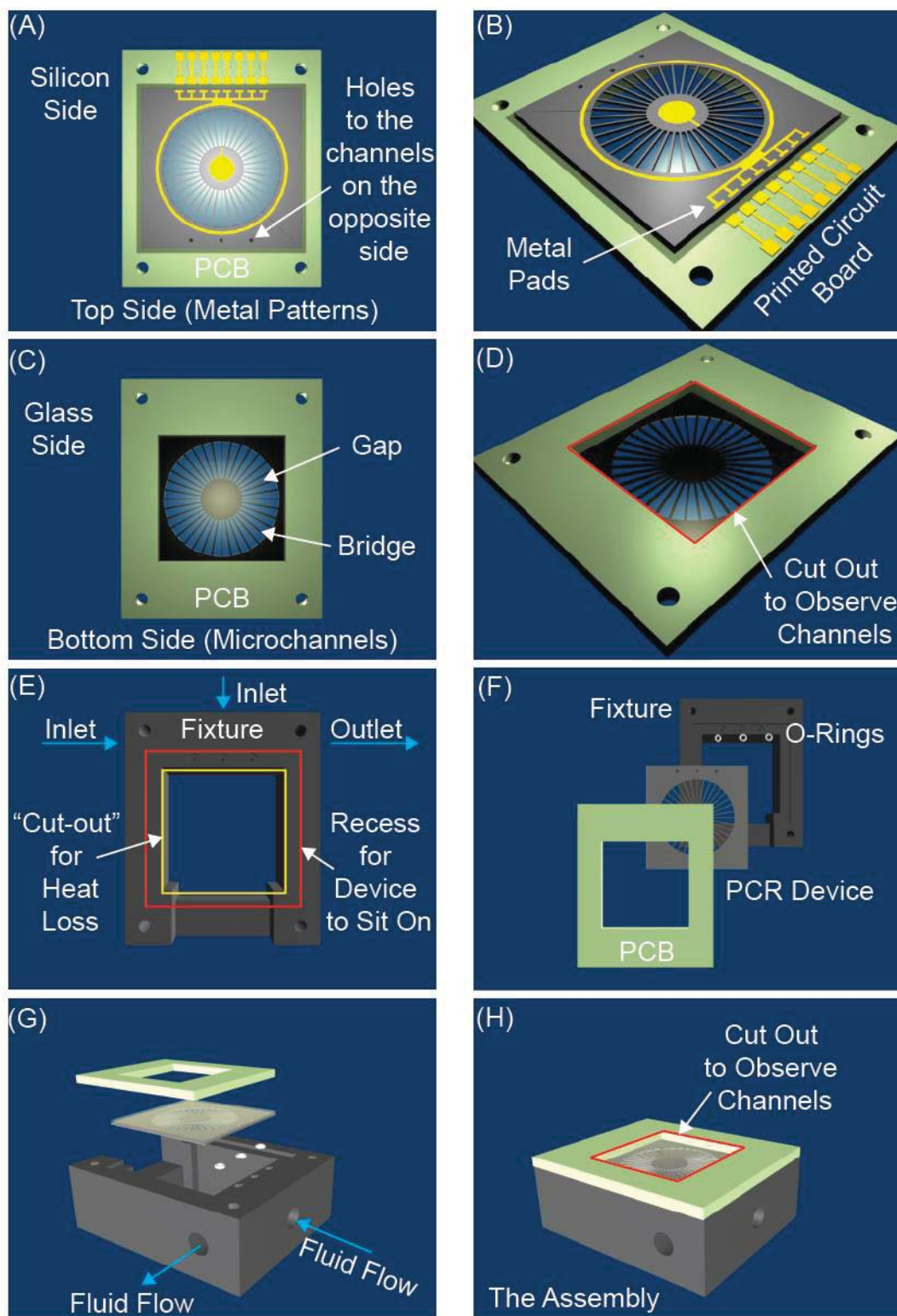


Figure 2.6. Schematics showing the electrical and fluidic interfaces. (A) The PCR device is attached to the PCB, with the metal patterns facing upwards. (B) The exposed metal pads on the device are aligned and connected to simple pass-through circuits on the PCB for electrical connections. (C-D) The glass side of the device is exposed through the cut-out of the PCB. (E) The fixture has a recess in which the device is placed. (F-G) The fluidic holes in the device are aligned with the O-rings and the fluidic holes in the fixture. (H) The complete assembly of the new PCR device.

For the electrical component, a printed circuit board (PCB) was used and attached to the PCR device. The PCB consists of simple pass-through circuits that are aligned to the metal pads on the PCR device (**Figure 2.4**). Electrical connections are made between the exposed metal pads on the device and the circuits on the PCB. The PCB is connected to proportional-integral-derivative (PID) controllers and power supplies, which control the metal thin-film heaters and temperature sensors on the device. The PCB is designed with a cut-out in the centre so that the fluidic channels may be observed visually under the microscope.

For the fluidic component, the PCR device is designed to sit in a polycarbonate fixture which has holes aligned to three holes (two inlets and one outlet) on the PCR device (**Figure 2.6**). O-rings are placed between the bore holes on the fixture and the holes on the PCR device to prevent leakage when fluids are pumped into the inlets and removed from the outlet. The polycarbonate fixture is designed with a cut-out in the centre to provide optical access to the PCR device and to promote heat loss to the surrounding air. These interfacing components are designed with the aim of reducing the footprint of the whole assembly so that the entire structures may be easily mounted on the stage of a microscope for visual observation or optical analysis.

In summary, the new design used silicon and glass as substrates for the PCR device, together with integrated metal thin-film resistive heaters and temperature sensors. Air gaps in the device were included to promote passive cooling and so create the required temperature gradient on the device. These components, together with the PCB and polycarbonate fixture, were designed to create a working PCR device with a much smaller footprint than the original design assembly.

2.3 THERMAL SIMULATION

Due to the use of passive cooling in the new design, the physical dimensions of the various components on the PCR device play a crucial role in generating a sufficient temperature difference for PCR. One way to determine the appropriate physical dimensions is to fabricate a physical PCR device with arbitrary dimensions and to measure its temperature gradient. The dimensions could then have been fine-tuned, iterating until a suitable temperature range for PCR was achieved. However, this approach would have been both costly and time-consuming. To reduce the number of physical iterations, thermal simulation studies were carried out. By using a computer-generated model of the new design, the effects on the temperature gradient of changing the device dimensions could be easily studied. The dimensions of the model which produced the most suitable temperature gradient for PCR could then be used for the physical

fabrication of the PCR device. This approach removed a lot of “guesswork” in determining the starting dimensions for fabricating the PCR device.

2.3.1 Building a Model and Generating a Solution

In order to conduct thermal simulation studies, a computer-generated model which approximated the real-life system was required. A basic starting model was created using the simulation software (ANSYS Icepak 12.1, USA) according to the following specifications (**Figure 2.7**).

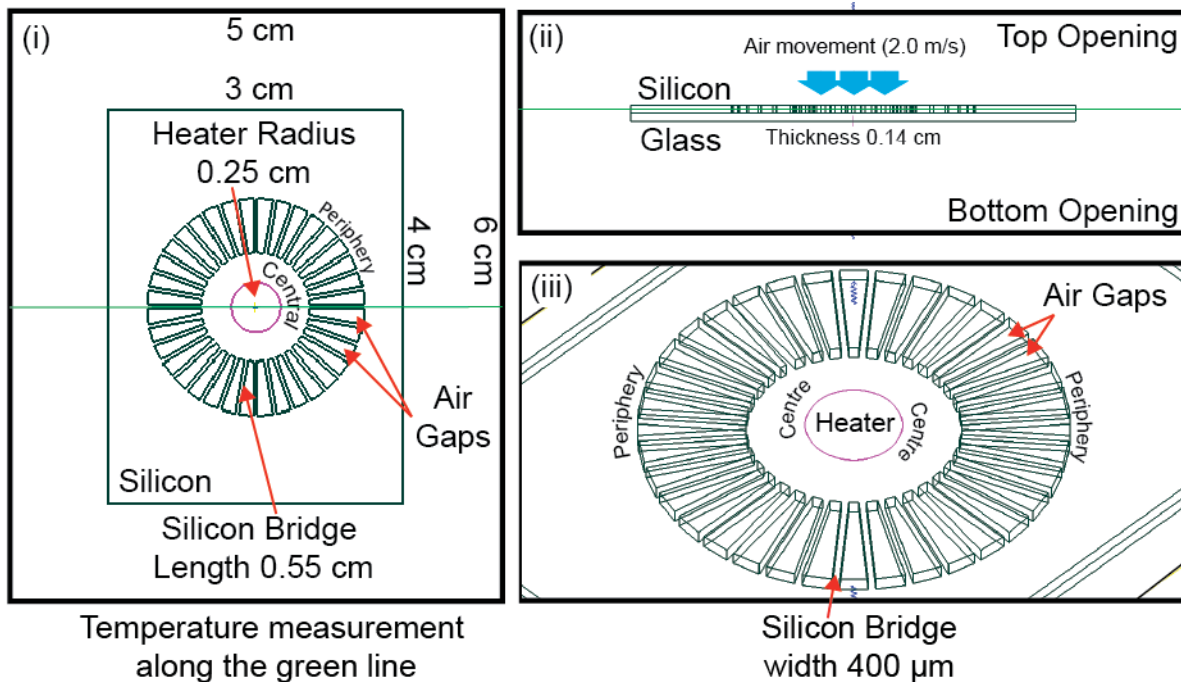


Figure 2.7. The starting model for thermal simulation. (i) Top view of the simulation model. The temperature gradient across the PCR chip was determined along the green line. The four sides were treated as closed boundaries where no heat and mass transfer was allowed. (ii) Side view of the simulation model. The green line indicates the cross-sectional region of the silicon layer (350 μm from the top surface of the silicon layer) where the temperature gradient was determined. The top and bottom of the model were treated as open, and air (at 25.0 °C) was moved from the top to bottom at 2.0 m/s. (iii) Isometric view of the simulation model. The pie-shaped spaces were defined as air spaces which functioned as gaps in the silicon layers. The remaining silicon spaces between the air gaps were the silicon bridges. The disc (radius: 0.25 cm) on the centre of the device was defined as a heat source with a constant temperature of 92.0 °C.

The initial dimensions of the silicon-glass chip were set at 4.0 cm × 3.0 cm × 0.14 cm (length × width × height). The chip was placed in a housing where the top and bottom boundaries were opened for heat and mass transfer, while the four sides were closed. The ambient temperature was maintained at 25.0 °C. Air was continuously moved through the system from the top to the bottom opening at a rate of 2.0 m/s (a typical speed for the air flow induced by a fan). A circular thin-film heater with a radius of 0.25 cm was positioned in the centre and on the silicon (top) side of the chip. The heater was assumed to have a fixed uniform temperature of 92.0 °C. The length of the silicon bridges was 0.55 cm and the width of the silicon bridges was 400 μm. The specific

heat capacities of the glass (pyrex) and silicon layers were fixed at 750 and 702 Jkg⁻¹K⁻¹ respectively^{19,24}, while the thermal conductivities of the glass (pyrex) and silicon layer were fixed at 1.25 and 124 Wm⁻¹K⁻¹, respectively.^{19,20} Heat transfer in the system was limited to conduction and convection, while radiative heat transfer was ignored. For the initial studies, there was no heating at the periphery.

With the created model, a computational mesh consisting of multiple discrete cells was generated (using the default automatic mesh generation tool in the software) and was imposed onto the model. Based specifications as defined in the model, each of the discrete cell had starting values for variables (temperature and velocity) that were used to solve the Navier-Stokes equations for the transport of mass, momentum and energy.²⁵ The simulation software iterated the calculations for each cell sequentially and updated the dependent variables until a steady-state condition was achieved. At the end of the calculations, each of these cells would have a resulting temperature value. By evaluating the temperatures of these cells along the green line (**Figure 2.7**), the temperature gradient across the PCR chip in the simulation studies was determined.

2.3.2 Varying Parameters for Simulation Studies

The dimensions of the following features on the PCR chip were varied and their effects on the temperature gradient was determined: (1) the width of the silicon bridges, (2) the length of the silicon bridges, (3) the radius of the central heater, and (4) the distance between the heater and the air gaps (**Table 2.2**). Based on the specifications of the basic starting model described above, the different features were varied individually, holding other parameters fixed.

Table 2.2. Variations of various parameters for thermal simulation studies

Parameter	Values
Width of silicon bridges	400, 600, 800 μm and no gap
Length of silicon bridges	0.15, 0.35, 0.55, 0.75 cm
Radius of central heater	0.25, 0.20, 0.15, 0.10 cm
Distance between heater and air gaps	0.70, 0.50, 0.30, 0.10 cm

2.4 RESULTS AND DISCUSSION

Starting with the basic model, iterative calculations were carried out by the simulation software until steady-state was reached. The final temperature distribution was plotted as a colour map to provide a visual representation of the temperature gradient on the PCR chip (**Figure 2.8**).

The temperature gradient obtained using the basic design was determined and evaluated for its suitability for PCR. In the proposed design, the hotter central region (92.0 °C) was assigned for

DNA denaturation step in PCR, while the cooler periphery was assigned for annealing of the primers and the extension of the annealed primers. Therefore, the objective of the thermal simulation was to vary the dimensions of various features (**Table 2.2**) of the PCR chip so as to achieve a suitable temperature gradient that had a low enough temperature (≤ 65.0 °C) at the periphery for the annealing and extension step in PCR to take place efficiently.

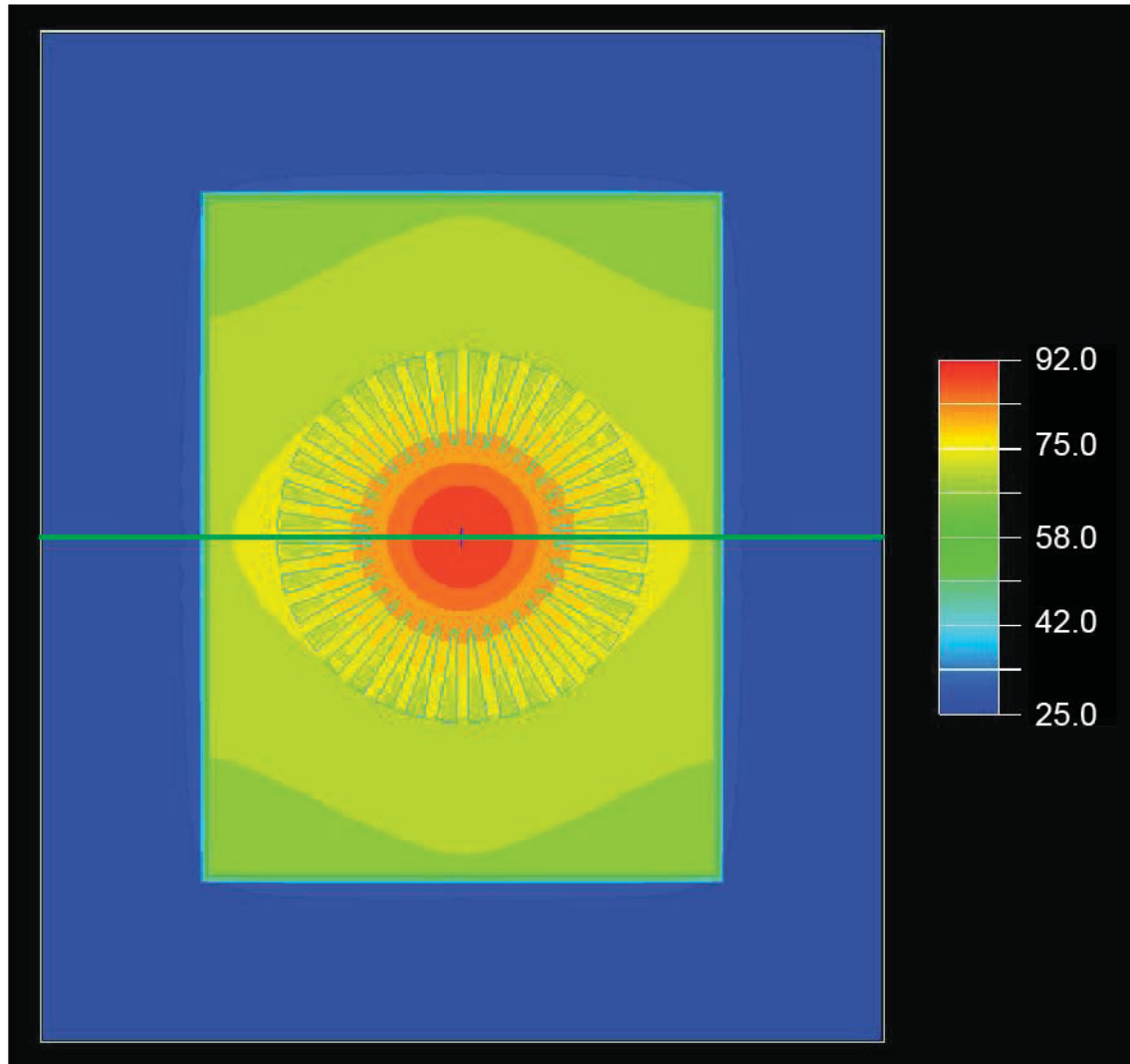


Figure 2.8. Colour map showing temperature distribution obtained using basic model. The green line across the PCR chip ($350.0 \mu\text{m}$ below the surface of the silicon) shows the line over which the temperature gradient was determined. As the heater in the central zone was the only heat source in the model and was defined with a constant temperature of 92.0 °C, the temperature was always highest at the centre, with the temperature reducing monotonically in moving away from the central zone to the periphery as a result of heat loss to the surroundings.

2.4.1 The Width of the Silicon Bridges

Without the presence of air gaps (no silicon bridges), heat from the central heater travelled radially outward and was lost to the environment by conduction and convection. This represented the natural heat loss of the silicon layer to the environment without additional

passive cooling due to air gaps. Under this condition, the temperature at the periphery was found to be 80.3 °C (**Figure 2.9**). When air gaps were introduced to the model, the temperature at the periphery dropped due to increased heat loss to the surroundings. As the width of the bridges increased from 400 μm to 600 μm and to 800 μm, the temperature at the periphery of the chip dropped from 56.6 °C to 59.9 °C and to 74.0 °C, respectively. The increase in temperature was due to the decrease in surface-area-to-volume ratio of the bridges, which allowed less heat loss to the environment as heat travelled from the heated central zone to periphery of the chip.

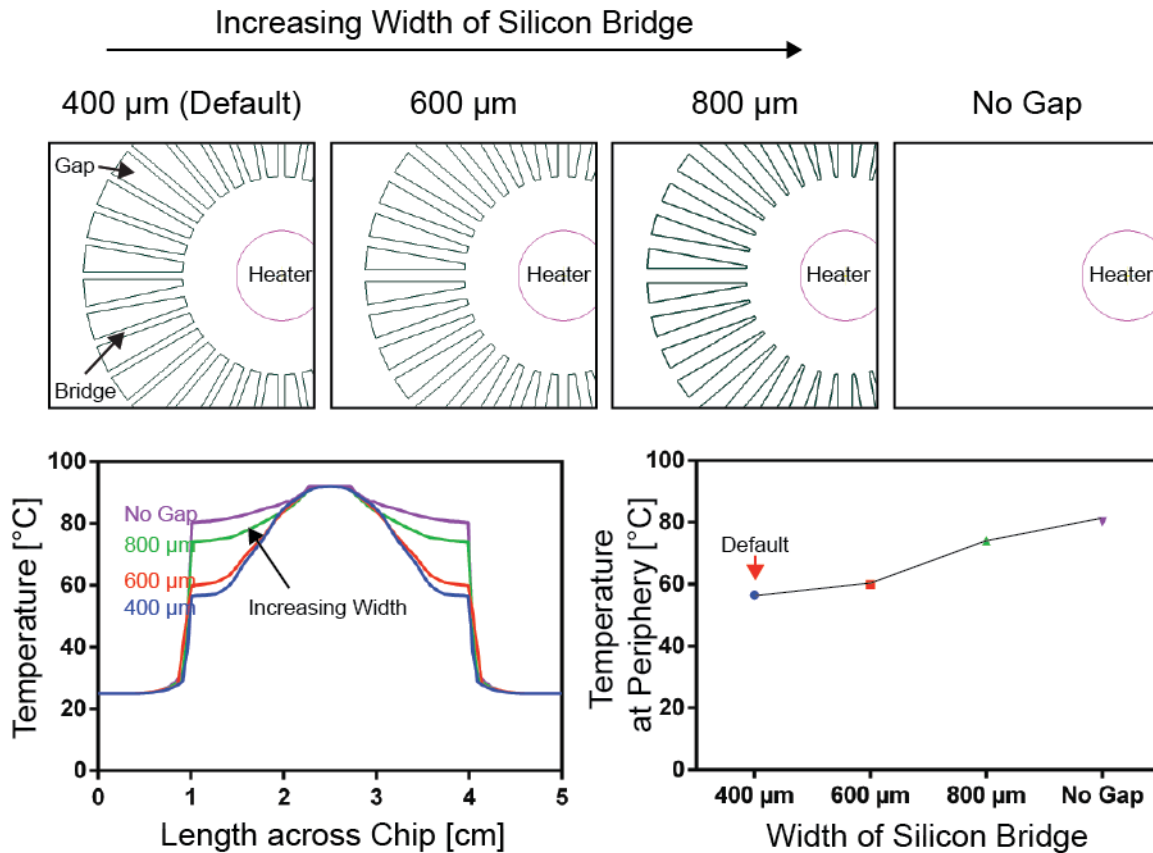


Figure 2.9. Effect of increasing the width of the silicon bridge. The default setup was based on the initial dimensions described in **Section 2.3.1** (i.e. the width of the silicon bridge was 400 μm, the length of the silicon bridge was 0.55 cm, the radius of the heater was 0.25 cm, and the distance between the heater and the gaps was 0.30 cm). Based on these initial dimensions, the width of the silicon bridge was increased from 400 μm to 600 μm and then to 800 μm. A model with no gap was also simulated. The temperature at the periphery increased as the width of the silicon bridge increased.

2.4.2 The Length of the Silicon Bridges

Increasing the length of the silicon bridges caused more heat exchange with the surrounding air (via the longer air gaps), resulting in a lower temperature at the periphery. Hence, as the length of the air gaps was increased from 0.15 cm to 0.35 cm, to 0.55 cm and to 0.75 cm by extending outwards (**Figure 2.10**), the temperature at the edge dropped from 69.8 °C to 67.8 °C, to 56.6 °C and to 51.7 °C, respectively.

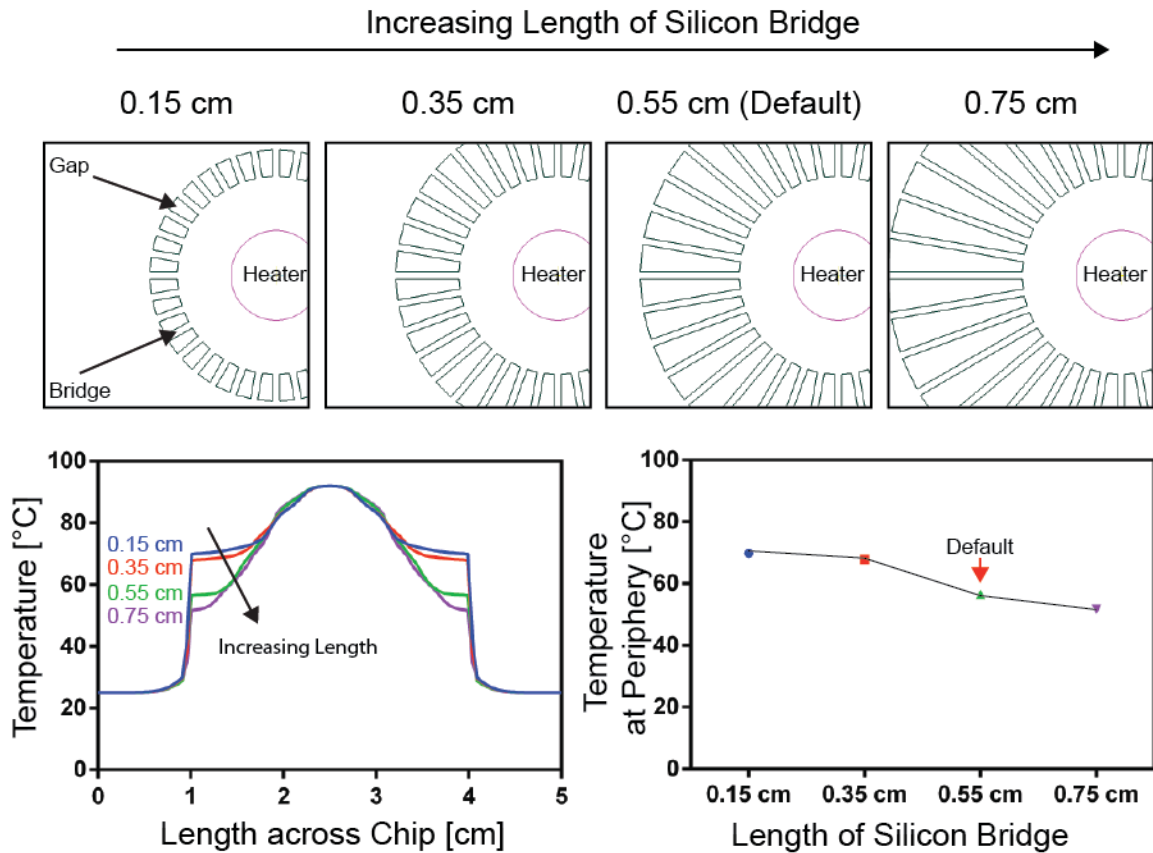


Figure 2.10. Effect of increasing the length of the silicon bridge. The default setup was based on the initial dimensions described in Section 2.3.1 (i.e. the width of the silicon bridge was 400 μm , the length of the silicon bridge was 0.55 cm, the radius of the heater was 0.25 cm, and the distance between the heater and the gaps was 0.30 cm). Based on these initial dimensions, the length of the silicon bridge was increased from 0.15 cm to 0.35 cm, to 0.55 cm, and to 0.75 cm. The temperature at the periphery decreased as the length of the silicon bridge increased.

2.4.3 The Radius of the Central Heater

The decrease in the radius of the heater from 0.25 cm to 0.20 cm, to 0.15 cm, and to 0.10 cm resulted in only a marginal decrease of the temperature (~ 55.0 °C) at the periphery of the chip (Figure 2.11). Changing the heater radius was not therefore found to be an effective way of controlling the temperature gradient.

As the temperature of the heater was fixed at 92.0 °C, a larger heater merely caused the central gap-free area to reach 92.0 °C at a faster rate. Once this constant temperature (steady state) had been reached, the temperature drop away from the gap-free central zone was the same regardless of the size of the heater. As a result, heat loss through the bridges was similar for all cases, leading to similar temperatures at the edge of the chip. As such, the size of the heater had little effect on the temperature at the periphery.

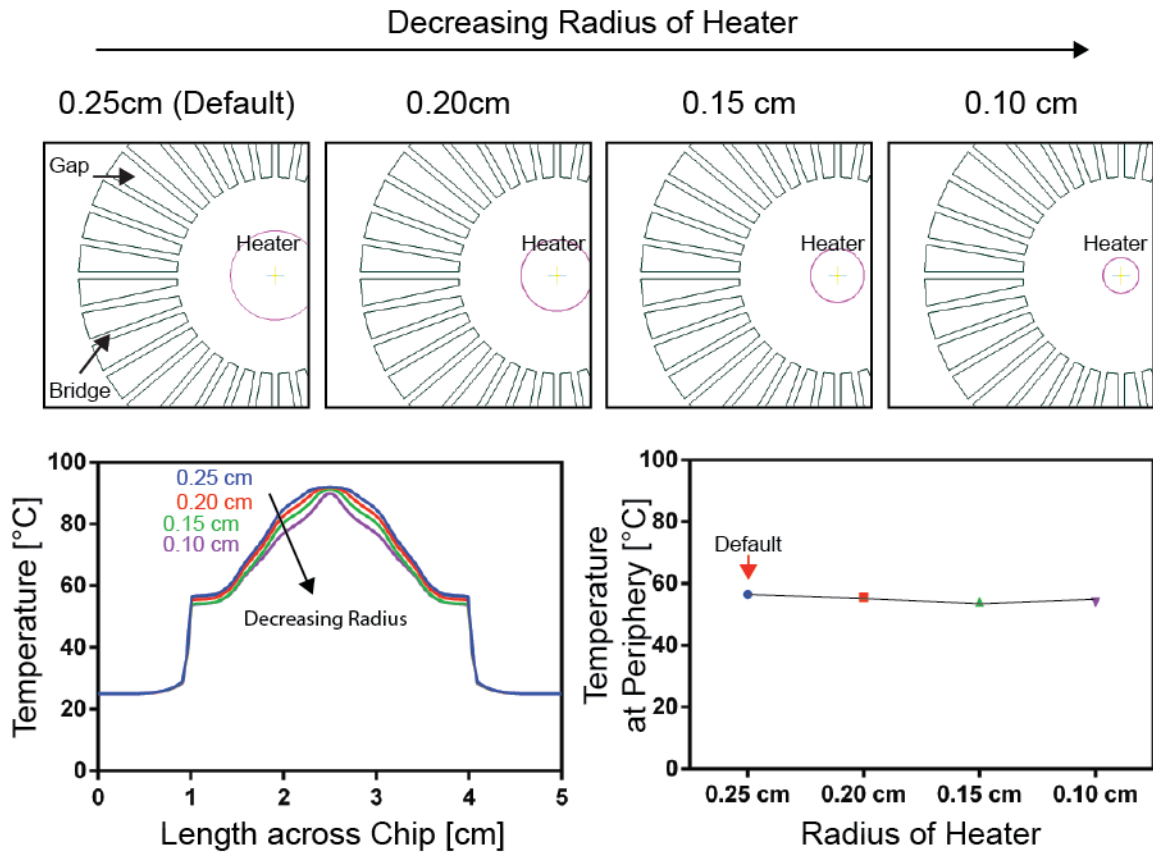


Figure 2.11. Effect of decreasing the radius of the heater. The default setup was based on the initial dimensions described in **Section 2.3.1** (i.e. the width of the silicon bridge was 400 μm , the length of the silicon bridge was 0.55 cm, the radius of the heater was 0.25 cm, and the distance between the heater and the gaps was 0.30 cm). Based on these initial dimensions, the radius of the heater was decreased from 0.25 cm, to 0.20 cm, to 0.15 cm, and to 0.10 cm. The temperature at the periphery was only weakly affected by the radius of the heater.

2.4.4 The Distance between the Heater and the Gaps

As the distance between the air gaps and the heater was increased, the length of the silicon bridges became longer and the area of the central zone became smaller (**Figure 2.12**). As the distance was decreased from 0.70 cm to 0.50 cm, to 0.30 cm, and to 0.10 cm, the effects of two competing phenomena could be observed. When the length of the silicon bridge was longer, more heat was lost to the environment. However, when the central area was smaller, less heat was required to achieve the constant temperature of 92.0 $^{\circ}\text{C}$ and the excess energy had to travel through the bridges to periphery.

When the distance was decreased from 0.70 cm to 0.50 cm and to 0.30 cm, the first effect dominated over the second. More heat loss resulted and therefore a lower temperature at the periphery was observed. When the distance was further reduced to 0.10 cm, the second effect dominated. An increase in the temperature at the periphery resulted. Given this trend, an optimal distance between the heater and the air gap existed (close to 0.3 cm) where the radial temperature gradient was highest.

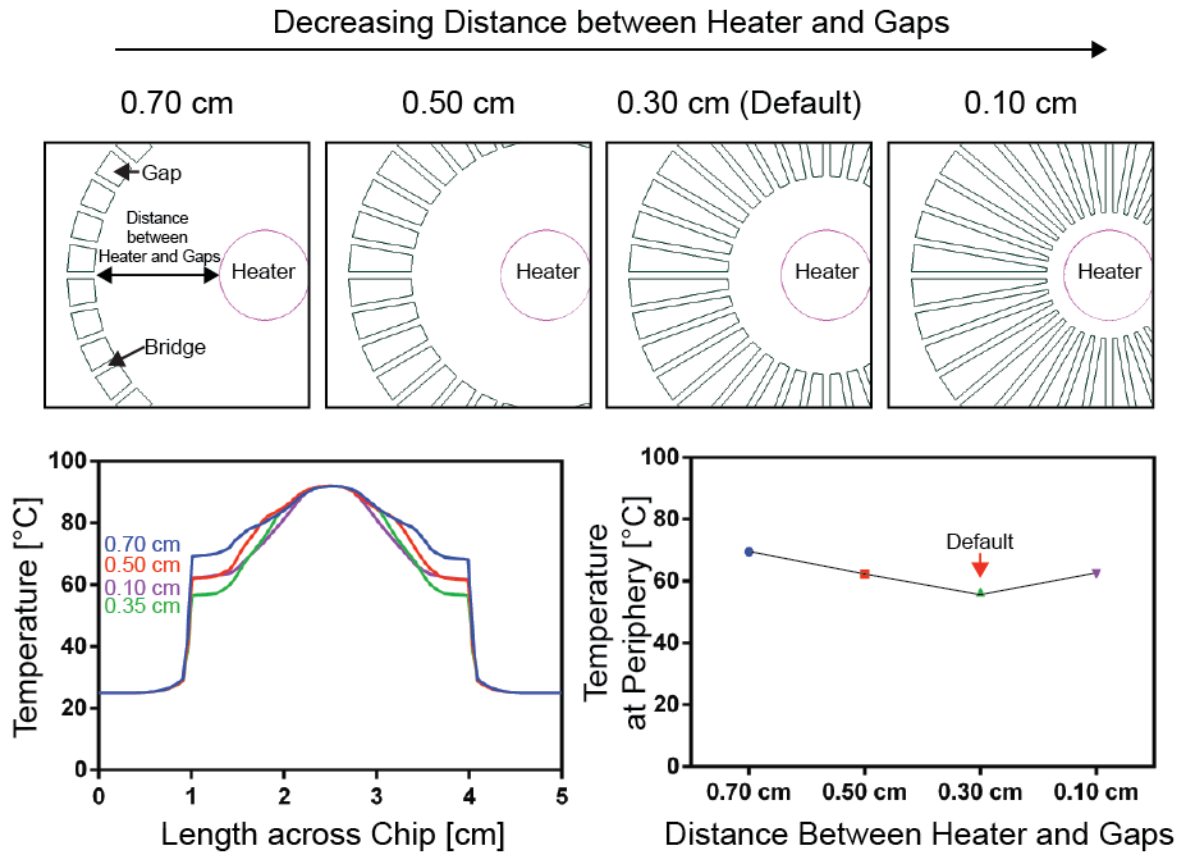


Figure 2.12. Effect of decreasing the distance between the heater and the gaps. The default setup was based on the initial dimensions described in **Section 2.3.1** (i.e. the width of the silicon bridge was 400 μm , the length of the silicon bridge was 0.55 cm, the radius of the heater was 0.25 cm, and the distance between the heater and the gaps was 0.30 cm). Based on these initial dimensions, the distance between the heater and the gaps were decreased from 0.70 cm to 0.50 cm, to 0.30 cm and to 0.10 cm. The temperature at the periphery was found to decrease initially and then subsequently increase below 0.3 cm.

2.4.5 Prototype: Finalised Dimensions

Based on the above results, certain design rules were formulated for achieving the steepest temperature gradient in the radial PCR chip. In summary, the silicon bridges should be long and narrow for the lowest possible temperature at the periphery of the PCR chip. The size of the heater had marginal effect on the temperature gradient, and an optimal distance between the heater and the air gaps existed.

Based on the above rules, the following dimensions for the chip were selected for fabrication: The silicon-glass chip was 4.0 cm \times 4.0 cm \times 0.12 cm. The length of the air gaps was fixed at 0.95 cm and the width of the silicon bridges was set to 400 μm . The radius of the heater was 0.25 cm and the distance between the heater and the air gaps was 0.30 cm. The simulation result using these dimensions revealed that a low temperature of $\sim 39^\circ\text{C}$ (with air cooling) and $\sim 63^\circ\text{C}$ (without air cooling) could be achieved at the periphery (**Figure 2.13**) when the central heater was fixed at 92.0°C . Even the temperature difference without air cooling was wide enough for applications in

PCR experiments, meaning it is possible to omit a fan from the final design and so further miniaturise the device footprint.

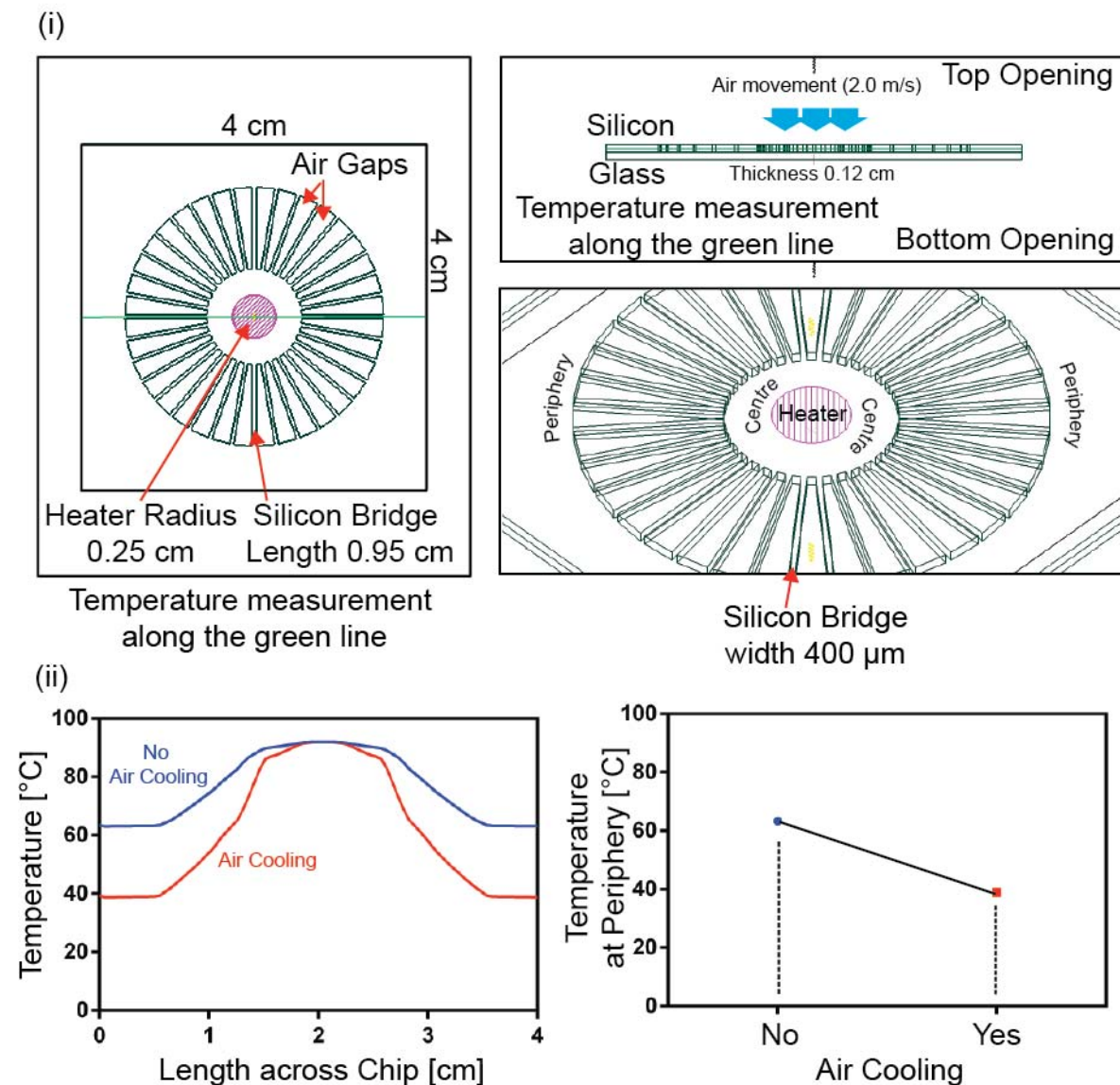


Figure 2.13. (i) Schematic showing the proposed dimensions for the prototype. (ii) Results of thermal simulation studies showing the expected variation in temperature across the width of the chip in the proposed prototype. On the basis of the simulations, it was concluded that temperatures of $\sim 39^\circ\text{C}$ with air cooling and $\sim 63^\circ\text{C}$ without air cooling at the periphery could be achieved.

2.5 CONCLUSIONS

In this chapter, I have proposed a modification of an earlier design for a radial thermal gradient PCR device reported by Schærli *et al.*¹. The new design used integrated heaters and temperature sensors, together with air gaps on the PCR device to generate a radial temperature gradient. The use of the integrated features in the design reduced the footprint of the device. At the same time, the integration of air gaps allowed high thermal conductivity materials such as silicon and glass

to be used as substrates for fabrication. The ability to use silicon is critical for the integration of heaters and temperature sensors, and hence achieve the intended miniaturisation of the design.^{7,8,16-18}

Thermal simulation studies of the new design were carried out to determine the optimum geometry and operating conditions needed to generate a suitable temperature gradient for PCR. On the basis of these studies, it was found that to achieve the steepest temperature gradient in the radial PCR chip, the silicon bridges should be long and narrow for the lowest possible temperature at the periphery of the PCR chip. The size of the heater had little effect on the temperature gradient. An optimal distance between the heater and the air gaps was also found to exist.

The final prototype had the following dimensions: The silicon-glass chip was 4.0 cm × 4.0 cm × 0.12 cm. The length of the air gaps was 0.95 cm, and the width of the silicon bridges was 400 μm. The radius of the heater was 0.25 cm, and the distance between the heater and the air gaps was 0.30 cm. Using these dimensions for thermal simulation studies, low periphery temperatures of 39 °C with air cooling and 63 °C without air cooling could be achieved. Importantly, even the temperature difference obtained without air cooling was sufficient for applications in PCR experiments, thus removing the need for fan cooling.

Chapter 3

This chapter describes the fabrication process for a new silicon-based radial PCR device based on the dimensions as determined by the thermal simulation studies described in the previous chapter.

3.1 INTRODUCTION

A wide variety of fabrication methods are available for PCR microfluidics.¹⁻³ The fabrication methods can be broadly classified into two groups – hard or soft fabrication methods, which are determined by the choice of substrate material.

3.1.1 Hard Fabrication Methods

Hard fabrication methods for microfluidics are rooted in the fields of microelectronics and micro-electro-mechanical systems (MEMS) engineering.^{1,2,4,5} Technologies such as photolithography, chemical and physical vapour deposition, ion and chemical etching, and bonding, which have been developed in the area of MEMS, provide highly-controllable methods for processing silicon substrates into high resolution and mechanically-stable microfluidic devices.^{1,6-9} The direct application of these established technologies to early silicon PCR device fabrication contributed greatly to the early advances in PCR microfluidics. However, silicon is a relatively expensive material to process, especially at the prototyping stage where designs can change frequently and fabrication runs are small.^{6,10,11} Compared to their polymeric counterparts, silicon microfluidic devices are time-consuming and costly to fabricate, making them less suitable for quick exploratory studies and iterative prototyping.^{1,4,12} Furthermore, silicon being opaque to visible and ultraviolet light, cannot be used with conventional optical detection methods.^{4,6,11} Glass overcomes the problem of opacity and is amenable to many of the same MEMS-based processing procedures as silicon, allowing intricate and high resolution microfluidic devices to be fabricated.^{1,6-9} However, it is also relatively expensive to process and does not permit easy integration of electronic components. For these reasons, most research in recent years has focused on polymer microfluidic devices.^{10,12-14}

3.1.2 Soft Fabrication Methods

Soft fabrication methods have been developed to enable inexpensive plastic microfluidic devices to be fabricated with relative ease.^{1,4,12} Many polymer-compatible fabrication methods have been developed, including soft lithography, injection moulding, casting, hot-embossing and laser ablation.^{1,9,13,15} The arrival of polymer-based devices has driven many of the recent advances in PCR microfluidics because it allows exploratory studies of new concepts and components in PCR devices to be carried out rapidly and cheaply. This has been particularly true for microfluidic devices fabricated using poly(dimethylsiloxane) (PDMS) due to their exceptional ease of fabrication and low cost.¹⁴ Besides PDMS, many other polymers have been used for the fabrication

of PCR devices, including polycarbonate (PC)¹⁶, poly(methylmethacrylate) (PMMA)¹⁷, poly(ethylene terephthalate) (PET)¹⁸, polyimide (PI)¹⁹, epoxy²⁰, and SU-8²¹.

3.1.3 Selecting an Appropriate Substrate Material

Even though much of the recent work in PCR microfluidics has involved polymer-based devices, silicon and glass are still of considerable interest because they possess favourable properties such as high thermal, chemical and mechanical stability (and high thermal conductivity in the case of silicon) that could be very useful for PCR devices.¹ Silicon also allows for the ready integration of electronic functionality, allowing for a higher level of integration than other substrate materials.^{1,6-9} Different materials have different advantages and disadvantages when used as substrates for the fabrication of microfluidic PCR devices. The appropriate choice of substrate material for fabrication depends on the fluidic, thermal and electrical requirements of the specific PCR device.

3.1.4 The Original Radial PCR Device: SU-8 and PMMA

The original device (by Schaeferli *et al.*²²) from which I developed my adapted design (**Chapter 2, Section 2.2.1**) was a polymer-based PCR device. SU-8 and PMMA were chosen as substrates for fabrication because replicates of the simple plastic device could be made inexpensively and rapidly. Multiple chip designs with varying radial temperature gradients could then be tested for their feasibility for PCR by making and testing multiple devices of varying architecture. However, although new prototypes could be designed and fabricated quickly, the need for rapid fabrication and testing required a simple design without any integrated features such as heaters and temperature sensors. The use of an external heating rod and an annular Peltier module for the generation of the radial temperature gradient resulted in a large footprint device that could not easily be miniaturised. In addition, the large footprint did not allow the device to be mounted on the microscope stage for visual observation and optical analysis.

3.1.5 The New Radial PCR Device: Silicon and Glass

The new radial PCR device (**Chapter 2, Section 2.2.2**) was designed to reduce the footprint of the original design by introducing integrated features such as heaters and temperature sensors. Silicon and glass were therefore chosen as the substrate materials for fabrication because silicon-based fabrication methods are well-established for such integration (while glass provides the transparency required for optical sensing).¹ As silicon and glass are highly thermally conductive, they allow stable temperature distributions to be established quickly, but cannot easily sustain

wide temperature distributions. To overcome this limitation, pie-shaped air gaps were introduced between the radial channels to promote passive cooling and to avoid the need for external bulky cooling systems as described in the previous chapter (**Chapter 2, Section 2.2.2**). The integration of air gaps is straightforward to realise with silicon-based fabrication methods.¹ Properties of silicon and glass of relevance to PCR device fabrication are considered below:

A. High Thermal and Structural Stability

Silicon and glass have high thermal and structural stability over the range of temperatures needed for PCR (typically between 55 to 100 °C). Materials that deform or melt within this temperature range are not suitable for PCR applications. PMMA, which was used in the original design, has a glass transition temperature of 105 °C and a melting point at 130 °C.²³⁻²⁵ It was therefore being used close to the upper limit of its working range. By contrast, the melting points of silicon and glass (pyrex) are 1697 and 560 °C respectively.^{26,27}

B. Reusability of PCR Devices

Due to the lower cost of fabrication, polymer-based PCR devices can be made thrown away after a single use, eliminating carry-over contamination between PCR experiments.^{28,29} Silicon and glass PCR devices, on the other hand, are too expensive for single use applications (at least, when they are fabricated on the small scale described here).^{1,12} However, since silicon and glass are inert and highly resistant to aqueous and organic solvents, the devices can be cleaned with various solvents such as ethanol and diluted acids after each use to remove any contamination. Furthermore, the new design focused on using water-in-oil droplets for PCR, preventing the PCR mixture inside the aqueous microdroplets from coming into contact with the surfaces of the substrates, thereby minimising contamination and (in principle at least) allowing the device to be re-used several times.³⁰⁻³²

C. Compatibility of Surfaces for PCR

Although the surfaces of bare silicon and glass are known to inhibit PCR due to the surface adsorption of polymerases and DNA templates, the surfaces can be easily modified for compatibility with PCR.³³⁻³⁵ A silicon dioxide layer for instance can be easily deposited on silicon to reduce the inhibitory effect of bare silicon^{1,35}. The approach of conducting PCR in droplets also prevents the surface adsorption and deactivation of polymerases and DNA templates.³⁶ Bovine serum albumin (BSA)³³ and other additives³⁷ may be added to the PCR aqueous mixture to further reduce any risk of surface inhibition of PCR.

D. Hydrophilic to Hydrophobic Surfaces

To make water-in-oil droplets, the microchannel surface must be hydrophobic so that the oil phase wets the channel walls preferentially over the aqueous phase (containing the PCR mixture), allowing the PCR mixture to be carried as aqueous droplets through the microchannels.³⁸ This is easy to ensure for polymer devices by careful selection of a hydrophobic polymer. However, both glass and silicon dioxide are inherently hydrophilic, causing the aqueous phase to wet the surfaces preferentially over the oil phase, leading to unwanted oil-in-water droplets. To prevent this, chemical modification of the surfaces is needed to form a hydrophobic layer that permits the generation of water-in-oil droplets.

E. Reduction of Flow or Velocity Fluctuations

Pressure capacitance in microfluidic devices can cause velocity fluctuations which are a potential concern for droplet-based PCR as they can affect the residence time of the droplets at the different temperature zones used for denaturation, annealing and extension.^{39,40} When liquids are pumped into microchannels at high pressure, mechanical deformation can cause localised pressure variations which directly affect the velocity of the droplets. Stiff and rigid materials reduce the fluctuations in the velocity of the droplets caused by pressure capacitance, potentially making silicon and glass more suitable as substrates than soft polymers for PCR.

F. Transparency

Polymers are typically transparent and therefore amenable to optical detection methods. Silicon being opaque does not allow the use of conventional optical detection methods.^{1,4} However, capping the silicon substrate with a glass layer allows observations under a microscope via the glass.¹ Various optical detection methods such as fluorescence detection can be carried out through the transparent glass layer.

In the remainder of this chapter, I describe the formulated silicon-based fabrication process for the new radial PCR device, using the dimensions and parameters determined by the aforementioned thermal simulation studies (**Chapter 2, Section 2.4.5**).

3.2 DEVICE FABRICATION

The fabrication process was formulated using available silicon-based fabrication methods at the Institute of Microelectronics (IME) in Singapore. **Figure 3.1** summarises the complete fabrication process.

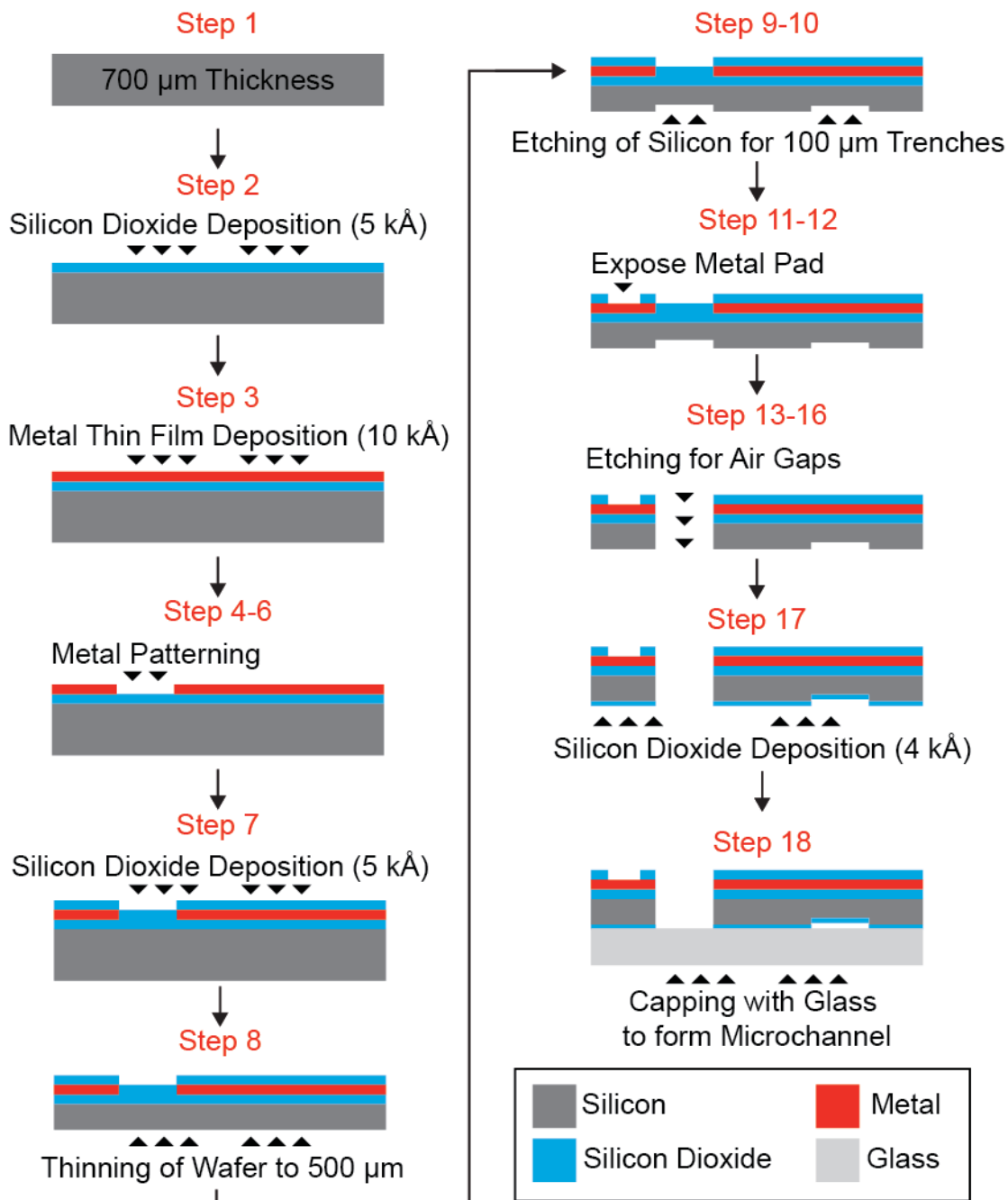


Figure 3.1. A summary of the fabrication process for the silicon-glass PCR device. The fabrication process consisted of four lithography stages (steps 4-6 for metal patterning, steps 9-10 for fluidic channel formation, steps 11-12 for exposing metal pads, and steps 13-16 for air gap formation). The fabrication process was concluded with the capping by the glass wafer in step 18 to form the microchannels.

3.2.1 Preparations of Starting Wafers

A. Step 1: Starting Silicon Wafers

A typical fabrication batch began with a set of five “reclaimed-grade” wafers that were stripped of any organic and metallic residues from the surfaces. The starting thickness of each wafer was 700 μm .

B. Step 2: Silicon Dioxide Deposition

5 kÅ of thin-film silicon dioxide was first deposited on the surface of the wafer using plasma-enhanced chemical vapour deposition (PECVD) (Novellus system, Lam Research, USA). This layer of oxide acted as an electrical insulator between the metal layer and the bare silicon surface.

3.2.2 Metal Thin-film Patterning

A. Step 3: Metal Thin-Film Deposition

10 kÅ of thin film aluminium was subsequently deposited on top of the silicon dioxide layer using physical vapour deposition (PVD) (Endura, Applied Materials, USA) (**Figure 3.2**).

B. Step 4: Lithography for Metal Thin-film Patterning

After the deposition of the aluminium layer, lithography was carried out to achieve the required metal patterns for the on-chip heaters and temperature sensors (**Figure 3.2(ii)**). The lithography process involved the following steps:

(1) 2 µm of positive photoresist (PFI26A, Sumitomo, Japan) was first spin-coated onto the wafer and soft-baked using product-recommended protocols. (2) The resist-coated wafer was then aligned to a lithography glass mask (**Mask 1, Appendix 9.1.1**) and was exposed to a mercury lamp to transfer the mask patterns onto the photoresist. (3) After exposure, the photoresist was developed using standard protocols. As PFI26A is a positive photoresist, the area of the photoresist which was exposed to light was removed by the developer (MF319, Microposit, Shipley, USA), exposing the metal layer underneath; the area of the photoresist which was covered by the mask (not exposed to light) remained intact on top of the metal surface. (4) After developing, the resist-coated wafer was then hard-baked and rinsed with deionised water using standard protocols. The wafer was then dried by spinning and purging with nitrogen gas.

C. Step 5: Metal Etching for Metal Thin-Film Patterning

After lithography, the wafer was placed in an aluminium etching solution (ratio of H₃PO₄ (85.0 %): CH₃COOH (99.0 %): HNO₃ (70.0 %): H₂O = 4: 4: 1: 1) to remove the exposed aluminium layer and uncover the silicon dioxide layer. The etching rate for this recipe was approximately 1 kÅ/min. After 10 min, the wafer was removed from the etching solution and placed under running deionized water bath to quench the etching. This step was done rapidly to minimise under-etching (etching of the side of the aluminium layer underneath the photoresist) which might

remove fine features and cause breaks to the metal patterns. The wafer was then rinsed thoroughly with deionised water and dried by spinning and purging with nitrogen gas. The wafers were then visually checked (**Figure 3.2(iii)**) for incomplete etching or over-etching.

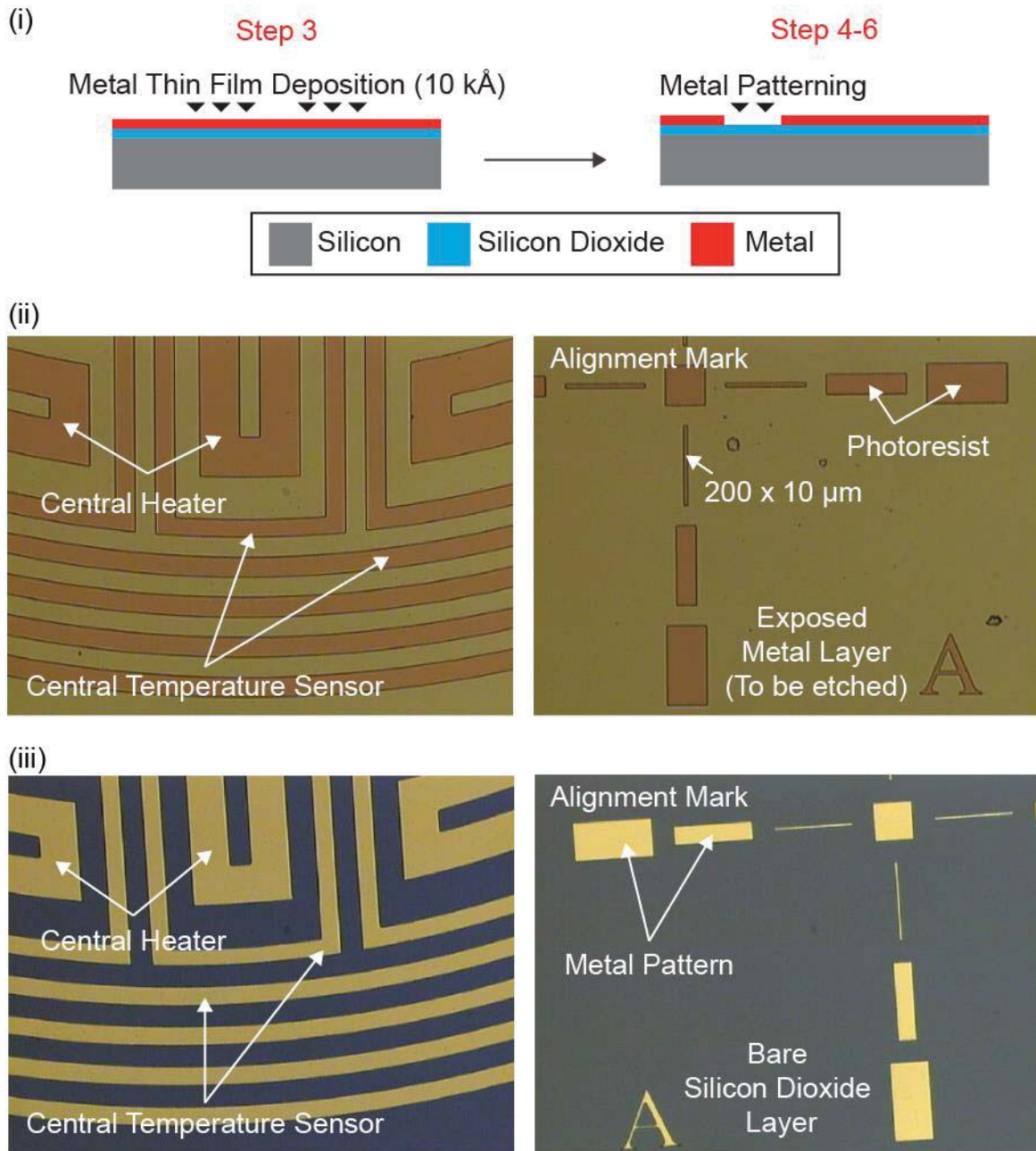


Figure 3.2. Metal-thin film patterning: step 3 to step 6. (i) Thin-film aluminium was deposited on the wafer in step 3 before lithography (steps 4-6) was conducted to pattern the metal layer. The metal patterns served as resistive heaters and temperature sensors in the completed PCR device. (ii) Step 4 of the fabrication process. Lithography was conducted to pattern the metal areas to be etched. (iii) Steps 5 and 6 of the fabrication process. After etching, the remaining metal areas formed the patterns that served as heaters and temperature sensors on the chip.

D. Step 6: Completion of Metal Patterning

After etching, the photoresist was removed completely from the surface of the wafer by immersing it completely in a stripping solution (PRS3000, J.T. Baker, USA) for 30 min. The wafer was then rinsed thoroughly with deionised water, and was dried by spinning and purging with nitrogen gas. The removal of the photoresist revealed the completed metal patterns (**Figure 3.2(iii)**) that in the final completed device formed the on-chip heaters and temperature sensors. The Ohmic resistances of the metal patterns were measured to determine electrical continuity of the patterns. Lower than expected resistances indicated a short-circuit in the metal patterns due to incomplete metal etching, while an open-circuit reading indicated a break in the circuit caused by under-etching (etching of the side of the aluminium layer underneath the photoresist) that resulted in the partial removal of the metal pattern.

3.2.3 Protection of Metal Patterns and Thinning Wafers

A. Step 7: Deposition of Silicon Dioxide

5 kÅ of silicon dioxide was then deposited on the surface of the wafer using plasma-enhanced chemical vapour deposition (PECVD) (790 Series, Plasma-Therm, USA) (**Figure 3.3**). This silicon dioxide layer was used to protect the fragile metal patterns from becoming scratched in the subsequent processing steps.

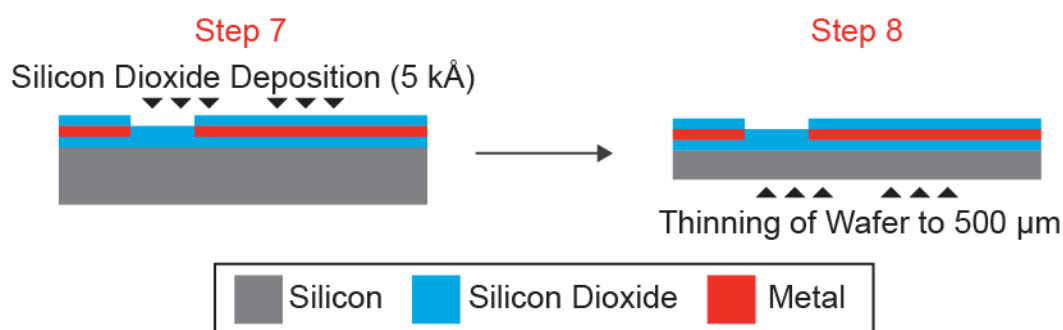


Figure 3.3. Protection of metal patterns and thinning wafers: step 7 to step 8. Silicon dioxide was deposited on top of the metal patterns for protection against scratching during subsequent handling. The silicon wafer was thinned from the back to 500 μm and was given a polished finish.

B. Step 8: Thinning of Silicon Wafers

With the metal patterns on the top of the wafer, the wafer was thinned from the back using back-grinding (GNX200 Grind-X, Okamoto, Japan) to match the thickness used in the simulation studies. Thinning the wafer also reduced the time needed to create the gaps in the wafers (step 15). The thickness of the wafer was thinned down from the original 700 μm to 500 μm. The back was also

polished to give a mirror finish. After thinning down the wafer, it was immersed in acetone for 10 min to remove any residues from back grinding. This was followed by immersion in isopropyl alcohol (IPA) for another 10 min, and then rinsing with deionised water. The wafer was then dried by spinning and purging with nitrogen gas.

3.2.4 Patterning of Fluidic Network

A. Step 9: Lithography for Fluidic Network

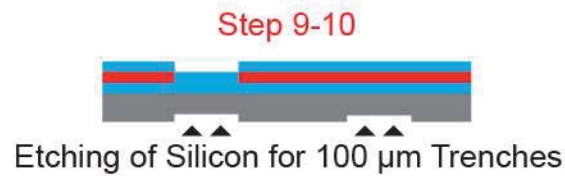
After back-grinding, lithography was carried out on the newly-polished side of the wafer to pattern the microchannel network (**Figure 3.4(i)**) through which fluids would flow in the PCR device. The lithography process involved the following steps:

(1) 10 μm of positive photoresist (SPR220, Microchem, USA) was first spin-coated onto the wafer and soft-baked using product-recommended protocols. (2) The coated wafer was then aligned to a lithography glass mask (**Mask 2, Appendix 9.1.2**) and was exposed using a mercury lamp to transfer the mask patterns onto the photoresist. (3) After exposure, the photoresist was developed using standard protocols.⁴¹ As SPR220 is a positive photoresist, the area of the photoresist which was exposed to light was removed by the developer (MF319, Microposit, Shipley, USA) to expose the underlying silicon layer; the area of the photoresist which was covered by the mask (not exposed to light) remained intact on top of the silicon surface. (4) After developing, the wafer with the exposed patterns was then hard-baked and rinsed with deionised water using standard protocols.⁴¹ The wafer was then dried by spinning and purging with nitrogen gas.

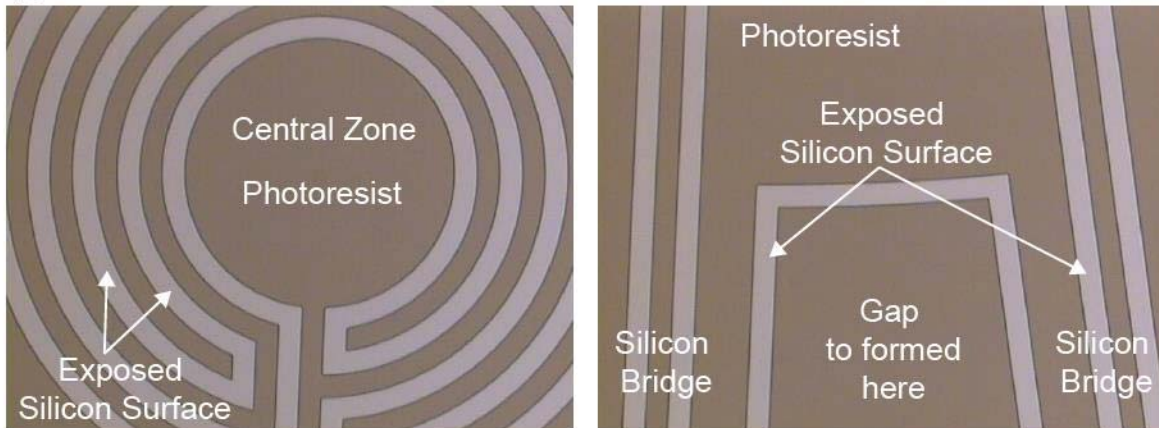
B. Step 10: Etching for Fluidic Network

After lithography (**Figure 3.4(ii)**), deep reactive ion etching (DRIE) (STS-MEMS, USA) was used to etch the exposed silicon areas to form trenches with a uniform depth of 100 μm (**Figure 3.4 (iii)**). After etching, the photoresist was removed completely from the surface of the wafer by immersing it completely in a stripping solution (PRS3000, J.T. Baker, USA) for 30 min. The wafer was then rinsed thoroughly with deionised water and was dried by spinning and purging with nitrogen gas. The trenches were checked visually under the microscope to ensure they were continuous. Blocked trenches due to incomplete etching of silicon were unusable as they would prevent fluid flow.

(i)



(ii)



(iii)

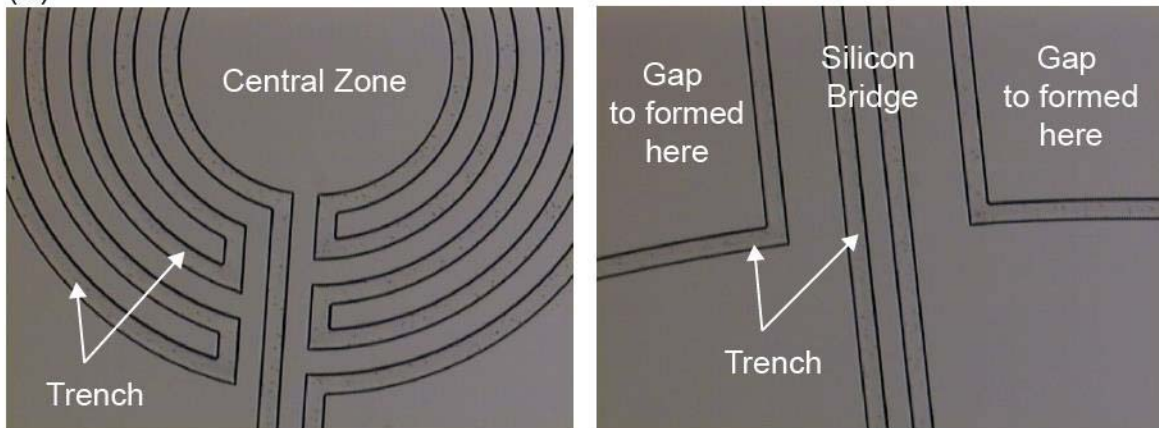


Figure 3.4. Patterning of fluidic network: step 9 to step 10. (i-ii) After thinning the wafer, lithography was carried out on the back side of the silicon wafer to pattern the microchannel network. (iii) Etching was subsequently carried out to create trenches for the microfluidic channels. Additional trenches were formed to mark out the areas for air gaps. In step 15, etch-through (aligned to these trenches) was done on the opposite side of the wafer to create the gaps.

3.2.5 Exposing Metal Pads

A. Step 11: Lithography for Exposure of the Metal Pads

After forming the trenches on the bottom side of the wafer, lithography was carried out on the top side (the side with the metal patterns) of the wafer to selectively remove the protective silicon dioxide and expose selected areas of the metal surface to allow electrical connection to power

supplies and temperature controllers (**Figure 3.5(i)**). The lithography process involved the following steps:

(1) A flat support was first taped to the bottom of the wafer to cover up the trenches so that the wafer could be held in place by suction on the underside during the spin-coating process. 10 μm of positive photoresist (SPR220, Microchem, USA) was then spin-coated onto the wafer and soft-baked using standard protocols.⁴¹ (2) After spin-coating, the taped support was separated from the wafer. The coated wafer was then aligned to a glass lithography mask (**Mask 3, Appendix 9.1.3**) and was exposed using a mercury lamp to transfer the mask patterns onto the photoresist. (3) After exposure, the photoresist was developed manually using standard protocols.⁴¹ As SPR220 is a positive photoresist, the area of the photoresist that was exposed to light was removed by the developer (MF319, Microposit, Shipley, USA) to expose the underlying silicon dioxide layer; the area of the photoresist which was covered by the mask (not exposed to light) remained intact on top of the wafer. (4) After developing, the wafer with the exposed patterns was then manually hard-baked on a hot plate and rinsed with deionised water using standard protocols. The wafer was then dried by spinning and purging with nitrogen gas.

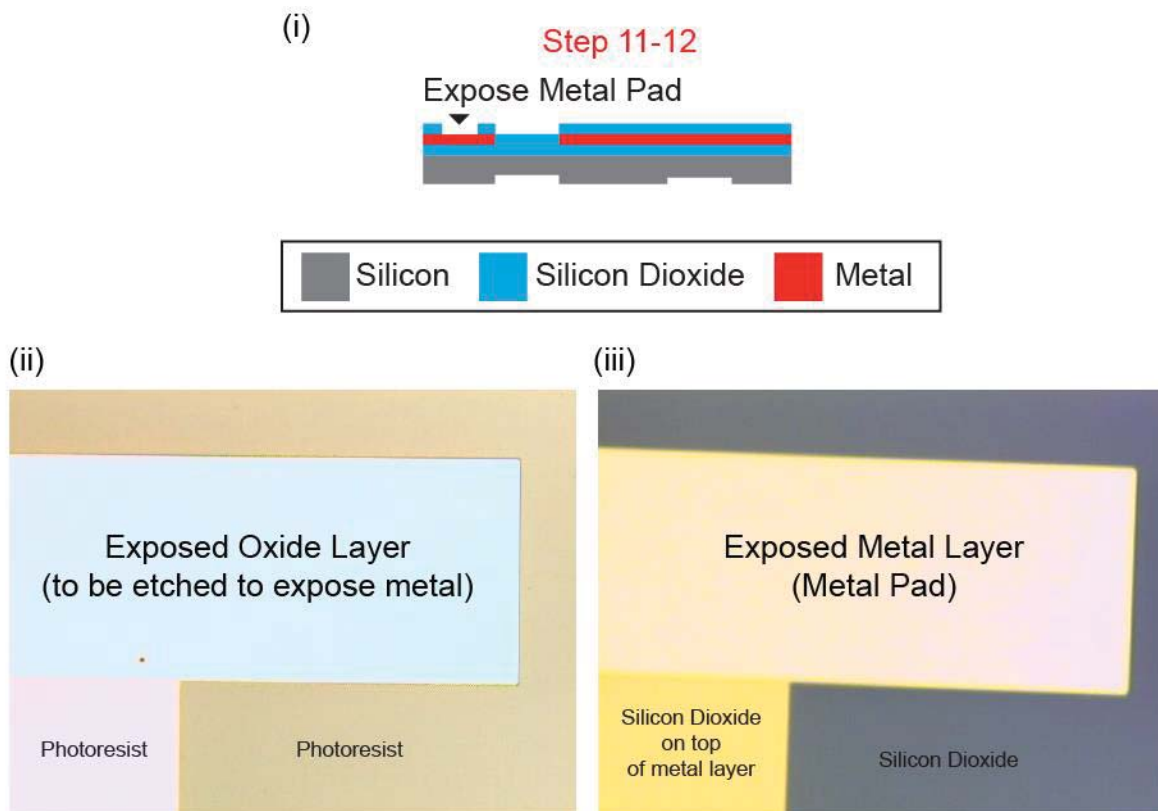


Figure 3.5. Exposing metal pads: step 11 to step 12 (i-ii) Lithography was carried out to pattern the silicon dioxide layer so that selected areas were removed by etching to expose the metal layer underneath. (iii) The exposed metal areas served as metal pads for connections to external electrical components (power supplies and PID controllers).

B. Step 12: Etching to Expose Metal Pads

After lithography, plasma etching (790 Series, Plasma-Therm, USA) was used to etch the exposed silicon dioxide (**Figure 3.5(ii)**). An etching depth of 5.5 kÅ was used to reach the metal surface (**Figure 3.5(iii)**). The resistances of the metal patterns were measured again at this point to verify the electrical continuity of the patterns. An open-circuit reading indicated that the silicon dioxide layer had not been removed completely. After etching, the photoresist was removed completely from the surface of the wafer by immersing it completely in a stripping solution (PRS3000, J.T. Baker, USA) for 30 min. The wafer was then rinsed thoroughly with deionised water and was dried by spinning and purging with nitrogen gas.

3.2.6 Formation of Air Gaps

A. Step 13: Lithography for Air Gaps Formation

After the exposure of the metal pads, lithography was carried out on the top side (the side with the metal patterns) so as to create openings on the wafer that functioned as air gaps on the devices for passive cooling of the silicon bridges (**Chapter 2, Figure 2.4**). The lithography process involved the following steps:

(1) A flat support was first taped to the bottom of the wafer to cover up the trenches so that the wafer could be held in place by suction on the underside during the spin-coating process. 10 µm of positive photoresist (SPR220, Microchem, USA) was then spin-coated onto the wafer and soft-baked using standard protocols.⁴¹ (2) After spin-coating, the taped support was separated from the wafer. The coated wafer was then aligned to a lithography glass mask (**Mask 4, Appendix 9.1.4**) and was exposed using a mercury lamp to transfer the mask patterns onto the photoresist. (3) After exposure, the photoresist was developed manually using standard protocols. As SPR220 is a positive photoresist, the area of the photoresist that was exposed to light was removed by the developer (MF319, Microposit, Shipley, USA) to expose the underlying silicon dioxide layer; the area of photoresist which was covered by the mask (not exposed to light) remained intact on top of the wafer. (4) After developing, the wafer with the exposed patterns was then manually hard-baked on a hot plate and rinsed with deionised water using standard protocols.⁴¹ The wafer was then dried by spinning and purging with nitrogen gas.

B. Step 14: Etching of Exposed Silicon Dioxide Layer

After lithography, plasma etching (790 Series, Plasma-Therm, USA) was used to etch the exposed silicon dioxide areas (**Figure 3.6**). An etching depth of 10.5 kÅ was targeted to reach the silicon surface.

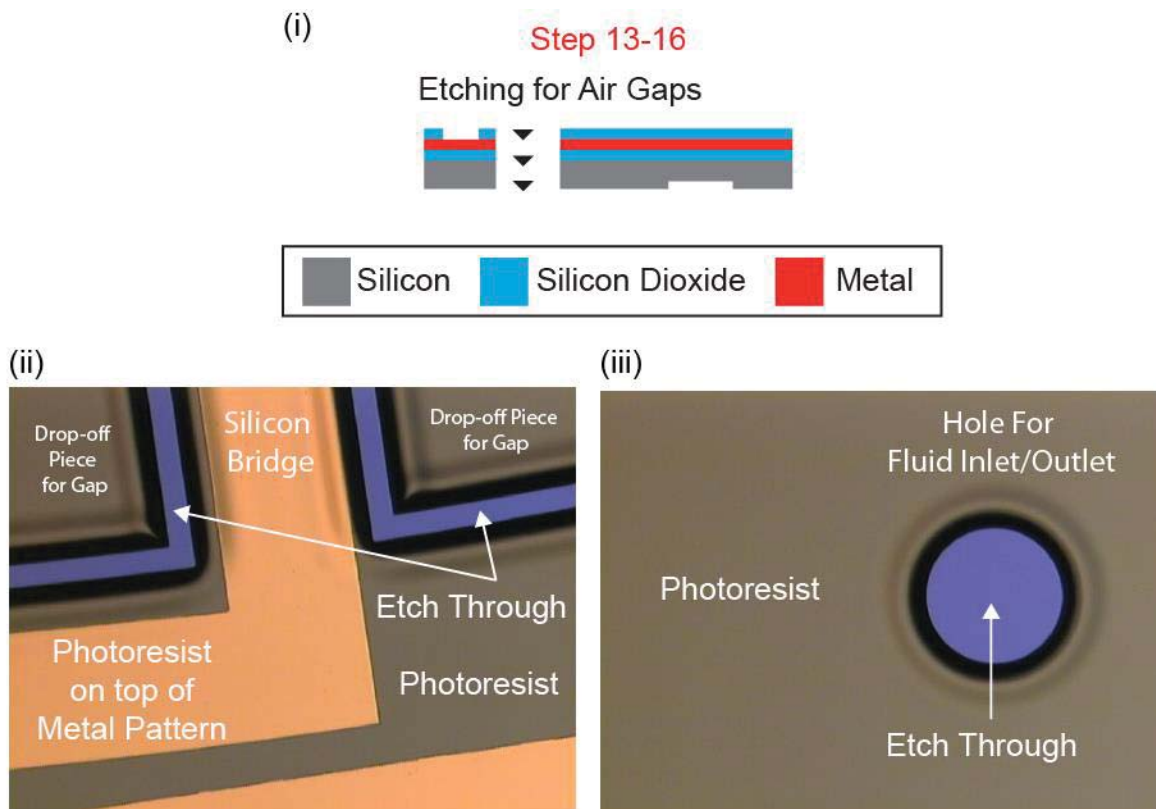


Figure 3.6. Formation of air gaps: step 13 to step 16. (i) Lithography was carried out to pattern the air gaps. Etching of the silicon dioxide layer was completed first before carrying out deep reactive ion etching to remove the silicon core layer to etch through the wafer. To etch through the wafer, an estimated 400 μm (instead of 500 μm) of the silicon layer was removed due to the initial 100 μm trench that was already etched on the opposite side in step 10. (ii) After etching through, pieces of the wafer dropped off to form openings or gaps. (iii) Holes for the inlets and outlets were etched in parallel with the formation of the air gaps.

C. Step 15: Etching Through the Silicon Wafer

Before etching through the wafer, it was first bonded to another flat support using a thermal release tape (90 °C REVALPHA, Nitto, USA) to cover up the trenches on the bottom side of the wafer. The bonded flat support allowed the wafer to be held in place by suction on the underside during the etching process. The bonding also ensured that small pieces of the wafer which were etched out to create openings were held in place. After attaching the flat support, deep reactive ion etching (DRIE) (STS-MEMS, USA) was used to etch the exposed silicon areas. An etching depth of 400 μm (instead of 500 μm) was targeted to create through openings on the wafer because an initial 100 μm trench had already been created on the opposite side in step 10. The wafer was

repeatedly checked under the microscope to determine if the etching had been successful in creating the openings.

D. Step 16: Completion of Air Gaps on Wafers

After etching, the wafer was thermally released from the flat support by placing it on a hot plate at 95 °C. Small pieces of unwanted wafer parts were removed. At this point, the wafer had many openings and was very fragile. The photoresist was removed completely from the surface of the wafer by immersing it completely in a stripping solution (PRS3000, J.T. Baker, USA) for 30 min. The wafer was then rinsed thoroughly with deionised water and gently brushed to remove any residues in the openings and microchannels. After brushing, the wafer was immersed in IPA for 10 min before drying on a hot plate at 40 °C. An air pistol was carefully used to remove any particles on the surface of the wafer.

3.2.7 Capping with Glass Wafers

A. Step 17: Silicon Dioxide Deposition

4 kÅ of thin-film silicon dioxide was deposited on the bottom side (the side with the trenches) of the wafer using plasma-enhanced chemical vapour deposition (PECVD) (790 Series, Plasma-Therm, USA) (**Figure 3.7**). After deposition, the wafer was then rinsed thoroughly with deionised water and gently brushed to remove any residues in the openings and microchannels. After brushing, the wafer was immersed in IPA for 10 min before drying on a hot plate at 40 °C. An air pistol was carefully used to remove any particles on the surface of the wafer.

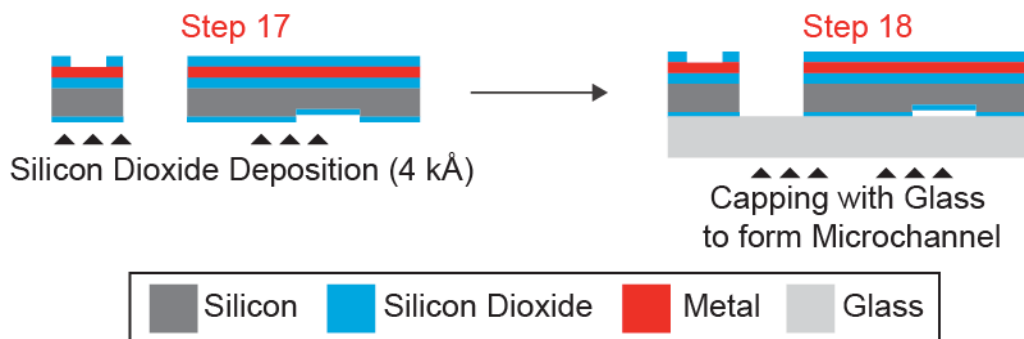


Figure 3.7. Capping with glass wafer: step 17 to step 18. Silicon dioxide was deposited to cover the trenches so that the oxide layer could later be used for modification. Glass was used to cap the trenches to form the microchannels.

B. Step 18: Capping the Trenches with Pyrex glass

Microchannels were formed by capping the trenches with a Pyrex glass wafer. The glass wafer was first cleaned by immersing it in freshly-prepared Piranha solution (a 3:1 mixture of

concentrated H₂SO₄ to 30% H₂O₂) for 20 min. After rinsing the glass wafer thoroughly with deionized water, it was dried by spinning and purging with nitrogen gas. Anodic bonding was used to bind the glass wafer on top of the trenches of the wafer (**Figure 3.7**).

3.2.8 Variations to the Fabrication Process

After several iterations, the above fabrication steps were finalised. Subsequent experiments were conducted using chips made using this fabrication process unless stated otherwise. The final device design used rounded microchannels that were 100 µm deep and wide. A variation of this design used angled microchannels that were 50 µm deep and wide (**Figure 3.8**).

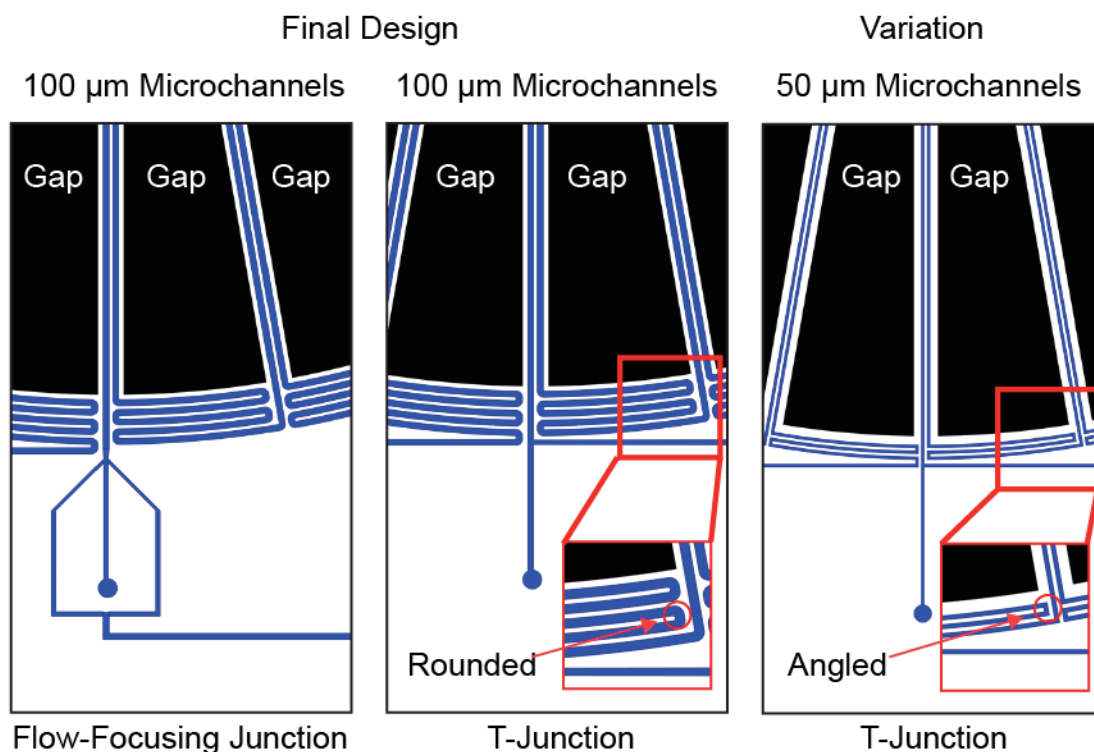


Figure 3.8. Variation to the fabrication process. The final fabrication process used rounded channels that were 100 µm deep and wide with two types of droplet generation junction – a flow-focusing junction⁴² and a T-junction⁴³. The initial fabrication process used angled microchannels that were 50 µm deep and wide. Only a T-junction type was used with the angled microchannels.

These chips were used primarily in the continuous-flow PCR experiment in **Chapter 4, Section 4.2.2**, and for the surface modification studies described in **Chapter 4, Section 4.3.1**. To make these narrower, shallower angled microchannels, the mask used in step 9 was replaced with **Mask 2A**. (**Appendix 9.1.5**) The etching in step 10 was specified to be 50 µm deep. The mask in step 13 was changed to **Mask 4A** (**Appendix 9.1.6**) so as to align the area for etch-through to the 50 µm wide trenches on the opposite side. No other changes to the fabrication process were required.

3.3 ELECTRICAL INTERFACE

The bonded wafer was diced (DFD6361 dicing saw, Disco, Japan) into 12 chips (4.0 x 4.0 cm) using a 250 μm thick diamond blade (MBT-284 SD280N50M42, Disco, Japan) (**Figure 3.9**). Each chip was then attached to a customised printed circuit board (PCB) (Tomcopy Solutions, Singapore).

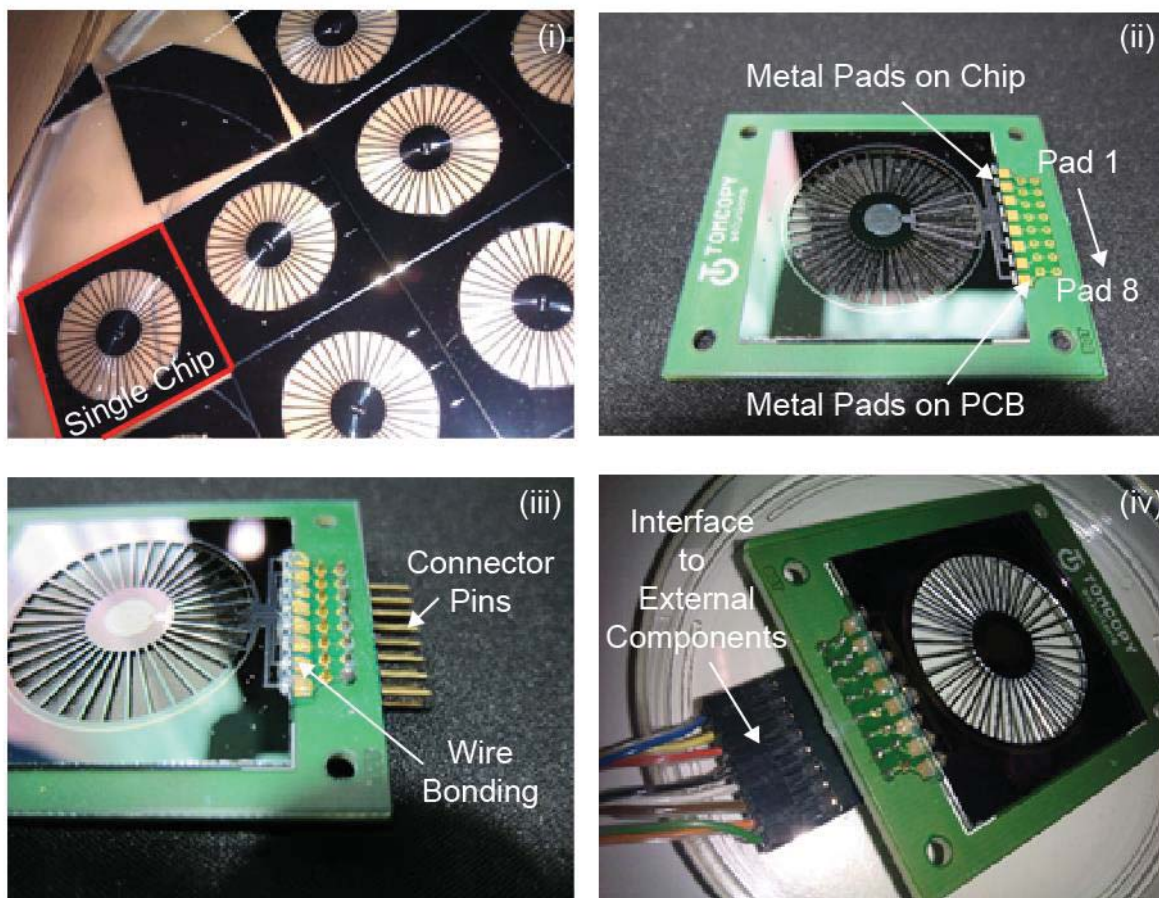


Figure 3.9. The components for the electrical interface. (i) The wafer was diced and individual chips (4.0 x 4.0 cm) were formed. (ii) A chip was attached to the customised PCB with the metal pads on the chip aligned to the printed metal pads on the PCB. The central heater was connected using pads 4 and 5, while the central temperature sensor was connected using pads 3-6 (**Chapter 2, Figure 2.4**). The periphery heater (when used) was connected using pads 1 and 8, while the periphery temperature sensors were connected using pads 2 and 3. (iii) The aligned metal pads were connected using wire bonding. Connector pins were soldered onto the PCB. (iv) A connector was attached to the soldered pins on the PCB for making connections to external electrical components.

After attaching the chip to the PCB board, wire bonding was carried out (ESEC3088, USA) to connect the exposed metal pads on the chips (**Section 3.2.5**) to the metal pads on the PCB using gold wires (25.4 μm in diameter). A dab of conductive silver epoxy was applied at each wire-bonding point to strengthen the connection. The silver epoxy had to be applied carefully to prevent spillage to neighbouring metal pads as this would cause a short circuit. Once the conductive silver epoxy had hardened, another epoxy glue (non-conductive) was liberally applied all over the connection pads to form a hard transparent protective layer to prevent the wires from breaking

during handling. After wire bonding, the PCB boards were soldered with connection pins where they could be used to interface to other electrical components such as the power supplies and the temperature controllers. The central heater on the chip was connected using pads 4 and 5, while the central temperature sensor was connected using pads 3-6. The periphery heater on the chip was connected using pads 1 and 8, while the periphery temperature sensors were connected using pads 2 and 3. The connection schematic is described in **Chapter 2, Figure 2.4**.

3.4 FLUIDIC INTERFACE

The chip together with the attached PCB was designed to sit in a customised polycarbonate fixture (6.0 cm x 5.0 cm x 2.0 cm) (CinTech Ad-venture, Singapore) (**Figure 3.10**).

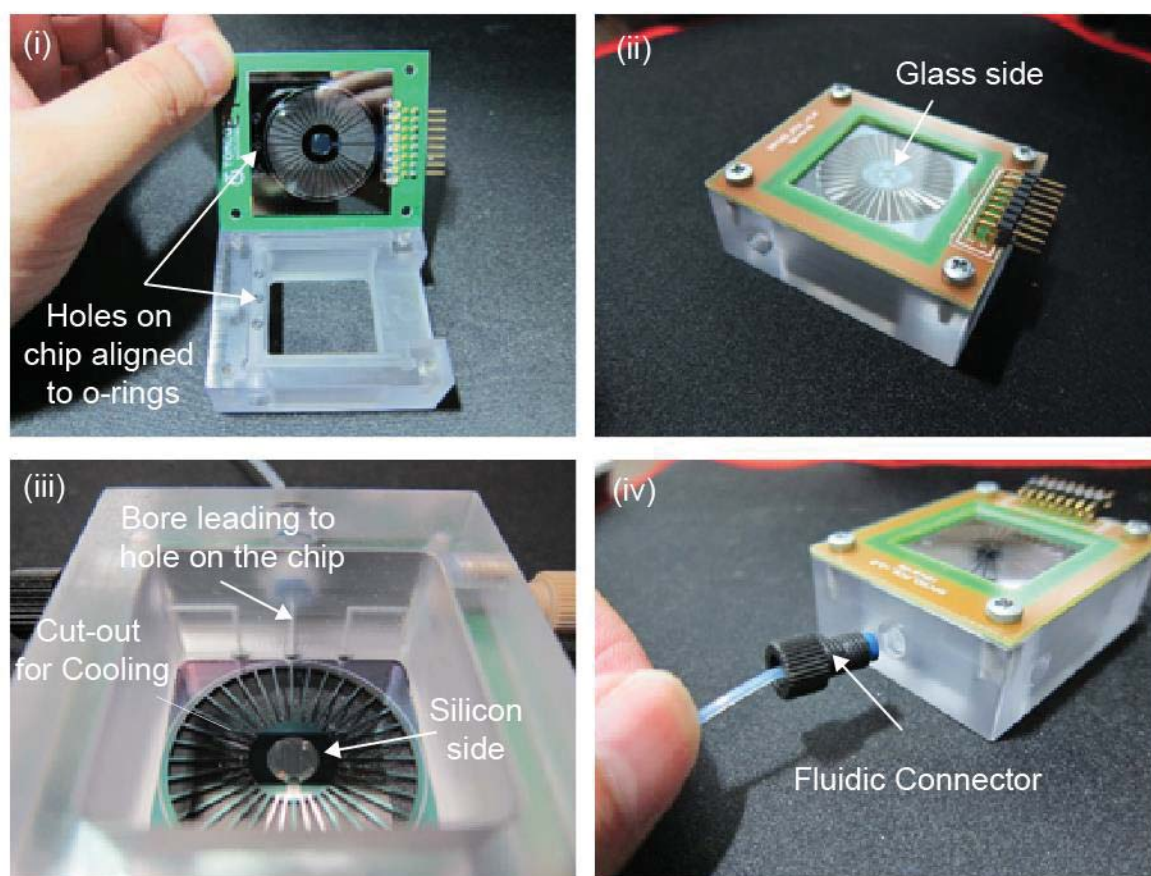


Figure 3.10. The components for the fluidic interface. (i) A customised polycarbonate fixture was designed and made to hold the fabricated PCR chip so as to handle fluid flow. O-rings were placed in between the holes on the chip and the bores in the fixture to prevent leakage. (ii) The complete assembly of the chip, PCB and the fixture. (iii) The fixture had a cut-out to expose the silicon side for passive cooling. (iv) Fluidic connectors were attached to the fixture so that fluids could be pumped into or out of the device via standard PEEK or Teflon tubing.

3.0 mm o-rings were placed between the bores and the aligned holes on the PCR device to prevent leakage when fluids were pumped into and removed from the microchannels. The o-rings were made of a synthetic fluoropolymer elastomer (Viton, DuPont, USA) that was resistant to the fluids

and reagents used in the PCR experiments. The polycarbonate fixture had a cut-out (3.2 x 3.2 cm) so that the silicon bridges and the gaps were exposed to the surrounding air to promote heat exchange. Polyether ether ketone (PEEK) or Teflon capillary tubes and connectors were connected to the polycarbonate fixture so that fluids could be pumped into and removed from the PCR chip via the fixture. The materials of the various components (o-rings, capillary tubes and connectors) for the fixture were inert and would not disrupt PCR by surface adsorption and deactivation of polymerases and DNA.³³

3.5 DISCUSSION

The fabrication process described above had four lithography steps and multiple etching steps. The fabrication process was time-consuming, taking about two months from start to end to complete a batch of five wafers. It was also costly, requiring the use of multiple pieces of specialized equipment and machines found in IME. Each 7" wafer produced only twelve chips because each chip was 4.0 cm x 4.0 cm. Due to the many potential failure points during the fabrication, the yield was low at ~20 %, meaning about 2-3 chips would work from each wafer. The low yield was due to errors incurred during the many steps in fabrication.

One of most common errors was a broken circuit or a short circuit in the heaters and/or temperature sensors due to problems during metal patterning and etching. As the finest features on the metal pattern were 10 μm , contamination by dust particles during exposure could prevent the positive photoresist from being properly exposed. As a result, the unexposed positive photoresist would not be developed and removed. Subsequent etching would fail to etch the area covered by the accidental unexposed resist, resulting in a short circuit. Another reason for short circuits was incomplete etching, which would leave metal residues (**Figure 3.11(i)**). Broken circuits were caused by scratching of the metal patterns during handling (**Figure 3.11(i)**). Another common mistake was over-etching, in which the etchant would cause sideways etching of the metal under the photoresist, removing the fine features. Both broken and short circuits would result in unusable chips. The measurement of the resistances of the heaters and the temperature sensors was used to verify the usability of the chips. If a resistance reading could not be measured, then an open or broken circuit had resulted. If a lower than expected resistance reading was measured, then a short circuit had resulted. Measuring the resistances of six random chips showed that only one was usable (**Table 3.1**). A fault in any of the integrated heater or temperature sensors would render the chip unusable for PCR experiments as heating and temperature control could not be accomplished.

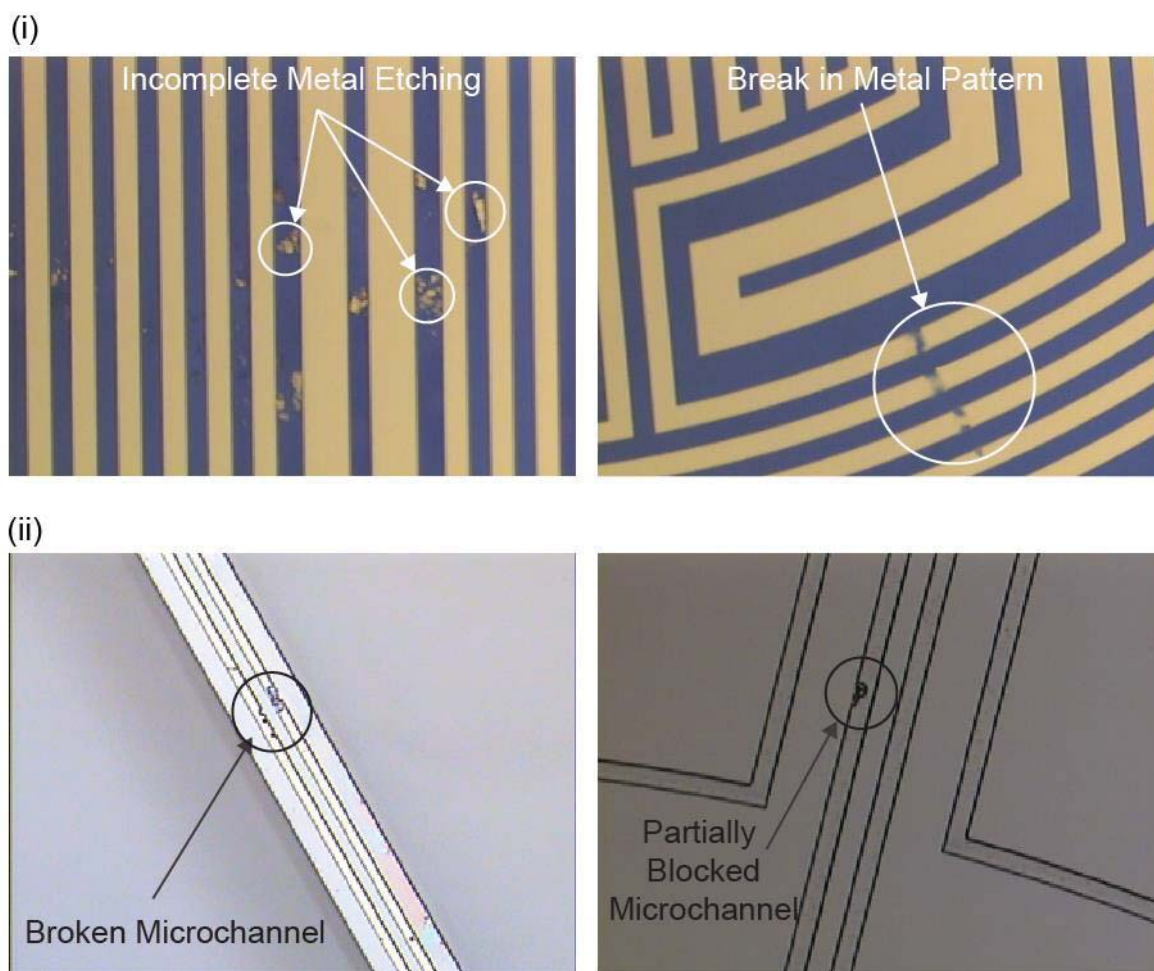


Figure 3.11. Defects arising from imperfect lithography and handling. (i) Defects in the metal pattern resulting from incomplete metal etching caused by imperfect lithography would result in a short circuit. A break in the metal pattern caused by scratching during handling would result in an open circuit. (ii) Imperfect lithography during channel patterning would result in broken or partially blocked microchannels.

Table 3.1. Resistance measurements of six random chips.

Chip Number	Resistance [Ω]				Note
	Periphery		Central		
	Heater	Sensor	Sensor	Heater	
	Pads 1-8	Pads 2-7	Pads 3-6	Pads 4-5	
1	74.4	446.3	730.0	82.9	Usable Chip
2	75.5	50.5 (low)	745.2	81.5	Short Circuit (Periphery Sensor)
3	74.2	No Reading	750.2	82.7	Open Circuit (Periphery Sensor)
4	73.2	No Reading	735.8	81.9	Open Circuit (Periphery Sensor)
5	73.8	450.4	25.5 (low)	83.8	Short Circuit (Central Sensor)
6	74.8	465.2	No Reading	83.5	Open Circuit (Central Sensor)

Another common error was broken or (partially or completely) blocked microchannels, which were caused by imperfect lithography (as with broken circuits and short circuits) (**Figure 3.11(ii)**). These would also render the chips unusable because they would hinder fluid flow and disrupt the formation of droplets.

To maximise the yield all possible precautions were taken to ensure the lithography was done properly. This included a thorough cleaning of the masks to remove any dust and resist residue that might block the patterns on the masks, purging the wafers with nitrogen gas to remove any particles that might have landed on the wafers, purging the surfaces of the exposure and aligner system to remove dust particles, use of class 100 cleanroom procedures, washing and spin drying, and thorough checking under a microscope.

The low yield was also due to the fragile nature of the silicon wafers. The wafers were thinned down from the original 700 μm to the final 500 μm thickness to promote rapid heat loss as determined by the thermal simulation (**Chapter 2**) and also to reduce the time needed to etch through the wafers for the formation of the air gaps. After thinning down and etching through the wafer, the silicon bridges were very thin and narrow, making them extremely fragile. A careless spray of water during cleaning could break or chip the bridges (**Figure 3.12(i)**), making the wafers difficult to handle and clean. As a result, poorly cleaned wafers would lead to residues (**Figure 3.12(ii) and (iii)**) in the microchannels, which would hamper fluid flow in PCR experiments.

Compared to the original device, the new radial PCR device was more complicated and harder to fabricate and replicate. However, given my objective of creating a small footprint device with integrated temperature sensors and heaters, this approach had to be taken. With sufficient time, many of these issues could have been avoided through appropriate changes to the fabrication process. In a production environment where the device design is finalised and the fabrication procedure is streamlined accordingly, it is likely that much higher yields would be achievable.

Although challenging, the described fabrication procedure was capable of producing working radial PCR devices, albeit at a low final yield of $\sim 20\%$. This yield was mostly due to human handling errors. Improvements to the yield could be made by using 12" wafers which would allow more chips to be made in a batch. Similarly, the chip size could be reduced so that more chips could be fitted onto a wafer. However, to reduce the chip size, further thermal studies would have to be undertaken to determine the right dimensions to achieve the temperature gradient needed for PCR. The change in the size of chip would also require the use of lower flow rates. The channels would also be shorter, potentially requiring different syringe pumps better suited to low flow rates. However, these are all surmountable issues, and it is clear that silicon-based micromachining is a viable route to integrated PCR device fabrication.

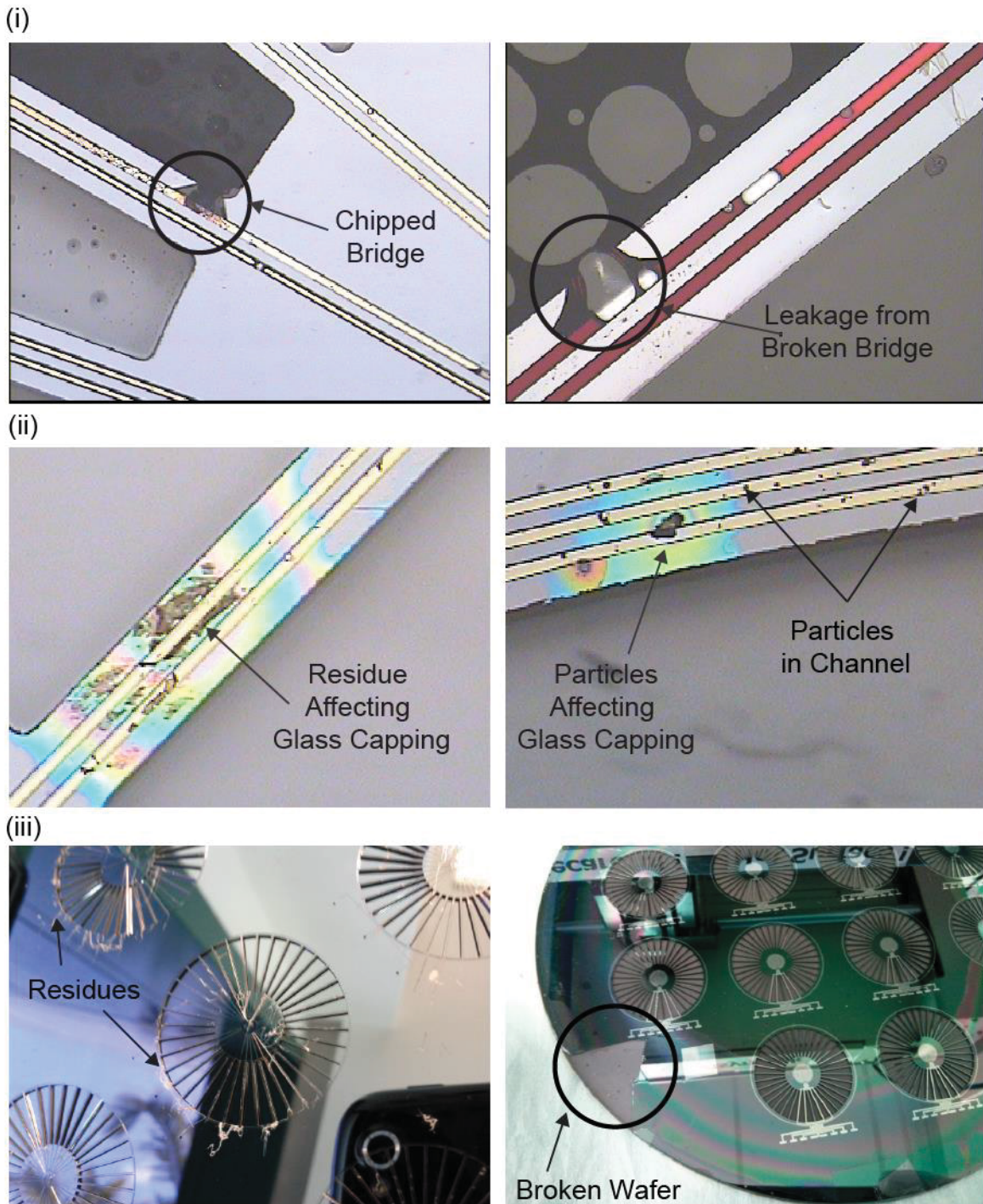


Figure 3.12. Common defects and issues arising during fabrication. (i) Broken or chipped silicon bridge resulting from handling of fragile wafer would render the chip unusable. Fluids passing through the broken bridge would leak, making microfluidic experiments impossible to conduct. (ii) As the wafer was fragile, cleaning was difficult and particles were sometimes left on the surfaces of the wafer or inside the channel. These residues would affect the glass capping and/or the fluid flow in PCR experiments. (iii) Residues on the wafer required extensive washing which had to be carried out carefully to avoid breaking a wafer.

3.6 CONCLUSIONS

In this chapter, the silicon-based fabrication process for the new radial PCR device (**Figure 3.13**) was described. With the fabrication process, a total of 30 wafers (360 chips) was processed. Out

of this number, 70 chips were considered usable after inspection of the metal patterns and the microfluidic channels. A quarter of these 70 chips were made using the 50 μm variation (**Section 3.2.8**), and the rest were made using the 100 μm fabrication process. Although challenging, the fabrication process yielded a sufficient number of devices for carrying out the PCR experiments described in the following chapters. The completed chip with its assembly (**Figure 3.13**) had a dimensions of 6.0 cm x 5.0 cm x 2.0 cm which was a major reduction in footprint compared to the original device (25.0 cm x 25.0 cm x 25.0 cm) by Schaerli *et al.*²².

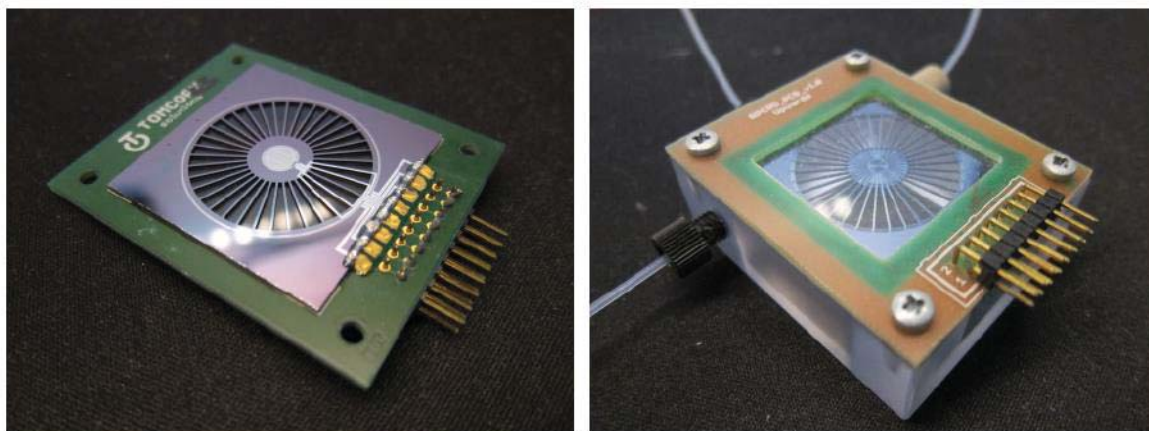


Figure 3.13. The fabricated device and complete assembly.

4 THERMAL AND FLUIDIC CHARACTERISATION OF THE RADIAL PCR DEVICE

Chapter 4

This chapter describes the thermal and fluidic characterisation of the newly fabricated radial PCR device. The built-in temperature sensors on the devices were calibrated and used to control the on-chip heaters using a proportional-integral-differential (PID) temperature controller. The hydrophilic surfaces of the microchannels were rendered hydrophobic by silanisation, allowing water-in-oil droplets to be formed using a T-junction or a flow-focusing junction. The generated droplets were characterised for their size, monodispersity and generation frequency.

4.1 INTRODUCTION

The PCR device was designed with two main functionalities. The first functionality was the ability to generate a temperature gradient between the centre and the perimeter using the integrated resistive heaters, temperature sensors, and air gaps. The second functionality was the ability to generate water-in-oil droplets using either a T-junction¹ or a flow-focusing junction² on the chip, allowing the PCR mixture to be encapsulated in aqueous droplets surrounded by an immiscible oil phase. The droplets could then be shuttled backwards and forwards along the radial temperature gradient to conduct PCR. The objective of this chapter is to describe the thermal and fluidic characterisation of the newly fabricated PCR device.

4.2 THERMAL CHARACTERISATION

We begin by describing how the newly fabricated PCR devices were calibrated and characterised for their temperature gradients.

4.2.1 Calibration and Generation of Temperature Gradient

A. Experimental

Before a temperature gradient could be controllably generated on the device, the integrated temperature sensors had to be calibrated. Electrical connections to the chip were made according to **Figure 4.1**. The periphery (metal pads 2-7) and the central temperature sensors (metal pads 3-6) were incorporated into Wheatstone bridges. A data acquisition (DAQ) device (USB 6501, National Instruments, USA) was used to apply 5.0 V DC across the two bridges and to measure the voltages (V_P and V_C) across the Wheatstone bridges.

The chip, fixed together with the polycarbonate fixture, was placed in a calibrated convection oven (Incubator IFE 500, Memmert, Germany) for the calibration process. Voltages across the Wheatstone bridges (V_P and V_C) were measured at constant temperatures (T) of 65.0, 75.0, 85.0 and 95.0 °C as maintained by the calibrated oven. To ensure constant temperature, the PCR device was kept in the oven for 1 h at each temperature before taking readings of V_P and V_C .

For the calibration graph, V_P and V_C were plotted against temperature (T). The graphs of V_P and V_C against temperature (T) were unique to each individual PCR chip, and therefore the temperature sensors on each chip had to be calibrated before use. The y-axis intersection and gradient were extracted from each plot to obtain a linear calibration function between T and V .

This information was passed to a proportional-integral-differential (PID) temperature controller (Labview, **Appendix 9.2**), which controlled the temperatures on the chip by measuring V_C and V_P continuously and adjusting the heater power to attain the required temperatures (**Figure 4.2**).

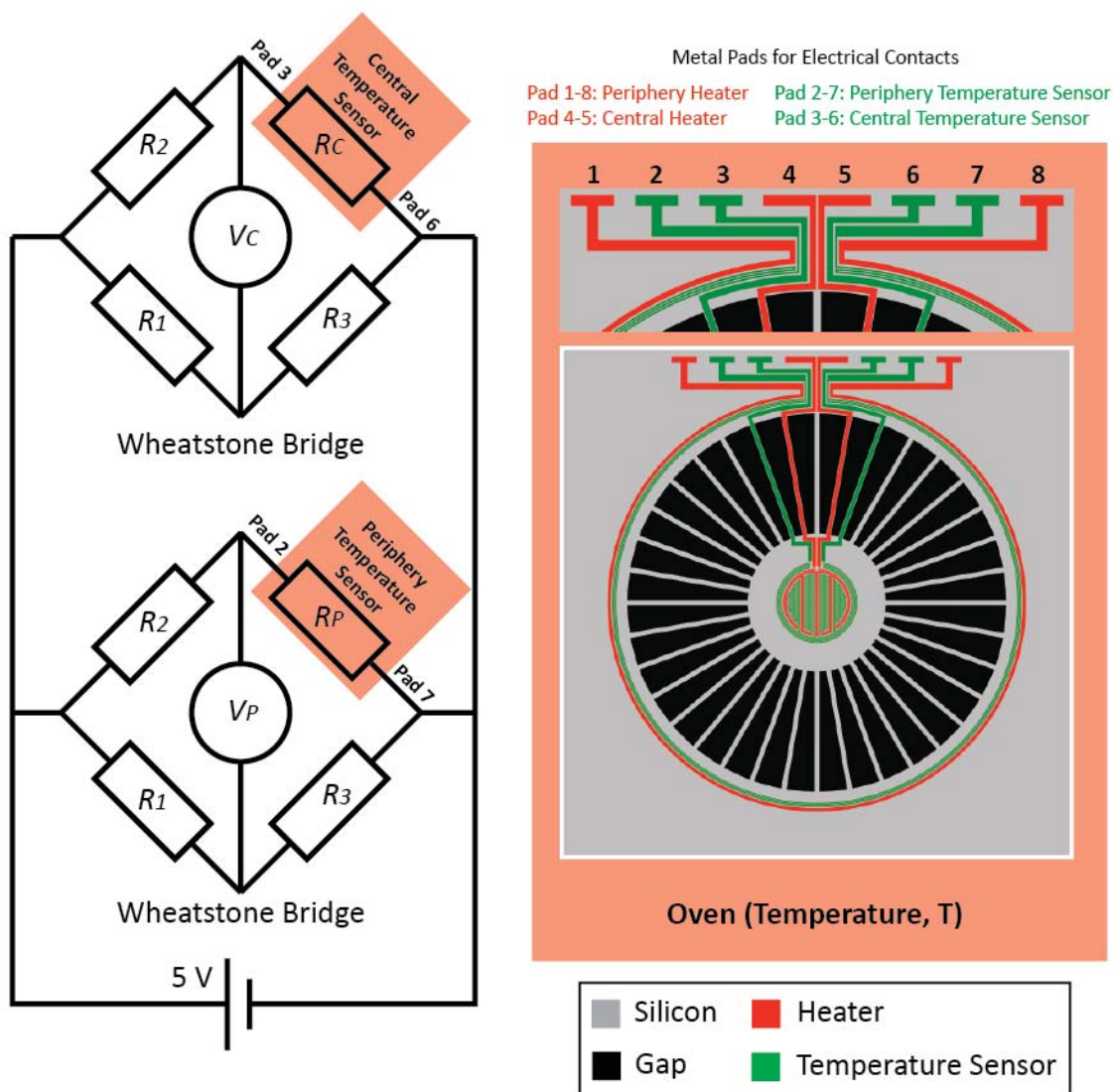


Figure 4.1. Schematic showing incorporation of the two temperature sensors into Wheatstone bridges. The Wheatstone bridges were connected in parallel to a DAQ device that supplied 5.0 V DC to the circuit. The fixed resistances R_1 , R_2 and R_3 in the bridge were each 680Ω . The variable resistors, R_C and R_P , represent the central (metal pad 3 and 6) and periphery (metal pads 2 and 7) metal-thin film temperature sensors respectively. As the temperature (T) of the oven was increased and the temperature of the chip increased, the resistances (R_C and R_P) of the temperature sensors increased, leading to an increase of the voltages (V_C and V_P) across the Wheatstone bridges. The voltages were measured by the DAQ device.

The temperature controller used a feedback control system (**Figure 4.2**) to maintain a fixed temperature difference between the centre and periphery of the chip. The resistive heaters integrated into the chips were used to heat up the centre and/or the periphery of the chips by an amount determined by the temperature controller.

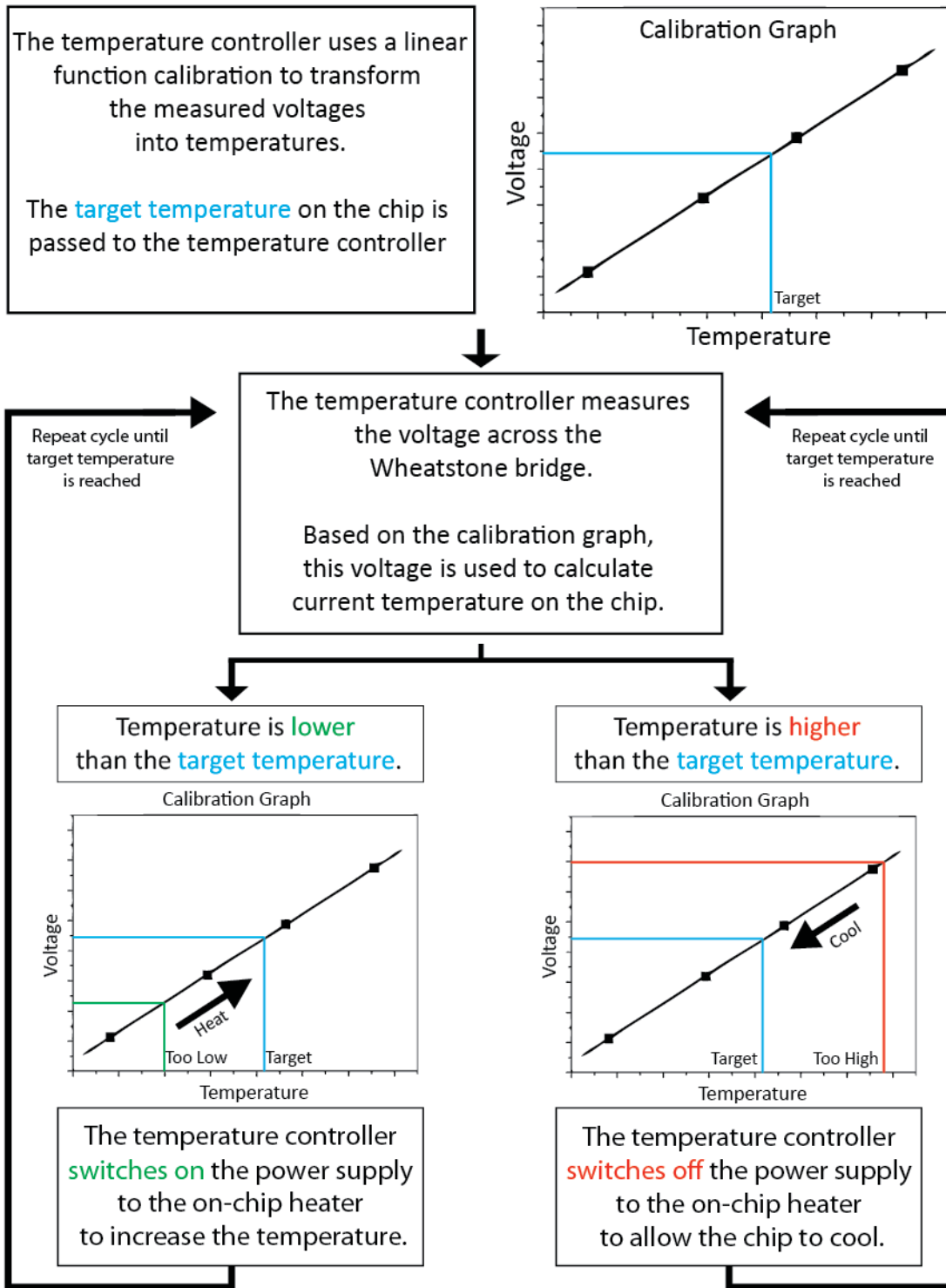


Figure 4.2. Schematic of the feedback loop used to control the temperature on the chip. The PID temperature controller used a linear calibration function to transform the voltages measured across a Wheatstone bridge into the current temperature on the chip. If the measured temperature on the chip was lower (higher) than the target temperature, the power supply to the heater was switched on (off). The cycle repeated so that the target temperature was reached and maintained.

If the temperature on the chip was lower than the required temperature, the temperature controller turned on the power supply to the heater (metal pads 1-8 for the periphery heater;

metal pads 4-5 for the central heater, **Figure 4.1**) to increase the temperature. If the temperature was too high, the temperature controller turned off the power supply to the heater so that the chip would cool. This control system enabled the chip to maintain a fixed temperature at the centre and/or periphery of the chip so that the temperature gradient could be generated.

For thermal characterisation, the central zone of the PCR device was heated using the integrated thin-film heater and maintained at 92 °C. The periphery heater was not used and no fan cooling was used because the simulation results (**Chapter 2, Section 2.4.5**) had shown that a wide-enough temperature gradient for PCR could be achieved without activating these features. The device was allowed to reach steady-state before a thermal image was taken using an IR camera (TVS-500EX, NEC-Avio, Japan). The thermal image showed the surface temperature profile of the PCR device and so gave an indication of the radial temperature gradient.

B. Results and Discussion

As the temperature (T) of the oven increased and therefore the temperature of the chip increased, the resistances of the aluminium metal thin-film temperature sensors increased, increasing the voltages (V_C and V_P) across the Wheatstone bridges. The plots (**Figure 4.3**) show a linear relationship between the temperature (T) and the respective voltage readings (V_C and V_P) over the selected temperature range. The calibration graphs were unique to each PCR chip differing in both their gradients and y-axis intersections. Consequently, each temperature sensor had to be calibrated before it could be used with the PID temperature controllers to control the heater.

The surface temperature profile of the fabricated PCR device was characterised using an IR camera. **Figure 4.4(i)** shows an IR image captured when the central zone of the PCR device was heated using the integrated thin-film heater to a constant temperature of 92.0 °C, while the periphery heater was deactivated. The thermal image revealed a radial temperature gradient along the silicon bridges, in which the temperature at the central zone dropped from ~95.0 °C to about ~65.0 °C at the periphery as extracted from the thermal image. At the same time, the on-chip thin-film temperature sensors indicated steady-state temperatures of 92.0 °C and 60.0 °C for the central zone and periphery, respectively (**Figure 4.4(ii)**).

When the central heater was first turned on, the temperature of the central zone increased quickly from ambient temperature (~22.0 °C) to a constant temperature of 92.0 °C within 25.0 s. When the target temperature was reached, the central heater was repeatedly turned on and off by the PID temperature controller based on the feedback system (**Figure 4.2**) to maintain the target temperature. The PID controller worked well in maintaining the target temperature (to

within ± 0.5 °C) as evidenced by the flat plateaus (**Figure 4.4(ii)**) in the plot indicating constant temperatures. As the central zone heated up, heat was rapidly conducted along the silicon bridges to the periphery, with heat being lost to the surrounding gaps as it travelled along the bridges. The temperature of the periphery reached a constant value of ~ 60.0 °C within 25.0 s. Once the central heater was turned off, both the central and periphery cooled to ambient temperature (~ 22.0 °C) within 15 s.

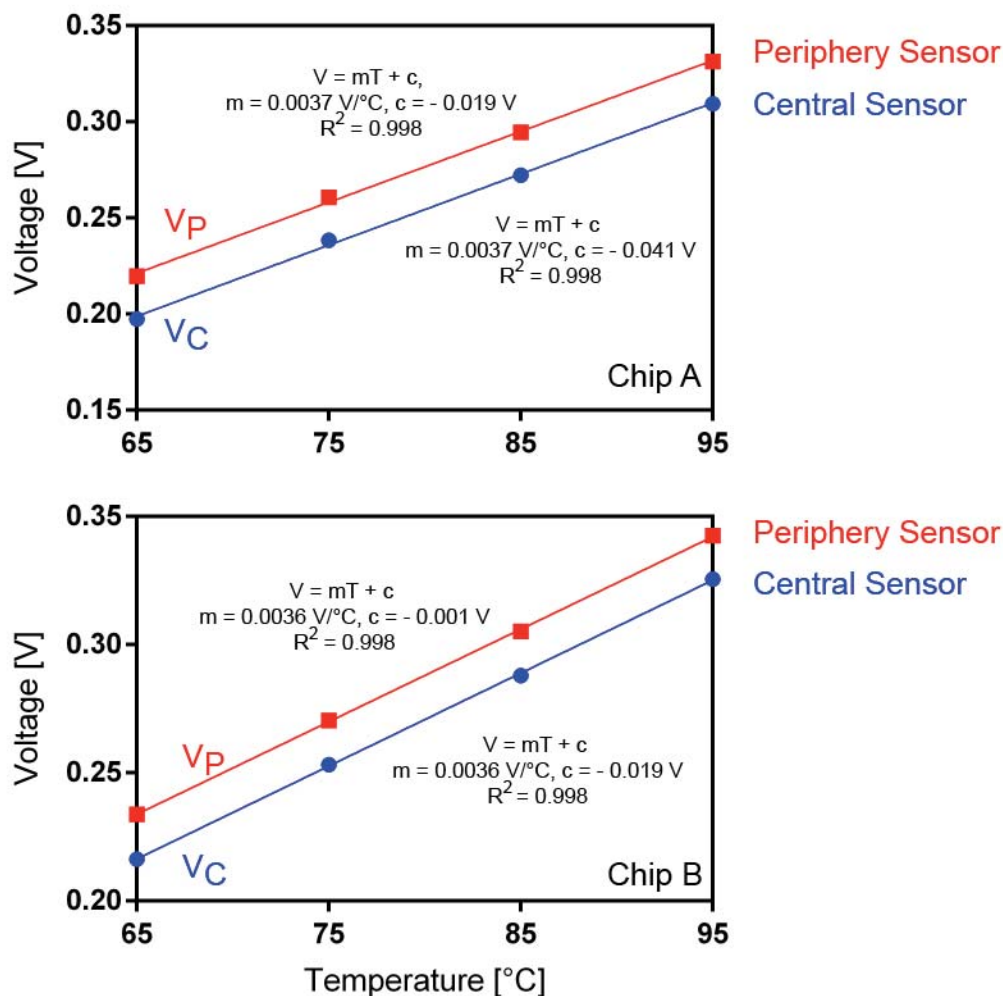


Figure 4.3. Calibration graphs of the central and periphery temperature sensors for two different chips (chip A and B). The calibration graphs were different for each sensor on each PCR chip, differing in both their gradients and the y-axis intersections. All sensors had to be calibrated before they could be used to generate the temperature gradient. A linear relationship was found between the voltages (V_C and V_P) and the temperature (T) on the chip.

The temperature readings from the IR images and from the on-chip temperature sensors were close to the temperature values obtained from the simulation studies (fixed 92.0 °C for the central zone and derived ~ 63 °C for periphery; **Chapter 2, Section 2.4.5**). The slight differences in values could be due to calibration errors or to the fact that the thermal imaging camera was capable of

extracting only the surface temperatures instead of the temperatures inside the microchannels; the simulation results were based on temperatures inside the microchannels.

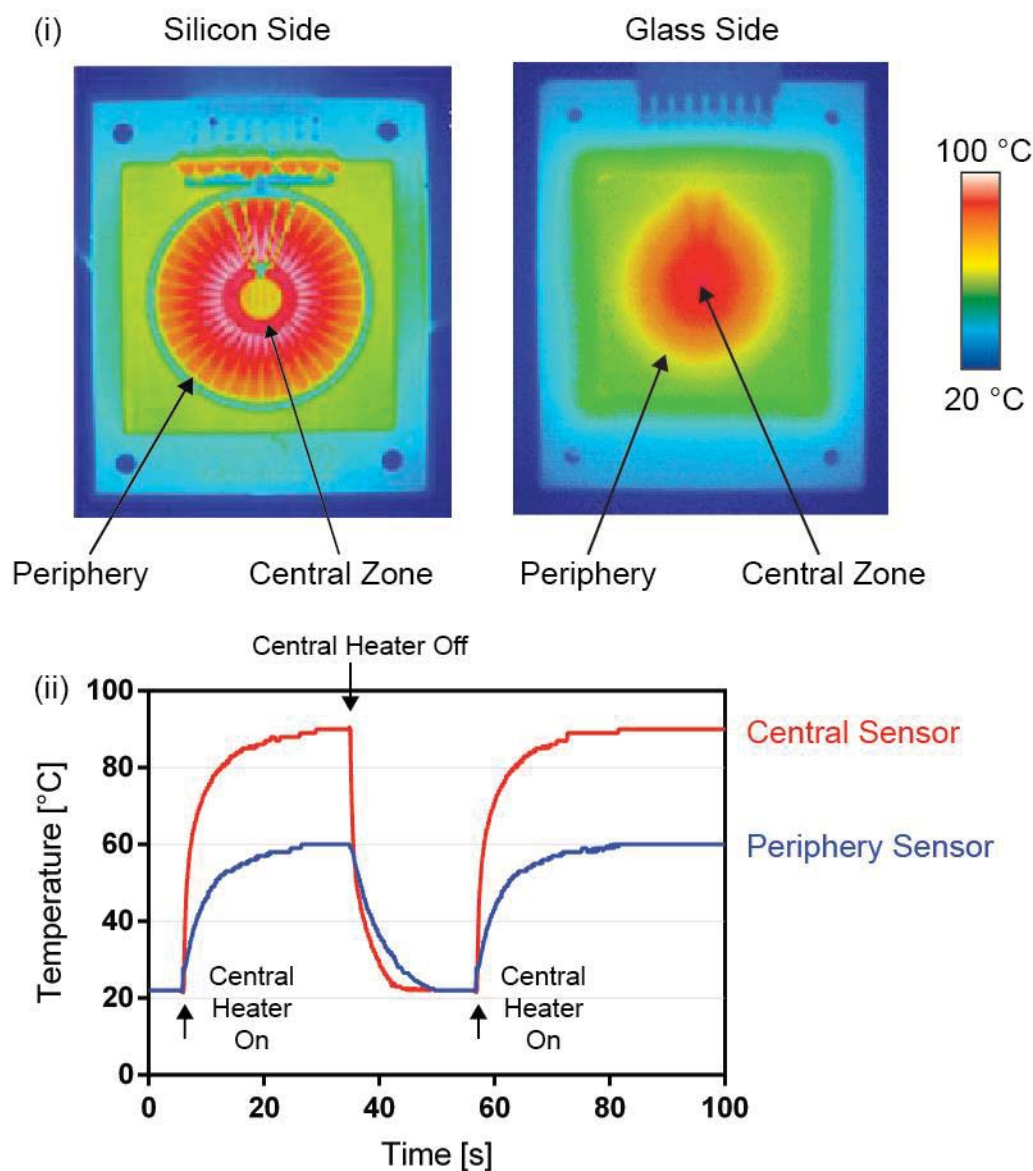


Figure 4.4. (i) IR image of a radial PCR device showing a temperature gradient in which the temperature at central zone is ~ 95 °C (whitish-red) while the temperature at the periphery is ~ 65 °C (orange-yellow). This temperature gradient was achieved by activating only the central heater; the periphery heater was not used at all. No fan cooling was used. (ii) Temperature versus time extracted from calibrated sensors at the centre and periphery of a chip. The set point of the central PID temperature controller was 92.0 °C. When the central heater was switched on, the temperature of the central zone and the periphery increased quickly (within ~ 25.0 s) from ambient temperature (~ 22.0 °C) to steady-state temperatures of 92.0 and 60.0 °C, respectively. The temperature difference between the central zone and the periphery established a temperature gradient along the silicon bridges. When the central heater was turned off, the whole chip cooled rapidly to ambient temperature (~ 22.0 °C).

In order to determine the empirical temperatures within the channels, further experiments utilizing thermochromic dyes could be used.³ By monitoring the colour change of the dyes flowing in the microchannel as a function of radial position, the temperature within the channel could be determined. Similarly, fluorescent probes could also be passed through the channels, and

temperature-dependent lifetime fluorescence studies could be made to determine the temperature profiles of the microchannels.^{4,5} Nevertheless, the temperature characterisations that were used in this work confirmed the existence of a sizeable temperature gradient induced by the presence of the air gaps. The achievable temperature difference across from centre to edge was suitable for PCR applications. On this basis, the temperature gradient was used to conduct continuous-flow PCR.

4.2.2 Employing the Radial Temperature Gradient for Continuous-flow PCR

A. Experimental

To confirm the usability of the temperature gradient for PCR, a “quick” (non-droplet-based) continuous flow PCR experiment was conducted using a centrally-heated chip. A 110 bp segment of the beta-globin gene from the human genomic DNA was used as the target for PCR. The PCR mixture was prepared by adding the following reagents into 200.0 μL of ultrapure distilled water (Invitrogen, USA): 100.0 μL of human genomic DNA templates (30.0 $\text{ng}/\mu\text{L}$) (Roche, USA), 100.0 μL of primers (5.0 μM of each primer: 5-ACACAAGTGTGTTCACTAGC-3, 5-CAACTTCATCCACGTTACC-3) (Roche, USA), 100.0 μL of 5.0 % (by mass) bovine serum albumin (Sigma Aldrich, USA) in ultrapure water (Invitrogen, USA), and 500.0 μL of the Ssofast Evagreen Supermix (Bio-Rad, USA) that contained a pre-mixed of Sso7d fusion polymerase, dNTPs, Evagreen dye in a buffer solution. A negative control was prepared in a similar manner, substituting the template with an equal amount of ultrapure distilled water.

20.0 μL of the negative control and 20.0 μL of the PCR mixture were first tested on a conventional bench-top thermal cycler (Lightcycler 2.0, Roche, USA) using a two-temperature PCR protocol that consisted of a first cycle of 30.0 s initial hot-start activation (92.0 $^{\circ}\text{C}$) and 15.0 s annealing/extension (60.0 $^{\circ}\text{C}$), followed by 35 cycles of 5.0 s denaturation (92.0 $^{\circ}\text{C}$) and 15.0 s annealing/extension (60.0 $^{\circ}\text{C}$). After PCR, sample 1 (negative control) and 2 (positive control) were collected (**Table 4.1**).

To perform continuous-flow PCR using the device (50 μm version, **Chapter 3, Section 3.2.8**), the negative control was loaded into a 1.0 mL plastic syringe (BD, USA) and was pumped into the PCR chip using a syringe pump (PHD Ultra, Harvard Apparatus, USA) at a rate of 0.5 $\mu\text{L}/\text{min}$. The heater on the PCR chip was initially switched off. The negative control was allowed to flow through the unheated chip for 5.0 min before collecting the sample. 20.0 μL of the out-flowing sample was collected (sample 3).

After collection of the first sample, the central heater on the PCR chip was turned on to achieve a constant central temperature of 92.0 °C. The flow rate was maintained at 0.5 µL/min. Once a stable radial temperature gradient had been established, two separate 20.0 µL samples were collected. The first 20.0 µL was discarded because it was subjected to varying temperature conditions while the temperature gradient was establishing. The second 20.0 µL (sample 5) was kept because it corresponded to a fully stabilised temperature distribution on the chip. At a flow rate of 0.5 µL/min, the mixture underwent a PCR duration similar to that on the bench-top thermal cycler: a first cycle of 30.0 s initial hot-start activation (92.0 °C) and 15.0 s annealing/extension (60.0 °C), followed by 35 cycles of 5.0 s denaturation (92.0 °C) and 15.0 s annealing/extension (60.0 °C).

Table 4.1. A summary of the collected samples

Sample	Template or No Template	Bench-top PCR or Chip-based PCR	Subjected to Temperature Gradient on the PCR Chip
1 (Negative Control)	No Template	Bench-top PCR	N.A. (Bench-top)
2 (Positive Control)	Template	Bench-top PCR	N.A. (Bench-top)
3	No Template	Chip-based PCR	No
4	Template	Chip-based PCR	No
5	No Template	Chip-based PCR	Yes
6	Template	Chip-based PCR	Yes

The above step was then repeated using the prepared positive control PCR mixture containing the DNA templates. To change solution, the heater of the PCR chip was first turned off, and the microchannels were flushed with ultrapure water for 10 min before loading with the prepared PCR mixture. Sample 4 was collected without activating the integrated central heater, while sample 6 was collected after subjecting the PCR mixture to the established temperature gradient.

All the collected samples (**Table 4.1**) were analysed for the presence of the 110 bp PCR product using electrophoresis (2100 Bioanalyser, Agilent Technologies, USA). The presence of the PCR product indicated that the PCR was successful.

B. Results and Discussion

Both sample 1 (negative control without DNA templates,) and 2 (positive control with DNA templates) were collected after undergoing a two-temperature PCR protocol on a conventional bench-top thermal cycler. Electrophoretic analysis of sample 2 showed the presence of the 110 bp PCR product (**Figure 4.5**), confirming the efficacy of the two-temperature protocol in inducing successful amplification. Electrophoretic analysis of sample 1 (negative control) showed an absence of the 110 bp PCR product as expected in the absence of DNA template.

Electrophoretic analysis of samples 3 (without DNA templates) and 4 (with DNA templates) – both of which were obtained from the radial PCR device with the heater switched off – did not show the presence of the 110 bp PCR product (**Figure 4.5**) due to the lack of thermal cycling. Electrophoretic analysis of sample 5 (without DNA templates), which was obtained with the heater switched on showed no evidence of the 110 bp PCR product, consistent with the absence of DNA template. Electrophoretic analysis of sample 6 (with DNA templates) however revealed the presence of the 110 bp PCR product (**Figure 4.5**), confirming the ability of the chip (with its in-built temperature gradient) to conduct continuous-flow PCR.

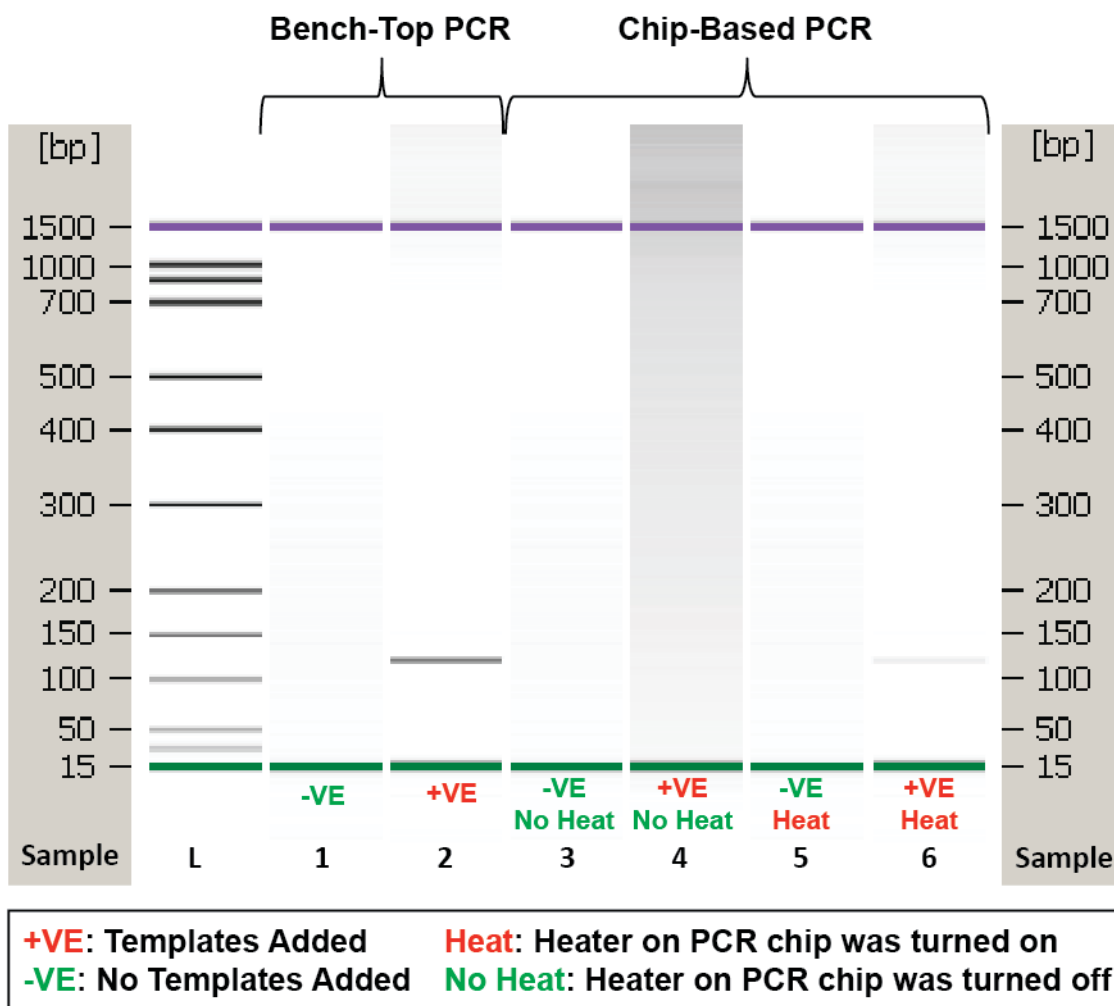


Figure 4.5. Electropherograms of all the collected samples from **Table 4.1**. Sample 6 (positive control obtained on the radial PCR device) showed a faint band at 110 bp, indicating a low yield of the PCR product. The product yield for sample 2 (positive control obtained on thermal cycler) was much higher as indicated by the darker band. Nevertheless, the band (albeit a faint one) in lane 6 indicated successful amplification using the chip.

Although the chip was found to be suitable for carrying out continuous-flow PCR, the yield of the 110 bp PCR product appeared to be lower on chip (Sample 6) than with the bench-top thermal cycler (Sample 2). In the latter case, the band was substantially darker, implying a larger concentration of PCR product. The low yield of the PCR product for the chip-treated sample

(sample 6) was expected because the experiment was done without any optimization of the PCR recipe for chip-based PCR and without any treatment of the microchannels. Continuous-flow PCR inevitably results in surface adsorption and deactivation of the polymerases as they flow through the device, so the low product yield was expected.⁶⁻⁸ The accumulation of residues within the channel over time was especially evident in the hot central zone, where thick residues were clearly visible, eventually clogging the channel and rendering the chip unusable (**Figure 4.6**). The droplet-based approach pursued in the rest of this thesis was intended to prevent surface adsorption and deactivation and to avoid the accumulation of other residues in the channels.^{5,9}

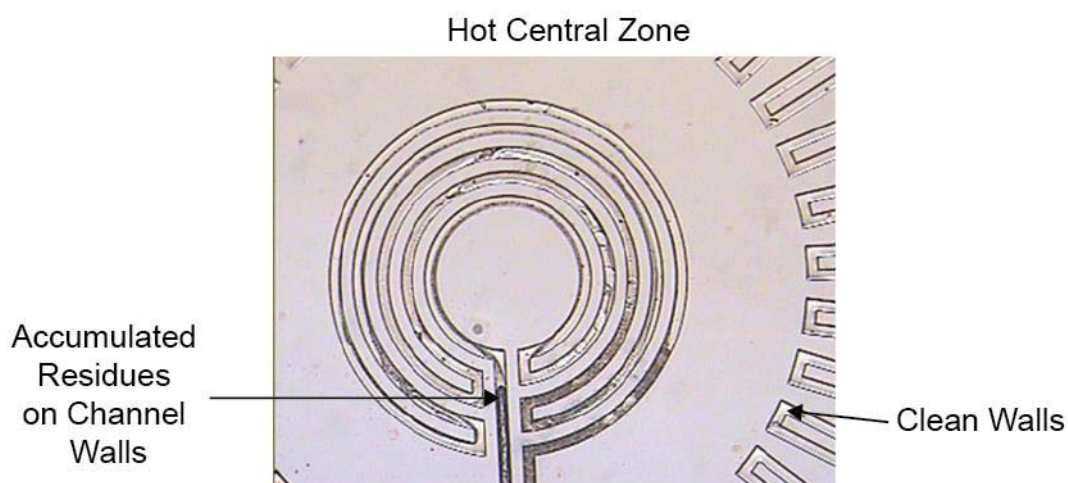


Figure 4.6. Photograph showing clogging of the microchannel in the central zone. The hot central zone was a prime spot for the accumulation of residue, resulting in eventual clogging of the chip. This accumulation was due to loss of polymerases and starting materials for PCR, and was a likely reason for the low PCR product yield.

4.2.3 Summary

In conclusion, following calibration of the temperature sensors, a PID temperature controller was used to control the integrated heaters within the chips and so maintain a stable temperature gradient using only the central heater to heat the central zone to a fixed high temperature of 92.0 °C while the periphery heater was switched off. A temperature gradient was observed along the silicon bridges from 92.0 °C at the central zone to 60.0 °C at the periphery as broadly predicted by the simulation discussed in **Chapter 2**, confirming the effectiveness of the air gaps in promoting cooling. The temperature gradient was shown to be suitable for PCR applications based on the successful (albeit low yield) amplification of a 110 bp PCR product in continuous-flow PCR.

4.3 FLUIDIC CHARACTERISATION

In this section, the fabricated PCR devices were characterised for their ability to form water-in-oil droplets. The ability to form water-in-oil droplets (as opposed to oil-in-water droplets) was essential for the PCR devices because the PCR mixtures are aqueous in nature and therefore must be carried in an oil-based fluid through the microchannels. The oil is used to encapsulate the PCR mixture and prevent it from coming into contact with the walls of the microchannels. It is also to prevent individual droplets from merging with one another.

4.3.1 Surface Modification and Water-in-oil Droplet Generation

A. Experimental: Surface Modification

Before water-in-oil droplets could be generated in the microchannels of the PCR chip, the naturally hydrophilic walls had to be treated to render them hydrophobic (and so prevent the formation of unwanted oil-in-water droplets). Surface modification of the walls with a hydrophobic coating agent was used to achieve the desired hydrophobicity. The chosen coating agent was a 2.0 % mixture of trichloro(1H,1H,2H,2H-perfluorooctyl)silane (97.0 %, Sigma Aldrich, USA) in anhydrous ethanol (Sigma Aldrich, USA). Before the silanising mixture was used in the actual device, its efficacy was first tested on the planar surfaces of glass and oxide-coated silicon substrates (similar to the walls of the microchannels). The substrates were briefly dipped in the silanising mixture and then incubated in an oven at 95.0 °C for 5.0 min. After 5.0 min, the substrate was washed with a fluorinated oil (FC-40, Fluorinert, 3M, USA). The above process was repeated three times. The contact angles of water before and after surface treatment were measured (DSA100, KRÜSS, Germany). Contact angles less than 90.0 ° indicate hydrophilicity, whereas contact angles greater than 90.0 ° indicate hydrophobicity (**Figure 4.7**).¹⁰ Successful silanisation was denoted by a change in contact angle from less than 90.0 ° to more than 90.0 °.

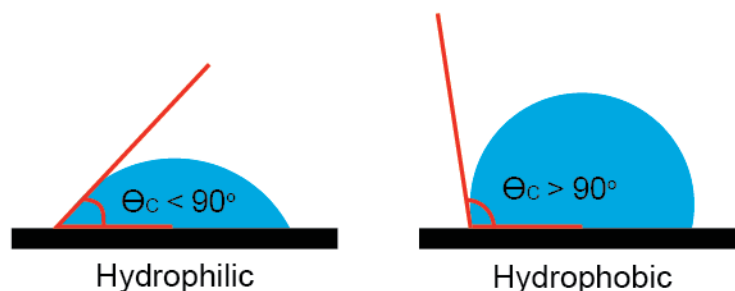


Figure 4.7. The contact angle of water on a planar surface. If the measured contact angle (θ_c) is less than 90 °, the surface is hydrophilic and the water droplet spreads out on the surface. If the measured contact angle is more than 90 °, the surface is hydrophobic and the water retracts from the surface.

The microchannels were treated by continuously pumping the silanising mixture into the PCR chip via the two inlets for 5.0 min. The pumps were then stopped, and the mixture was allowed to remain in the microchannels. The chip together with the fixture (**Figure 3.10**) was then placed in an oven at 95.0 °C for 5.0 min. The above process was repeated three times. The microchannels were then thoroughly flushed with FC-40 (Fluorinert, 3M, USA) to remove any loose silanising mixture in the microchannels. The fluorinated oil was allowed to remain in the chip. At this point, the chip was ready to generate water-in-oil droplets for PCR experiments.

To determine whether the silanisation procedure had successfully changed the walls of the microchannels from hydrophilic to hydrophobic, an aqueous solution of red food dye and FC-40 (Fluorinert Electronic liquid, 3M) were pumped into the microchannels using syringe pumps. In an untreated PCR chip, oil-in-water (clear oil surrounded by red aqueous solution) droplets were expected to form as the red aqueous solution would wet the hydrophilic walls in preference to the oil phase. After silanisation, a switch to water-in-oil (red aqueous dye surrounded by clear oil) droplets was expected since the oil phase would now wet the hydrophobic walls in preference to the red aqueous dye.

B. Experimental: Characterisation of Generated Droplets

After surface treatment of the microchannels, water-in-oil droplet that were generated using two different on-chip droplet generation methods were characterised (**Figure 4.8**).

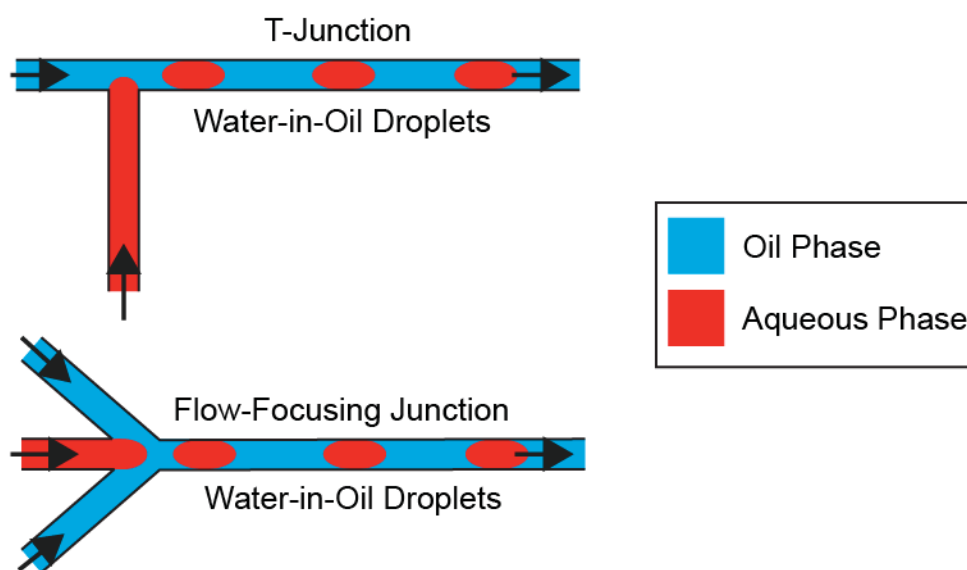


Figure 4.8. The T-junction¹ and flow-focusing junction².

The first method was the use of a T-junction where the oil phase would flow in a straight microchannel while the aqueous phase would enter perpendicularly to the straight

microchannel.¹ In this configuration the oil phase shears the incoming aqueous phase to form water-in-oil droplets. The second method was the use of a flow-focusing junction where the aqueous phase would flow in the middle microchannel and the oil phase would flow in from two side-channels to squeeze, focus and break the central aqueous stream into water-in-oil droplets.²

Important features such as the size and monodispersity of the droplets and droplet generation frequency were characterised for these two droplet generation methods using a confocal laser-induced fluorescence detection system (as described in the PhD thesis by Monpichar Srisa-Art) was used (Figure 4.9).¹¹

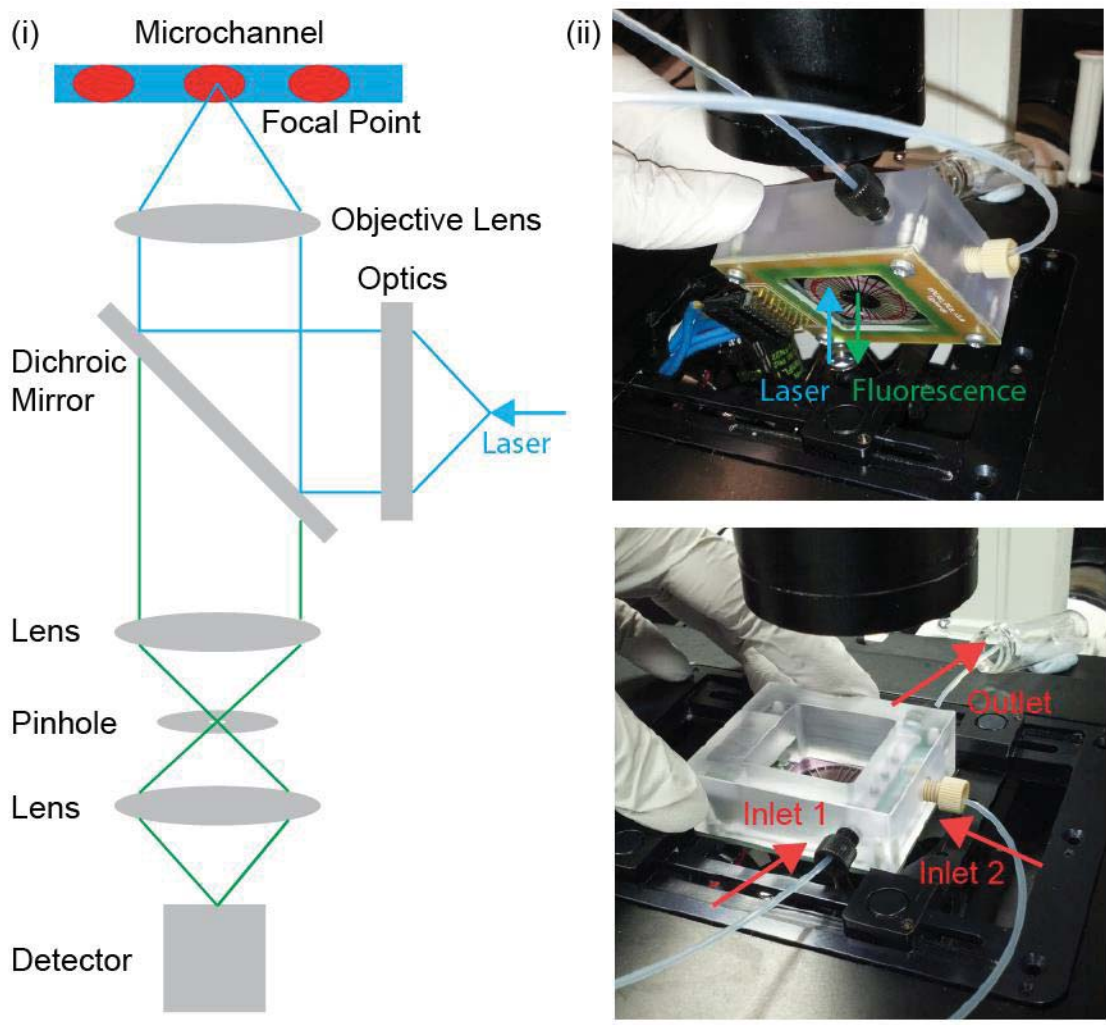


Figure 4.9. (i) Schematic of confocal laser-induced fluorescence detection setup used for droplet characterisation. (ii) Photographs showing the setup of the PCR device on the microscope stage. The laser was focused into a microchannel via the transparent glass side of the chip. For chips using the T-junction, the PCR mixture and oil were pumped into the chip using inlets 1 and 2 respectively; for chips using the flow-focusing junction, the PCR mixture and oil were pumped in using inlets 2 and 1 respectively. The droplets passed through the outlet of the PCR device, and were collected in a vial.

Briefly, as shown in Figure 4.9, the detection system used a cyan (488 nm wavelength) laser as an excitation source. The laser was focused to a point in the middle of the microchannel via the

transparent glass side of the PCR device using a 10x objective. As the generated droplets flowed downstream, droplets containing the PCR mixture plus a fluorescent dye (fluorescein isothiocyanate or FITC) passed sequentially through the excitation point, causing them to emit with a peak wavelength of 518 nm. The fluorescence was monitored using an avalanche photodiode (APD) over a period of 45.0 s, recording one data point every 25.0 μ s. Besides the detection system, a high-speed camera was also used to capture moving and still images of the generated droplets.

250.0 μ L of the aqueous PCR mixture (**Table 4.2**) was prepared by adding the following to 162.5 μ L of ultrapure water (Invitrogen, USA): 50.0 μ L of 5X standard reaction buffer (5X) (OneTaq, NED, USA), 2.5 μ L of 1.0 μ M single-stranded lab-synthesized DNA templates copying the 110 bp segment of the beta-globin gene from the human genomic DNA (**Table 4.3**) (Eurofins, Germany), 6.25 μ L of primers mix (**Table 4.3**) (10.0 μ M each) (Eurofin, Germany), 5.0 μ L of 10.0 mM dNTPs (NED, USA), 5.0 μ L of 5.0 U/ μ L polymerase (OneTaq, NEB, USA), 12.5 μ L of 1.0 % (by mass) bovine serum albumin (Sigma Aldrich, USA) in ultrapure water (Invitrogen, USA), and 6.25 μ L of 10.0 μ M fluorescein isothiocyanate (FITC) (Sigma Aldrich, USA). The actual PCR mixture (as prepared above) was used to characterise the droplets because the PCR mixture had multiple constituents which affected the viscosity of the aqueous phase and so could potentially affect the process of droplet generation.¹²

Table 4.2. Preparation of the PCR mixture

Component	Volume Added		Starting Concentration		Final Concentration	
Ultrapure Water	162.5	μ L	-	-	-	-
Standard Reaction Buffer	50.0	μ L	5	parts	1	parts
DNA Template	2.5	μ L	1.0	μ M	0.01	μ M
Primers Mix	6.25	μ L	10	μ M	0.25	μ M
dNTPs	5.0	μ L	10.0	mM	0.2	mM
Polymerase	5.0	μ L	5.0	U/ μ L	0.1	U/ μ L
Bovine Serum Albumin(BSA)	12.5	μ L	1.0	%	0.05	%
Fluorescein Isothiocyanate (FITC)	6.25	μ L	10.0	μ M	0.25	μ M

Table 4.3. The sequence of the DNA template, and the forward and reverse primers

Component	Sequence	Number of Bases
DNA Template	5-ACACAACCTGTGTTCACTAGCAA CCTCAAACAGACACCATGGTGC ATCTGACTCCTGAGGAGAAGTC TGCCGTTACTGCCCTGTGGGGC AAGGTGAACGTGGATGAAGTTG-3	110
DNA Forward Primer	5-ACACAACCTGTGTTCACTAGCAACC-3	24
DNA Reverse Primer	5-CAACTTCATCCACGTTACCTTG-3	23

During droplet generation, the central heater was set to a target temperature of 92.0 °C. The periphery heater was deactivated. No fan cooling was used. The heater was switch on before droplet generation to allow the stabilisation of the temperature gradient so as to reproduce the operating conditions in a typical PCR run.

The droplets were generated under various flow rates as summarised in **Table 4.4** below. Syringe pumps (PHD Ultra, Harvard Apparatus, USA) were used to control the flow rates of the oil phase and the aqueous phase and hence control the water fraction(W_f), where the water fraction is defined by the following equation:

$$W_f = \frac{U_{aq}}{U_{aq} + U_{oil}} \quad (4.9)$$

where U_{oil} and U_{aq} are the volumetric flow rates of the aqueous phase (PCR mixture) and the oil phase, respectively. The aqueous phase was formed from the PCR mixture described above, while the oil phase was a 1.8 % (by mass) surfactant mixture in FC-40 (Fluorinert, 3M, USA). The surfactant was a perfluorinated polyethers-polyethyleneglycol block-copolymer (PFPE-PEG, **Appendix 9.3**) that was synthesised by a PhD student, Soong-Won Cho.¹³ The surfactant was added to the oil phase to stabilise the droplets after formation. Polyether ether ketone (PEEK) capillary tubes and connectors were connected to the polycarbonate fixture so that fluids could be pumped into and removed from the PCR chip via the fixture (**Chapter 3, Section 3.4**).

Table 4.4. Summary of the various flow rates used for droplet generation

Total Flow Rate (μL/min)	Aqueous Flow Rate (μL/min)	Oil Flow Rate (μL/min)	Water Fraction
0.6	0.12	0.48	0.2
	0.18	0.42	0.3
	0.24	0.36	0.4
	0.30	0.30	0.5
0.8	0.16	0.64	0.2
	0.24	0.56	0.3
	0.32	0.48	0.4
	0.40	0.40	0.5
1.2	0.24	0.96	0.2
	0.36	0.84	0.3
	0.48	0.72	0.4
	0.60	0.60	0.5
1.8	0.36	1.44	0.2
	0.54	1.26	0.3
	0.72	1.08	0.4
	0.90	0.90	0.5
2.4	0.48	1.92	0.2
	0.72	1.68	0.3
	0.96	1.44	0.4
	1.20	1.20	0.5

C. Results and Discussion

Before the surface modification, the water contact angles were $\sim 50^\circ$ and $\sim 70^\circ$ for the glass and oxide-coated silicon substrates, respectively (**Figure 4.10**), indicating partial wetting of the substrates by water in both cases ($\theta_c < 90.0^\circ$). After surface treatment, the contact angles increased to $\sim 103^\circ$ and $\sim 100^\circ$ for the glass and oxide-coated silicon substrates, respectively, confirming the silanisation procedure had rendered the surfaces hydrophobic.

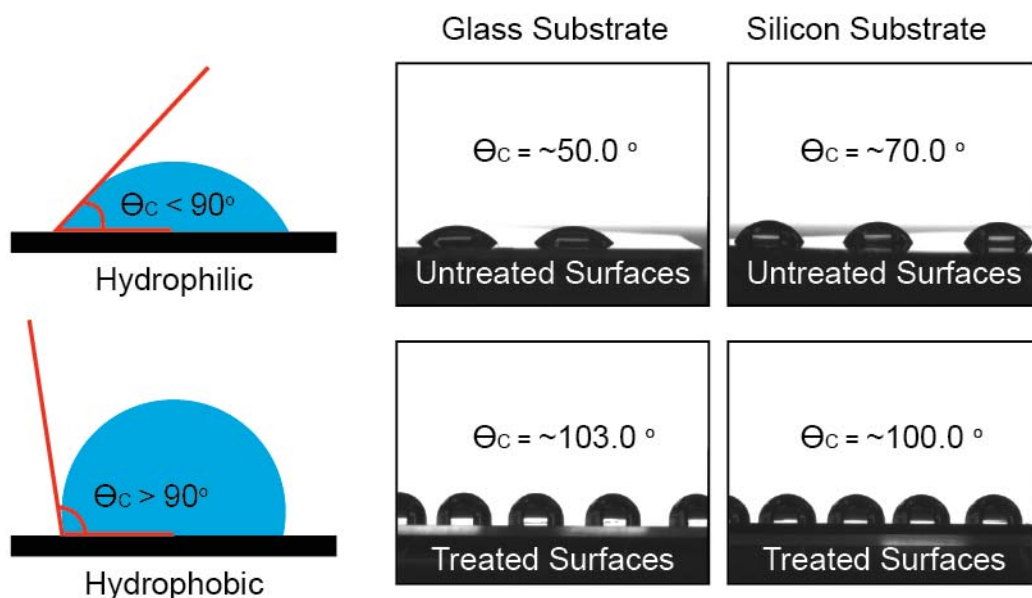


Figure 4.10. Measurement of the contact angles before and after surface treatment. Before surface treatment, the contact angles were $\sim 50^\circ$ and $\sim 70^\circ$ for the glass and oxide-coated silicon substrate, respectively, implying hydrophilicity ($\theta_c < 90^\circ$). After surface treatment, the contact angles increased to $\sim 103^\circ$ and $\sim 100^\circ$ for the glass and oxide-coated silicon substrates, respectively, indicating hydrophobicity ($\theta_c > 90^\circ$). The change of the surfaces from hydrophilic to hydrophobic confirmed the efficacy of the chosen silanisation procedure.

After verifying that the silanisation procedure was effective on planar substrates, the same silanising mixture was used on the microchannels as described above. Before surface treatment, the walls of the microchannels were inherently hydrophilic. As red aqueous dye and FC-40 oil were pumped into the untreated microchannels, oil-in-water droplets formed naturally due to the red aqueous solution wetting the walls in preference to the FC-40 oil phase (**Figure 4.11(i)**).

After surface treatment using the silanisation procedure, a switch to water-in-oil droplets was observed. A photograph showing the formation of oil-in-water droplets in treated microchannels is shown in **Figure 4.11(ii)**. The silanisation process was evidently successful in changing the walls of the microchannels from hydrophilic to hydrophobic, resulting in the FC-40 oil wetting the surface in preference over the aqueous red solution.

Water-in-oil droplets were generated using the T-junction¹ and the flow-focusing junction². A high-speed camera was used to obtain pictures and videos of the droplet generation process. In principle, information concerning the size, monodispersity and generation frequency could be extracted from the still images and videos. However, this was not pursued as the fluorescence analysis using the laser-induced confocal detection system offered a more convenient approach that did not require computationally intensive image processing. A quick observation of the still images of droplet generation using both the T-junction (**Figure 4.12**) and the flow focusing junction (**Figure 4.13**) confirmed that water-in-oil droplets were formed successfully in both cases after the channels had been silanised.

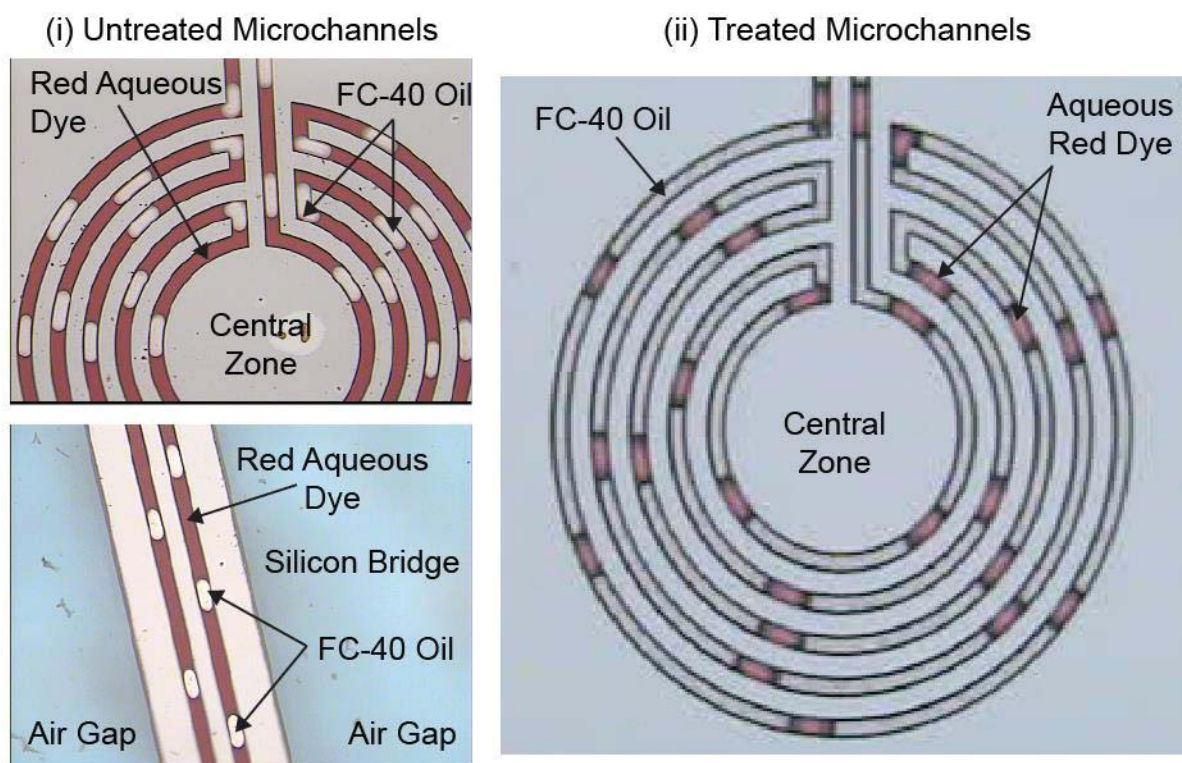


Figure 4.11. Photographs showing switch from oil-in-water droplets to water-in-oil droplet after surface treatment of the microchannels. (i) Pumping red aqueous dye and FC-40 oil into the untreated microchannels of the PCR chip (50 μm variation, **Chapter 3, Section 3.2.8**) led to the formation of (clear oil) droplets surrounded by (red) water due to the hydrophilicity of glass and oxide-coated silicon. (ii) After surface treatment using the silanisation procedure, (red) water droplets in (clear) oil were formed due to the hydrophobic nature of the surface coating.

Using both droplet generation methods, the length of each droplet was observed to increase as the water fraction increased, while holding the total flow rate constant. The increase in droplet length was expected because the increase in the flow rate of the aqueous phase requires the flow rate of the oil to decrease in order to maintain a constant total flow rate (**Equation 4.1**). Therefore, more of the aqueous phase is injected into the channel per unit time, resulting in the formation of a larger volume (i.e. longer) droplets. For both methods, the length of the droplets was observed to decrease if the total flow rate was increased while holding the water fraction constant. This

decrease in length was likely due to the higher flow velocity of the immiscible phase which would cause the aqueous stream to break more readily into smaller droplets.

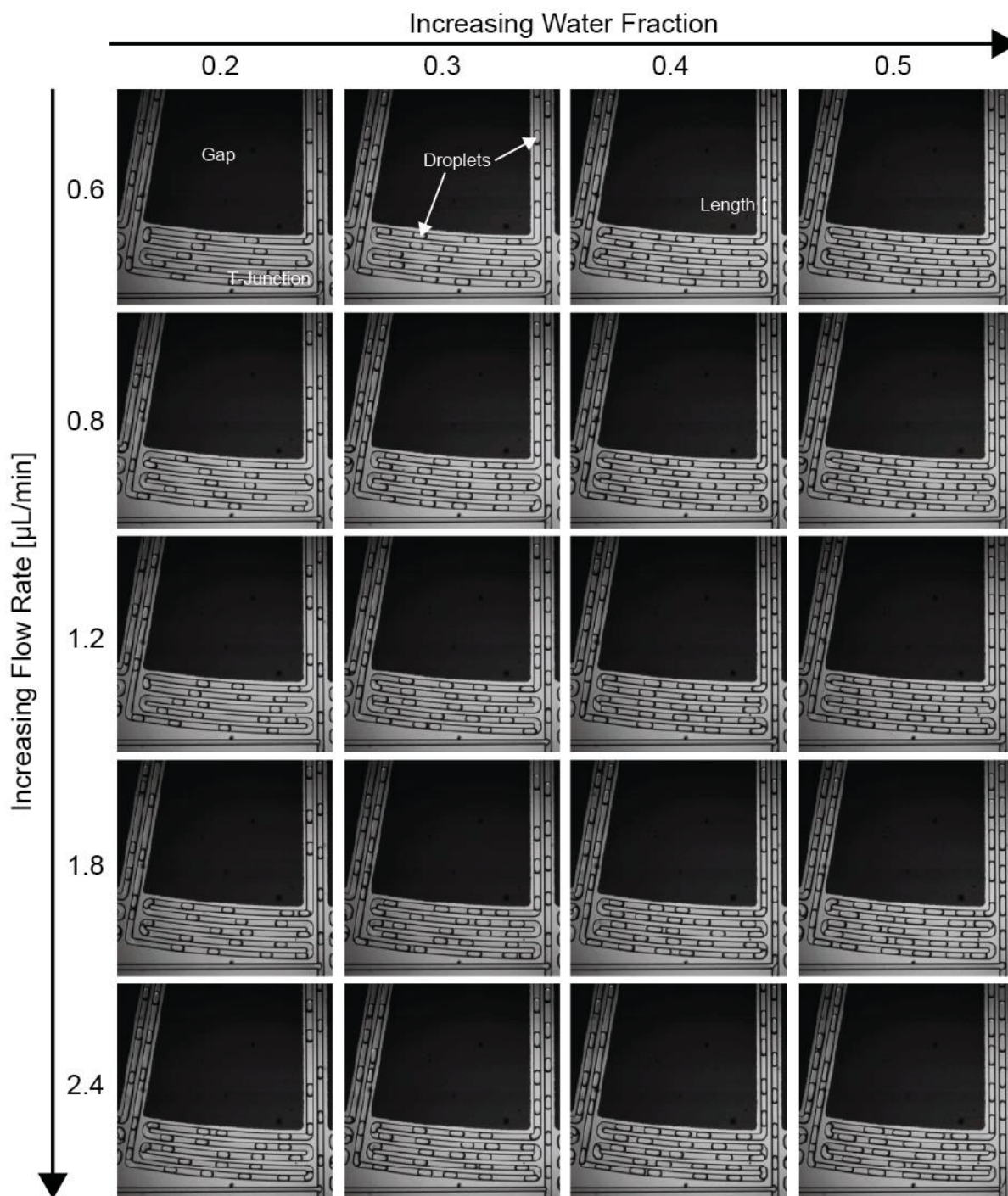


Figure 4.12. A series of still images of droplets generated by the T-junction¹ as total flow rate and water fraction were varied. The oil phase flowed in a straight microchannel while the aqueous phase was introduced perpendicularly from the side of the straight microchannel. The oil phase sheared the incoming aqueous phase to form water-in-oil droplets. As the water fraction increased, the length of each droplet was observed to increase. When the flow rate was increased while holding the water fraction constant, the length of the droplet each droplet was observed to decrease. Water-in-oil droplets were generated successfully using the T-junction in the hydrophobic microchannels.

With the detection system, laser-induced fluorescence from the flowing droplets was monitored for 45.0 s at 25.0 μs interval. A plot of intensity against time showed periodic signal peaks (**Figure**

4.14), corresponding to the arrival of successive droplets. I have written a MATLAB code (Appendix 9.4) to facilitate analysis of the data to allow quick determination of the average volume of the droplet and the monodispersity, and also the droplet generation frequency.

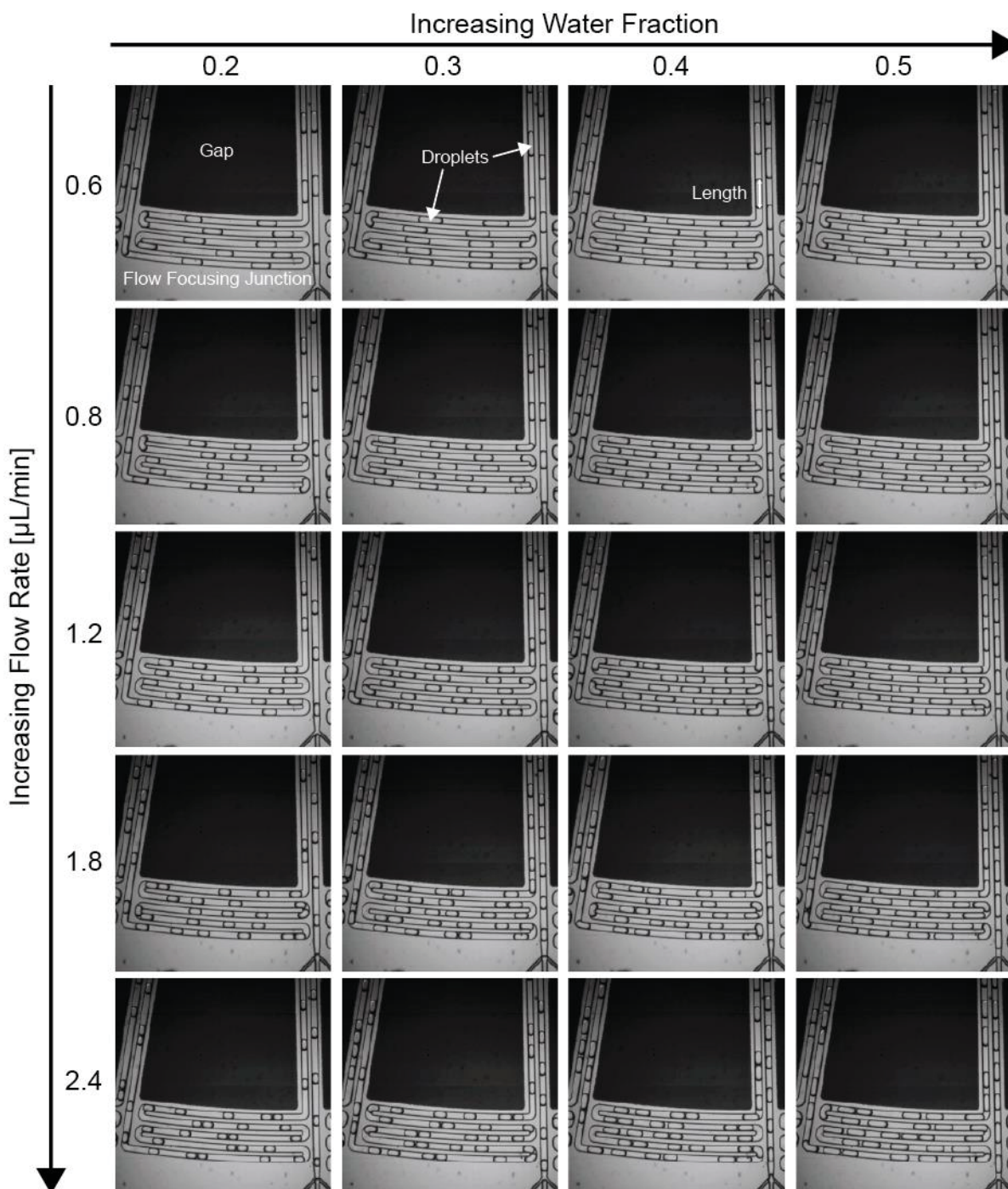


Figure 4.13. A series of still images of droplets generated by the flow-focusing junction² as total flow rate and water fraction were varied. The flow-focusing junction was used to generate water-in-oil droplets. The aqueous phase flowed in the middle microchannel and the oil phase was introduced from two side microchannels to squeeze, focus and break the central aqueous stream into water-in-oil droplets. As the water fraction increased, the length of each droplet was observed to increase. When the flow rate was increased while holding the water fraction constant, the length of each droplet was observed to decrease. Water-in-oil droplets were generated successfully using the flow-focusing junction in the hydrophobic microchannels.

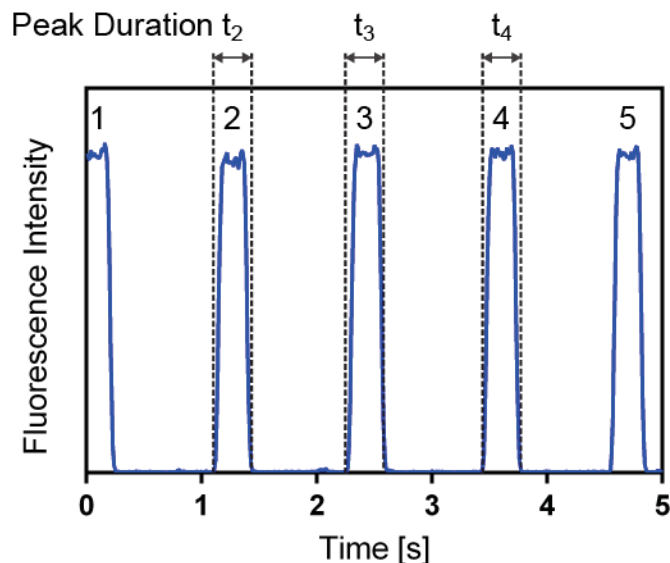


Figure 4.14. Graph showing fluorescence intensity versus time. Each peak corresponds to the arrival of a new FITC-containing droplet at the laser excitation point in the microchannel. By measuring the duration of peak (t_1), the size of droplet 1 in terms of length or volume could be derived from the total flow rate. Measuring multiple peaks (t_1, t_2, \dots, t_n) would then allow for the determination of the average volume and the standard deviation of n droplets. The droplet generation frequency could also be determined by counting the number of signals per unit time.

As a droplet passed through the excitation point at a fixed total flow velocity, the duration of each peak signal allowed length of each droplet to be determined (**Figure 4.14**). In turn, the volume of each droplet could be derived from the known channel dimensions (width and height). By measuring the volume of many droplets, the average volume could be determined (**Figure 4.15**). As previously observed using the still images from the high-speed camera (**Figure 4.12 and 4.13**), for both droplet generation methods, the average volume of the droplets increased as the water fraction increased while the total flow rate was held constant. The average volume of the droplets decreased as the total flow rate increased, while the water fraction was held constant.

Comparing the two methods for the generation of droplets, the average volume of droplets formed from the flow-focusing junction was generally smaller than that formed from the T-junction under the same volumetric flow rates. The reason for the smaller droplets was likely due to the pinching effect from the two oil-phase side-streams, which would cause the central aqueous phase to break more readily into smaller droplets. The T-junction used the oil phase to shear off the single side-stream of the aqueous phase. This process was expected to occur less readily than in the flow-focusing junction, resulting in larger droplets.

The standard deviation of the volume of the droplets was also determined. The derived relative standard deviation (RSD) would give an indication of the monodispersity of the generated droplets. The RSD value of the T-junction was generally higher (between 7.3 to 15.4 %) than the flow-focusing junction (between 3.5 to 14.0 %) (**Table 4.5**). The flow-focusing junction was therefore more likely to generate similar droplets (higher monodispersity) than the T-junction.

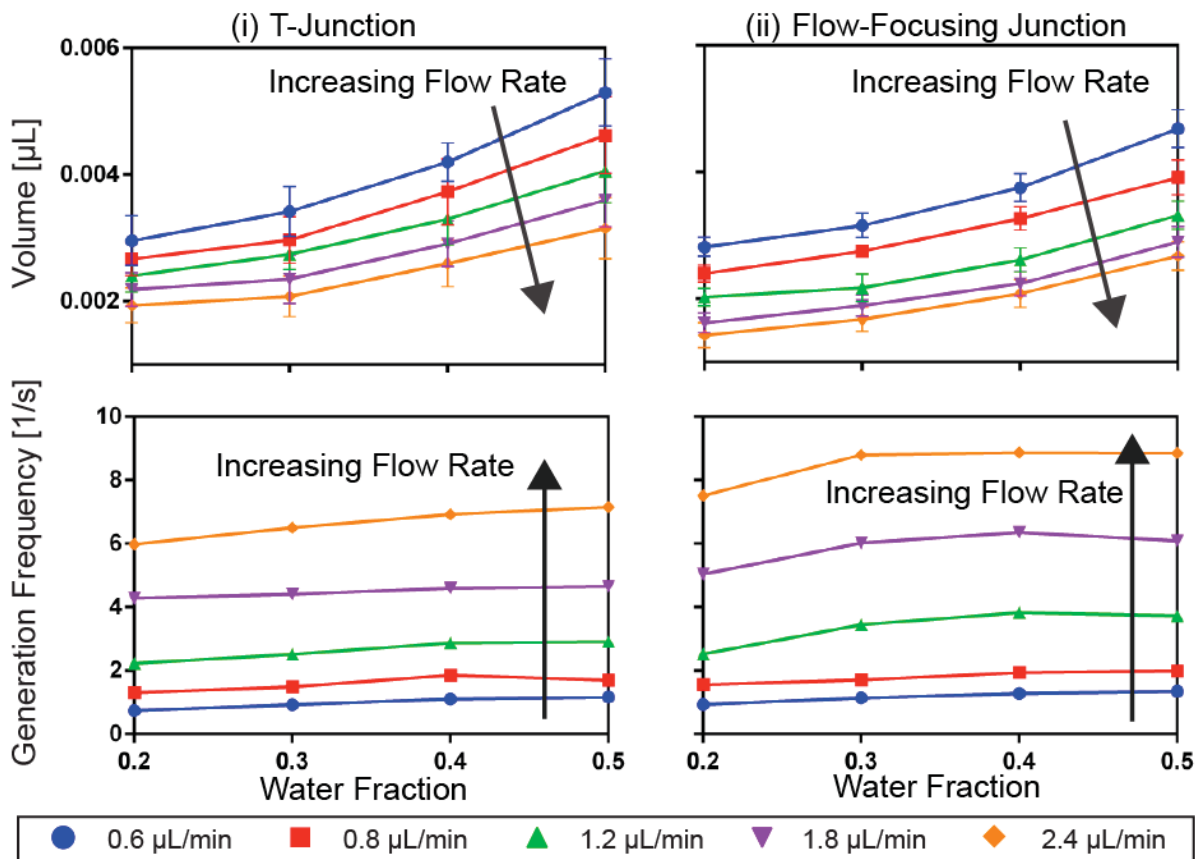


Figure 4.15. Graphs showing volume and generation frequency versus water fraction for droplet generation via a T-junction (i) and flow-focusing junction (ii). For the T-junction, the average volume of the droplets increased as the water fraction was increased. The average volume of the droplets decreased as the total flow rate was increased, while holding the water fraction constant. The droplet generation frequency did not vary appreciably with water fraction but showed a relatively strong increase with flow-rate. (ii) The general trends for the flow-focusing junction were similar to those observed with the T-junction. The average volume of droplets formed by the flow-focusing junction was generally smaller than for the T-junction under the same conditions. The droplet generation frequency of the flow-focusing junction was generally higher than for the T-junction under the same conditions.

Table 4.5. The RSD at various total flow rates and water fractions for a T-junction and a flow-focusing junction.

Water Fraction	T-Junction					Flow-focusing Junction				
	RSD [%] at Various Total Flow Rate					RSD [%] at Various Total Flow Rate				
	[$\mu\text{L}/\text{min}$]					[$\mu\text{L}/\text{min}$]				
	0.6	0.8	1.2	1.8	2.4	0.6	0.8	1.2	1.8	2.4
0.2	13.3	10.0	10.7	12.3	14.0	5.4	5.7	6.9	9.9	14.0
0.3	11.4	12.2	8.9	16.3	15.3	6.1	3.5	9.8	9.0	11.6
0.4	7.3	14.0	12.2	12.3	14.3	6.0	5.7	7.2	8.6	10.6
0.5	10.0	13.2	12.4	11.8	15.4	6.4	7.0	6.7	8.4	8.4

The droplet generation frequency (number of droplets generated per unit time) could also be determined by counting the number of signals for a fixed duration (**Figure 4.15**). For the T-junction, the droplet generation frequency remained fairly constant as the water fraction increased while keeping the total flow rate constant. However, it increased substantially when the total flow rate was increased while keeping the water fraction constant. This general behaviour was also observed for the flow-focusing junction. Comparing the two methods in the high flow-rate regime, the flow-focusing junction tended to have a higher droplet generation frequency under equivalent flow conditions, consistent with the previously described formation

of smaller droplets. As such, the empirical results showed that flow-focusing junction might be better suited to achieving high droplet generation frequencies when working at high total flow rates (more than 1.8 $\mu\text{L}/\text{min}$). At lower total flow rates (less than 0.8 $\mu\text{L}/\text{min}$), both the T-junction and flow-focusing junction had similar droplet generation frequencies of less than 2 droplets/s.

The size and monodispersity of the droplets and the droplet generation frequency are important parameters for PCR experiments and were duly characterised for both the T-junction¹ and the flow-focusing junction². The average size of the droplet determines the volume of PCR mixture encapsulated in each droplet. For digital PCR, the volume is a critical parameter as it determines the number of DNA templates that are encapsulated in each droplet at high dilution.^{14,15} For accurate and reliable digital PCR, it is obviously important to achieve high monodispersity so that all the droplets are of uniform size and so encapsulate the same volume of PCR mixture.^{14,15} The droplet generation frequency determines the throughput of the chip. A high droplet generation rate will result in many droplets being detected (and analysed) per unit time. Being able to probe more droplets in a given time period improves the reliability of the digital PCR data analysis.^{14,15} On this basis, the flow-focusing junction appeared to be a better choice than the T-junction as it formed smaller and more monodisperse droplets at a slightly higher frequency.

4.3.2 Summary

In conclusion, the newly fabrication PCR device was able to generate water-in-oil droplets using both the T-junction and the flow-focusing junction after changing the hydrophilic walls of the microchannels to hydrophobic. The flow-focusing junction was able to form smaller and more monodisperse droplets than the T-junction. The flow-focusing junction had a slightly higher droplet generation frequency than the T-junction.

4.4 CONCLUSIONS

In this chapter, the newly fabricated devices were characterised for their thermal and fluidic functionalities. The integrated central heaters, temperature sensors and air gaps were used together to create a temperature gradient on the chip, varying from 92.0 °C at the centre to 60.0 °C at the periphery. This temperature gradient was used successfully for continuous-flow PCR, although the yield of the PCR product was low. Water-in-oil droplets were also generated successfully on the chip after treating the microchannel surfaces with a silanising agent. After the thermal and fluidic characterisation of the PCR device, the chip was ready to be used to conduct droplet-based PCR experiments as described in the **Chapter 6**.

Chapter 5

A model PCR reaction was optimised on a bench-top thermal cycler for subsequent translation to the PCR devices for droplet-based PCR. In this chapter, the steps required to optimise the PCR recipe are described.

5.1 INTRODUCTION

Before droplet-based PCR was performed, the various reaction components were optimised on a bench-top thermal cycler. A typical PCR experiment requires the following components (**Chapter 1, Section 1.1.2**): a DNA template containing a specific target sequence for amplification, a pair of primers that determines which specific sequence on the DNA template will be targeted, a probe which provides a real-time (usually fluorescence-based) signal to report the progress of the reaction, a polymerase which uses the available dNTPs to extend the annealed primers to replicate the target sequence, and finally a buffer solution (with various additives) which affects the stability and yield of the reaction.

5.1.1 DNA Template

For the work reported here, a 110 bp segment of the beta-globin gene was targeted. This segment is of interest since sickle cell anaemia is caused by a single-base substitution or a point mutation¹ in this gene segment (**Figure 5.1**).

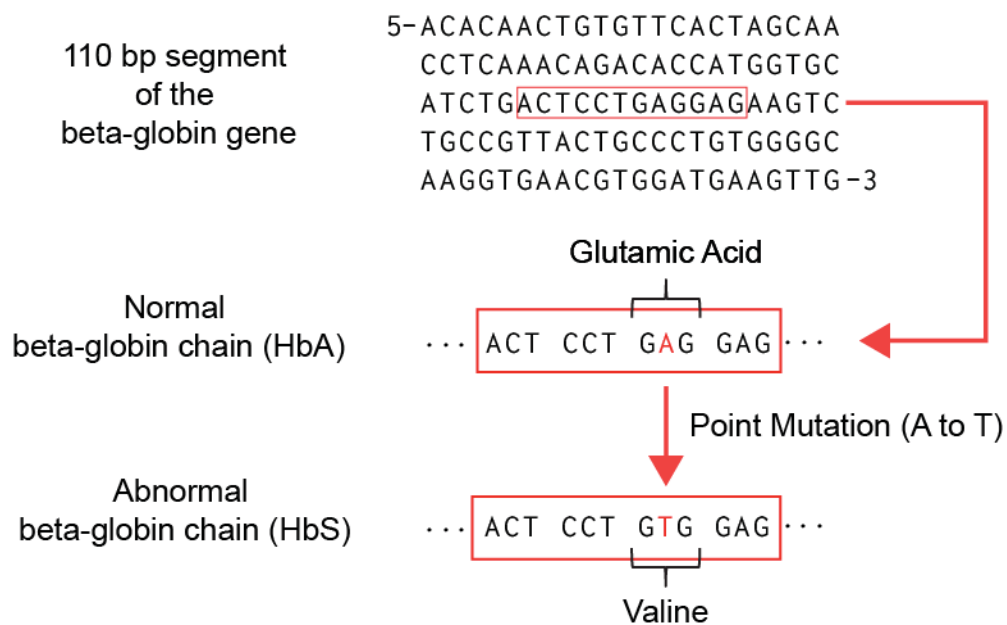


Figure 5.1. The sequence of the 110 bp segment of the beta-globin gene. Sickle cell anaemia is caused by a point mutation¹ in the segment where the base adenine (A) is substituted with thymine (T). As a result of this mutation, the amino acid glutamic acid is replaced with valine, which causes the red-blood cell to take on an abnormal “sickle” shape.

As a result of the mutation, the codon GAG is replaced by GTG which results in the replacement of the hydrophilic amino acid glutamic acid with the hydrophobic amino acid valine.^{2,3} The hydrophobic region in the protein causes the red blood cell to warp and adopt a “sickle” shape. Such sickle-shaped red blood cells are destroyed prematurely in the body, leading to a reduction of red blood cells that in turn causes anaemia.

The selected template was a lab-synthesised (Eurofins, Germany) 110 bp segment of the beta-globin gene (**Figure 5.1**) (as opposed to the whole human genomic DNA previously in the continuous-flow PCR experiment (**Chapter 4, Section 4.2.2**)). Moreover, instead of using double-stranded DNA, only the single-stranded sequence was used to avoid the need for an initial incubation period in which the double-stranded DNA is denatured prior to primer annealing.

5.1.2 Primers

In the previous continuous-flow PCR experiments (**Chapter 4, Section 4.2.2**), the primers (F1 and R1, **Table 5.1**) that were used to target the 110 bp beta-globin segment had 20 bases each. The forward primer (F1) and the reverse complimentary (R1) primer had melting temperatures of 55.3 and 57.3 °C, respectively, as reported by the manufacturer (Eurofins, Germany).

Table 5.1. Sequences of the primers F1, R1 and F2, R2.

Primer	Sequence	Number of Base	Melting Temperature [°C]*	Annealing Temperature [°C]
F1	5'-ACACAACCTGTGTTCACTAGC-3'	20	55.3	61.9
R1	5'-CAACTTCATCCACGTTCCACC-3'	20	57.3	62.5
F2	5'-ACACAACCTGTGTTCACTAGCAACC-3'	24	61.0	63.6
R2	5'-CAACTTCATCCACGTTCCACCTTG-3'	23	60.6	63.5

*The melting temperatures were provided by Eurofins, Germany.

The melting temperature is defined as the temperature at which the duplex DNA dissociates to single strands, and indicates the stability of the duplex.⁴ The melting temperature has a strong influence on the annealing temperature, which is defined as the temperature at which the primer binds to the DNA template to form a primer-template hybrid.^{5,6} At a working temperature higher than the annealing temperature of the primer, insufficient primer-template hybridization will occur, resulting in a low yield of the PCR product. At a working temperature lower than the annealing temperature of the primer, non-specific PCR products will be generated due to non-specific primer association with the DNA template.

The annealing temperature can be determined from the melting temperatures of the PCR product and the primers according to^{5,6}

$$T_a = 0.3 \times T_{m(\text{primer})} + 0.7T_{m(\text{product})} - 14.7 \quad (5.10)$$

where $T_{m(\text{primer})}$ is the melting temperature (°C) of the primers, and $T_{m(\text{product})}$ is the melting temperature (°C) of the product (86 °C, determined empirically by melting analysis).

From **Equation 5.1**, F1 and R1 were estimated to have annealing temperatures of 61.9 and 62.5 °C, respectively (**Table 5.1**). For the PCR reaction to proceed on-chip, the annealing temperature

must lie within the working range of the fabricated device. With a central zone temperature of 92.0 °C, the steady-state temperature at the periphery was 60.0 °C (**Chapter 4, Section 4.2.1**), assuming the periphery heater is switched off and no fan-cooling is used. The maximum working temperature at the central zone was 99.0 °C, i.e. just below the boiling point of water. With a central temperature of 99.0 °C, the periphery temperature was 67.0 °C. Accordingly, due to the constraints on the central temperature, the temperature at the periphery was restricted to lie between 60.0 to 67.0 °C.

Comparing the working temperature range (60.0 to 67.0 °C) of the PCR device and the annealing temperatures of F1 and R1 (61.9 and 62.5 °C), the primers F1 and R1 were expected to anneal to the DNA template efficiently. However, the PCR device was required to work near its lower temperature limit (60.0 °C) in order for F1 and R1 to work. If the periphery temperature was too high (> 62.5 °C), then a low PCR product yield was expected. If a low periphery temperature (< 60.0 °C) was used, the central temperature should then be reduced (< 92.0 °C) and denaturation of the DNA template might not be possible. Hence, the usable temperature range at the periphery was narrowed to be between 60.0 to 62.5 °C.

To obtain a wider usable temperature range it was decided to use primers with higher annealing (and therefore melting) temperatures. This was achieved by extending the length of F1 and R1. F1 was lengthened by four bases, while R1 was lengthened by three bases. The new primers (F2 and R2) had melting temperatures of 61.0 and 60.6 °C, respectively as reported by the manufacturer (Eurofins, Germany). From **Equation 5.1**, the expected annealing temperatures for F2 and R2 were 63.6 and 63.5 °C, respectively. Though the calculated increase was relatively small (around 1.0 °C), the effective working range of 60.0 to 63.5 °C provided greater operational flexibility.

The length of the primers could not be increased much further to increase the melting temperature, since longer primers have a greater tendency to form self-dimers and primer-dimers, lowering reaction yields.⁷ The recommended length range for primers is between 18 and 22 bases.⁴ The new primers F2 and R2 were already 24 and 23 base long, so increasing the length was avoided.

5.1.3 Probe

A TaqMan probe^{8,9} was required in the PCR mixture to provide a real-time fluorescence signal that would vary with the concentration of the PCR product. The TaqMan probe contained a complementary base sequence to the 110 bp DNA template where the point mutation was located,

ensuring selectivity. (**Table 5.2**). Besides the base sequence, the TaqMan probe contained a fluorophore attached at the -5' end and a quencher dye attached at the -3' end of the base sequence.⁸ The selected fluorophore for P1 was carboxyfluorescein or FAM that has an excitation peak (λ_{ex}) at 494 nm and an emission peak (λ_{em}) at 518 nm.¹⁰ The corresponding quencher dye was "black hole quencher 1" (BHQ1) that has an absorption peak (λ_{abs}) at 535 nm and absorbs over between 480 to 580 nm.⁹⁻¹¹ Due to the close proximity of the reporter and the quencher dye, the fluorescence of FAM is partially quenched by BHQ1 due to fluorescence resonance energy transfer (FRET).^{9,12}

Table 5.2. Sequences of the TaqMan probes.

Primer	Sequence	Number of Base	Melting Temperature [°C]*	Annealing Temperature [°C]
P1	5'-FAM-CCTGAGGAGAAGTCTGCCGT-BHQ1-3'	20	61.4	63.7
P2	5'-F-CCTGTGGAGAAGTCTGCCGT-Q-3'	20	NA	NA

*The melting temperatures were provided by Eurofins, Germany

During PCR (**Figure 5.2**), the probe anneals specifically to its target sequence on the DNA template. As the polymerase extends the primer, the polymerase eventually reaches the location where the TaqMan probe is bound, cleaving the bound TaqMan probe due to its 5'-3' exonuclease activity. Once the TaqMan probe is cleaved, the reporter dye is released into solution and its fluorescence is no longer quenched by BHQ1, causing the fluorescence intensity of FAM to increase.^{8,12} With every cycle of PCR, the above process repeats itself, with more TaqMan probes being cleaved and the fluorescence intensity increasing proportionally. Only one probe (P1) (**Table 5.2**) was used at this stage because only the DNA template of the normal sequence (not the mutated one) was used for PCR.

The annealing temperature of the TaqMan probe is an important parameter controlling real-time detection. If the working temperature is higher than the annealing temperature of the probe, insufficient probe-template hybridization will occur. Hence, a low fluorescence signal will result. If the working temperature is lower than the annealing temperature, the probe may undergo hybridization with other primers or with other probes in the PCR mixture. Fluorescence due to non-specific products may therefore occur.

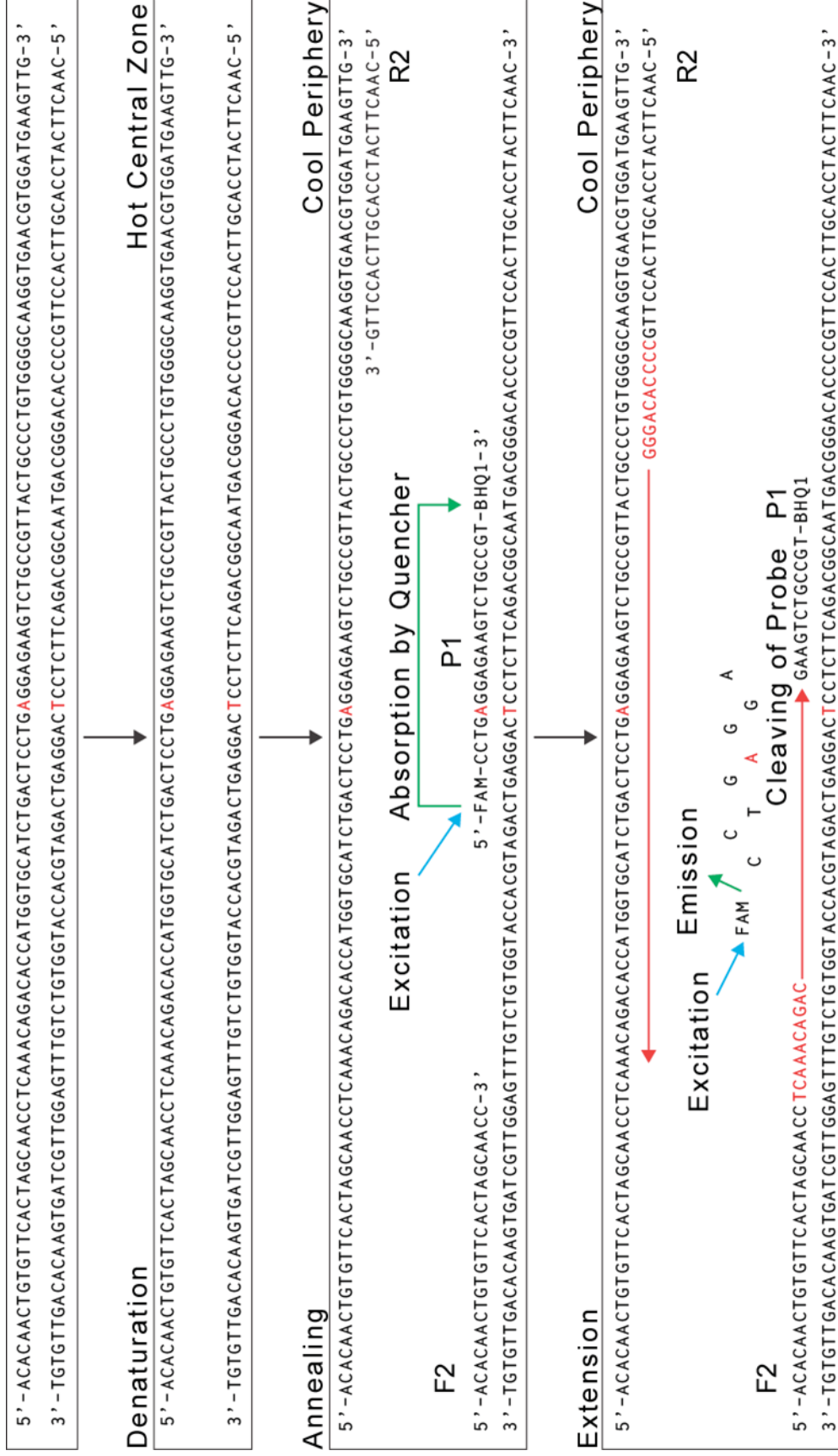


Figure 5.2. Flow chart showing PCR (at cycle > 1) with the selected DNA template, primers (F2 and R2) and TaqMan probe (P1). At the hot central zone, the double-stranded DNA template accumulated during previous cycles undergoes denaturation to form two individual strands. When the mixture is moved to the cool periphery, annealing of the primers and probe occur. This is immediately followed by extension of the primers by the polymerase. As the polymerase replicates the template, the annealed TaqMan probe is cleaved to release the reporter dye.

As such, the TaqMan probe should have an annealing temperature that matches that of the primers. If their annealing temperatures are similar, the probe and primers will anneal to the DNA template under similar conditions at their respective sites once the PCR mixture has flowed into the cool periphery (60.0 to 67.0 °C depending on the central temperature). The probe was therefore designed to contain a 20 base sequence with a melting temperature of 61.4 °C (Eurofins, Germany). The calculated annealing temperature was 63.7 °C based on **Equation 5.1**, closely matching the annealing temperature of F2 (63.6 °C) and R2 (63.5°C).

5.1.4 Polymerase

In a typical flow-based PCR experiment the PCR mixture is left standing in a syringe at room temperature for an extended period of time (before being injected into the PCR device). There is therefore a risk that the PCR mixture might develop some PCR activity, leading to the formation of non-specific PCR products. False positives might also be possible due to PCR product being formed before entering the chip. This can be avoided by using a so-called “hot-start” polymerase that is designed to exhibit minimal PCR activity at low temperatures.¹³

The chosen polymerase was the *OneTaq* Hot-Start DNA Polymerase (NEB, USA). According to the manufacturer, *OneTaq* is a mix of *Taq* and *Deep Vent* DNA polymerases. The included *Deep Vent* DNA polymerase in the blend increases the fidelity of the PCR reaction.¹⁴ The *Taq* DNA polymerase has 5'-3' exonuclease activity which is needed to cleave the TaqMan probe to release the reporter dye during the extension cycle in PCR (**Figure 5.2**). *OneTaq* contains an aptamer-based inhibitor, that ensures that PCR is not initiated until the hot-start polymerase is activated above 45.0 °C (at which temperature the aptamer inhibitor is released from the polymerase).¹⁴ Thermal activation is easily achievable on the fabricated PCR device because a cycle of polymerase activation at the hot central zone (typically above 90.0 °C) is implemented in the first cycle.

5.1.5 Buffer

Two different buffers for PCR are provided with the *OneTaq* DNA polymerase (NEB, USA). The first buffer is the standard reaction buffer (**Table 5.3**) recommended by the manufacturer for products containing less than 50 % GC in the sequence, while the second buffer is the GC reaction buffer (**Table 5.4**) recommended for products containing more than 65 % GC in the sequence.¹⁴ The GC reaction buffer is also recommended when working with difficult amplicons or when PCR does not work with the standard reaction buffer. The GC reaction buffer includes DMSO that disrupts the base pairing, allowing easier splitting of DNA templates into single strands for

annealing by primers.^{15,16} Glycerol is believed to reduce secondary conformations (dimer structures) of the DNA templates that might lead to decreased product yield or failure in PCR.^{17,18} The 110 bp PCR product had a GC content of 51.8 %. As such, for the initial experiments standard reaction buffer was chosen for the PCR experiments first even though the GC content of the PCR product was slightly more than 50 %.

Table 5.3. Constituents in 1X OneTaq standard reaction buffer¹⁴

Component	Concentration	
Tris-HCl (pH 8.9 at 25 °C)	20.0	mM
MgCl ₂	1.8	mM
NH ₄ Cl	22.0	mM
KCl	22.0	mM
IGEPAL CA-630	0.06	%
Tween 20	0.05	%

Table 5.4. Constituents in 1X OneTaq GC reaction buffer¹⁴

Component	Concentration	
Tris-SO ₄ (pH 9.2 at 25 °C)	80.0	mM
MgSO ₄	2.0	mM
(NH ₄) ₂ SO ₄	20.0	mM
Glycerol	5.0	%
DMSO	5.0	%
IGEPAL CA-630	0.06	%
Tween 20	0.05	%

5.1.6 Other Components

Bovine serum albumin (BSA) (Sigma Aldrich, USA) was added to the PCR mixture as an additive because it is known to increase PCR yields from low purity templates and also to prevent the adhesion of polymerase to surfaces.¹⁹ Deoxynucleotides or dNTPs (NEB, USA)²⁰ were added because they are the building blocks which the polymerase uses to extend the primers. Water was added to dilute the components in the PCR mixture to the required concentrations. Water of RT-PCR grade (Ambion, USA) was used to ensure no nuclease and DNA contamination. With the above selected components, the PCR mixture was prepared and then tested on a bench-top thermal cycler. The recipe was optimized by varying the concentrations of the TaqMan probe, the primers and also the DNA template.

5.2 EXPERIMENTAL

5.2.1 Starting Recipe

To test the PCR mixture on a bench-top thermal cycler, a starting PCR mixture was first prepared by mixing the selected components at concentrations recommended by the manufacturer of *OneTaq* polymerase.

To prepare 250.0 μL of the PCR mixture, the following components were added to 162.5 μL of water: 50.0 μL of the standard reaction buffer (5x) (**Section 5.1.5**), 2.5 μL of the lab-synthesised 110 bp DNA templates (1.0 μM) (**Section 5.1.1**), 6.25 μL of the primer mixture with F2 and R2 (each at a concentration of 10.0 μM) (**Section 5.1.2**), 5.0 μL of dNTPs (10.0 mM), 5.0 μL of the polymerase (5.0 U/ μL) (**Section 5.1.4**), 12.5 μL of bovine serum albumin in ultrapure water (1.0 % by mass) (**Section 5.1.6**), and 6.25 μL of the TaqMan probe P1 (10.0 μM) (**Section 5.1.3**). To prepare the negative control, an equal volume of RT-PCR grade water was used in place of the DNA template solution. The above recipe is summarised in **Table 5.5**.

Table 5.5. Recipe of the starting PCR mixture

Component	Volume Added		Starting Concentration		Final Concentration	
		μL				
Water (RT-PCR Grade)	162.5	μL	-	-	-	-
Standard Reaction Buffer	50.0	μL	5	parts	1	parts
DNA Template*	2.5	μL	1.0	μM	10^{-2}	μM
Primer Mix (F2 and R2)	6.25	μL	10.0	μM	0.25	μM
dNTPs	5.0	μL	10.0	mM	0.2	mM
OneTaq Hot-Start Polymerase	5.0	μL	5.0	U/ μL	0.1	U/ μL
Bovine Serum Albumin(BSA)	12.5	μL	1.0	%	0.05	%
TaqMan Probe (P1)	6.25	μL	10.0	μM	0.25	μM

*To prepare a negative control, an equal volume of ultrapure water was used in place of the DNA template.

Though precautionary measures such as the addition of BSA (**Section 5.1.6**) to the PCR mixture and surface treatments with a silanising mixture were carried out, four times the recommended concentration of polymerase was used so as to compensate for any possible loss of polymerase to the surfaces of the glass syringes and the microchannels used in chip-based PCR.¹⁹ This use of additional polymerase was costly but ensured a higher chance of successful chip-based PCR. Once chip-based PCR was successful, the amount of polymerase could be scaled back to determine if the excessive polymerase is crucial.

Bench-top PCR experiments were conducted using the Lightcycler 2.0 (Roche, USA). This system uses glass capillaries instead of plastic PCR tubes. As polymerase is known to adsorb and deactivate on glass surfaces, the capillaries were silanised before use.¹⁹ The silanising mixture consisted of a 2.0 % mixture of trichloro(1H,1H,2H,2H-perfluorooctyl)silane (97.0 %, Sigma Aldrich, USA) in anhydrous ethanol (Sigma Aldrich, USA). 20.0 μL of the silanising mixture was injected into the glass capillaries which were left in a sterile oven (40.0 $^{\circ}\text{C}$) for 1 h. The openings of the glass capillaries were sealed to prevent evaporation of the mixture. After 1 h, the mixture inside the glass capillaries was removed by centrifugation (2000 rpm for 10.0 s). To flush the inside of the capillaries, 20.0 μL of ultrapure water (Invitrogen, USA) was injected into the capillaries and then removed by centrifugation (2000 rpm for 10.0 s). This flushing was repeated

three times. Thereafter, the glass capillaries were left in a sterile oven (40.0 °C) overnight to remove any remaining water.

To conduct PCR, 20.0 µL of the prepared PCR mixture was injected into a capillary. An equal volume of negative control was injected into a second capillary. A two-temperature PCR protocol which consisted of 36 cycles was used. The two-temperature PCR protocol was chosen to match that performed on the PCR microdevice at a total flow rate of 1.2 µL/min (**Chapter 2, Table 2.1**). The first cycle comprised 30.0 s at 94.0 °C for the initial hot-start activation of the polymerase and then 7.0 s at 62.0°C for the annealing and extension of the primers F2 and R2 (**Figure 5.3**).

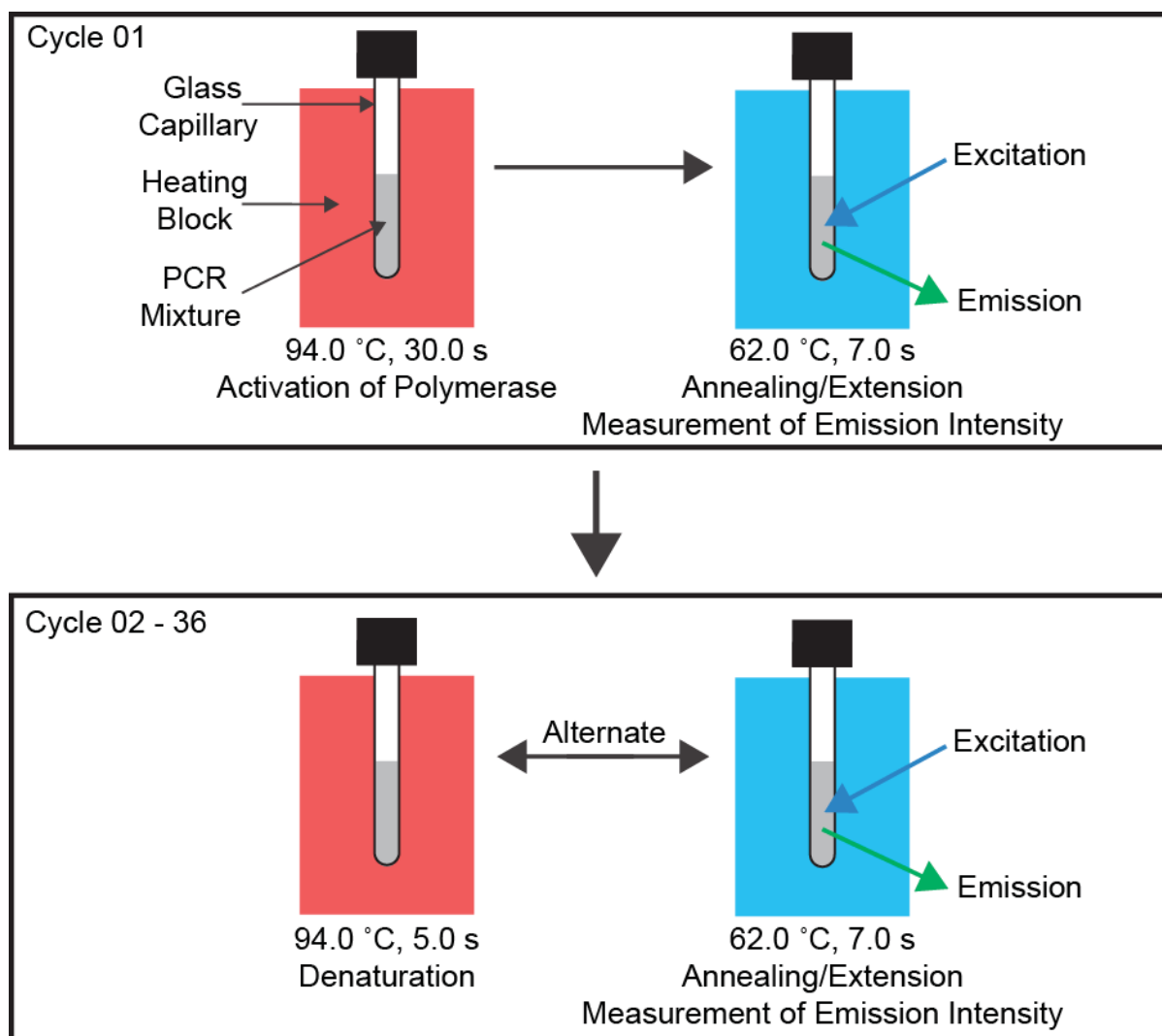


Figure 5.3. A summary of the PCR protocol as carried out on the Lightcycler 2.0 thermal-cycler. At every annealing/extension stage, a measurement of the fluorescence signal was made.

The remaining 35 cycles (**Figure 5.3**) were conducted by alternating between denaturation of DNA templates (5.0 s at 94.0 °C) and annealing/extension (7.0 s at 62.0°C) until completion. For real-time PCR, fluorescence signals from the excited fluorophore FAM (released from the TaqMan

probe) were measured at the end of every annealing and extension cycle. After PCR, samples from the positive control (labelled P_C) and the negative control (labelled N_C) were collected for further analysis by gel electrophoresis.

The gel slabs used for gel electrophoresis were prepared as follows. 0.75 g of agarose (Sigma, Aldrich) was added to 50 mL of TBE (Tris/Borate/EDTA) buffer (Novex TBE running buffer, Invitrogen, USA). The two were mixed and placed in a microwave oven for 2 min at medium power. After heating the mixture, 2.5 μ L of ethidium bromide (EtBr) solution (10 mg/mL, Sigma Aldrich, USA) was added into the mixture and mixed well. EtBr was incorporated into the gel at this stage, so that DNA stains could be visualised immediately after electrophoresis. The mixture was then poured over an assembled container that consisted of a tray and a comb. The mixture was then allowed to stand for 45 min to let it cool and harden into a gel state. Once hardened, the comb bridge was pulled out from the agarose gel slab to reveal wells for loading samples. The tray with the agarose gel slab was then loaded onto the gel electrophoresis station (Sub-Cell GT Cell, Bio-Rad, USA) and immersed completely in TBE buffer.

To conduct gel electrophoresis, 8.0 μ L of the collected PCR sample (N_C or P_C) was mixed thoroughly with 2.0 μ L of loading dye (Novex Hi-Density TBE sample buffer, Invitrogen, USA). The mixture was then loaded into a well of the agarose gel. 4.0 μ L of a 50 bp DNA ladder (TrackIt 50 bp DNA ladder, Invitrogen, USA) was also loaded into a well for use as a DNA size (bp) reference. A power supply (Power Pac 300, Bio-Rad, USA) was connected to the electrodes of the electrophoresis station, and gel electrophoresis was conducted at a constant voltage of 140.0 V for 40.0 min. After electrophoresis, a computer with image-capturing software (Gene-Snap, Syngene, USA) was used to obtain images of the stained DNA bands on the agarose gel.

5.2.2 Varying Concentration of the TaqMan Probe (P1)

The final concentration of the probe (P1) was varied from 0.50 to 0.25 to 0.125 μ M, while the concentrations of the other components in the PCR mixture were kept the same as the starting recipe (**Table 5.5**). Using the same two-temperature PCR protocol (**Section 5.2.1**), the prepared PCR mixtures underwent thermal-cycling on the Lightcycler 2.0 system. After PCR, the collected samples were labelled PP1_0.50, PP1_0.25 and PP1_0.125, respectively (**Table 5.6**). Negative controls without DNA template were also employed for each concentration of the probe. The collected samples were labelled NP1_0.50, NP1_0.25 and NP1_0.125, respectively.

Table 5.6. The collected samples with varying concentration of P1

Sample	DNA Template Added	Final Concentration of P1 [μM]
PP1_0.50	Yes	0.50
PP1_0.25	Yes	0.25
PP1_0.125	Yes	0.125
NP1_0.50	No	0.50
NP1_0.25	No	0.25
NP1_0.125	No	0.125

5.2.3 Varying Concentration of the Primers (F2 and R2)

The final concentration of the primers (F2 and R2) was varied from 0.50 to 0.25 to 0.125 μM , while the concentrations of the other components in the PCR mixture were kept the same as the starting recipe (**Table 5.5**). Using the same two-temperature PCR protocol (**Section 5.2.1**), the prepared PCR mixtures underwent thermal-cycling on the Lightcycler 2.0 system. After PCR, the collected samples were labelled PF2R2_0.50, PF2R2_0.25 and PF2R2_0.125, respectively (**Table 5.7**). Negative controls without DNA template were also employed for each primer concentration. After PCR, the collected samples were labelled NF2R2_0.50, NF2R2_0.25 and NF2R2_0.125, respectively.

Table 5.7. The collected samples with varying concentration of F2 and R2

Sample	DNA Template Added	Final Concentration of F2 and R2 [μM]
PF2R2_0.50	Yes	0.50
PF2R2_0.25	Yes	0.25
PF2R2_0.125	Yes	0.125
NF2R2_0.50	No	0.50
NF2R2_0.25	No	0.25
NF2R2_0.125	No	0.125

5.2.4 Varying Concentration of the DNA Template

The final concentration of template was varied between 0 and 10^{-5} μM , while the concentrations of the other components in the PCR mixture were kept the same as the starting recipe (**Table 5.5**). Using the same two-temperature PCR protocol (**Section 5.2.1**), the prepared PCR mixtures underwent thermal-cycling on the Lightcycler 2.0 system. After PCR, the collected samples were labelled P_10-2, P_10-3, P_10-4, P_10-5 and 0, respectively (**Table 5.8**).

Table 5.8. The collected samples with varying concentration of DNA template

Sample	DNA Template Added	Final Concentration of template [μM]
P_10-2	Yes	10^{-2}
P_10-3	Yes	10^{-3}
P_10-4	Yes	10^{-4}
P_10-5	Yes	10^{-5}
0	No	0

5.3 RESULTS AND DISCUSSION

5.3.1 Starting Recipe

94.0 °C was selected for initial activation of the polymerase (in the first cycle for 30 s), and also for denaturation of the template (from the second cycle onwards for 5.0 s each time). This temperature was much higher than the activation temperature (45.0 °C) of the hot-start polymerase, so activation was expected to occur in a much shorter time than the allotted 30 s.¹⁴ This temperature was also high enough to disrupt the hydrogen bonds in the base pairing of duplex DNA templates. The splitting of duplex templates is typically fast and a 5.0 s duration was expected to be sufficient.²¹

62.0 °C was selected for annealing of the TaqMan probe (P1) and the primers (F2 and R2), and also for the extension of the primers by the polymerase (first cycle onwards for 7.0 s each time). This temperature was chosen to be slightly lower than their calculated annealing temperatures (P1: 63.7 °C, F2: 63.6 °C and R2: 63.5 °C), so they would efficiently anneal to their target sites on the templates without many secondary hybridizations.^{4,7} As a two-temperature PCR protocol was used, 62.0 °C was also the temperature for the polymerase to extend the annealed primers. According to the specification by the manufacturer, *OneTaq* polymerase has an extension rate of 1 kb/min at 68.0 °C. At a lower temperature of 62.0 °C, the extension rate was expected to be substantially lower but still sufficient for extension to occur within the allotted 7 s.¹⁴

The significance of the selected temperatures and durations in the two-temperature PCR protocol was that they corresponded to the same PCR conditions that would be used on the fabricated microdevice. When the central heater of the fabricated device was set to 94.0 °C, the periphery had a temperature of 62.0 °C. If the water-in-oil droplets containing the PCR mixture were flowing at a total flow rate of 1.2 µL/min in the fabricated PCR device, then the PCR mixture would have the same residence times at the hot central and the cool periphery as the durations used in the bench-top PCR.

From the gel electropherograms (**Figure 5.4(i)**), the positive control (P_C) was found to contain a DNA band at the 110 bp, indicating successful formation of the target PCR product. PCR was therefore verified to work on the bench-top thermal cycler, using the selected components at the stated concentrations. The selected DNA template, the primers (F2 and R2), the polymerase, the standard reaction buffer solution, and the other additives were confirmed to work properly together for PCR. The negative control (N_C) showed no DNA band, confirming that no DNA amplification was possible in the absence of the DNA template.

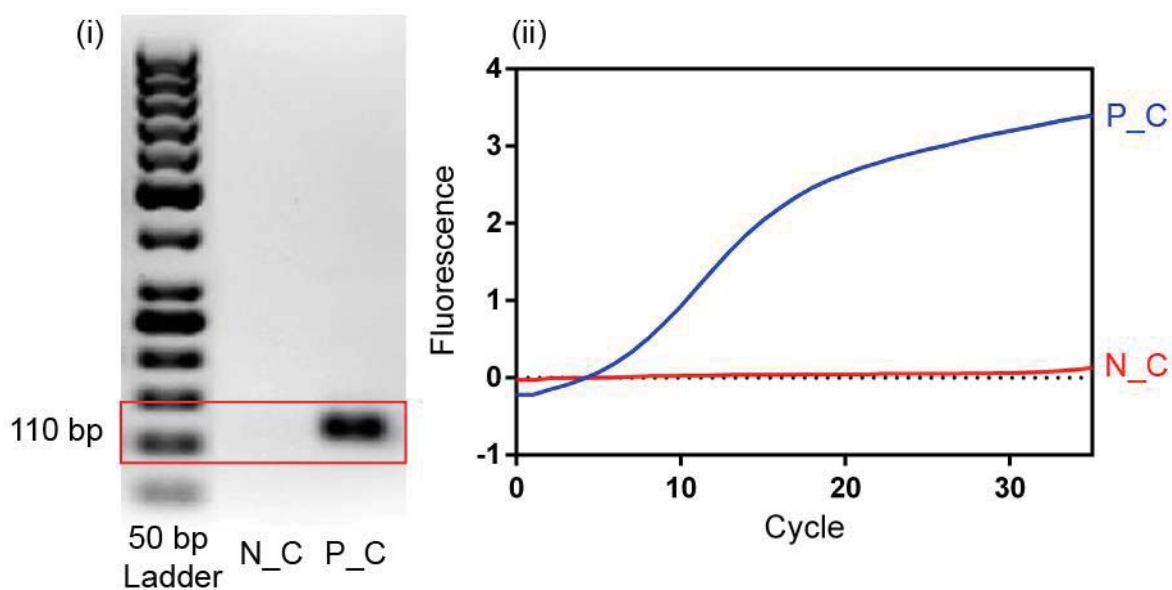


Figure 5.4. (i) Gel electrophoresis result of negative control (N_C) and positive control (P_C). P_C shows a band at the 110 bp while the N_C does not have a band. (ii) Real-time PCR for N_C and P_C. The emission signal of P_C increases over successive cycles of PCR, while N_C remains constant.

The gel electrophoresis analysis showed only the end-point result of PCR. Real-time PCR was used to confirm if the TaqMan probe (P1) was annealing successfully to the DNA template and was being cleaved at the end of every extension cycle. This experiment provided important confirmation that the selected fluorophore and quencher dye were working in tandem to quench the emission before being cleaved apart by the polymerase.

The Lightcycler 2.0 system was programmed to excite each sample in the glass capillary with a LED light source and to take measurements of the emission signal at the end of each cycle (**Figure 5.3**). The emission signal of the prepared PCR mixture (P_C) started increasing from around cycle four onwards (**Figure 5.4(ii)**). The build-up of the fluorescence signal over successive cycles confirmed that P1 annealed successfully onto the template and was cleaved by the 5'-3' exonuclease activity of the polymerase during extension. The two-temperature PCR protocol worked well for the prepared PCR mixture as indicated by the formation of the 110 bp PCR product (**Figure 5.4(i)**). The emission signal of the negative control (N_C) remained broadly constant, consistent with there being no amplification in the absence of DNA template.

Having verified that PCR proceeded successfully using the two-temperature protocol on the bench-top thermal cycler, it was hoped that the same protocol would also work when translated to the fabricated PCR device.

5.3.2 Variation of the Concentration of the TaqMan Probe (P1)

Based on the starting recipe, the concentration of the probe was varied to determine its effect on the PCR reaction and the resulting fluorescence signals. The concentration that gave the highest fluorescence intensity would then be translated to the fabricated PCR device for coupling with the laser-induced confocal detection system (**Chapter 4, Figure 4.11**).

With template present, decreasing the concentration of P1 from 0.50 to 0.25 to 0.125 μM resulted in a drop in the signal intensity (**Figure 5.5**).

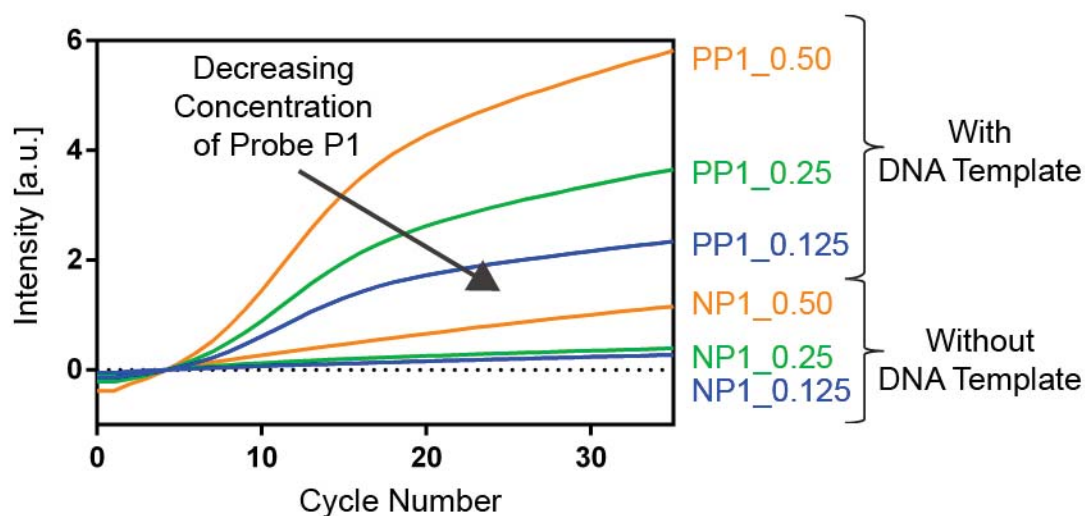


Figure 5.5. Fluorescence intensity versus cycle number for decreasing concentrations of P1 (Table 5.6).

The decrease in intensity (**Figure 5.5**) was consistent with there being less P1 being available to anneal to the template for cleaving by the polymerase during extension; consequently, less FAM was released into the solution, resulting in a lower signal.⁸ Without template present, samples NP1_0.25 and NP1_0.125 showed a broadly constant fluorescence signal with cycle number, indicating zero amplification. Without any template for annealing by P1, no P1 was cleaved during extension to release the fluorophore. For sample NP1_0.50, a slight increase in fluorescence was observed with increasing cycle number against expectation. A possible explanation is that an overly high concentration of P1 can cause it to form secondary dimers with itself and the included primers, leading to unwanted PCR products. The formation of these products would also cause the TaqMan probe to cleave and release the fluorophore, thus causing a build-up of emission signal. Given the non-ideal behaviour of NP1_0.50, 0.25 μM was deemed the optimal concentration of P1 for translation to chip-based PCR, providing a moderate increase in signal intensity with increasing cycle number in the presence of template and a flat response in its absence.

5.3.3 Variation of the Concentration of the Primers (F2 and R2)

Using the optimum concentration of TaqMan probe P1, the negative controls (NF2R2_0.25, NF2R2_0.50, NF2R2_0.12) showed a flat response with cycle number for all tested primer concentrations in the absence of DNA template as expected (**Figure 5.6**).

As the concentration of the primers was decreased from 0.50 to 0.25 to 0.125 μM with template present, the fluorescence intensity decreased. Although PF2R2_0.50 gave the highest amplification in the presence of template and a flat response without, the response obtained using PF2R2_0.25 was adequate and using less primers was more economical. Therefore, 0.25 μM was chosen as the primer concentration to be used in chip-based experiments.

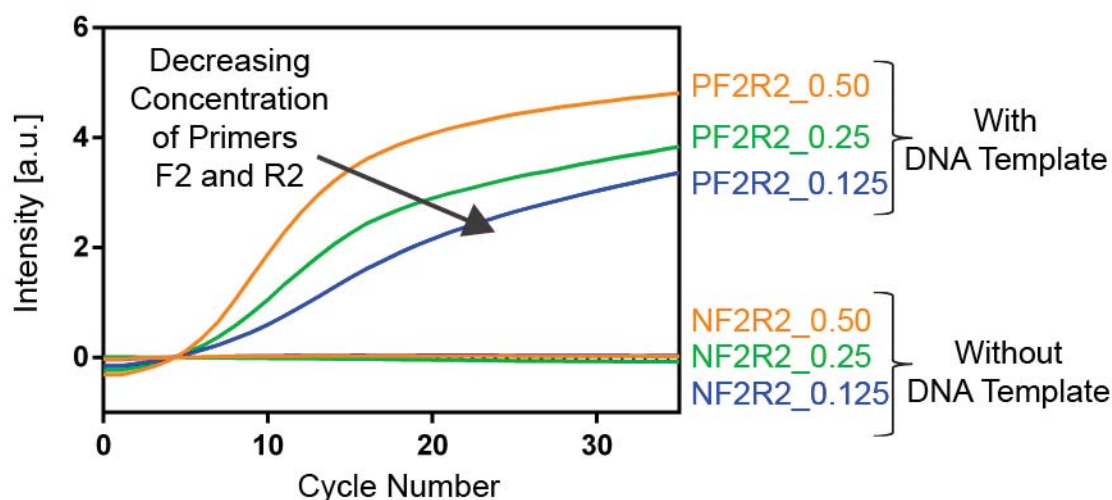


Figure 5.6. Fluorescence intensity versus cycles number for decreasing concentrations of primers F2, R2 (**Table 5.7**).

5.3.4 Variation of the Concentration of DNA Template

As the concentration of the template decreased, the amplification per cycle decreased and the number of cycles needed to reach a certain intensity threshold consequently increased (**Figure 5.7**). With 10^{-2} μM of template, around four cycles were required to reach the threshold level (denoted by the arbitrary black line in **Figure 5.7**). For 10^{-3} , 10^{-4} and 10^{-5} μM , ~ 8 , ~ 11 and ~ 16 cycles were required, respectively. This is attributed to the reduction in the initial number of templates available for amplification. At higher concentrations, more templates are available for annealing by the primers and the TaqMan probe. As polymerase extends the primers and cleaves the probe, more of the reporter dye is released into solution and more DNA is replicated. The newly-replicated DNA acts as a template for the next cycle of annealing by the primers and the TaqMan probe. Therefore, with a higher concentration of starting template, the signal builds up

faster. As a result, PCR mixtures with higher concentrations of template reach the threshold level earlier. The negative control did not exhibit an increasing signal because no template was available for amplification. Since the sample containing $10^{-2} \mu\text{m}$ showed the fastest rate of amplification, this concentration was selected for translation to chip-based PCR.

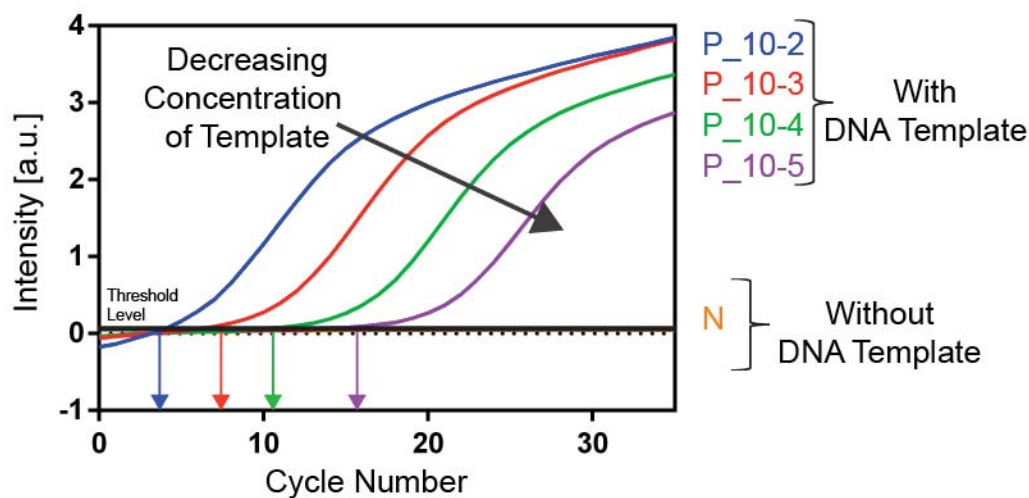


Figure 5.7. Fluorescence intensity versus cycles number for decreasing concentration of DNA templates (Table 5.8).

A standard curve was generated by plotting the natural logarithm of the concentrations of DNA template against their corresponding threshold cycles (Figure 5.8). Based on Equation 1.5 in Chapter 1, the efficiency (E) of the PCR reaction can be determined based on the gradient (m) of the straight calibration line.²²

$$E = e^{-m} - 1 \quad (5.11)$$

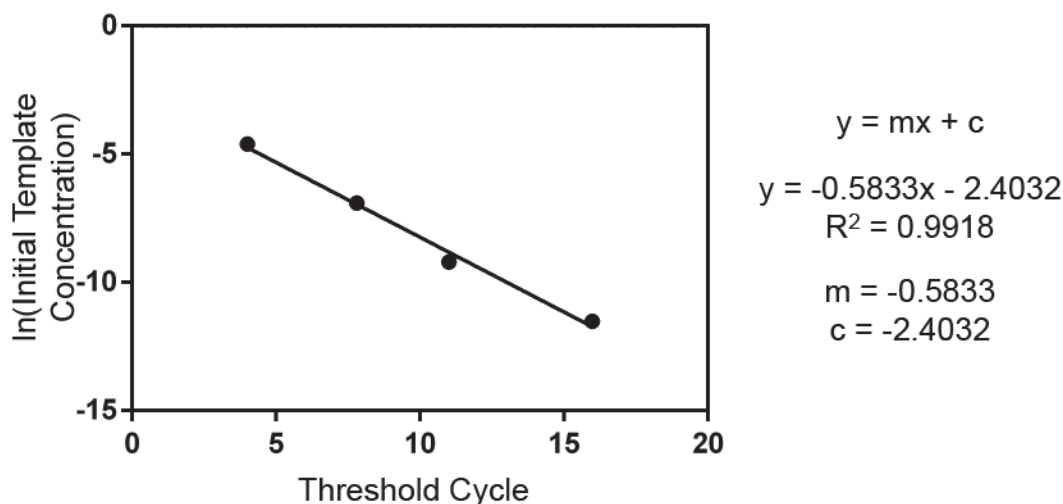


Figure 5.8. A straight line plot of $\ln(\text{initial template concentration})$ against threshold cycle. The gradient of the plot is used to determine the efficiency of the PCR.

Using **Equation 1.2²²**, the efficiency of the PCR using the described recipe and protocol was ~ 0.8 . The amplification efficiency is considered perfect case when $E = 1$. Therefore, a 0.8 value for E in this case was good, and the described PCR recipe and protocol were considered efficient enough for testing on the fabricated PCR device.

5.3.5 Optimised PCR Recipe for Droplet-based PCR

Based on the above experiments, a final optimised recipe for the PCR mixture was fixed for subsequent use in droplet-based PCR. The recipe is summarised in **Table 5.9**.

Table 5.9. Optimised Recipe for Droplet-based PCR

Component	Volume Added		Starting Concentration		Final Concentration	
		μL				
Water (RT-PCR Grade)	162.5	μL	-	-	-	-
Standard Reaction Buffer	50.0	μL	5	parts	1	parts
DNA Template*	2.5	μL	1.0	μM	10^{-2}	μM
Primer Mix (F2 and R2)	6.25	μL	10.0	μM	0.25	μM
dNTPs	5.0	μL	10.0	mM	0.2	mM
OneTaq Hot-Start Polymerase	5.0	μL	5.0	U/ μL	0.1	U/ μL
Bovine Serum Albumin(BSA)	12.5	μL	1.0	%	0.05	%
TaqMan Probe (P1)	6.25	μL	10.0	μM	0.25	μM

*To prepare a negative control, an equal volume of ultrapure water was used in place of the DNA template.

5.4 CONCLUSIONS

PCR was verified to work with the selected components on a bench-top thermal cycler. The working recipe was then optimised by varying the concentration of the TaqMan probe, primers and DNA templates to obtain a formula that was most likely to work in a droplet-based format on the fabricated PCR microdevice.

Chapter 6

Droplet-based PCR was conducted on the fabricated PCR microdevice, and the effects of varying the central temperature and flow rate were investigated. Serial dilution of the DNA template was carried out to determine the lowest concentration of DNA template required for successful amplification.

6.1 INTRODUCTION

In **Chapter 5**, an optimised PCR recipe was defined using a conventional bench-top thermal cycler. In this chapter, we report the initial testing of the fabricated PCR microdevice. In particular, we evaluate the use of an immiscible oil to carry the aqueous PCR mixture as water-in-oil droplets, and the use of a radial temperature gradient to conduct droplet-flow PCR. The central temperature and flow rate were varied to determine the effects on the reaction yield. The concentration of DNA template was varied to determine the lowest concentration needed for successful amplification on the PCR device.

6.2 CHIP-BASED DROPLET PCR

In this section, we describe the adaption of the optimised PCR recipe (**Chapter 5**) to a droplet-flow format using the following experimental setup (**Figure 6.1**).

6.2.1 Experimental

A. Recipe: Aqueous Phase

The aqueous phase for the water-in-oil droplets was made up of the optimised PCR mixture defined in **Chapter 5, Table 5.9**. A negative control was prepared by replacing the DNA template with an equal volume of ultrapure water. The preparation of the PCR mixture was the same in all experiments unless stated otherwise.

B. Recipe: Oil Phase

The oil phase for the water-in-oil droplets was a 1.8 % (by mass) surfactant mixture in FC-40 (Fluorinert, 3M, USA). The surfactant was a perfluorinated PFPE-PEG synthesized by Soong-Won Cho.¹ The surfactant was added to the oil phase to stabilize the droplets during and after formation. The same oil phase was used in all experiments unless stated otherwise.

C. Treatment of Internal Surfaces of Glass Syringes

In all flow experiments, the PCR mixture was injected from glass syringes using precision syringe pumps. To prevent loss of material during storage, the internal surfaces of the glass syringes were treated before use.^{2,3}

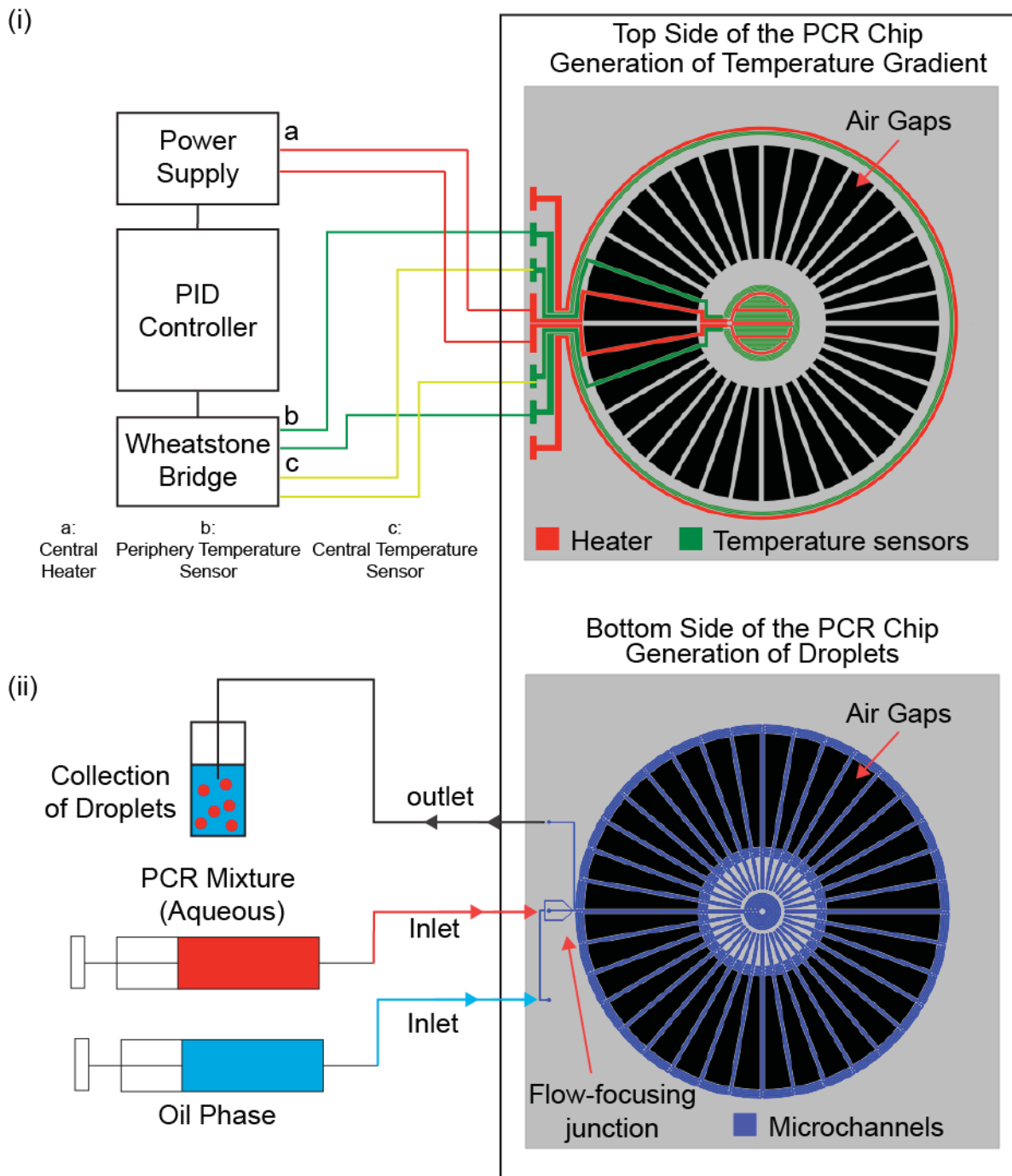


Figure 6.1. Schematic showing (i) the thermal setup for the temperature profile (Section 6.2.1.E) and (ii) the fluidic setup for droplet generation on the chip (Section 6.2.1.D). (i) For the thermal setup, both central and periphery temperature sensor were used to monitor temperature on-chip. Only the central heater was used. (ii) Both the aqueous PCR mixture (Section 6.2.1.A) and the oil phase (Section 6.2.1.B) were loaded into glass syringes (Section 6.2.1.C) and injected into the chip using syringe pumps. The droplets were collected from the outlet of the chip and merged (Section 6.2.1.F) prior to electrophoretic analysis (Section 6.2.1.G).

A 2.0 % mixture of trichloro(1H,1H,2H,2H-perfluorooctyl)silane (97.0 %, Sigma Aldrich, USA) in anhydrous ethanol (Sigma Aldrich, USA) was prepared as a silanising mixture. The silanising mixture was loaded into the glass syringe, and allowed to remain in the syringe overnight. The syringe was then flushed with deionized water, and thoroughly air-dried before loading the PCR

mixture. After each experiment, the glass syringe was again flushed with deionized water and air-dried. The above silanisation process was repeated before re-using the glass syringe.

D. Flow Profile on Chip

The aqueous phase and the oil phase were loaded into their respective 250.0 μL treated glass syringes (Hamilton, Switzerland). They were then injected into the PCR device at flow rates of 0.48 and 0.72 $\mu\text{L}/\text{min}$, respectively using syringe pumps (PHD ultra, Harvard Apparatus, USA) to form water-in-oil droplets (**Figure 6.1(ii)**). The negative control PCR mixture (N) without added DNA template was injected into the PCR device first. Once the experiments were complete, the positive control PCR mixture (P) with added DNA template was injected into the device.

The droplets flowed through the chip undergoing a PCR protocol (**Chapter 2, Table 2.1**) that consisted of 36 cycles. At a total flow rate of 1.2 $\mu\text{L}/\text{min}$, the droplets had a residence time of 30.0 s in the hot central zone where the initial hot-start activation of the polymerase occurred, and 7.0 s in the cool periphery where the annealing/extension of the primers took place. Thereafter, the droplets would alternate 35 times between the hot zone for denaturation of DNA templates (5.0 s) and the cool periphery for annealing/extension (7.0 s). The droplets were collected for analysis after flowing through the PCR chip. The above conditions were used for all experiments unless stated otherwise.

E. Temperature Profiles on Chip

The temperature sensors on each PCR chip were first calibrated (**Chapter 4, Section 4.2.1**) before use. After calibration, the central heater was set to a target temperature (T_c) of 94.0 $^{\circ}\text{C}$, using the integrated thin-film temperature sensor, and the PID temperature controller (**Figure 6.1(i)**). Once the central zone reached the target temperature of 94.0 $^{\circ}\text{C}$, the temperature difference between the central zone and the periphery (62.0 $^{\circ}\text{C}$) created a temperature gradient that could be used for PCR. The periphery heater was deactivated and no fan cooling was used. The above conditions were the same for all experiments unless stated otherwise.

F. Merging of Collected Water-in-Oil Droplets

To merge the collected water-in-oil droplets, an excess of FC-40 was slowly added to the water-in-oil droplets to reduce the stabilising effect of the added surfactant. The mixture was agitated and centrifuged until the droplets coalesced into a large aqueous globule that floated on the oil.

The globule was then carefully removed by a pipette for analysis by gel electrophoresis. The above procedures were the same for all experiments unless stated otherwise.

G. Gel Electrophoresis

A polyacrylamide gel (Novex TBE gel, 10.0 %, 10 well, Invitrogen, USA) was placed in an electrophoresis chamber (XCell SureLock Mini-Cell, Invitrogen, USA), which was filled with TBE (Tris/Borate/EDTA) buffer (Novex TBE running buffer, Invitrogen, USA). 8.0 μ L of the collected aqueous PCR sample was mixed thoroughly with 2.0 μ L of loading dye (Novex Hi-Density TBE sample buffer, Invitrogen, USA). The mixture was then loaded into a well of the polyacrylamide gel. 4.0 μ L of a 50 bp DNA ladder (TrackIt 50 bp DNA ladder, Invitrogen, USA) was also loaded into a well of the polyacrylamide gel for use as a DNA size (bp) reference. A power supply (Power Pac 300, Bio-Rad, USA) was connected to the electrodes of the electrophoresis chamber, and gel electrophoresis was conducted at a constant voltage of 200.0 V for 20.0 min. After gel electrophoresis, the polyacrylamide gel was removed from its plastic cartridge and immersed in a solution containing 40.0 mL of TBE buffer and 6.0 μ L of DNA dye (SYBR Safe DNS gel stain) for 10.0 min to achieve DNA staining. After immersion, the gel was placed in a gel imaging system (Dyversity, Syngene, USA) under UV transmission mode. A computer with image-capturing software (Gene-Snap, Syngene, USA) was used to obtain images of the stained DNA bands on the polyacrylamide gel. The above procedures were the same for all experiments unless stated otherwise.

H. Bench-top Thermal Cycler: Control Experiments

Control experiments were conducted on a conventional bench-top thermal cycler (TC-5000, Techne, USA). 20.0 μ L of PCR mixture with the added DNA template was used as a positive control, while an equal volume of the PCR mixture without template was used as a negative control. A two-temperature PCR protocol consisting of 36 cycles was used. The first cycle lasted 30.0 s at 94.0 $^{\circ}$ C for the initial hot-start activation of polymerase and then 7.0 s at 62 $^{\circ}$ C for annealing/extension of the primers. The remaining 35 cycles were conducted by alternating between denaturation of DNA templates (5.0 s at 94.0 $^{\circ}$ C) and annealing/extension (7.0 s at 62.0 $^{\circ}$ C) until completion. This protocol was analogous to the one used on-chip at a total flow rate of 1.2 μ L/min (**Chapter 2, Table 2.1**). The bench-top control experiments were used to ensure that the two-temperature PCR protocol worked for the prepared PCR mixture, and that no amplification was possible in the absence of DNA template. After PCR, the negative control (N_C) and positive control (P_C) samples were collected for gel electrophoresis. The procedures for the control tests were the same in all experiments unless stated otherwise.

6.2.2 Results and Discussion

The water-in-oil droplets appeared stable throughout the collection process, alternating between the hot central zone (94.0 °C) and the cool periphery (62.0 °C) without coalescing. The droplets were collected and successfully merged (**Section 6.2.1.F**) for gel electrophoresis analysis. No accumulation of droplets was observed in the microchannels for the duration of the experiment, even in the hottest central region that was most prone to fouling in continuous-flow. This observation contrasted to the non-droplet continuous-flow PCR experiment in **Chapter 4, Figure 4.6** where the microchannels were rapidly blocked from the accumulation of residues, confirming the efficacy of droplet flow in preventing fouling.

The optimised PCR recipe (**Chapter 5, Table 5.9**) worked successfully on the bench-top thermal cycler as evidenced by the presence of the 110 bp band in the positive control (P_C) in the gel electropherogram (**Figure 6.2**). The 110 bp band was not observed for the negative control (N_C).

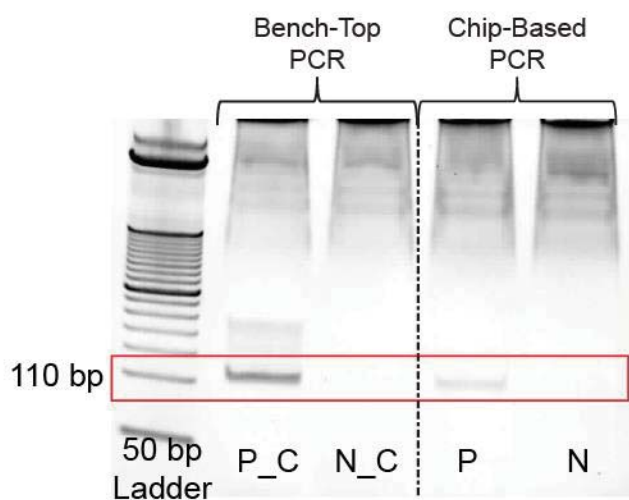


Figure 6.2. Gel electropherograms of the bench-top positive (P_C) and negative (N_C) controls, and the chip-based samples with (P) and without (N) DNA template. Using the bench-top cycler, P_C showed a dark 110 bp band while the negative control (N_C) showed no band. Using the chip, the PCR mixture with added DNA template (P) showed a very faint 110 bp band, while the PCR mixture without added DNA template (N) showed no band. Hence, the PCR device was able to conduct droplet-based PCR successfully, although the product yield appeared to be low from the low band intensity.

The PCR mixture with added DNA template (P) showed a very faint band in the gel electrophoresis analysis, while the PCR mixture without the added DNA template (N) showed no visible product band (**Figure 6.2**). Hence it was evident that the PCR device was able to conduct droplet-based PCR successfully, even though the product yield appeared to be lower than observed for the bench-top thermal cycler (P_C).

The low yield was most likely due to the discrepancy between the measured temperatures on the chip and the actual temperatures in the microchannels. When the central temperature was fixed to a nominal temperature of 94.0 °C (as indicated by the calibrated central temperature sensors and controlled by the PID controller), a radial temperature gradient was established and the periphery had a nominal temperature of ~62.0 °C as measured by the calibrated periphery temperature sensor. These nominal temperatures matched those used in the bench-top thermal cycler, and it was therefore hoped that the PCR reaction would progress in a similar manner, leading to a comparable product yield. However, since the temperature sensors were located on the surface of the PCR device and not within the microchannel, it was not certain that they would accurately report the temperatures within the droplets (**Figure 6.3**).

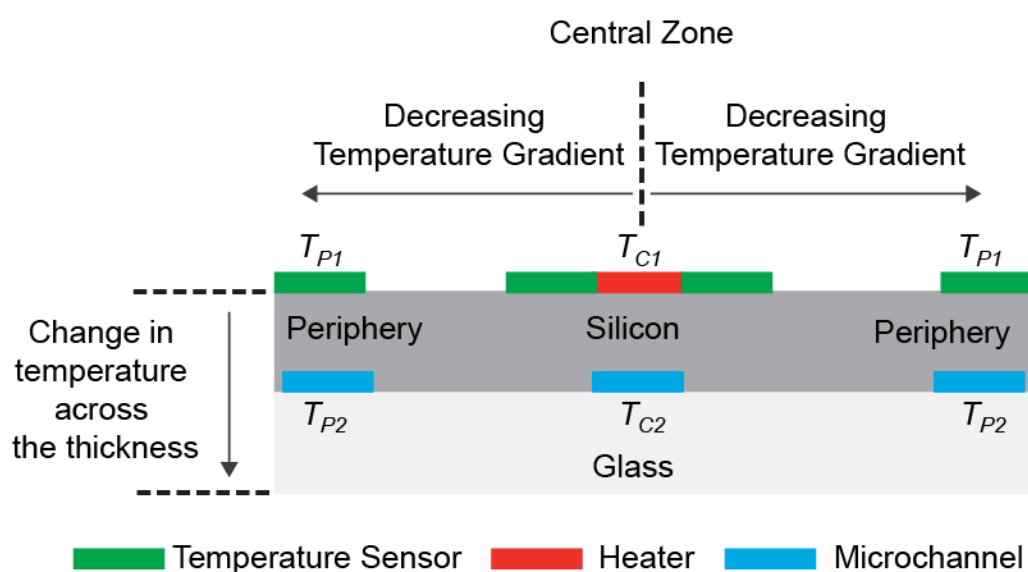


Figure 6.3. Schematic showing the placement of the heater, the temperature sensors and the microchannels. The heater and the temperature sensors were on the surface of the exposed side, while the microchannels were on the opposite side capped by a glass layer. The temperature sensors measured the temperatures on the surface (T_{P1} and T_{C1}) which were likely to be higher than the temperatures in the microchannel (T_{C2} and T_{P2}).

As the temperature sensors were on the exposed surface, they were subjected to cooling by air convection, causing them to adopt a different temperature than in the glass-capped microchannels on the opposite side. As a result, the surface temperatures (T_{C1} and T_{P1}) as measured by the calibrated temperature sensors were likely to be lower than the internal temperatures (T_{C2} and T_{P2}) of the microchannels. This speculation was supported by the thermal simulation studies in **Chapter 2, Section 2.4.5**. When the central heater was fixed at 92.0 °C, the temperature at the periphery on the surface was ~61.0 °C, while the temperature in the microchannel was ~63.0 °C. Higher temperatures within the microchannels may have adversely affected the PCR reaction since the chosen primers were designed to work within the range of 60.0 to 63.5 °C (**Chapter 5, Table 5.1**). If the periphery temperature sensors indicated a local

temperature of 62.0 °C, the temperature inside the microchannel was likely to be more than 62.0 °C (i.e. near or beyond the upper limit of the working temperature of the primers).⁴ As noted in earlier chapters, higher temperatures can potentially reduce the efficiency with which the primers anneal onto the single-stranded DNA templates for extension by the polymerase, leading to a lower yield of the PCR product (**Figure 6.2**).

Although the reaction yield was reduced, the experiment provided important confirmation that the fabricated PCR device was able to carry out droplet-based PCR successfully. The radial temperature gradient generated by the integrated heaters and the gaps on the chip were evidently able to induce the denaturation, annealing and extension steps required for PCR. The droplet-based approach was also shown to be effective in preventing blockages of the microchannel previously encountered in continuous-flow PCR.

One way to achieve a higher yield of the PCR product would have been to more accurately determine the temperatures of the microchannels, so that the temperatures on the chip could be adjusted appropriately to achieve the optimum temperatures for PCR. (Potential ways to determine the actual temperatures in the microchannels were discussed in **Chapter 4, Section 4.2.1.B**). However, even then differences would exist between the bench-top thermal cycler and the device due to the different rates of heating and cooling. Hence, a more empirical approach was taken here by monitoring the effect of lowering the temperature of the central zone on the yield of the PCR product.

6.3 EFFECTS OF VARYING THE CENTRAL TEMPERATURE

In this section, the effects of decreasing the central temperature on the reaction yield are investigated.

6.3.1 Experimental

For the following set of experiments, the conditions specified in **Section 6.2.1** were used, except for a slight modification of the recipe for the aqueous phase (**Section 6.2.1.A**). The buffer solution in the aqueous PCR mixture was changed from the standard reaction buffer solution to the GC reaction buffer solution (**Chapter 5, Section 5.1.5**). The reason for the buffer change was to allow a lower central temperature (≤ 90.0 °C) on the fabricated device for the denaturation of DNA templates. Higher temperatures (≥ 96.0 °C) at the central zone were observed to cause droplet instabilities, resulting in boiling and rupturing of the water-in-oil droplets. The GC reaction buffer allowed a lower central temperature to be used because the DMSO in the GC buffer destabilises

the hydrogen bonds in the double-helix DNA templates, reducing the thermal energy required to split the double strands into single strands.^{5,6} Consequently, more single strands form at lower temperature. They are then annealed by the primers which are in turn extended by the polymerase to form more DNA replicates. The overall effect should therefore be to increase the PCR yield, allowing a lower central temperature to be used. The recipe of the PCR mixture is summarised in **Table 6.1**.

Table 6.1. New recipe after change in buffer solution

Component	Volume Added		Starting Concentration		Final Concentration	
Water (RT-PCR Grade)	162.5	μL	-	-	-	-
GC Reaction Buffer	50.0	μL	5	parts	1	parts
DNA Template*	2.5	μL	1.0	μM	0.01	μM
Primer Mix (F2 and R2)	6.25	μL	10	μM	0.25	μM
dNTPs	5.0	μL	10.0	mM	0.2	mM
OneTaq Hot-Start Polymerase	5.0	μL	5.0	U/μL	0.1	U/μL
Bovine Serum Albumin(BSA)	12.5	μL	1.0	%	0.05	%
TaqMan Probe (P1)	6.25	μL	10.0	μM	0.25	μM

*To prepare a negative control, an equal volume of ultrapure water was used in place of the DNA template.

The effects of decreasing the central temperature (T_c) from 96.0, to 90.0 °C were investigated. A PCR chip was first calibrated (**Chapter 4, Section 4.2.1**). The central heater was then set to a target temperature of 96.0 °C using the approach described in **Chapter 4, Section 4.2.1**. Once the central zone had reached the target temperature of 96.0 °C, a temperature difference of ~32.0 °C was established between the central zone and the periphery. As before, the periphery heater was deactivated and no fan cooling was used. The PCR mixture and the oil phase were injected into the PCR device to form the water-in-oil droplets. At a total flow rate of 1.2 μL/min, the flow rate of PCR mixture was 0.48 μL/min, while the flow rate of the oil phase was 0.72 μL/min.

Once the droplet generation and temperature gradient on the chip had stabilized, a waiting time of 20 min was required to ensure that the collected samples were made up entirely of droplets that were subjected to steady-state conditions. 20.0 μL sample (sample P_96) was then collected from the outlet of the PCR device. After collection of sample P_96, T_c was then turned down to 94.0 °C. Once again, a 20 min waiting time was used to ensure collection of a consistent product. Thereafter, another 20.0 μL sample (sample P_94) was collected. This process was repeated for 92.0 and 90.0 °C, yielding samples P_92 and P_90, respectively (**Table 6.2**).

The above experiment was repeated by decreasing the central temperature from 95.0 to 90.0, to 85.0 °C (**Table 6.2**) to determine if PCR could take place even when the central temperature (used for denaturation) was below 90.0 °C. As in **Section 6.2.1.H**, positive (P_C) and negative (N_C) control experiments were conducted on the bench-top thermal cycler.

All the collected droplet samples (**Table 6.2**) were separately collected and merged for analysis by gel electrophoresis. The presence of a 110 bp product band would indicate that PCR had been successful. A darker product band would indicate a higher yield of the PCR product.

Table 6.2. Collected samples from varying the central temperature, T_c

Experiment	Sample	DNA Template Added	Template Concentration [pM]	Type of PCR	Central Temperature (T_c) [°C]	Total Flow Rate [μ L/min]
Control	N_C	No	10000	Bench-top	N.A. (Bench-top)	N.A. (Bench-top)
	P_C	Yes		Bench-top	N.A. (Bench-top)	N.A. (Bench-top)
1	P_96	Yes		Chip-based	96	1.2
	P_94	Yes		Chip-based	94	
	P_92	Yes		Chip-based	92	
	P_90	Yes		Chip-based	90	
2	P_95	Yes		Chip-based	95	
	P_90	Yes		Chip-based	90	
	P_85	Yes		Chip-based	85	

6.3.2 Results and Discussion

The generated water-in-oil droplets were observed to be unstable when the central temperature was at the highest value of 96.0 °C. The water-in-oil droplets appeared to rupture as they entered the hot central zone, possibly due to boiling of the aqueous phase. Although the measured temperature was 96.0 °C, the temperature within the microchannels in the central zone may have been higher than 100.0 °C, causing boiling to take place.

The GC buffer in the PCR recipe worked successfully on the bench-top thermal cyclers as evidenced by the presence of the 110 bp band in the positive control (P_C) (**Figure 6.4**). As expected no product band at 110 bp was observed for the negative control (N_C). Although the water-in-oil droplets were unstable when the central temperature was fixed at 96.0 °C, a sample of the aqueous phase (P_96) was collected.

Droplets were found to be stable when the central temperature was reduced below 96.0 °C. Using central temperatures of 94.0, 92.0 and 90.0 °C (**Table 6.2**), the droplets in each sample were collected and merged for analysis by gel electrophoresis (**Figure 6.4(i)**). A second set of experiments (**Table 6.2**), was then carried out using the same procedure at temperatures of 95.0, 90.0 and 85.0 °C to determine if PCR could still take place when the central temperature (used of denaturation) was below 90.0 °C; the gel electrophoresis results are shown in **Figure 6.4(ii)**.

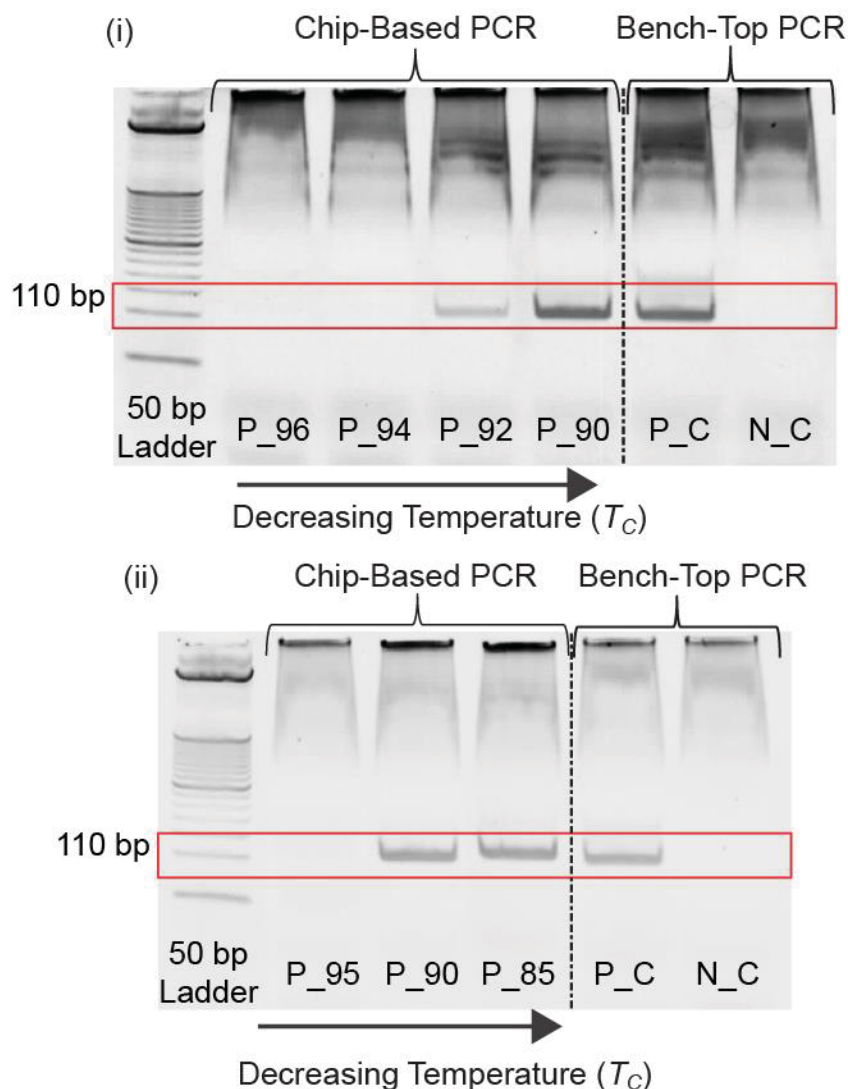


Figure 6.4. Gel electrophoresis results of samples (Table 6.2) obtained using different central temperatures on the chip. (i) In the first experiment, the central temperature was varied from 96.0 °C to 90.0 °C in 2.0 °C intervals. The 110 bp band appeared at 92.0 °C and became darker at 90.0 °C. No band was observed at 96.0 or 94.0 °C. The 110 bp band showed up only in the positive control (P_C) and not in the negative control (N_C). (ii) In the second experiment, the central temperature was varied from 95.0 °C to 85.0 °C in 5.0 °C intervals. The 110 bp band appeared at 90.0 °C and at 85.0 °C. No band was observed at 95.0 °C. The 110 bp band showed up only in the positive (P_C) and not in the negative control (N_C).

When the central temperature was decreased from 96.0 °C to 90.0 °C in 2.0 °C intervals, the 110 bp PCR product band appeared faintly at 92.0 °C and became darker at 90.0 °C (Figure 6.4(i)), indicating that droplet-based PCR took place successfully on the device when the central temperature was below 92.0 °C with the yield of the PCR product increasing for the lower central temperature.

A similar trend was also observed in the second experiment when the central temperature was lowered from 95.0 °C to 85.0 °C in 5.0 °C intervals (Figure 6.4(ii)). As with the first experiment, a 110 bp band was observed at 90.0 °C, and this band remained even when the central temperature was lowered to 85.0 °C. The low working temperature was made possible by the

presence of the DMSO in the GC buffer which helps to destabilise the double stranded DNA template, thereby lowering the denaturation temperature relative to the standard reaction buffer (**Figure 6.5**).^{5,6} With the standard reaction buffer, denaturation would most likely not have taken place below 90.0 °C and PCR would have failed although this was not tested directly.

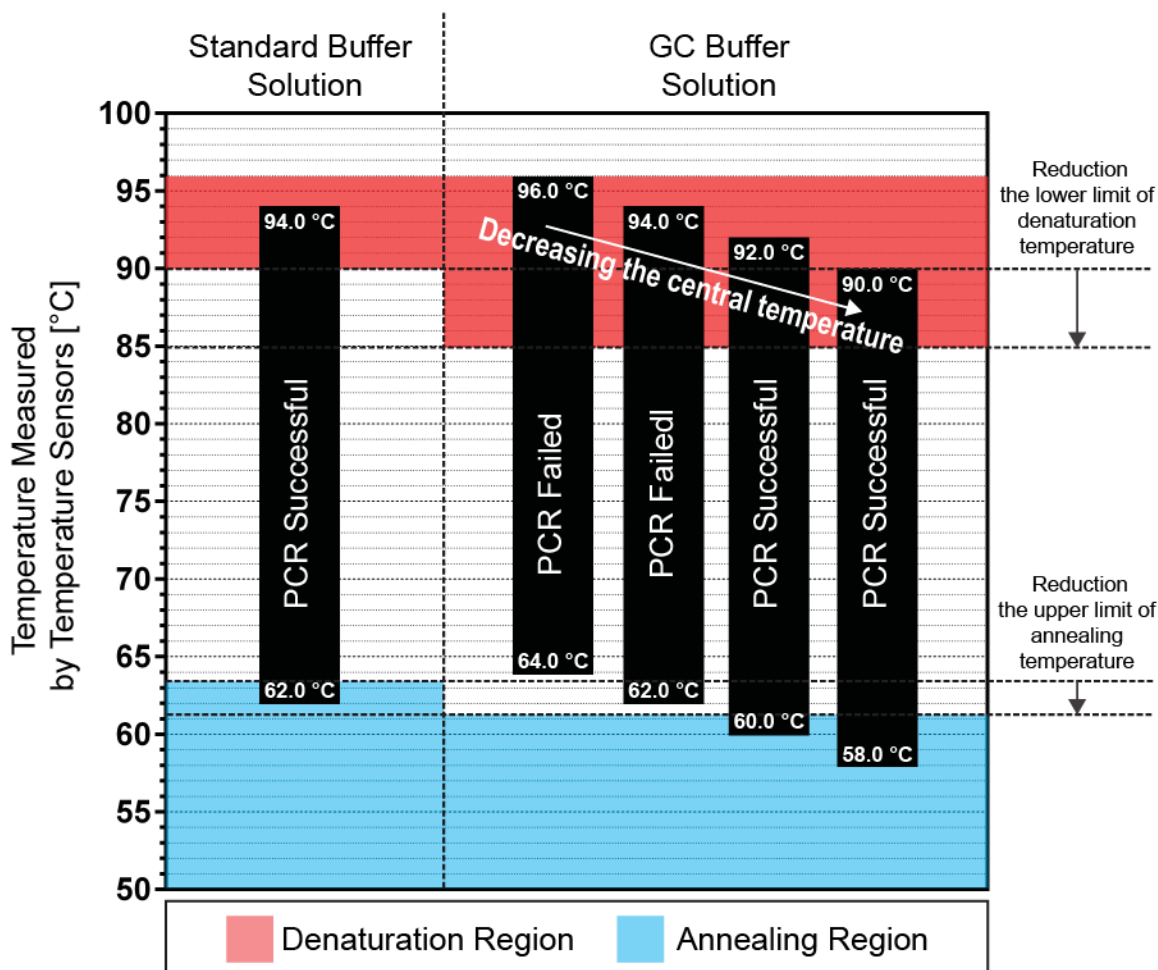


Figure 6.5. A diagram illustrating the reduction of the lower temperature limit for denaturation and the upper temperature limit for annealing when the buffer is switched from a standard reaction buffer to GC reaction buffer. The red and blue regions represent the usable temperature ranges for denaturation and annealing, respectively. The black bar represents the temperature across the PCR device. For example, when the central temperature is 94.0 °C, the resulting periphery temperature is 62.0 °C. The black bar must overlap with red and blue regions for PCR to take place. The temperature difference between the central zone (upper limit of the black bar) and the periphery (lower limit of the black bar) of the PCR device was approximately constant, so the overlap could be maximised by adjusting the central temperature.

Comparing the gel electrophoresis results obtained using the standard buffer (**Figure 6.2**) and the GC buffer (**Figure 6.4(i)**) at the same temperature of 94.0 °C, a faint band was evident with the standard reaction buffer solution, while no the band was observed when using the GC buffer solution. The band appeared at a lower temperature of 92.0 °C with the GC buffer solution due to the destabilising effect of DMSO on the primers. Besides lowering the denaturation temperature, the DMSO in the GC buffer also shifted the working temperature range of the primers to a lower temperature (**Figure 6.5**).^{5,6} DMSO has the effect of destabilising the template-primer hybrid

formed when the primers anneal onto the DNA template.^{5,6} As a result, the primers need a lower working temperature in order to anneal onto the template to form the stable template-primer hybrids needed for PCR.

The primers had an upper annealing temperature of 63.5 °C (**Chapter 5, Table 5.1**). When working with a central temperature of 94.0 °C, the periphery temperature was more or less ideal for the standard reaction buffer at ~62.0 °C, leading to a 110 bp band (**Figure 6.2**). However, when working with the GC buffer, the periphery temperature of ~62.0 °C was too high for the primers to anneal onto the template for extension by the polymerase. Consequently, little or no PCR product was formed, and no 110 bp showed up in the gel electrophoresis analysis (**Figure 6.4(i)**). When the central temperature was reduced to 92.0 °C, the periphery temperature was ~60.0 °C (**Figure 6.5**). This temperature was low enough for annealing to take place, and as a result PCR was successful. When the central temperature was further lowered to 90.0 °C, the yield of the PCR product increased as shown by the darker 110 bp band in the gel electropherogram (**Figure 6.4(i)**). The yield increased because the central and the periphery temperatures were suitable for denaturation and the annealing, respectively.

The positive control (P_C) underwent successful PCR on the bench-top thermal cycler (**Figure 6.4(i)**). The denaturation and the annealing/extension temperatures used on the bench-top thermal cycler were 94.0 and 62.0 °C, respectively. Using the same nominal temperatures on the fabricated PCR device, PCR (P_94) failed. The denaturation and annealing/extension temperatures had to be lowered to 90.0 and 58.0 °C for PCR (P_90) to work on chip, supporting the view that the temperatures measured by the sensors were lower than the temperatures in the channels. A measured temperature of 90.0 °C might have roughly corresponded to 94.0 °C in the bench-top thermal cycler because these two bands (P_C and P_90) were similar in intensity according to the gel electrophoresis analysis.

As the dimensions of the air gaps (for passive cooling) on the fabricated PCR device were fixed, the output by the central heater was the sole factor determining the radial temperature difference between the central zone and the periphery. The difference in the temperature between the two zones was observed to be approximately constant at 32.0 °C for the temperatures investigated (**Figure 6.5**). With a target central temperature of 96.0 °C, the periphery had a temperature of ~64.0 °C. Lowering the central to 94.0 °C, 92.0 °C and 90.0 °C reduced the periphery temperature to 62.0 °C, 60.0 °C and 58.0 °C, respectively. For situations where greater flexibility was required, a heater was integrated at the periphery (**Chapter 2, Figure 2.4**) and a fan cooling system (**Chapter 2, Figure 2.13**) could be used. However, the use of the periphery heater and the air

cooling system to generate the radial temperature gradient were not pursued at this point in order to keep the experimental set-up as simple as possible.

On the basis of the above investigations, it was evident that the microdevice allowed droplet-based PCR to be carried out using the generated temperature gradient. The yield of the PCR product when using a central temperature of 90.0 °C was high and, on the basis of gel electrophoresis analysis, was qualitatively comparable to the bench-top thermal cycler. This temperature was therefore used for all subsequent droplet-based PCR experiments.

6.4 EFFECTS OF VARYING THE TOTAL FLOW RATE

In this section, the effect of varying the total volumetric flow rate of the aqueous PCR mixture and the immiscible oil is described.

6.4.1 Experimental

The same conditions described previously (**Section 6.2.1**) were used, except for the following changes: the central temperature of the fabricated PCR device was fixed at 90.0 °C; the buffer used in the PCR mixture was the GC buffer solution. The effects of increasing the flow rate from 0.6 to 1.2 to 2.4 to 4.8 $\mu\text{L}/\text{min}$ were investigated (**Table 6.3**).

Table 6.3. Summary of the flow rates used in the chip-based PCR

Total Flow Rate ($\mu\text{L}/\text{min}$)	Aqueous Flow Rate ($\mu\text{L}/\text{min}$)	Oil Flow Rate ($\mu\text{L}/\text{min}$)	Water Fraction
0.6	0.24	0.36	0.4
1.2	0.48	0.72	
2.4	0.96	1.44	
4.8	1.92	2.88	

The aqueous PCR mixture (with DNA template) and the oil phase were first injected into the PCR device at flow rates of 0.24 and 0.36 $\mu\text{L}/\text{min}$, respectively, to form water-in-oil droplets. At a total flow rate of 0.6 $\mu\text{L}/\text{min}$ (**Table 6.4**), the droplets spent 60.0 s flowing through the hot central zone for the initial hot-start activation of the polymerase and 14.0 s in the cool periphery for the annealing/extension of primers. Thereafter, the droplets alternated 35 times between the centre and periphery spending 10.0 s per cycle in the hot zone for denaturation and 14.0 s in the cool periphery for annealing/extension.

The PID temperature controller was set to target a central temperature of 90.0 °C. Once a stable temperature gradient on the chip had been established, a 20.0 μL sample (sample P_0.6) was collected from the outlet of the PCR device (after a 40 min waiting time for complete stabilisation).

Table 6.4. The flow rate and its corresponding PCR protocol

Total Flow Rate ($\mu\text{L}/\text{min}$)	Process	Duration (s)	Cycle Number
0.6	Hot-Start Activation	60.0	1
	Annealing and Extension	14.0	
	Denaturation	10.0	2 to 36
	Annealing and Extension	14.0	
1.2	Hot-Start Activation	30.0	1
	Annealing and Extension	7.0	
	Denaturation	5.0	2 to 36
	Annealing and Extension	7.0	
2.4	Hot-Start Activation	15.0	1
	Annealing and Extension	3.5	
	Denaturation	2.5	2 to 36
	Annealing and Extension	3.5	
4.8	Hot-Start Activation	7.5	1
	Annealing and Extension	1.8	
	Denaturation	1.3	2 to 36
	Annealing and Extension	1.8	

After collection of sample P_0.6, the total flow rate was increased to 1.2 $\mu\text{L}/\text{min}$ (while keeping the water fraction fixed at 0.4 (**Table 6.3**)). This time, a 20 min waiting time was required after the temperature gradient had been established. Thereafter, another 20.0 μL sample (sample P_1.2) was collected. This process was repeated at 2.4 and 4.8 $\mu\text{L}/\text{min}$. Samples P_2.4 and P_4.8 were collected after respective waiting times of 10 and 5 min. All the collected droplets (**Table 6.5**) were merged for gel electrophoresis. As before, positive (P_C) and negative (N_C) control experiments were also conducted on the bench-top thermal cycler (**Section 6.2.1.H**).

Table 6.5. Collected samples from varying the total flow rate.

Sample	DNA Template Added	Template Concentration [μM]	Type of PCR	Central Temperature (T_c) [$^{\circ}\text{C}$]	Total Flow Rate [$\mu\text{L}/\text{min}$]
N_C	No	-	Bench-top	N.A (Bench-top)	N.A. (Bench-top)
P_C	Yes	10000	Bench-top	N.A. (Bench-top)	N.A (Bench-top)
P_0.6	Yes		Chip-based	90	0.6
P_1.2	Yes		Chip-based		1.2
P_2.4	Yes		Chip-based		2.4
P_4.8	Yes		Chip-based		4.8

6.4.2 Results and Discussion

As expected the positive control (P_C) worked successfully on the bench-top thermal cycler as evidenced by the presence of the 110 bp band in the gel electrophoresis analysis (**Figure 6.6**), while no 110 bp band was observed for the negative control (N_C).

The 110 bp band of the PCR product in the gel electrophoresis analysis was observed to become darker when the total flow rate decreased (**Figure 6.6**), implying a higher yield of the PCR

product. Hence the PCR yield could be maximised by tuning the total flow rate through the fabricated PCR device.

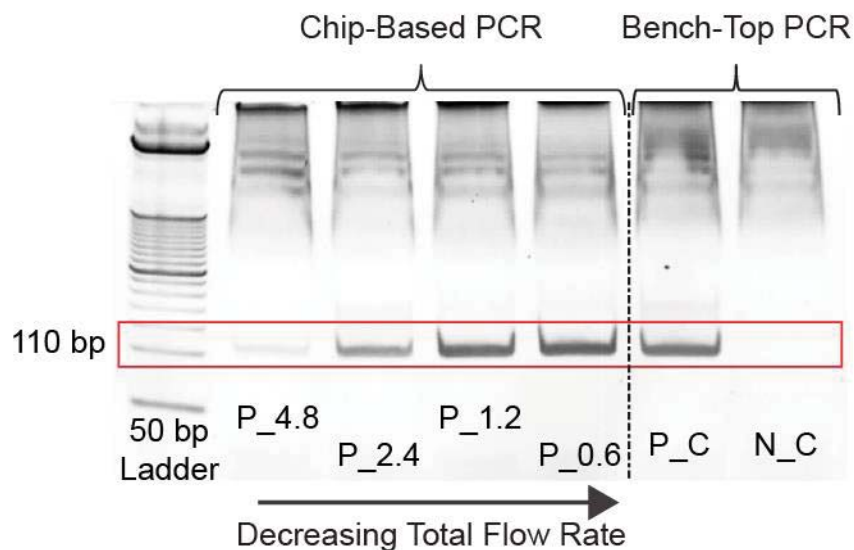


Figure 6.6. Gel electropherograms of collected PCR samples (Table 6.5) subjected to different total flow rates on the chip at a fixed water fraction of 0.4. As the total flow rate decreased from 4.8 to 2.4 to 1.2 to 0.6 $\mu\text{L}/\text{min}$, the 110 bp PCR product band became darker in intensity, indicating an increased yield of the PCR product. The 110 bp band showed up only with the positive control (P_C) and not with the negative control (N_C).

When the flow rate was decreased, the water-in-oil droplets passed more slowly through the chip, allowing more time for denaturation and extension/annealing (Table 6.4). It should be noted that the denaturation duration does not strongly affect the PCR yield because denaturation of DNA templates is virtually instantaneous.^{7,8} Once the denaturation temperature is reached, the hydrogen bonds between DNA strands break immediately. Hence no incubation time is needed. As such, the duration of denaturation should not affect yield significantly. This is important because it means that the flow process may be fully optimised by controlling the extension/annealing time.⁷

Given the above discussion, it is probable that the increase in yield observed at lower total flow rates is attributable to the increased duration of the annealing/extension process.⁷ When the annealing temperature is reached, the primers anneal onto the single-stranded DNA template. The polymerase then extends the annealed primers to replicate the DNA strand. According to the manufacturer's manual, *OneTaq* polymerase has a processivity of 1 kb/min at 68.0 $^{\circ}\text{C}$ meaning around 6.6 s is required to form a 110 bp PCR product.⁹ Given that the temperature at the periphery was 58.0 $^{\circ}\text{C}$, the processivity was expected to be lower, increasing the time required to make the 110 bp PCR product. At the highest total flow rate of 4.8 $\mu\text{L}/\text{min}$, only 1.8 s was spent in the periphery, meaning the polymerase would not have had enough time to fully extend the primers. At the lowest total flow rate of 0.6 $\mu\text{L}/\text{min}$, 14.0 s was spent in the periphery, meaning

the polymerase had sufficient time to fully extend a primer (and potentially move on to extend another primer). Increasing the annealing/extension time would therefore be expected to result in more DNA strands being replicated, leading to a higher PCR yield.

A high throughput is preferred for digital PCR since many droplets must be processed to achieve a usable statistical analysis.^{10,11} To enhance throughput, a high total flow-rate is needed. However, as shown in this experiment, the highest total flow rate resulted in the lowest yield of PCR product. A reasonable compromise between throughput and PCR yield was obtained at 1.2 $\mu\text{L}/\text{min}$. At this flow rate, the yield was high and similar to 0.6 $\mu\text{L}/\text{min}$ (as shown by the similar intensity of the 110 bp band). 2.4 $\mu\text{L}/\text{min}$ gave a much lower PCR yield. 1.2 $\mu\text{L}/\text{min}$ was therefore chosen as the default total flow rate for the subsequent droplet-based PCR experiments on the fabricated PCR device.

6.5 EFFECTS OF VARYING THE CONCENTRATION OF DNA TEMPLATE

Here the effects of serially diluting the DNA template were investigated to determine the lowest concentration at which the on-chip amplification was sufficient for detection by gel electrophoresis.

6.5.1 Experimental

In this experiment, all the conditions described previously (**Section 6.2.1**) were kept the same except for the following changes: the central temperature of the fabricated PCR device was fixed at 90.0 °C; the buffer in the PCR mixture was the GC buffer solution; the total flow rate was 1.2 $\mu\text{L}/\text{min}$. DNA template was successively reduced in concentration from 10000 to 100 to 1.0 and 0.01 pM to determine the lowest concentration of template that could be successfully detected by gel electrophoresis (after amplification).

The starting 1.0 μM DNA template solution was serially diluted three times by a factor of 100 each time (**Figure 6.7**), yielding DNA template solutions of concentration 1.0, 10^{-2} , 10^{-4} and 10^{-6} μM . These starting solutions were then used to prepare PCR mixtures, in which the final concentration of DNA template ranged from 10000 to 0.01 pM. The recipe for the PCR mixtures is summarised in **Table 6.6**.

A negative control was carried out by injecting the oil phase and PCR mixture with no added DNA template, using a flow rate of 0.48 $\mu\text{L}/\text{min}$ for the PCR mixture and 0.72 $\mu\text{L}/\text{min}$ for the oil phase. At the same time, the central temperature was set to 90.0 °C using the PID controller. After a 20

min waiting time (i.e. once a stable temperature gradient had been established), a 20.0 μL sample (sample CN) was collected from the outlet of the PCR device.

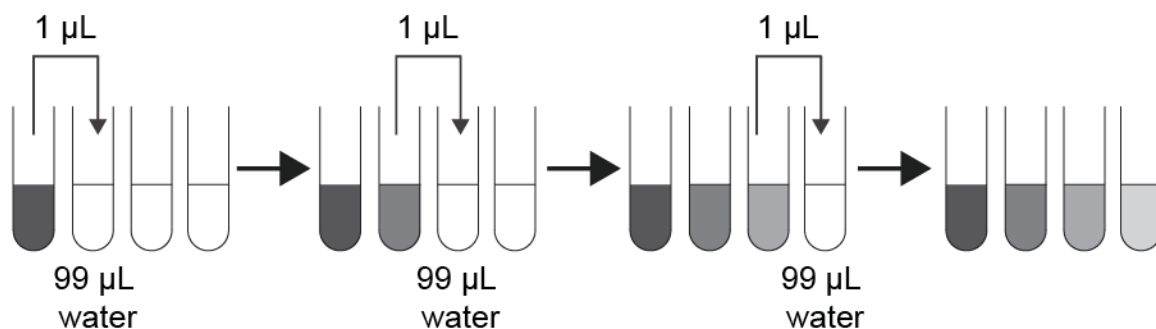


Figure 6.7. Schematic showing serial dilution of an initial 1.0 μM DNA template solution. In each step, the solution was diluted by a factor of 100. After serial dilution, DNA template solutions with concentrations of 1.0, 10^{-2} , 10^{-4} and 10^{-6} μM were used to prepare the PCR mixtures.

Table 6.6. PCR mixtures with varying concentration of DNA template

Component	Volume Added		Starting Concentration		Final Concentration	
Water (RT-PCR Grade)	162.5	μL	-	-	-	-
GC Reaction Buffer	50.0	μL	5	parts	1	parts
DNA Template*	2.5	μL	1.0	μM	10000	pM
			10^{-2}		100	
			10^{-4}		1.0	
			10^{-6}		0.01	
Primers Mix	6.25	μL	10	μM	0.25	μM
dNTPs	5.0	μL	10.0	mM	0.2	mM
Polymerase	5.0	μL	5.0	U/ μL	0.1	U/ μL
Bovine Serum Albumin(BSA)	12.5	μL	1.0	%	0.05	%
TaqMan Probe	6.25	μL	10	μM	0.25	μM

*To prepare a negative control, an equal volume of ultrapure water was used in place of the DNA template.

After collection of sample CN, the heater of the PCR chip was turned off, and the microchannels were flushed with oil phase for 10 min before injecting the PCR mixture with the lowest concentration of DNA template (0.01 pM). At this point, the central heater was set to 90.0 $^{\circ}\text{C}$. Once the droplet generation and temperature gradient were stable, a 20.0 μL sample (sample CP0.01) was collected from the outlet of the PCR device (allowing a 20.0 min waiting time). This procedure was repeated using DNA template concentrations of 1.0, 100 and 10000 pM; the collected samples were labelled CP1.0, CP100 and CP10K, respectively (**Table 6.7**). Droplets from each sample were merged for gel electrophoresis.

20.0 μL of each of the prepared PCR mixtures and a negative control were used for PCR on the bench-top thermal cycler (TC-5000, Techne, USA). The usual two-temperature PCR protocol consisting of 36 cycles was used. In the first cycle, 30.0 s was spent at 94.0 $^{\circ}\text{C}$ for the initial hot-start activation of polymerase, followed by 7.0 s at 62.0 $^{\circ}\text{C}$ for the annealing/extension of primers. The remaining 35 cycles were conducted by alternating between denaturation of DNA templates

(5.0 s at 94.0 °C) and annealing/extension (7.0 s at 62.0 °C) until completion. The collected samples (**Table 6.7**) were analysed by gel electrophoresis.

Table 6.7. Collected samples from varying the DNA template concentration.

Sample	DNA Template Added	Final Template Concentration [pM]	Type of PCR	Central Temperature (T_c) [°C]	Total Flow Rate [μ L/min]
CN	No	-	Chip-based	90	1.2
CP0.01	Yes	0.01	Chip-based		
CP1.0	Yes	1.0	Chip-based		
CP100	Yes	100	Chip-based		
CP10K	Yes	10000	Chip-based		
BN	No	-	Bench-top	N.A. (Bench-top)	N.A. (Bench-top)
BP0.01	Yes	0.01	Bench-top		
BP1.0	Yes	1.0	Bench-top		
BP100	Yes	100	Bench-top		
BP10K	Yes	10000	Bench-top		

6.5.2 Results and Discussion

For both the chip-based PCR (**Figure 6.8(i)**) and the bench-top thermal cycler (**Figure 6.8(ii)**), the 110 bp PCR product band reduced in intensity as the concentration of the DNA template decreased in accordance with expectation.

In the bench-top experiment, the 110 bp band disappeared at a DNA template concentration of 0.01 pM while, in the chip-based experiment, a faint band was still visible at 0.01 pM. It is important not to over interpret this observation since it might be due to these two experiments being analysed separately by gel electrophoresis. As a result, the contrast and brightness settings during the imaging of bands on the gel slab were different. However, it seems that the chip-based PCR was at the very least as effective as the bench-top PCR.

If chip-based PCR was indeed able to generate a higher yield than bench-top PCR at 0.01 pM, this observation could be due to the small volume of the aqueous droplets (~2.5 nL) used on chip, allowing them to reach the target temperatures rapidly due to their small thermal mass.¹²⁻¹⁴ In chip-based PCR heat transfer is rapid, whilst the large volume samples used on the bench-top thermal cycler require more time to reach the desired temperatures, meaning only a fraction of the nominal time at each temperature is fully exploited.^{7,12,13} The rapid heat transfer and more homogenous temperature achieved with small droplets provides an ideal environment for PCR, potentially allowing the primers and polymerase to anneal and extend earlier, thus leading to a higher PCR yields.¹³

It is evident from these results that PCR could be performed with high efficiency on the integrated chip even when using low concentration of DNA template (~15 DNA template molecules per 2.5 nL droplet). From the gel electrophoresis analysis, the PCR yield from the fabricated device was comparable (or better) than the conventional bench-top thermal cycler.

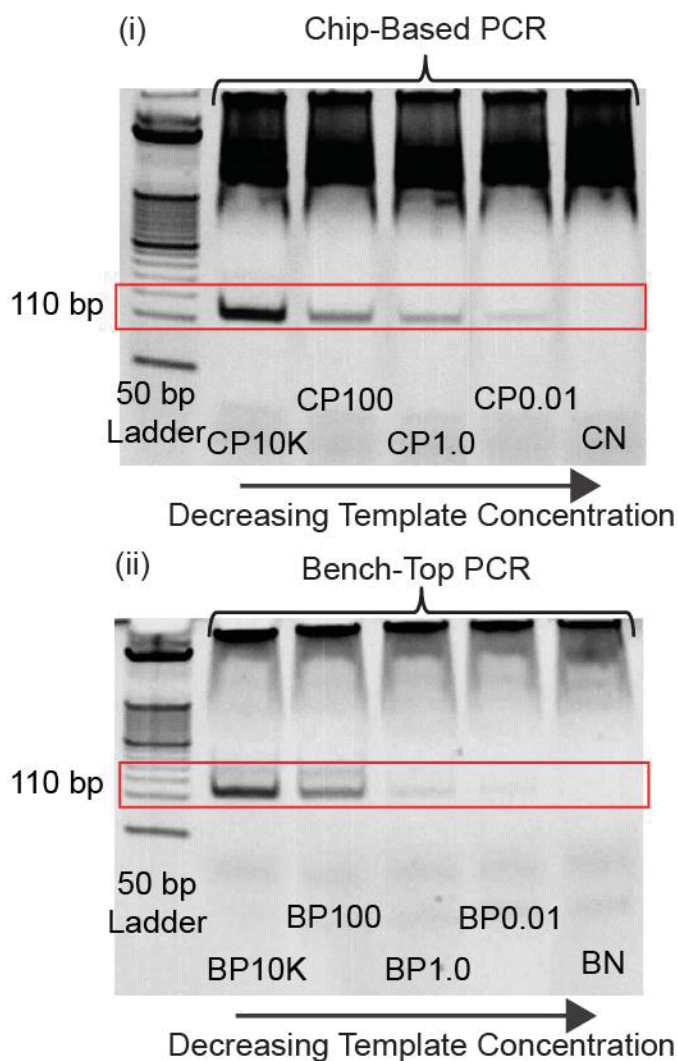


Figure 6.8. Gel electropherograms of collected PCR samples from chip-based and bench-top PCR, **Table 6.7**) at different template concentrations. (i) Chip-based droplet PCR experiment. The final concentration of the DNA template used in the PCR mixture was lowered from 10000 (CP10K) to 100 (CP100) to 1.0 (CP1.0) to 0.01 (CP0.01), to 0 pM (CN). The intensity of the 110 bp band decreased with decreasing template concentration; no band was observed in the absence of template (CN). (ii) Bench-top thermal cycler PCR experiment. The final concentration of the DNA template used in the PCR mixture was lowered from 10000 (BP10K) to 100 (BP100) to 1.0 (BP1.0) to 0.01 (BP0.01) to 0 pM (BN). The intensity of the 110 bp band was observed to decrease with decreasing template concentration; no band was observed at concentration 0.01 pM (BP0.01) and in the absence of template (BN).

6.6 CONCLUSIONS

In this chapter, the fabricated PCR microdevice was successfully applied to droplet-based PCR. The generated radial temperature gradient (as effected by the integrated heater, temperature sensors and air gaps) was successfully used to conduct continuous-flow droplet-based PCR. By varying the central temperature and the flow rate on the fabricated PCR, the PCR yield could be adjusted. 90.0 °C and 1.2 $\mu\text{L}/\text{min}$ were empirically determined to be the best central temperature and total flow rate for the highest PCR yield. Using these conditions, droplet-based PCR could be carried out successfully even at a low DNA template concentration of 0.01 pM (as detectable by gel electrophoresis).

Chapter 7

A confocal fluorescence detection system was coupled with the fabricated PCR device to allow real-time droplet-flow PCR.

7.1 INTRODUCTION

Chapter 5 described the implementation of droplet-based PCR within a microfabricated device. Successful amplification was confirmed by determining the presence of the 110 bp DNA band using gel electrophoresis post reaction. To obtain real-time information regarding the reaction, the fabricated device was coupled with a laser-induced fluorescence confocal detection system as previously described in **Chapter 4, Figure 4.9**.

The real-time fluorescence signal was generated using the TaqMan probe that, as discussed previously (**Chapter 5, Section 5.1.3**), was designed with a complementary sequence to the target sequence in the 110 bp DNA template. The probe was designed with a fluorophore (FAM) attached at the -5' end and a quencher dye (BHQ1) attached at the -3' end of the sequence.¹⁻³ Due to the close proximity of the reporter and the quencher dye, the fluorescence of FAM is partially quenched by BHQ1 when FAM is excited by a laser source. During PCR, the probe and primers anneal onto the DNA template and, when the primers extend, the polymerase cleaves the TaqMan probe to release the fluorophore into solution, causing its fluorescence intensity to increase. The fluorescence signal increases as PCR progresses because more probes are released as more DNA molecules are replicated by the polymerase.

This chapter describes the coupling of the microfluidic device with the laser-induced fluorescence confocal detection system so that the resulting real-time emission signal from the TaqMan probe in the droplets could be determined and measured during successive PCR cycles.

7.2 MEASURING EMISSION INTENSITY OF FITC-CONTAINING DROPLETS

Before testing the laser-induced confocal system using (expensive) TaqMan probes, droplets containing varying concentrations of fluorescein isothiocyanate (FITC) were first assayed. FITC has similar spectral properties to the FAM fluorophore in the TaqMan probe ($\lambda_{ex} = 494$ nm and $\lambda_{em} = 518$ nm).⁴ By varying the concentration of FITC in the droplets, the ability of the detection system (**Chapter 4, Figure 4.9**) to quantitatively measure the change in fluorescence intensity was investigated. This test was intended to imitate the expected situation in real-time PCR where the concentration of the FAM fluorophore would increase during successive PCR cycles.

7.2.1 Detection of Droplets

A. Experimental

Based on the optimal PCR mixture recipe described in the previous chapter (**Chapter 6, Table 6.1**), all the constituents and their concentrations were kept the same, except the TaqMan probe, which was replaced by FITC. The concentration of FITC was varied from 0.10 to 1.00 μM . The PCR recipe is summarised in **Table 7.1**.

Table 7.1. Various concentrations of FITC in the aqueous PCR mixture.

Component	Volume Added		Starting Concentration		Final Concentration	
Water (RT-PCR Grade)	162.5	μL	-	-	-	-
GC Reaction Buffer	50.0	μL	5	parts	1	parts
DNA Template*	2.5	μL	1.0	μM	0.01	μM
Primer Mix (F2 and R2)	6.25	μL	10	μM	0.25	μM
dNTPs	5.0	μL	10.0	mM	0.2	mM
OneTaq Hot-Start Polymerase	5.0	μL	5.0	U/ μL	0.1	U/ μL
Bovine Serum Albumin(BSA)	12.5	μL	1.0	%	0.05	%
Fluorescein Isothiocyanate (FITC)	6.25	μL	4.0	μM	0.10	μM
			10.0		0.25	
			20.0		0.50	
			30.0		0.75	
			40.0		1.00	

*To prepare a negative control, an equal volume of ultrapure water was used in place of the DNA template.

The oil phase used was a 1.8 % (by mass) surfactant mixture in FC-40 (Fluorinert, 3M, USA). The surfactant was a PFPE-PEG block-copolymer.⁵ To make water-in-oil droplets, the PCR mixture and the oil phase were injected into the PCR device at respective flow rates of 0.48 and 0.72 $\mu\text{L}/\text{min}$. The PCR mixtures were tested in sequence, starting with the lowest concentration of FITC and finishing with the highest concentration. The central heater was set to a target temperature (T_c) of 90.0 $^{\circ}\text{C}$ to create a temperature gradient between the central zone and the periphery. As before, the periphery heater was switched off and no fan cooling was used.

Once the droplet formation and the temperature gradient had stabilised, the laser excitation source (488 nm, 10% power, attenuation 20) was focused into a point in the microchannel just after the generation point (**Figure 7.1(i)**) using a 4X objective. The fluorescence intensity was measured for each FITC concentration. As the experiment involved a change of solution for each concentration of FITC, it was necessary to remove the fabricated PCR device from the microscope stage and replace it several times. Precautions had to be taken to ensure the laser point was focused in a consistent fashion (**Figure 7.1(ii)**).

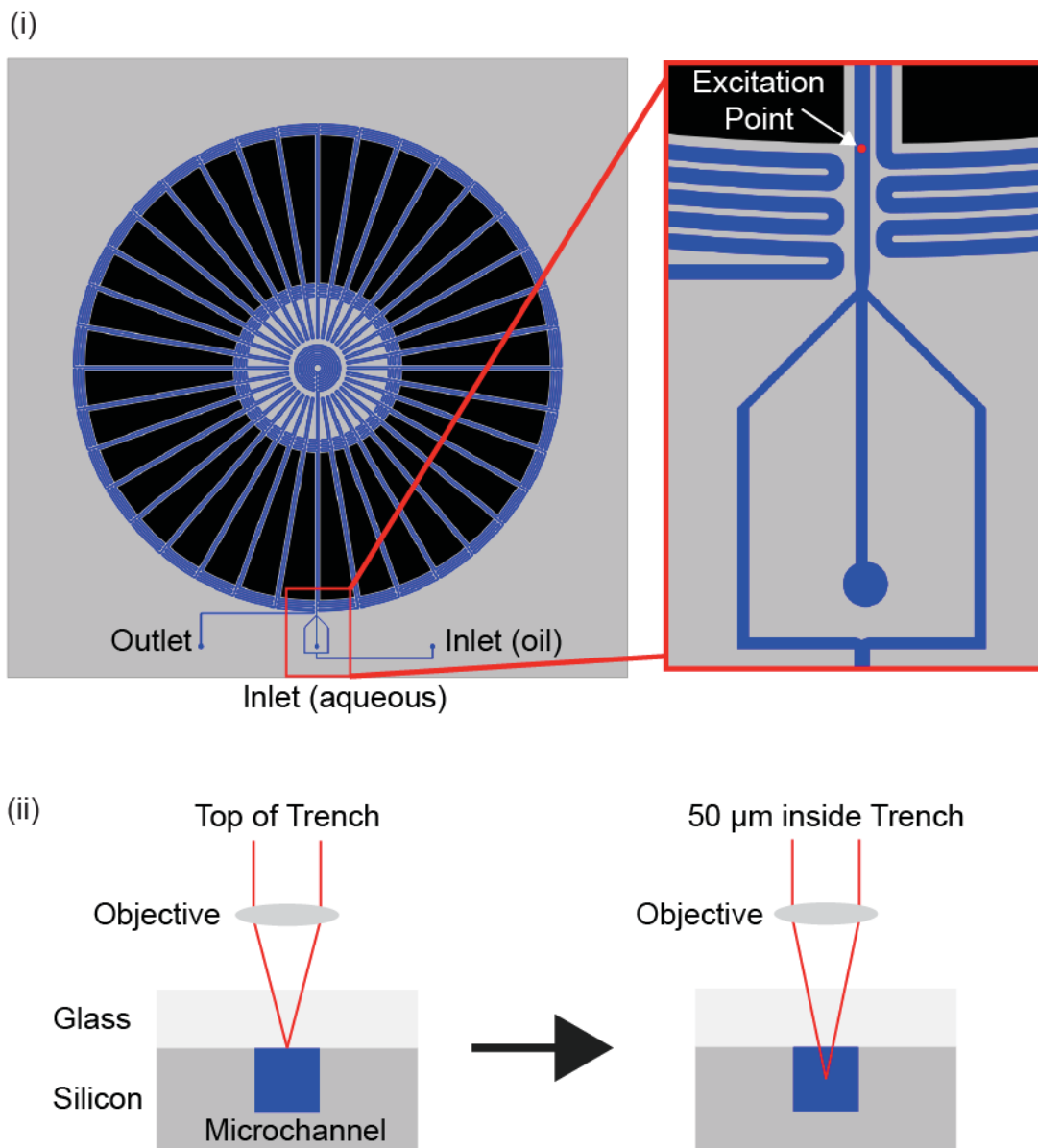


Figure 7.1. Schematic showing the position of the laser excitation point in the microchannel during confocal detection. (i) A 488 nm laser is focused into the microchannel to form an excitation point near the flow-focusing junction where the droplets are formed. As droplets flow through the excitation point, the encapsulated FITC in the droplets is excited, resulting in emission. (ii) The placement of the laser spot is done by first visually focusing the top of the trench and then using the fine-adjustment focusing knob on the microscope to bring the laser point down 50.0 μm into the trench.

As each droplet flowed through the excitation volume, the laser ($\lambda_{ex} = 494 \text{ nm}$) excited the encapsulated FITC molecules within the droplet, resulting in green emission ($\lambda_{max} = 518 \text{ nm}$).⁴ For each concentration of, the signal was recorded using an avalanche photodiode (APD) for a period of 10.0 s, with a data point taken every 50 μs . The average signal per droplet and standard deviation were then determined for each concentration of FITC.

B. Results and Discussion

As the concentration of FITC was increased from 0.1 to 1.0 μM , the intensity of the fluorescence from each droplet increased as expected (**Figure 7.2(i)**).

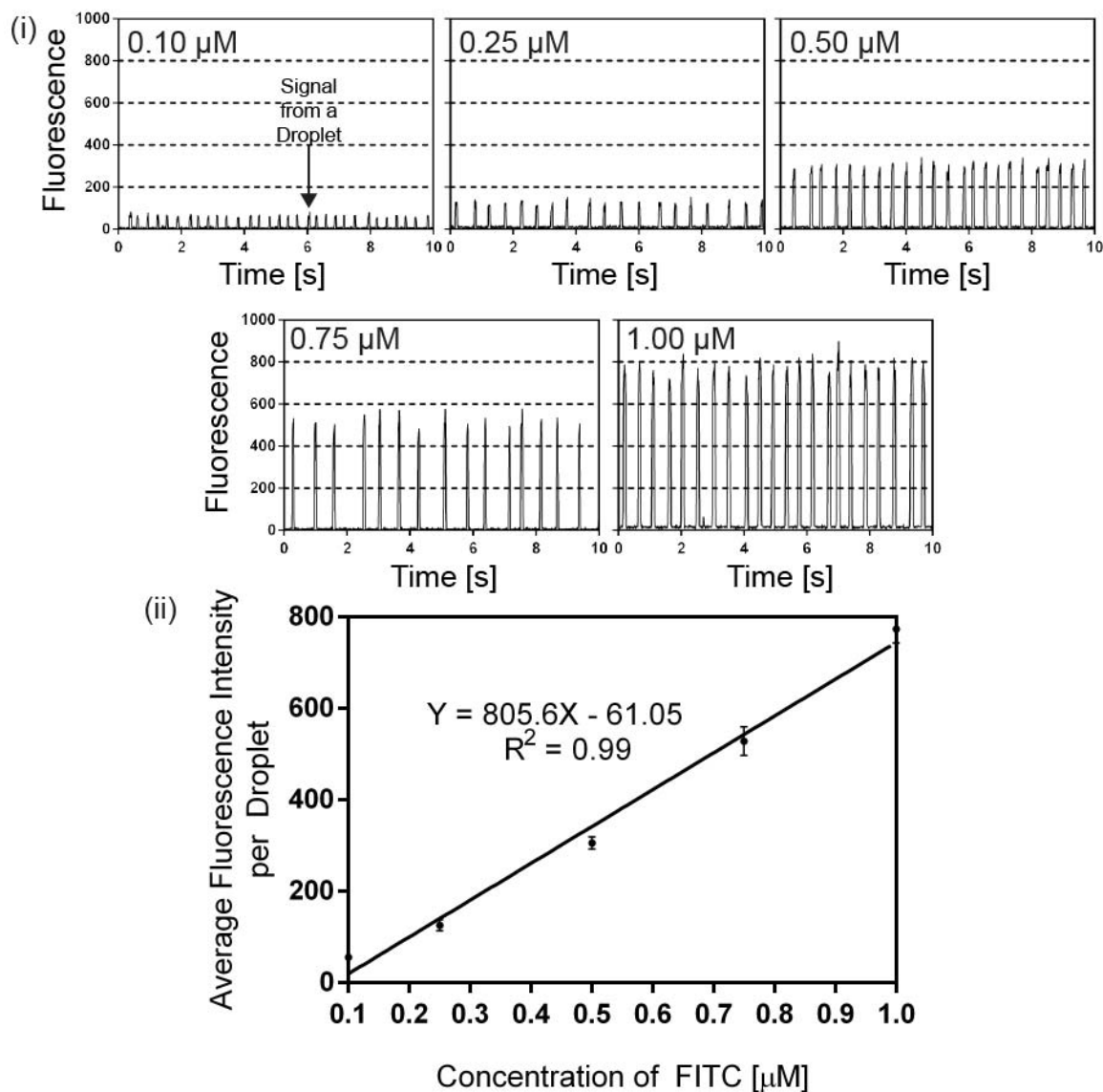


Figure 7.2. (i) Time resolved data obtained from the confocal detection system, showing an increase in the fluorescence intensity from each droplet with increasing concentration of FITC. Each peak corresponds to a droplet flowing through the laser excitation volume in the microchannel. (ii) Plot of average peak signal versus FITC concentration, showing an approximately linear relationship.

As can be seen in **Figure 7.2(ii)**, the average peak signal was linearly proportional to the concentration of FITC. Hence, given a solution of unknown FITC concentration, measurement of the average peak signal allowed the determination of its concentration via a simple linear interpolation. The detection system was able to readily measure droplets with FITC concentrations in the range 0.1 to 1.0 μM .

The ability of the detection system to measure the increase in the intensity of the FITC emission from within droplets suggests that the detection system would also be able to detect the increase in the FAM emission (from 0.25 μM of TaqMan probe in the recipe) with the progression of PCR.

7.3 MEASURING EMISSION INTENSITY OF THE PCR MIXTURE (WITH TAQMAN PROBE) IN DROPLETS

For the experiments described in this section, the TaqMan probe was re-introduced into the PCR mixture, and its emission monitored using the confocal detection system.

7.3.1 Injecting Bench-top PCR Samples into Microdevice as Droplets

A. Experimental

The same working recipe for the PCR mixture described in **Table 6.1** was used. The final concentration of TaqMan probe in the PCR mixture was 0.25 μM . A negative control was also prepared by replacing the DNA template solution with water. The PCR mixture and the negative control were aliquoted into 10 separate PCR tubes to undergo varying numbers of PCR cycles as summarised in **Table 7.2**.

Table 7.2. The prepared samples undergoing varying number of PCR cycles on a bench-top thermal-cycler.

Sample	DNA Template Added	Total Number of PCR Cycle
P0	Yes	0
P6		6
P12		12
P24		24
P36		36
N0	No	0
N6		6
N12		12
N24		24
N36		36

Samples P0 (with DNA template) and N0 (without DNA template) did not undergo thermal-cycling at all. For the other pairs, PCR was conducted on the bench-top thermal cycler using the same two-temperature protocol described in **Chapter 6, Section 6.2.1.H**. Briefly, in the first cycle, 30 s was spent at 94.0 $^{\circ}\text{C}$ for the initial hot-start activation of polymerase and then 7 s was spent at 62.0 $^{\circ}\text{C}$ for the annealing/extension of primers. The next cycles involved denaturation of DNA templates (5.0 s at 94.0 $^{\circ}\text{C}$) and the annealing/extension of primers (7.0 s at 62.0 $^{\circ}\text{C}$). P6 and N6, P12 and N12, P24 and N24, P36 and N36 underwent 6, 12, 24 and 36 total cycles, respectively. After completion of thermal-cycling, the samples were analysed using gel electrophoresis.

The collected samples from the bench-top PCR reaction were injected into the PCR microdevice in the form of water-in-oil droplets to determine whether the emission could be measured using the detection system. As before the oil phase was a 1.8 % (by mass) PFPE-PEG block-copolymer surfactant mixture⁵ in FC-40. The aqueous samples processed in the bench-top thermal cycler and the oil phase were injected into the PCR device at respective flow rates of 0.48 and 0.72 $\mu\text{L}/\text{min}$. The central heater was set to a target central temperature (T_c) of 90.0 °C so as to create a temperature gradient. The periphery heater was switched off and no fan cooling was used.

Once the formation of the droplets and the temperature gradient had stabilised, the laser excitation source (488 nm, 10 % power, attenuation 10) was focused using a 4X objective into the microchannel immediately after the droplet generation point (**Figure 7.1(i)**). The negative samples (in the order of N0, N6, N12, N24, N36) were injected into the fabricated device and measured first. This was followed by P0, P6, P12, P24, P36 in order to minimise carry-over contamination.

As the droplets flowed through the excitation volume, fluorescence emitted within the detection zone was measured. The signal from each measurement point was recorded for a duration of 30 s, with data points recorded every 50 ms.

B. Results and Discussion

The bench-top thermal cycler was used to conduct thermal-cycling on the prepared PCR mixtures (P0 to P36 and N0 to N36). After thermal-cycling, PCR mixtures were injected into the PCR microdevice as water-in-oil droplets. The purpose of this experiment was to observe how the emission signal from the TaqMan probe changed with the number of PCR cycles.^{1,6}

From the gel electrophoresis results (**Figure 7.3(i)**), it was found that the 110 bp band for the positive samples (P0 to P36 which contained the DNA templates) became more intense as the number of PCR cycles increased due to the expected increase in PCR product. P36 which had gone through the greatest number of cycles (36 cycles) had the highest amount of PCR product as represented by the darkest band on the gel slab, while P0 (which did not go through any PCR cycles) had the least product. No band was observable in this case.

With an increasing number of PCR cycles, more TaqMan probe is cleaved as more DNA templates are replicated. An increase in the build-up of free FAM fluorophore in the aqueous solution is therefore expected with increasing cycle number, resulting in a higher fluorescence intensity.

This trend was observed empirically (**Figure 7.3(ii)**). The fluorescence intensity increased from P0 to P36, consistent with the gel electrophoresis results (**Figure 7.3(i)**).

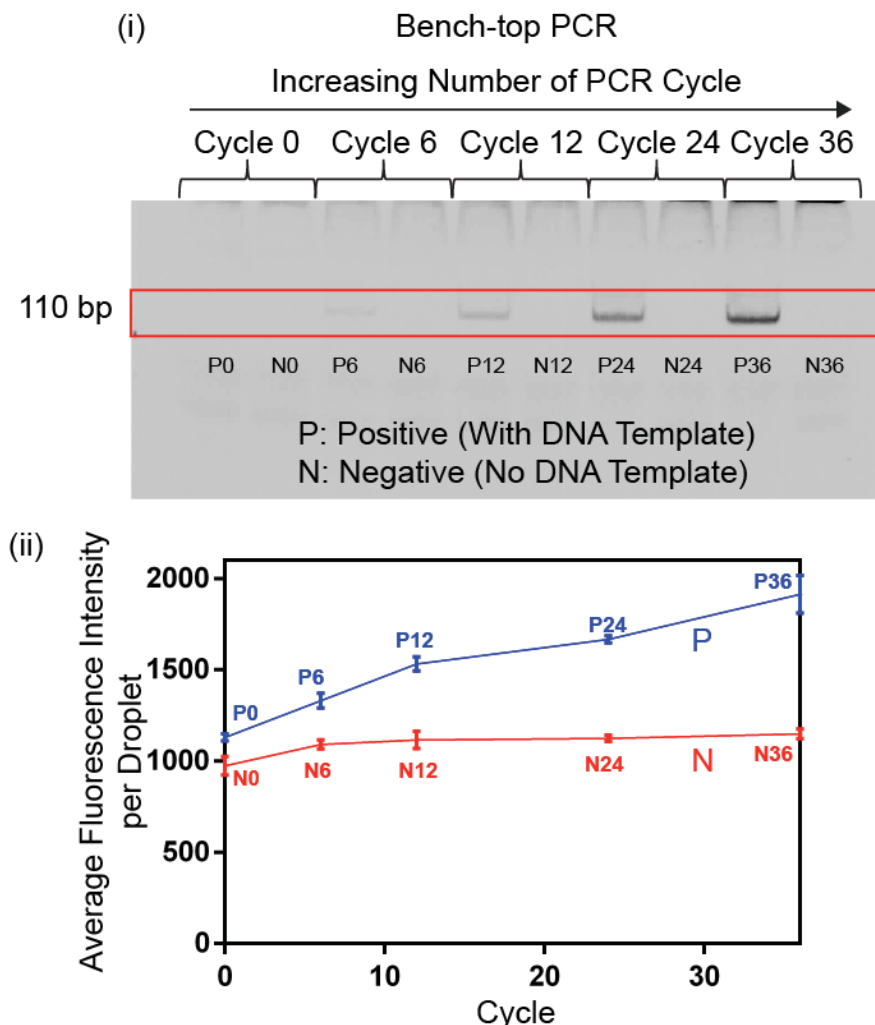


Figure 7.3. (i) The results of the gel electrophoresis of samples subjected to varying numbers of PCR cycles on the bench-top thermal cycler (**Table 7.2**). With increasing cycle number, the 110 bp band became progressively darker from P0 (zero cycle) to P36 (36 cycles) due to increasing PCR yield. No 110 bp band was observed for N0 to N36 because no DNA template was added. (ii) Plot of average peak emission signal from the TaqMan probe versus PCR cycle number. The average intensity of the fluorescence increased from P0 to P36; the average intensity of the fluorescence remained largely the same for N0 to N36.

No product band was observed for the negative samples (N0 to N36) that contained no DNA templates (**Figure 7.3(i)**). This observation confirmed that no amplification occurred in the absence of DNA templates. The corresponding emission signal showed a flat response, consistent with gel electrophoresis results (**Figure 7.3(ii)**).

From this experiment, it was clear that the laser-induced fluorescence confocal detection system was able to measure the increase in the fluorescence intensity from cycle 0 to cycle 36 caused by increasing amounts of TaqMan probe being cleaved during PCR. The detection system was also able to differentiate the signals from samples with and without the DNA template.

The data obtained from the confocal system indicated that the background signal from the TaqMan probe was high. As seen in the negative samples (N0 to N36), though the TaqMan probe was not cleaved after successive cycles of PCR, there was a high emission signal. This signal was due to the partial (as opposed to total) quenching of the FAM fluorophore by the quencher, BHQ1 with only partial transfer of the excitation energy occurring to the quencher.^{1,7} This incomplete quenching resulted in an unwanted strong background signal from the fluorophore even in the absence of the DNA template, resulting in a smaller signal difference between the positive and negative samples.

7.3.2 Conducting Droplet-flow PCR with and without Temperature Gradient

A. Experimental

The same working recipe for the PCR mixture described in **Chapter 6, Table 6.1** was used for all experiments. The final concentration of TaqMan Probe in the PCR mixture was 0.25 μM . As before the oil phase consisted of 1.8 % (by mass) PFPE-PEG block-copolymer surfactant⁵ mixture in FC-40. The PCR mixture and the oil phase were injected into the PCR device at respective flow rates of 0.48 and 0.72 $\mu\text{L}/\text{min}$.

Two sets of fluorescence measurements were measured using the PCR microdevice. The first set of measurements was taken when the central heater was switched off and hence no temperature gradient was generated on the PCR chip. The second set of measurements was taken when the central heater was set to a central temperature (T_c) of 90.0 $^{\circ}\text{C}$. In both cases, the periphery heater was switched off and no fan cooling was used.

In each case, the emission signals were measured by focusing the laser excitation source (488 nm, 10 % power, attenuation 10) using a 10X objective into the microchannel at point C0 and C36 in the microchannel sequentially (**Figure 7.4**). C0 was close to the point of droplet generation, while C36 was close to the exit point of the PCR device. As an individual droplet flowed through the excitation point (C0 or C36), the APD measured the intensity of the fluorescence emitted. The signal from each measurement point was recorded for 60 s, with a data point recorded every 5 ms. Using the recorded data, the average peak magnitude and the standard deviation were determined. At the same time, effluent droplets were collected and merged to enable analysis by gel electrophoresis analysis.

Positive (with DNA template) and negative (without DNA template) control experiments were also conducted on the bench-top thermal cycler using the conditions described in **Chapter 6**,

Section 6.2.1.H. The positive control was used to confirm that the PCR mixture recipe was working before the introduction of the PCR mixture into the microdevice, while the negative control was used to ensure that amplification was not possible without the addition of the specific DNA template.

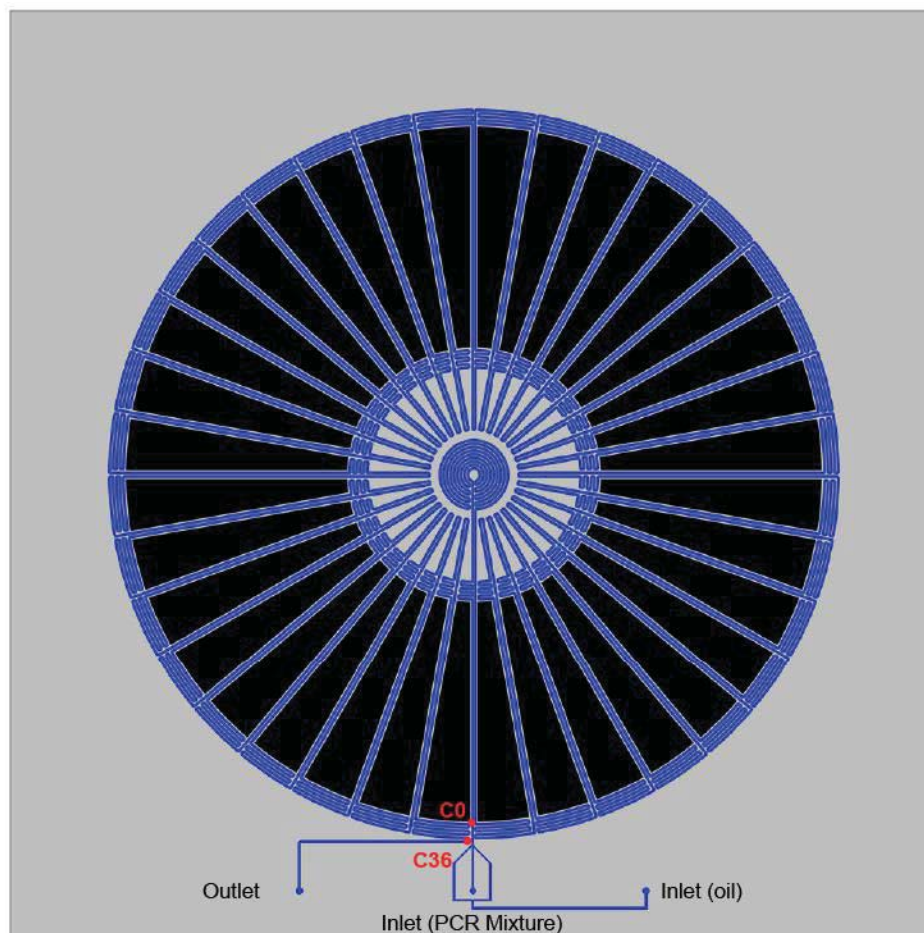


Figure 7.4. Schematic showing the position of the laser excitation points (C0 and C36) in the PCR device. The laser source was focused into the microchannel at points C0 and C36 in the microchannel sequentially for measurement of fluorescence emission. Droplets at C0 had not undergone PCR; droplets at C36 had undergone 36 cycles of PCR.

B. Results and Discussion

Gel electropherograms of the positive control from the bench-top thermal cycler showed a 110 bp band corresponding to the targeted PCR product (**Figure 7.5(i)**), while no band was observed for the equivalent negative control.

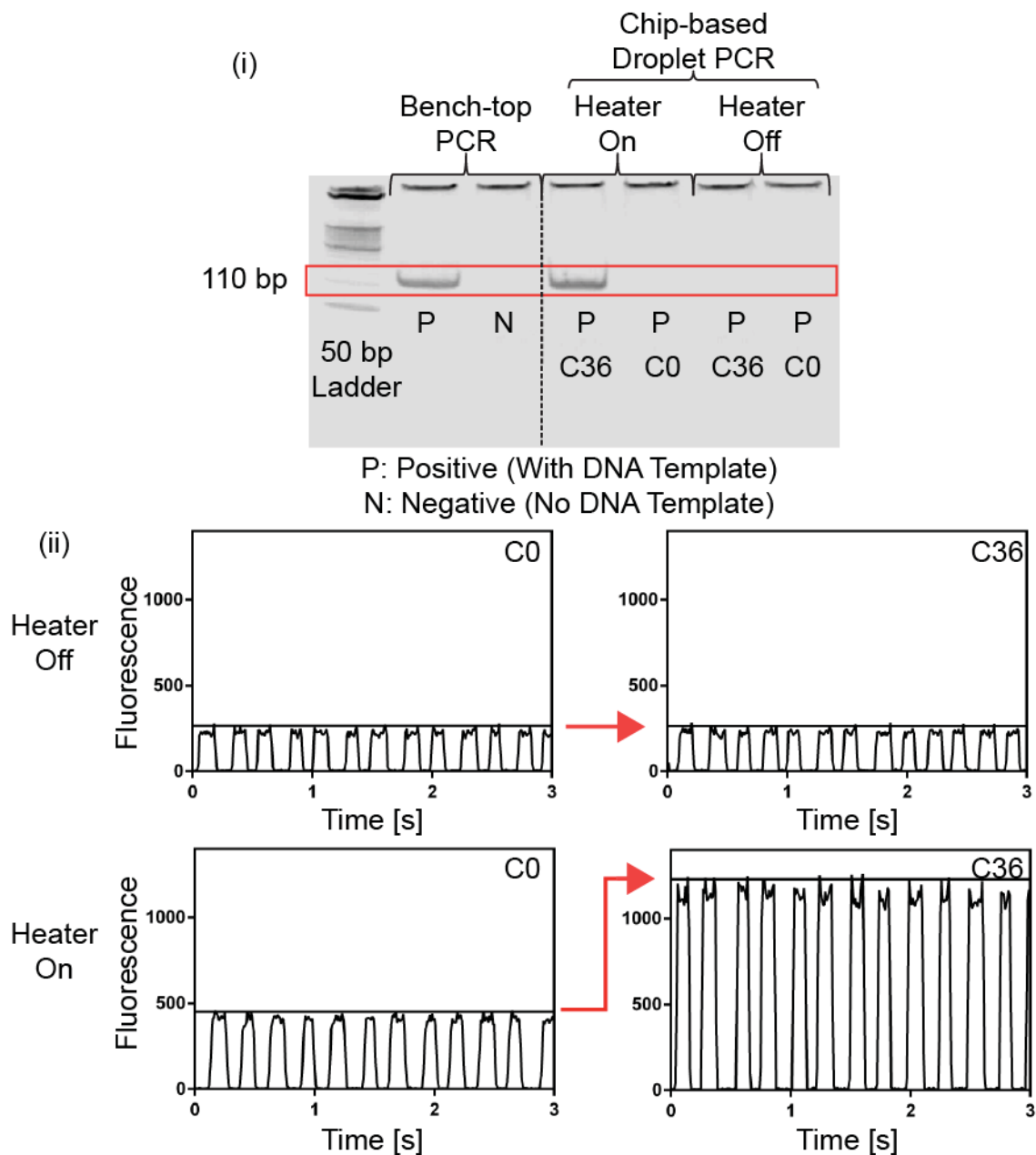


Figure 7.5. (i) Gel electropherograms for samples that had been processed on a bench-top thermal cycler and on chip (with the central heater switched off and on). The positive control from the bench-top thermal cycler showed a 110 bp band, while the negative control showed no band. With the central heater on the PCR device switched off, the collected droplets showed no 110 bp band for either C36 or C0. With the central heater on the PCR device switched on, the collected droplets showed no 110 bp band for C0 but a clear 110 bp band for C36. (ii) Plot of fluorescence intensity versus time for template-containing droplets passing through the detection zone on the PCR device. With the heater switched off, the magnitude of the fluorescence signal remained approximately constant from C0 to C36. With the heater switched on, the magnitude of the fluorescence changed increased by an approximate factor of two from C0 to C36, indicating successful amplification.

The collected droplets from the PCR chip were merged and the accumulated aqueous phase was used for analysis by gel electrophoresis (**Figure 7.5(i)**). When the central heater on the PCR device was turned on (90.0 °C), the template-containing droplets showed no 110 bp band for C0 but a clear 110 bp band for C36, indicating successful amplification on-chip. When the central

heater on the device was turned off, the collected droplets showed no 110 bp band for either C0 or C36, confirming the necessity of the radial temperature gradient for PCR (**Figure 7.5(i)**).

The emission signal before cycling (C0) and after cycling (C36) were determined using the confocal detection system. Time-resolved traces of emission from the flowing droplets are shown in **Figure 7.5(ii)**. With the heater switched off, the C0 and C36 signals were broadly the same. In both cases, a fluorescence intensity peak was observed each time a droplet passed through the detection zone due to incomplete quenching of the TaqMan probe.⁷

With the heater switched on, clear differences were observed between the C36 and C0 signals. As before, the traces showed an increase in emission every time a droplet passed through the detection zone. However, the C36 signal intensity was approximately twice as strong as the C0 signal intensity (**Figure 7.5(ii)**) due to the thermal-cycling induced by the temperature gradient on the device. The increase in the magnitude of the signal from C0 to C36 confirms that droplet-based PCR occurred successfully on the PCR device, and is consistent with the electropherograms.

The fluorescence signal at C0 with the heater switched on was approximately twice as strong as the fluorescence signal with the heater switched off. (**Figure 7.5(ii)**). The fluorescence quantum yield (efficiency of converting absorbed light into emitted light) of FAM is known to decrease with increasing temperature.⁸ Therefore, one would ordinarily expect the intensity of the fluorescence to be lower when the heater is turned on. The unexpected increase in intensity observed in this experiment suggests that quenching (non-radiative energy transfer from FAM to BHQ1) is less efficient at higher temperature, and that the reduction in FRET may have dominated over the drop in the fluorescence quantum yield, resulting a higher fluorescence intensity.

7.3.3 Measuring Emission Intensity at Various Cycles on the PCR Microdevice

A. Experimental

The same PCR mixture described in **Chapter 6, Table 6.1** was used. The final concentration of TaqMan Probe in the PCR mixture was 0.25 μM . As before the oil phase was a 1.8 % (by mass) PFPE-PEG block-copolymer surfactant mixture⁵ in FC-40. The PCR mixture and the oil phase were injected into the PCR device at respective flow rates of 0.48 and 0.72 $\mu\text{L}/\text{min}$. The central heater was set to a target temperature (T_c) of 90.0 $^\circ\text{C}$. The periphery heater was switched off and no fan cooling was used.

Once the formation of the droplets and the temperature gradient had been stabilised, the laser excitation source (488 nm, 10 % power, attenuation 10) was focused at various points along the microchannel (C0, C1, C12, C20, C24, C30, C36 in **Figure 7.6**), and the resulting emission signal was measured. In this way, it was possible to monitor the change in fluorescence signal during the course of thermal cycling and so monitor the progress of the PCR. As the laser point was moved around the PCR device, care had to be taken to ensure that focusing was consistent (**Figure 7.1(ii)**).

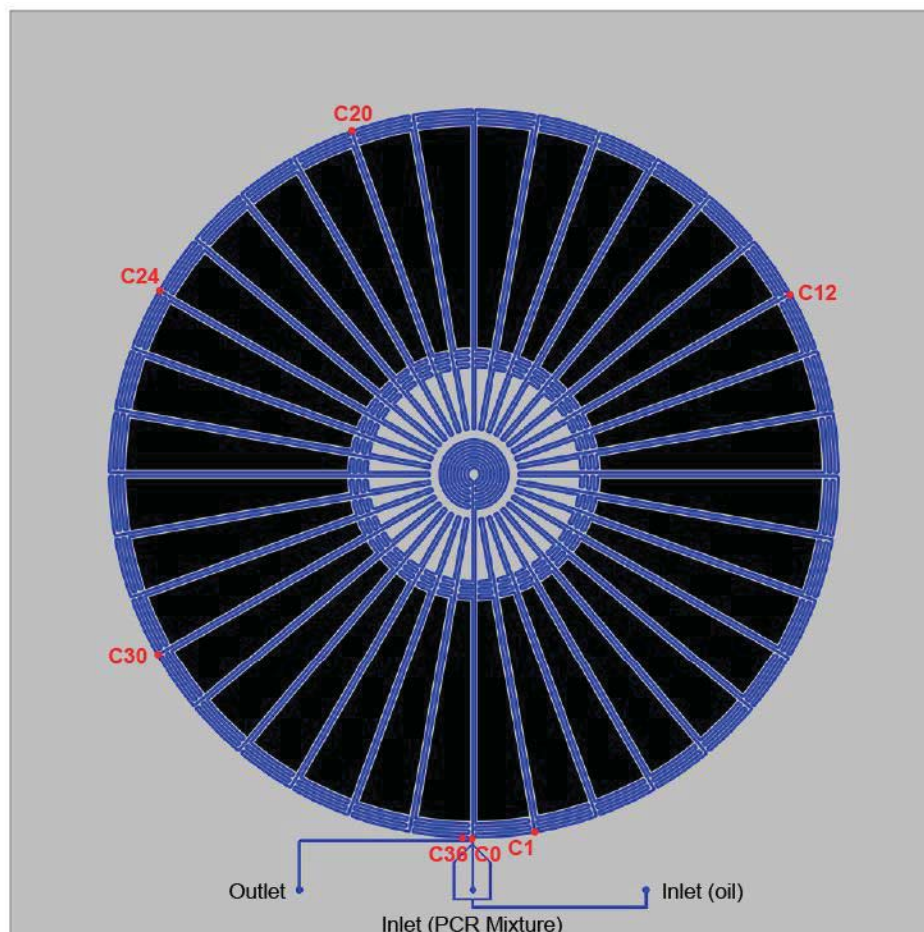


Figure 7.6. Schematic showing the sequential positioning of the laser excitation point in the PCR device, allowing PCR to be monitored on a cycle-by-cycle basis. The laser was focused at point C0 for measurement of the fluorescence intensity at cycle 0 of PCR. The laser was then moved in turn to C1, C12, C20, C24, C30 and C36. All points except C36 were located in the microchannel just before the droplets flowed back into the hot central zone; point C36 was located just before the droplets exited the microdevice.

At each excitation point, the signal from the avalanche photodiode (APD) was recorded for 60 s, with a data point recorded every 1 ms. In each case, the average peak magnitude and the standard deviation were determined. The exiting droplets were collected and merged for analysis by gel electrophoresis. The experimental procedure was then repeated with a negative control that contained all the same components in the same concentrations except that the DNA template was replaced with water. Positive and negative control experiments were also conducted on the

bench-top thermal cycler using an equivalent two-temperature PCR protocol (**Chapter 6, Section 6.2.1.H**).

B. Results and Discussion

The positive control from the bench-top PCR showed a 110 bp band on the gel slab (**Figure 7.7(i)**), confirming that the PCR was working. As expected, no band was observed for the negative control without the use of the DNA template.

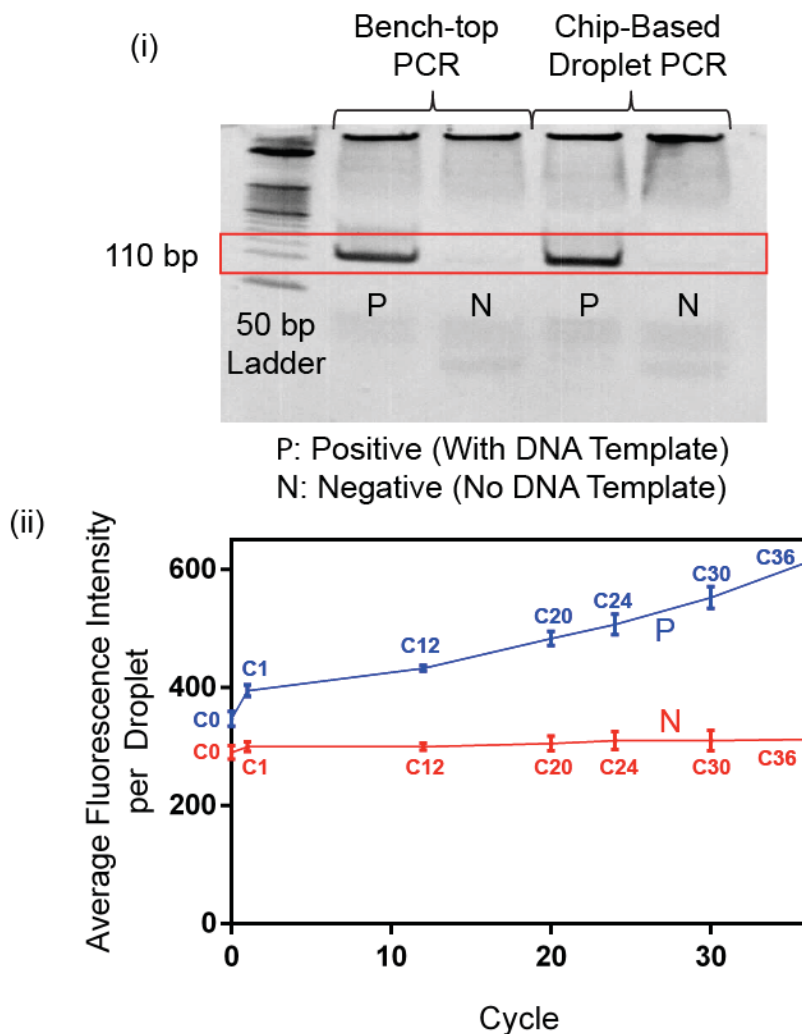


Figure 7.7. (i) Gel electropherograms for positive (with DNA template) and negative (without DNA template) control samples that had undergone PCR on a bench-top thermal cycler or on a chip. For both the bench-top thermal cycler and the PCR device, only the positive control showed the 110 bp product band. (ii) Plot of average peak signal versus PCR cycle number. In the case of the positive control (P), the fluorescence signal increased progressively with cycle number. In the case of the negative control (N), no increase in fluorescence signal was seen.

The collected droplets from the PCR chip were merged for gel electrophoresis analysis (**Figure 7.7(i)**). A 110 bp band was observed for the positive control droplets containing DNA template (P), while no band was observed for the negative control droplets without template (N). These

observations confirmed that droplet-based PCR on the fabricated device was successful and behaving as expected.

The intensity of the emission was measured at C0, C1, C12, C20, C24, C30 and C36. At cycle zero (C0) the droplets containing the PCR mixture had just been generated and were about to enter the first cycle. C1 corresponded to the completion of cycle 1, in which the droplets had undergone the first cycle for the initial activation of the polymerase at the central zone (30.0 s, 90.0 °C) and then a cycle of annealing and extension at the periphery (7.0 s, 58.0 °C). C12 represented the completion of cycle 12 in which the droplets had undergone another 11 cycles (after cycle 1) of denaturation at the central zone (5.0 s, 90.0 °C) and annealing/extension at the periphery (7.0 s, 58.0 °C) on top of cycle 1. C20, C24, C30 and C36 represented analogous situations.

In the presence of DNA template (P), the fluorescence increased in a super-linear fashion with cycle number, indicating successful cycle-by-cycle amplification on the device (**Figure 7.7(ii)**). In the absence of DNA template (N), no increase in the fluorescence intensity was observed with cycle number (**Figure 7.7(ii)**), consistent with there being no amplification.

The behaviour of the negative control on the chip (**Figure 7.7(ii)**) was similar to that observed for samples processed on the bench-top thermal cycler (**Figure 7.3(ii)**). In both cases, a flat response was observed with cycle number with a substantial non-zero background. The behaviour of the positive control was also broadly similar for both the chip- and the bench-top-processed samples. Both showed an increase in fluorescence intensity over successive PCR cycles, indicating a build-up of free FAM fluorophores during the amplification process.³ Both the chip (**Figure 7.7(ii)**) and the bench-top thermal cycler (**Figure 7.3(ii)**) gave a similar increase (an approximate two-fold increase) from cycle 0 to cycle 36. Given the similarity in the signal responses of both negative and positive control, it is evident that the chip-based droplet-flow PCR progressed in a similar manner to the bench-top PCR. The on-chip temperature gradient was clearly able to conduct droplet-flow PCR successfully and in a manner (PCR yield and fluorescence response) that was comparable to the bench-top thermal cycler.

The above results confirmed that the PCR device could be readily coupled to the laser-induced confocal detection system to allow the progression of PCR to be monitored on a cycle-by-cycle basis. It is clear that what limits the performance of the system at present is not the design of the device but the performance of the TaqMan probe (P1) (**Chapter 5, Section 5.1.3**), which gives an unacceptably high background signal. To achieve a higher signal difference between the positive and negative control and hence improve the sensitivity of detection, the background signal needs

to be reduced. This could potentially be achieved by modifying the length and sequence of the TaqMan probe so that FRET occurs more readily to the quencher molecule, thereby increasing the quenching efficiency.^{1,7} Modifying the length and sequence of the TaqMan probe will also lead to better stability in the pairing of the probe with the DNA template so that more of the probe could anneal and be cleaved by the polymerase during PCR to release more of the fluorophore, leading to a higher fluorescence intensity.^{1,7}

Alternatively, it may be necessary to use a different kind of fluorescent probe (intercalating dyes^{9,10}, dual hybridisation probes^{9,10} or molecular beacons^{10,11}) as described in **Chapter 1, Section 1.1.5**). At this stage, intercalating dyes (such as SYBR Green) would be the easiest and cheapest to implement because they do not require a complementary sequence to be designed or a FRET pair to be identified (unlike the TaqMan probe, dual hybridisation probes and molecular beacons). The main disadvantage of using intercalating dyes is their non-specificity; they will bind to all double-stranded DNA and emit.¹⁰ This disadvantage is not an issue at this point because all the gel electrophoresis results (e.g. **Figure 7.7(ii)**) of the PCR mixtures using the current recipe only show a single 110 bp band, indicating only the presence of only one DNA product. As such, the non-specificity of the intercalating dye would not pose a problem. Later on, however, when examining mixed systems containing multiple DNA templates, a more selective probe would be needed.

7.4 CONCLUSIONS

The droplet-based PCR microdevice was coupled with the laser-induced fluorescence detection system and successfully used to conduct droplet-based PCR. The fluorescence from the water-in-oil droplets was successfully measured on a cycle-by-cycle basis by the detection system, and a progressive increase in fluorescence signal was observed, yielding results at least as good as those obtained from the bench-top thermal cycler. Having determined the suitability of the chip and fluorescence detection system for carrying out and monitoring the droplet-based PCR reaction, further work is now needed to find a better fluorescent probe for monitoring progression of the PCR reaction in real-time.

Chapter 8

This chapter concludes the thesis and describes some promising avenues for further work.

8.1 CONCLUSIONS

This thesis has described work undertaken to implement a continuous-flow droplet-based method for conducting PCR in an integrated silicon-based microfluidic device.

The microfluidic device built upon previous work by Schaerli *et al.*¹, in which a polymer-based PCR device utilised a radial temperature gradient to thermally cycle water-in-oil droplets loaded with a PCR mixture. In the original design, the radial temperature gradient was generated using bulky external heaters, fans, and a thermoelectric cooler. Accordingly, the assembly of the device with such external heating and cooling components resulted in a large device footprint (25.0 cm x 25.0 cm x 25.0 cm).

The novel design described in this work reduced the footprint of the original device through the integration of heaters, temperature sensors and air gaps (for passive cooling) to generate a radial temperature gradient. The new silicon-glass devices were designed with metal thin-film patterns on one side of the silicon substrate that served as resistive heaters and temperature sensors; on the other side, a network of microchannels (silicon trenches capped by glass) was etched to carry the droplets. Pie-shaped gaps (through-holes on the silicon) were positioned around the central zone to promote passive cooling from the centre to the periphery. The microchannels were arranged in a spoke-like geometry, allowing the droplets to be shuttled back and forth along the temperature gradient between the hot central zone and cool periphery. Silicon was chosen as the substrate material because silicon-based processing methods provide a straightforward means of integrating the heaters, temperature sensors and air gaps on the chip.

Based on this new design, thermal simulation studies were carried out to determine the physical dimensions of the chip, the integrated heaters and air gaps that were needed to generate a radial temperature gradient suitable for PCR. On the basis of these studies the silicon-glass chip was chosen to have dimensions of 4.0 cm x 4.0 cm x 0.12 cm; the length and the width of the silicon bridges were 0.95 cm and 400 μm , respectively. The radius of the central heater was 0.25 cm, and the distance between the heater and air gaps was 0.30 cm. With these dimensions, simulations showed that a low temperature of ~ 39 $^{\circ}\text{C}$ (with air cooling) and ~ 63 $^{\circ}\text{C}$ (without air cooling) could be achieved at the periphery when the central zone had a fixed temperature of 92.0 $^{\circ}\text{C}$. Importantly, the simulations showed that a broad temperature gradient (92.0 $^{\circ}\text{C}$ at the hot end, and ~ 63 $^{\circ}\text{C}$ at the cool end) for PCR could be achieved without the use of the periphery heater and fan cooling, further reducing the footprint of the device.

Using the dimensions from the thermal simulations, a silicon-based fabrication process was formulated and successfully used to make the new PCR chip. The yield of usable chips was relatively low at ~20 % for each batch of fabrication due to the compounded results of defective microchannels and metal patterns resulting from imperfect lithography and etching, and broken wafers arising from the handling of fragile perforated wafers. These issues are easily overcome when the process of the fabrication is automated and streamlined. Though the yield of usable chip was low, a sufficient number of chips was made to enable them to be evaluated for PCR. Including a polycarbonate housing for fluidic interfacing and a PCB for electrical connections, the completed device had dimensions of 6.0 cm x 5.0 cm x 2.0 cm, which was a major reduction in footprint compared to the previous assembly (25.0 cm x 25.0 cm x 25.0 cm) and highlights the potential for point-of-care or in-the-field application.

The fabricated chip was characterised for its thermal and fluidic functionalities. A temperature gradient (a drop from 92.0 °C at the central zone to 60.0 °C at the periphery) was successfully generated on the chip using the integrated heaters, temperature sensors and air gaps. Water-in-oil droplets were also successfully generated after silanising the hydrophilic walls of the microchannels to render them hydrophobic.

A PCR recipe was optimised using a bench-top thermal cycler. With this recipe, droplet-flow PCR was successfully conducted on the PCR device by flowing droplets back and forth along the radial temperature gradient. Gel electrophoretic analysis of the collected droplets from the device confirmed the presence of the PCR product, and verified the ability of the integrated device to conduct droplet-flow PCR. The yield of the PCR product could be tuned by varying the central temperature of the PCR device (to modify the temperature gradient) and the flow rate of the droplets (to change the residence time of droplets on the chip). By varying the concentration of the DNA template, the PCR device was found to be able to amplify template concentrations as low as 0.01 pM to a level detectable by gel electrophoresis.

A lower detection limit (than gel electrophoresis) is possible when a laser-induced fluorescence detection system is used to probe the droplets containing the fluorescent probe and the PCR mixture. When the PCR device was coupled with a laser-induced fluorescence detection system, the fluorescent signals from the PCR mixture in the water-in-oil droplets were successfully detected and measured on a cycle-by-cycle basis. The observed progressive increase in the fluorescence confirmed the feasibility of carrying out real-time droplet-based PCR on the integrated device.

In conclusion, a silicon-based device was successfully developed for conducting droplet-based PCR using a radial temperature gradient to induce thermal cycling. With the use of integrated heaters, temperature sensors and air gaps, it was possible to make a fully integrated device that was substantially smaller than previously reported chip-based devices for droplet PCR. Despite the small footprint, the device was able to generate a sizeable temperature gradient that could be used to conduct droplet-flow PCR.

8.2 FURTHER WORKS

8.2.1 The Periphery Heater

In the work described above, only the central heater was used to generate the radial temperature gradient. The periphery heater was switched off throughout (**Chapter 4, Figure 4.1**) since the approximate 32 °C temperature difference between the centre and periphery was considered sufficient for PCR. In future work, it would be useful to investigate whether improved amplification could be achieved by activating both the central and periphery heaters to further tune the temperature gradient. In this way greater flexibility in the temperature gradient could be achieved, potentially leading to more controlled thermal-cycling.

8.2.2 Optimisation of TaqMan Probe or Selection of New Probe

In **Chapter 7**, the PCR device was coupled to a laser-induced confocal detection system to allow the progression of PCR to be monitored on a cycle-by-cycle basis. However, the fluorescent TaqMan probe gave a high background signal when used with a negative control that contained no DNA templates. This high background signal was due to incomplete quenching of the FAM fluorophore by FRET.² To achieve a greater signal difference between the positive and negative control, and hence achieve higher sensitivity, the background signal of the TaqMan probe should be reduced, e.g. by modifying its length and sequence so that FRET will occur more readily. The modification of the length and sequence might also result in a more stable hybridisation of the TaqMan probe with the DNA template, resulting in more fluorophore being released and hence a stronger positive response. Alternatively, a different kind of fluorescent probe such as an intercalating dye^{3,4}, dual hybridisation probe^{3,4} or molecular beacon^{4,5} could be used.

At this stage of the work, intercalating dyes (such as SYBR Green) would be the easiest and cheapest to implement because they do not require the design of complementary sequences⁶ or the selection of a FRET pair⁷. Even though intercalating dyes are non-specific (as they emit when they bind to all double-stranded DNA)⁴, the gel electrophoresis results of the current PCR

mixtures showed the presence of only one DNA product. As such, the non-specificity of the intercalating dye is not an issue at the current stage of development where the performance of the device is still being assessed and have freedom in choosing the composition of the PCR mixture. However, in order to apply the chip to a real sample containing multiple DNA templates, it would clearly be necessary to use a more selective fluorescent probe.

8.2.3 Real-time PCR

Once an appropriate fluorescent probe has been identified, the experiment reported in **Chapter 6, Section 6.5** should be repeated using the laser-induced confocal detection system to monitor the signal strength as a function of DNA template concentration. For each concentration of DNA template, cycle-by-cycle measurements of the fluorescence signal should be made to generate a real-time PCR curve showing the build-up of the emission signal over successive cycles. The generated PCR curve for each template concentration should be similar to the curves generated on the real-time Lightcycler thermal cycler (**Chapter 5, Figure 5.7**), and these curves could therefore be used to create a standard curve (**Chapter 5, Figure 5.8**) for quantitation.^{8,9}

8.2.4 Digital PCR

The PCR device has potential to conduct digital PCR. To conduct digital PCR (**Chapter 1, Section 1.1.6**), a pool of DNA templates needs to be diluted and divided into multiple aliquots, with most of the aliquots containing no templates and some aliquots containing only one templates.^{10,11} These independent aliquots then undergo thermal-cycling for PCR, and are subsequently probed for positive ("1") or negative ("0") signal according to whether or not they contain the target template. By its nature, digital PCR requires the handling of a large number of aliquots of very small volumes. Continuous-flow droplet-based PCR is a perfect platform for digital PCR because of its ability to generate droplets at very high throughput. The developed PCR device coupled with real-time online fluorescence detection has the definite potential to be applied to digital PCR applications.

In this work, the PCR device was able to amplify DNA template concentrations as low as 0.01 pM to a level detectable by gel electrophoresis (**Chapter 6, Figure 6.8**). With the water-in-oil droplets having an average volume of ~2.5 nL each, the template concentration of 0.01 pM corresponds to an average of ~15 DNA templates per droplet. For the purposes of digital PCR, the volume of the droplet should be further reduced. For example, if 1.0 nL droplets were used, the same template concentration of 0.01 pM would give an average of ~6 DNA templates in each droplet. Further reducing the droplet volume would consequently reduce the number of DNA

template molecules per droplet to below one as required for digital PCR. The volume of the droplet could be straightforwardly reduced by adjusting the ratio of aqueous to oil flow rate as well using smaller channels (50 μm variation, **Chapter 3, Section 3.2.8**). Besides reducing the droplet volume, digital PCR could also be conducted by further diluting the initial pool of DNA templates. For example, instead of 0.01 pM of DNA template, using a 100-fold diluted pool would result in average of ~ 0.15 DNA templates in a 2.5 nL droplet.

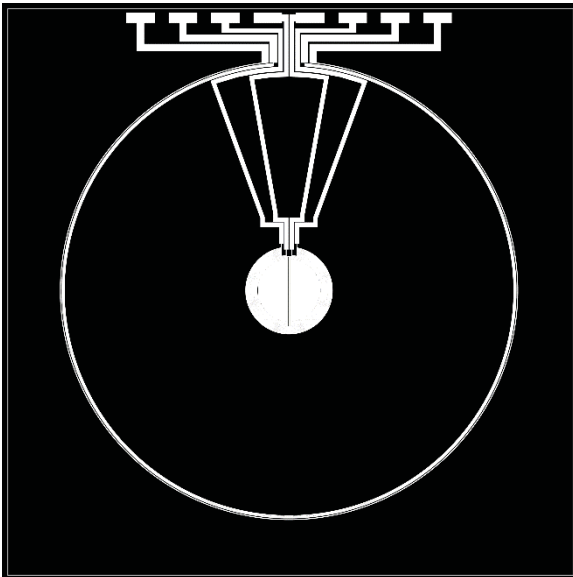
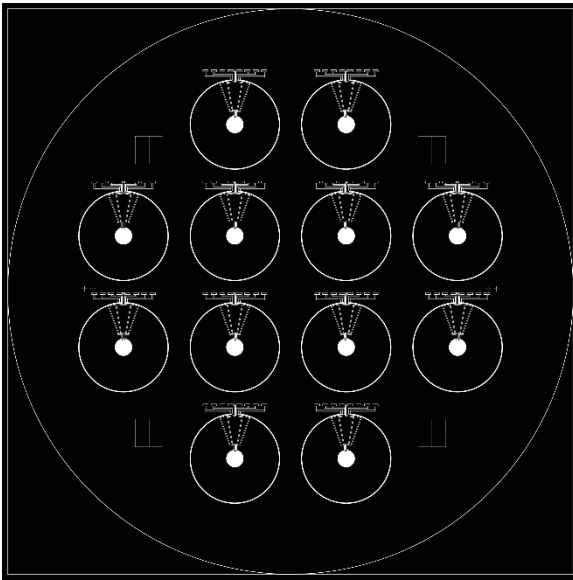
The device developed in this thesis is in principle ideally suited to conducting digital PCR because it can handle many independent small volume aliquots as water-in-oil droplets. At the same time, the generated temperature gradient can be used to thermally cycle the flowing droplets. Lastly, the coupled laser-induced confocal system can be used to probe each droplet. An obstacle towards digital PCR is the selection of an appropriate fluorescent probe (**Section 8.2.2**). With an appropriate probe, it should be easy to differentiate droplets with and without templates, and count them using the laser-induced confocal detection system. The ability to conduct digital PCR on the chip would allow it to be used for absolute quantitation. This will then allow the amplification of DNA templates with concentrations that are below the current detection limit of 0.01 pM to be quantified.

Appendix

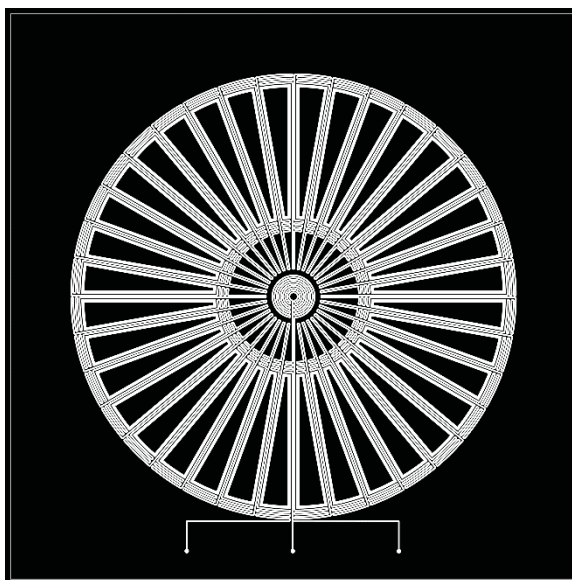
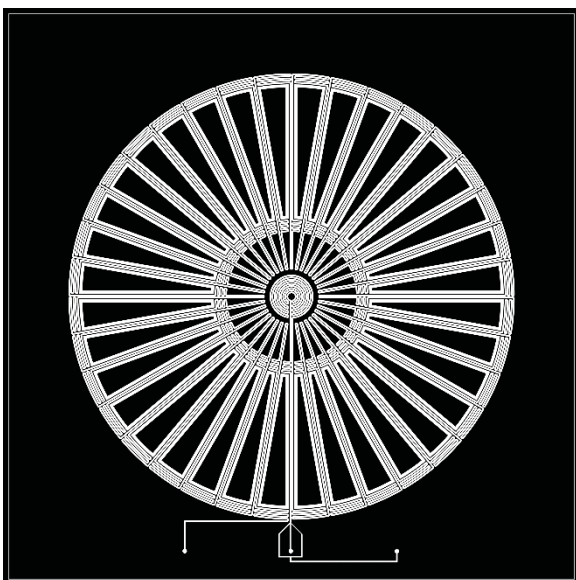
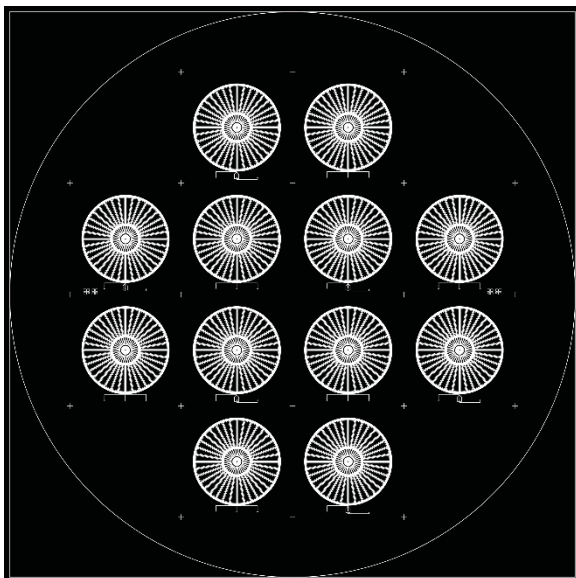
9.1 MASKS

Below are the masks used for the lithography processes mentioned in **Chapter 3**. The black areas represent the regions that are opaque and the white areas represents regions that are transparent on the mask. The whole mask is shown first and is followed by a zoom-in of a single chip. Due to the very fine features in the mask, the images below may not capture all the details. To view the fine features, the soft-copies of the masks are available.

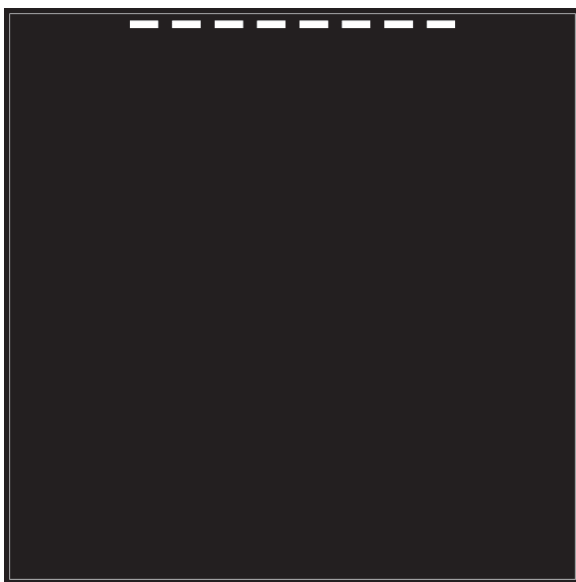
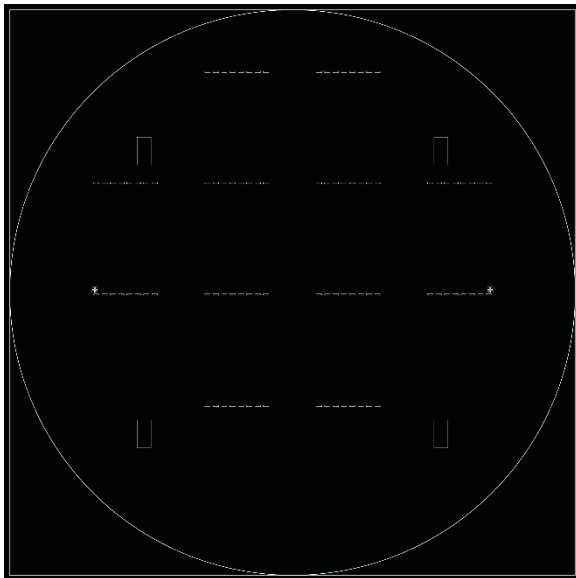
9.1.1 Mask 1



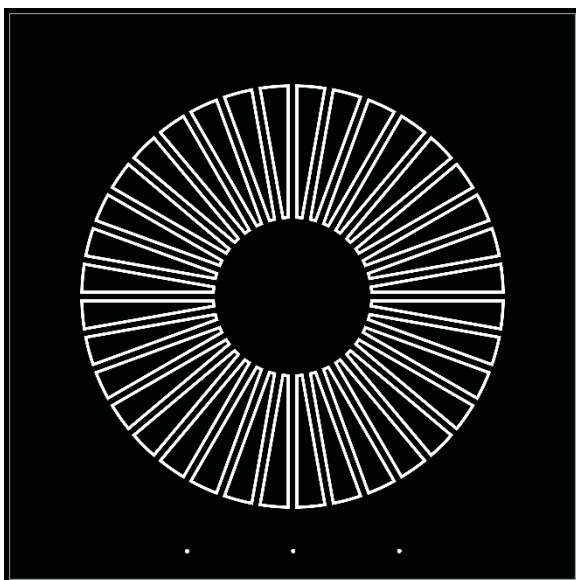
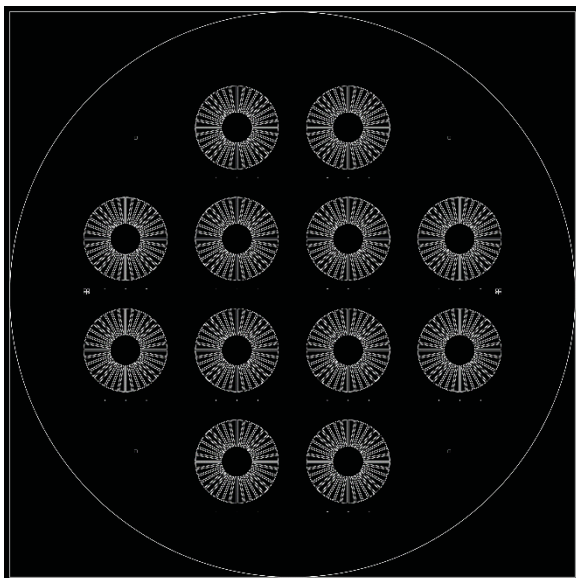
9.1.2 Mask 2



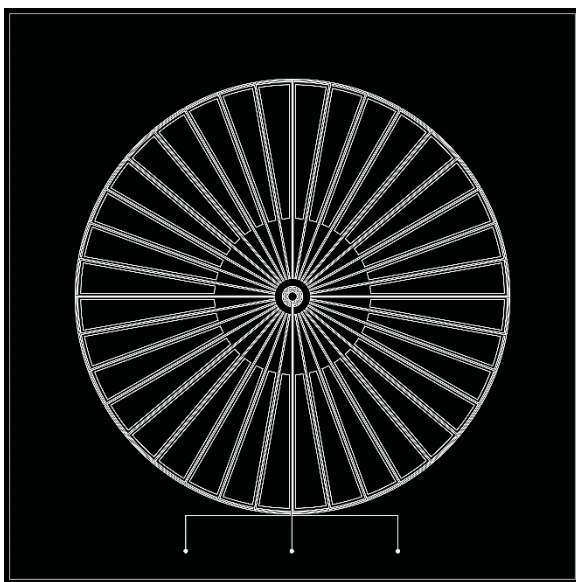
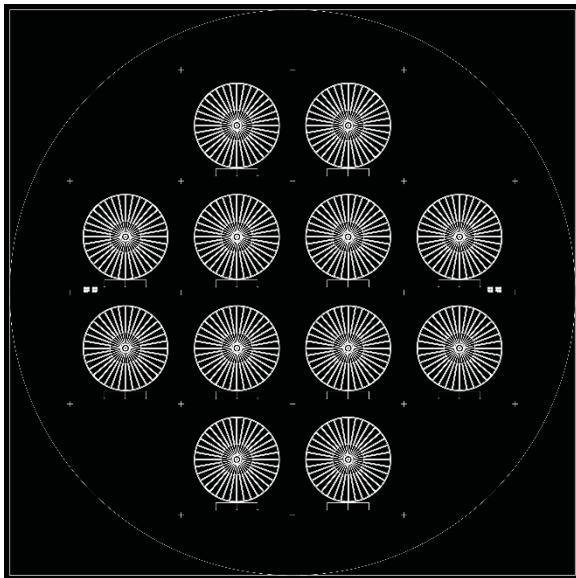
9.1.3 Mask 3



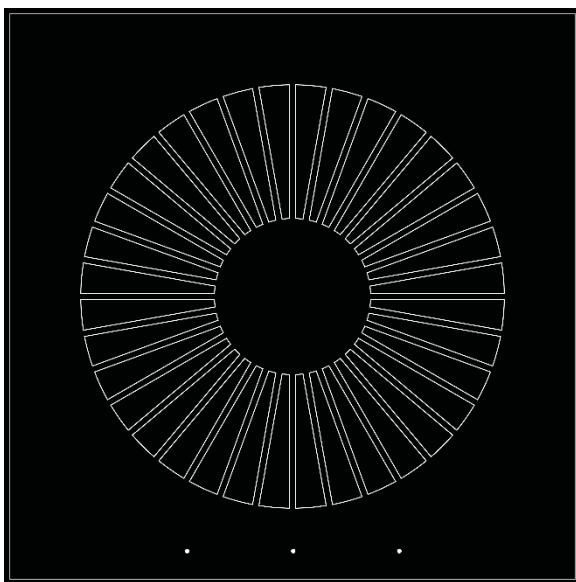
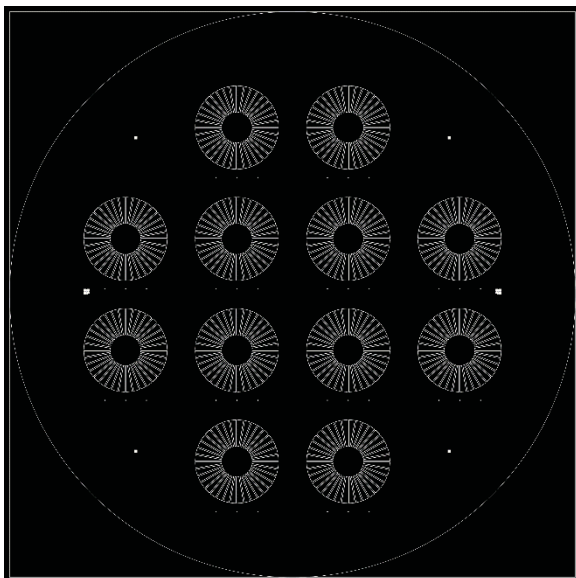
9.1.4 Mask 4



9.1.5 Mask 2A

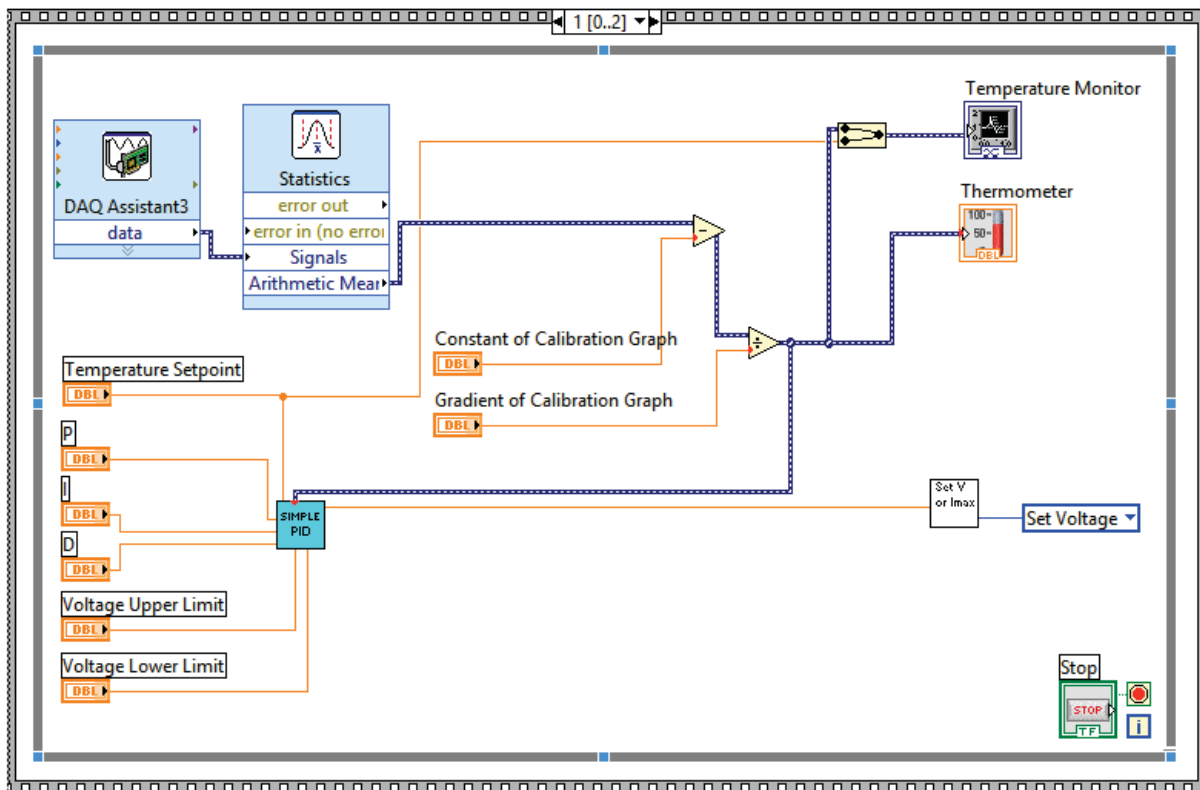


9.1.6 Mask 4A



9.2 LABVIEW

The following code was written to measure the voltages across the Wheatstone bridges by using a DAQ board. The central temperature value was extracted from the measured voltages using the previously determined linear calibration. The measured temperature was then used as an input to the PID controller (SIMPLE PID)¹ which set the voltage output of the power supply (**Chapter 4, Section 4.2**).




```
end
```

9.4.2 To Analyse Data (dataanalysis)

```
x = data(:,1); %Extract data column 1 to x
y = data(:,2); %Extract data column 2 to y

%Create x1 to predefined duration with resolution ms interval
x1 = (res/1000:res/1000:(numel(y)*res/1000))';

%To change y to y1 with digital 1 and 0
i = 1; %Initiate i with a value of 1
while (i<=numel(y))
    if y(i) > peak %Change value for selectivity of peaks
        y1(i,1) = 1;
    else
        y1(i,1) = 0;
    end
    i = i + 1;
end

%To determine the address n for start and end of peak
i = 1; %Initiate i with a value of 1
ii = 1; %Initiate ii with a value of 1
while (i<numel(y1))
    if ((y1(i+1) - y1(i)) ~= 0) & (y1(i+1)==1)
        n(ii,1) = i+1;
        ii = ii + 1;
    elseif ((y1(i+1) - y1(i)) ~= 0) & (y1(i)==1)
        n(ii,1) = i;
        ii = ii + 1;
    else
        end
    i = i+1;
end

%To determine the time (or length) of the droplet
i = 1; %Initiate i with a value of 1
ii = 1; %Initiate ii with a value of 1
if y1(n(1))==1 & y1(n(1)+1)==0 %1/2 starting peaks
    if y1(n(numel(n)))==1 & y1(n(numel(n))-1)==1 %Full ending peak
        while (i<numel(n))
            time(ii,1) = x1(n(i+2))-x1(n(i+1));
            ii=ii+1;
            i=i+2;
        end
    elseif y1(n(numel(n)))==1 & y1(n(numel(n))-1)==0 %1/2 ending
peak
        while (i<numel(n)-1)
            time(ii,1) = x1(n(i+2))-x1(n(i+1));
            ii=ii+1;
            i=i+2;
        end
    else
        end
end
```

```

elseif y1(n(1))==1 & y1(n(1)+1)==1 %Full starting peak
    if y1(n(numel(n)))==1 & y1(n(numel(n))-1)==1 %Full ending peak
        while (i<=numel(n))
            time(ii,1)= x1(n(i+1))-x1(n(i));
            ii=ii+1;
            i=i+2;
        end
    elseif y1(n(numel(n)))==1 & y1(n(numel(n))-1)==0 %1/2 ending
peak
        while (i<numel(n))
            time(ii,1)= x1(n(i+1))-x1(n(i));
            ii=ii+1;
            i=i+2;
        end
    else
    end
else
end

%To determine the time (or length) between droplets
i = 1; %Initiate i with a value of 1
ii = 1; %Initiate ii with a value of 1
if y1(n(1))==1 & y1(n(1)+1)==0 %1/2 starting peaks
    if y1(n(numel(n)))==1 & y1(n(numel(n))-1)==1 %Full ending peak
        while (i<numel(n))
            t1(ii,1)= x1(n(i+1))-x1(n(i));
            ii=ii+1;
            i=i+2;
        end
    elseif y1(n(numel(n)))==1 & y1(n(numel(n))-1)==0 %1/2 ending
peak
        while (i<numel(n))
            t1(ii,1)= x1(n(i+1))-x1(n(i));
            ii=ii+1;
            i=i+2;
        end
    else
    end
elseif y1(n(1))==1 & y1(n(1)+1)==1 %Full starting peak
    if y1(n(numel(n)))==1 & y1(n(numel(n))-1)==1 %Full ending peak
        while (i<numel(n)-1)
            t1(ii,1)= x1(n(i+2))-x1(n(i+1));
            ii=ii+1;
            i=i+2;
        end
    elseif y1(n(numel(n)))==1 & y1(n(numel(n))-1)==0 %1/2 ending
peak
        while (i<numel(n))
            t1(ii,1)= x1(n(i+2))-x1(n(i+1));
            ii=ii+1;
            i=i+2;
        end
    else
    end
else
end

```

```

end

%To determine the period (start to start of peak)
i = 1; %Initiate i with a value of 1
ii = 1; %Initiate ii with a value of 1
if y1(n(1))==1 & y1(n(1)+1)==0 %1/2 starting peaks
    if y1(n(numel(n)))==1 & y1(n(numel(n))-1)==1 %Full ending peak
        while (i<numel(n)-2)
            period(ii,1)= x1(n(i+3))-x1(n(i+1));
            ii=ii+1;
            i=i+2;
        end
    elseif y1(n(numel(n)))==1 & y1(n(numel(n))-1)==0 %1/2 ending
peak
        while (i<numel(n)-1)
            period(ii,1)= x1(n(i+3))-x1(n(i+1));
            ii=ii+1;
            i=i+2;
        end
    else
    end
elseif y1(n(1))==1 & y1(n(1)+1)==1 %Full starting peak
    if y1(n(numel(n)))==1 & y1(n(numel(n))-1)==1 %Full ending peak
        while (i<numel(n)-1)
            period(ii,1)= x1(n(i+2))-x1(n(i));
            ii=ii+1;
            i=i+2;
        end
    elseif y1(n(numel(n)))==1 & y1(n(numel(n))-1)==0 %1/2 ending
peak
        while (i<numel(n))
            period(ii,1)= x1(n(i+2))-x1(n(i));
            ii=ii+1;
            i=i+2;
        end
    else
    end
else
end

%To determine total number of droplets for a duration
%To determine droplet generation frequency
if y1(n(1))==1 & y1(n(1)+1)==0 %1/2 starting peaks
    if y1(n(numel(n)))==1 & y1(n(numel(n))-1)==1 %Full ending peak
        totaltime = x1(n(numel(n)))-x1(n(2));
        totalnumber = numel(time);
        frequency = totalnumber/totaltime;
    elseif y1(n(numel(n)))==1 & y1(n(numel(n))-1)==0 %1/2 ending
peak
        totaltime = x1(n(numel(n)-1))-x1(n(2));
        totalnumber = numel(time);
        frequency = totalnumber/totaltime;
    else
    end
elseif y1(n(1))==1 & y1(n(1)+1)==1 %Full starting peak

```

```

    if y1(n(numel(n)))==1 & y1(n(numel(n))-1)==1 %Full ending peak
        totaltime = x1(n(numel(n)))-x1(n(1));
        totalnumber = numel(time);
        frequency = totalnumber/totaltime;
    elseif y1(n(numel(n)))==1 & y1(n(numel(n))-1)==0 %1/2 ending
peak
        totaltime = x1(n(numel(n)-1))-x1(n(1));
        totalnumber = numel(time);
        frequency = totalnumber/totaltime;
    else
    end
else
end

%To determine average time (or length) of droplets
time_average = mean(time);
time_std = std(time);
time_rsd = time_std/time_average * 100;

%To determine average time between droplets
t1_average = mean(t1);
t1_std = std(t1);
t1_rsd = t1_std/t1_average * 100;

%To determine average period
period_average = mean(period);
period_std = std(period);
period_rsd = period_std/period_average * 100;

%To print all values to screen
fprintf('Total number of droplet is %g.\n', totalnumber);
fprintf('Total time is %g s.\n', totaltime);
fprintf('Droplet generation frequency is %g per s.\n\n', frequency);

fprintf('Time (length): Average : %g s.\n', time_average);
fprintf('Time (length): SD : %g s.\n', time_std);
fprintf('Time (length): RSD : %g per cent.\n\n', time_rsd);

fprintf('Time (between droplets): Average : %g s.\n', t1_average);
fprintf('Time (between droplets): SD : %g s.\n', t1_std);
fprintf('Time (between droplets): RSD : %g per cent.\n\n', t1_rsd);

fprintf('Period: Average : %g s.\n', period_average);
fprintf('Period: SD : %g s.\n', period_std);
fprintf('Period: RSD : %g per cent.\n\n', period_rsd);

%To plot graphs
plot(x1,y);
hold;
plot(x1,y1);
plot(x1(n),1,'x','color','red');
pause; %to pause before next analysis
hold; %to release the graph

```


References

- 1 Hodge R. *The molecules of life: DNA, RNA, and proteins*. Facts On File: New York, 2009.
- 2 Alberts B, Wilson J, Hunt T. *Molecular biology of the cell*. Garland Science: New York, 2008.
- 3 Bartlett JMS, Stirling D. A Short History of the Polymerase Chain Reaction. In: *PCR Protocols*. Humana Press: Totowa, NJ, 2003, pp 3–6.
- 4 Elliott WH, Elliott DC. *Biochemistry and molecular biology*. Oxford University Press: Oxford; New York, 2009.
- 5 Mullis KB, Faloona FA. Specific synthesis of DNA in vitro via a polymerase-catalyzed chain reaction. *Methods in enzymology* 1987; **155**: 335.
- 6 Wittwer CT, Farrar JS. Magic in solution: an introduction and brief history of PCR. In: *PCR Troubleshooting and Optimization: The Essential Guide*. Caister Academic Press: Norfolk, UK, 2011, pp 1–21.
- 7 Garibyan L, Avashia N. Polymerase Chain Reaction. *Journal of Investigative Dermatology* 2013; **133**: 1–4.
- 8 Cox MM, Doudna JA, O'Donnell M. *Molecular biology: principles and practice*. W.H. Freeman and Co.: New York, NY, 2012.
- 9 Saiki R, Scharf S, Faloona F, Mullis K, Horn G, Erlich H *et al*. Enzymatic amplification of beta-globin genomic sequences and restriction site analysis for diagnosis of sickle cell anemia. *Science* 1985; **230**: 1350–1354.
- 10 Saiki R, Gelfand D, Stoffel S, Scharf S, Higuchi R, Horn G *et al*. Primer-directed enzymatic amplification of DNA with a thermostable DNA polymerase. *Science* 1988; **239**: 487–491.
- 11 Weiss J. Luminaries in laboratory medicine: Kary Mullis: microbiology and clinical chemistry. *Laboratory Medicine* 2009; **40**: 441–442.
- 12 Post JC, Ehrlich GD. The impact of the polymerase chain reaction in clinical medicine. *Jama* 2000; **283**: 1544–1546.
- 13 Rutledge RG. Mathematics of quantitative kinetic PCR and the application of standard curves. *Nucleic Acids Research* 2003; **31**: 93e–93.
- 14 Hyndman DL, Mitsuhashi M. PCR Primer Design. In: *PCR Protocols*. Humana Press: Totowa, NJ, 2003, pp 81–88.
- 15 Cha RS, Thilly WG. Specificity, efficiency, and fidelity of PCR. *Genome Research* 1993; **3**: S18–S29.
- 16 Watson JD, Crick FH. Molecular structure of nucleic acids. *Nature* 1953; **171**: 737–738.

- 17 Pray L. Discovery of DNA structure and function: Watson and Crick. *Nature Education* 2008; **1**: 100.
- 18 Rychlik W, Spencer WJ, Rhoads RE. Optimization of the annealing temperature for DNA amplification in vitro. *Nucleic acids research* 1990; **18**: 6409–6412.
- 19 Chou Q, Russell M, Birch DE, Raymond J, Bloch W. Prevention of pre-PCR mis-priming and primer dimerization improves low-copy-number amplifications. *Nucleic Acids Research* 1992; **20**: 1717–1723.
- 20 Singh VK, Govindarajan R, Naik S, Kumar A. The effect of hairpin structure on PCR amplification efficiency. 2000.
- 21 Cline J, Braman JC, Hogrefe HH. PCR fidelity of pfu DNA polymerase and other thermostable DNA polymerases. *Nucleic Acids Research* 1996; **24**: 3546–3551.
- 22 Pelt-Verkuil E, Belkum A, Hays JP. Taq and Other Thermostable DNA Polymerases. In: *Principles and Technical Aspects of PCR Amplification*. Springer Netherlands: Dordrecht, 2008, pp 103–118.
- 23 Wittwer CT, Garling DJ. Rapid cycle DNA amplification: time and temperature optimization. 1991.
- 24 Kunkel TA. DNA Replication Fidelity. *Journal of Biological Chemistry* 2004; **279**: 16895–16898.
- 25 Yang L, Arora K, Beard WA, Wilson SH, Schlick T. Critical Role of Magnesium Ions in DNA Polymerase β 's Closing and Active Site Assembly. *J Am Chem Soc* 2004; **126**: 8441–8453.
- 26 Gundry CN, Poulson MD. Obtaining maximum PCR sensitivity and specificity. In: *PCR Troubleshooting and Optimization: The Essential Guide*. Caister Academic Press: Norfolk, UK, 2011, pp 79–96.
- 27 Gallup JM. qPCR inhibition and amplification of difficult templates. In: *PCR troubleshooting and optimization: the essential guide*. Caister Academic Press: Norfolk, UK, 2011, pp 23–65.
- 28 Smith KT, Long CM, Bowman B, Manos MM. Using cosolvents to enhance PCR amplification. *Amplifications* 1990; **5**: 617.
- 29 Varadaraj K, Skinner DM. Denaturants or cosolvents improve the specificity of PCR amplification of a G+ C-rich DNA using genetically engineered DNA polymerases. *Gene* 1994; **140**: 1–5.
- 30 Frackman S, Kobs G, Simpson D, Storts D. Betaine and DMSO: enhancing agents for PCR. *Promega notes* 1998; **65**: 27–29.

- 31 Musso M, Bocciardi R, Parodi S, Ravazzolo R, Ceccherini I. Betaine, dimethyl sulfoxide, and 7-deaza-dGTP, a powerful mixture for amplification of GC-rich DNA sequences. *The Journal of Molecular Diagnostics* 2006; **8**: 544–550.
- 32 Ralser M, Querfurth R, Warnatz H-J, Lehrach H, Yaspo M-L, Krobitch S. An efficient and economic enhancer mix for PCR. *Biochemical and biophysical research communications* 2006; **347**: 747–751.
- 33 Kodzius R, Xiao K, Wu J, Yi X, Gong X, Foulds IG *et al.* Inhibitory effect of common microfluidic materials on PCR outcome. *Sensors and Actuators B: Chemical* 2012; **161**: 349–358.
- 34 Heid CA, Stevens J, Livak KJ, Williams PM. Real time quantitative PCR. *Genome research* 1996; **6**: 986–994.
- 35 Bizouarn F. Digital PCR: Improving Nucleic Acid Quantification. 2012.<http://online.liebertpub.com/doi/full/10.1089/gen.32.9.15> (accessed 28 Jan2016).
- 36 Sochivko DG, Fedorov AA, Varlamov DA, Kurochkin VE, Petrov RV. Accuracy of quantitative real-time PCR analysis. *Doklady Biochemistry and Biophysics* 2013; **449**: 105–108.
- 37 VanGuilder HD, Vrana KE, Freeman WM. Twenty-five years of quantitative PCR for gene expression analysis. *Biotechniques* 2008; **44**: 619.
- 38 Fraga D, Meulia T, Fenster S. Real-time PCR. *Current Protocols Essential Laboratory Techniques* 2008; : 10.3. 1–10.3. 40.
- 39 Tichopad A, Dilger M, Schwarz G, Pfaffl MW. Standardized determination of real-time PCR efficiency from a single reaction set-up. *Nucleic acids research* 2003; **31**: e122–e122.
- 40 Gál ÁB, Carnwath JW, Dinnyes A, Herrmann D, Niemann H, Wrenzycki C. Comparison of real-time polymerase chain reaction and end-point polymerase chain reaction for the analysis of gene expression in preimplantation embryos. *Reproduction, Fertility and Development* 2006; **18**: 365–371.
- 41 Grossman PD, Colburn JC. *Capillary electrophoresis: Theory and practice*. Academic Press, 2012.
- 42 Ozawa T, Tanaka M, Ikebe S, Ohno K, Kondo T, Mizuno Y. Quantitative determination of deleted mitochondrial DNA relative to normal DNA in parkinsonian striatum by a kinetic PCR analysis. *Biochemical and biophysical research communications* 1990; **172**: 483–489.
- 43 Valasek MA, Repa JJ. The power of real-time PCR. *Advances in physiology education* 2005; **29**: 151–159.
- 44 Kubista M, Andrade JM, Bengtsson M, Forootan A, Jonák J, Lind K *et al.* The real-time polymerase chain reaction. *Molecular aspects of medicine* 2006; **27**: 95–125.

- 45 Gevertz JL, Dunn SM, Roth CM. Mathematical model of real-time PCR kinetics. *Biotechnology and bioengineering* 2005; **92**: 346–355.
- 46 Higuchi R, Dollinger G, Walsh PS, Griffith R. Simultaneous amplification and detection of specific DNA sequences. *Bio/technology* 1992; **10**: 413–417.
- 47 Higuchi R, Fockler C, Dollinger G, Watson R. Kinetic PCR analysis: real-time monitoring of DNA amplification reactions. *Biotechnology* 1993; **11**: 1026–1030.
- 48 Wittwer CT, Herrmann MG, Moss AA, Rasmussen RP. Continuous fluorescence monitoring of rapid cycle DNA amplification. *Biotechniques* 1997; **22**: 130–139.
- 49 Livak KJ, Flood SJ, Marmaro J, Giusti W, Deetz K. Oligonucleotides with fluorescent dyes at opposite ends provide a quenched probe system useful for detecting PCR product and nucleic acid hybridization. *Genome Research* 1995; **4**: 357–362.
- 50 Jothikumar P, Hill V, Narayanan J. Design of FRET-TaqMan probes for multiplex real-time PCR using an internal positive control. *Biotechniques* 2009; **46**: 519.
- 51 Tyagi S, Kramer FR. Molecular beacons: probes that fluoresce upon hybridization. *Nature biotechnology* 1996; **14**: 303–308.
- 52 Tyagi S, Bratu DP, Kramer FR. Multicolor molecular beacons for allele discrimination. *Nature biotechnology* 1998; **16**: 49–53.
- 53 Didenko VV. DNA probes using fluorescence resonance energy transfer (FRET): designs and applications. *Biotechniques* 2001; **31**: 1106.
- 54 Marras SA, Kramer FR, Tyagi S. Efficiencies of fluorescence resonance energy transfer and contact-mediated quenching in oligonucleotide probes. *Nucleic acids research* 2002; **30**: e122–e122.
- 55 Ginzinger DG. Gene quantification using real-time quantitative PCR: An emerging technology hits the mainstream. *Experimental Hematology* 2002; **30**: 503–512.
- 56 Klein D. Quantification using real-time PCR technology: applications and limitations. *Trends in Molecular Medicine* 2002; **8**: 257–260.
- 57 Hindson CM, Chevillet JR, Briggs HA, Gallichotte EN, Ruf IK, Hindson BJ *et al.* Absolute quantification by droplet digital PCR versus analog real-time PCR. *Nature Methods* 2013; **10**: 1003–1005.
- 58 Kubista M. emerging real-time PCR applications. *Drug Discovery* 2008; : 57.
- 59 Vogelstein B, Kinzler KW. Digital PCR. *Proceedings of the National Academy of Sciences* 1999; **96**: 9236–9241.

- 60 Pohl G, Shih I-M. Principle and applications of digital PCR. *Expert review of molecular diagnostics* 2004; **4**: 41–47.
- 61 Pavsic J, Zel J, Milavec M. Assessment of the real-time PCR and different digital PCR platforms for DNA quantification. *Analytical and Bioanalytical Chemistry* 2016; **408**: 107–121.
- 62 Sykes PJ, Neoh SH, Brisco MJ, Hughes E, Condon J, Morley AA. Quantitation of targets for PCR by use of limiting dilution. *Biotechniques* 1992; **13**: 444–449.
- 63 Blow N. PCR's next frontier. *Nature Methods* 2007; **4**: 869–875.
- 64 Piggee C. Research Profile: Drop, stop, and cycle: digital microfluidics meets digital PCR. *Analytical Chemistry* 2007; **79**: 8828–8828.
- 65 McCaughan F, Dear PH. Single-molecule genomics. *The Journal of Pathology* 2010; **220**: 297–306.
- 66 Lin CQ, Yao B. Recent Advance in Digital PCR. *Progress in Chemistry* 2012; **24**: 2415–2423.
- 67 Corbisier P, Bhat S, Partis L, Rui Dan Xie V, Emslie KR. Absolute quantification of genetically modified MON810 maize (*Zea mays* L.) by digital polymerase chain reaction. *Analytical and Bioanalytical Chemistry* 2010; **396**: 2143–2150.
- 68 Sanders R, Huggett JF, Bushell CA, Cowen S, Scott DJ, Foy CA. Evaluation of Digital PCR for Absolute DNA Quantification. *Analytical Chemistry* 2011; **83**: 6474–6484.
- 69 Barrett AN, McDonnell TCR, Chan KCA, Chitty LS. Digital PCR Analysis of Maternal Plasma for Noninvasive Detection of Sick Cell Anemia. *Clinical Chemistry* 2012; **58**: 1026–1032.
- 70 Belgrader P, Tanner SC, Regan JF, Koehler R, Hindson BJ, Brown AS. Droplet digital PCR measurement of HER2 copy number alteration in formalin-fixed paraffin-embedded breast carcinoma tissue. *Clinical chemistry* 2013; **59**: 991–994.
- 71 Li M, Chen W, Papadopoulos N, Goodman SN, Bjerregaard NC, Laurberg S *et al*. Sensitive digital quantification of DNA methylation in clinical samples. *Nature Biotechnology* 2009; **27**: 858–863.
- 72 Heredia NJ, Belgrader P, Wang S, Koehler R, Regan J, Cosman AM *et al*. Droplet Digital™ PCR quantitation of HER2 expression in FFPE breast cancer samples. *Methods* 2013; **59**: S20–S23.
- 73 Henrich TJ, Gallien S, Li JZ, Pereyra F, Kuritzkes DR. Low-level detection and quantitation of cellular HIV-1 DNA and 2-LTR circles using droplet digital PCR. *Journal of Virological Methods* 2012; **186**: 68–72.
- 74 Manoj P. Droplet digital PCR technology promises new applications and research areas. *Mitochondrial DNA* 2016; **27**: 742–746.

- 75 Zimmermann BG, Grill S, Holzgreve W, Zhong XY, Jackson LG, Hahn S. Digital PCR: a powerful new tool for noninvasive prenatal diagnosis? *Prenatal Diagnosis* 2008; **28**: 1087–1093.
- 76 Day E, Dear PH, McCaughan F. Digital PCR strategies in the development and analysis of molecular biomarkers for personalized medicine. *Methods* 2013; **59**: 101–107.
- 77 Auroux P-A, Koc Y, deMello A, Manz A, Day PJR. Miniaturised nucleic acid analysis. *Lab on a Chip* 2004; **4**: 534.
- 78 Zhang Y, Ozdemir P. Microfluidic DNA amplification—A review. *Analytica Chimica Acta* 2009; **638**: 115–125.
- 79 Zhang C, Xu J, Ma W, Zheng W. PCR microfluidic devices for DNA amplification. *Biotechnology Advances* 2006; **24**: 243–284.
- 80 Zhang C, Xing D. Miniaturized PCR chips for nucleic acid amplification and analysis: latest advances and future trends. *Nucleic Acids Research* 2007; **35**: 4223–4237.
- 81 Taly V, Kelly BT, Griffiths AD. Droplets as Microreactors for High-Throughput Biology. *ChemBioChem* 2007; **8**: 263–272.
- 82 Chen L, Manz A, Day PJR. Total nucleic acid analysis integrated on microfluidic devices. *Lab on a Chip* 2007; **7**: 1413.
- 83 Manz A, Graber N, Widmer H áM. Miniaturized total chemical analysis systems: a novel concept for chemical sensing. *Sensors and actuators B: Chemical* 1990; **1**: 244–248.
- 84 Baker M. Digital PCR hits its stride. *nature methods* 2012; **9**: 541–544.
- 85 Didelot A, Kotsopoulos SK, Lupo A, Pekin D, Li X, Atochin I *et al.* Multiplex Picoliter-Droplet Digital PCR for Quantitative Assessment of DNA Integrity in Clinical Samples. *Clinical Chemistry* 2013; **59**: 815–823.
- 86 Nakano M, Komatsu J, Matsuura S, Takashima K, Katsura S, Mizuno A. Single-molecule PCR using water-in-oil emulsion. *Journal of biotechnology* 2003; **102**: 117–124.
- 87 Leamon JH, Link DR, Egholm M, Rothberg JM. Overview: methods and applications for droplet compartmentalization of biology. *Nature methods* 2006; **3**: 541–543.
- 88 Li M, Diehl F, Dressman D, Vogelstein B, Kinzler KW. BEAMing up for detection and quantification of rare sequence variants. *Nature Methods* 2006; **3**: 95–97.
- 89 Griffiths AD, Tawfik DS. Miniaturising the laboratory in emulsion droplets. *Trends in biotechnology* 2006; **24**: 395–402.
- 90 Schaerli Y, Hollfelder F. The potential of microfluidic water-in-oil droplets in experimental biology. *Molecular BioSystems* 2009; **5**: 1392.

- 91 Tanaka H, Yamamoto S, Nakamura A, Nakashoji Y, Okura N, Nakamoto N *et al.* Hands-Off Preparation of Monodisperse Emulsion Droplets Using a Poly(dimethylsiloxane) Microfluidic Chip for Droplet Digital PCR. *Analytical Chemistry* 2015; **87**: 4134–4143.
- 92 Anna SL, Bontoux N, Stone HA. Formation of dispersions using ‘flow focusing’ in microchannels. *Applied physics letters* 2003; **82**: 364–366.
- 93 Thorsen T, Roberts RW, Arnold FH, Quake SR. Dynamic pattern formation in a vesicle-generating microfluidic device. *Physical review letters* 2001; **86**: 4163.
- 94 Ding Y, Casadevall i Solvas X, deMello A. ‘V-junction’: a novel structure for high-speed generation of bespoke droplet flows. *Analyst* 2015; **140**: 414–421.
- 95 Sim SPC, Kang TG, Yobas L, Holtze C, Weitz DA. The shape of a step structure as a design aspect to control droplet generation in microfluidics. *Journal of Micromechanics and Microengineering* 2010; **20**: 035010.
- 96 Whitesides GM. The origins and the future of microfluidics. *Nature* 2006; **442**: 368–373.
- 97 deMello AJ. Control and detection of chemical reactions in microfluidic systems. *Nature* 2006; **442**: 394–402.
- 98 Polson NA, Hayes MA. Peer Reviewed: Microfluidics: Controlling Fluids in Small Places. *Analytical chemistry* 2001; **73**: 312 A–319 A.
- 99 Janasek D, Franzke J, Manz A. Scaling and the design of miniaturized chemical-analysis systems. *Nature* 2006; **442**: 374–380.
- 100 Ohno K, Tachikawa K, Manz A. Microfluidics: applications for analytical purposes in chemistry and biochemistry. *Electrophoresis* 2008; **29**: 4443–4453.
- 101 Abou-Hassan A, Sandre O, Cabuil V. Microfluidics in inorganic chemistry. *Angewandte Chemie International Edition* 2010; **49**: 6268–6286.
- 102 Marre S, Roig Y, Aymonier C. Supercritical microfluidics: Opportunities in flow-through chemistry and materials science. *The Journal of Supercritical Fluids* 2012; **66**: 251–264.
- 103 Theberge AB, Courtois F, Schaerli Y, Fischlechner M, Abell C, Hollfelder F *et al.* Microdroplets in microfluidics: an evolving platform for discoveries in chemistry and biology. *Angewandte Chemie International Edition* 2010; **49**: 5846–5868.
- 104 Kelly BT, Baret J-C, Taly V, Griffiths AD. Miniaturizing chemistry and biology in microdroplets. *Chemical Communications* 2007; : 1773.
- 105 Beebe DJ, Mensing GA, Walker GM. Physics and applications of microfluidics in biology. *Annual review of biomedical engineering* 2002; **4**: 261–286.

- 106 Holmes D, Gawad S. The application of microfluidics in biology. *Microengineering in Biotechnology* 2010; : 55–80.
- 107 Mitchell P. Microfluidics-downsizing large-scale biology. *Nature biotechnology* 2001; **19**: 717–721.
- 108 Weibel DB, Whitesides GM. Applications of microfluidics in chemical biology. *Current opinion in chemical biology* 2006; **10**: 584–591.
- 109 Breslauer DN, Lee PJ, Lee LP. Microfluidics-based systems biology. *Molecular BioSystems* 2006; **2**: 97–112.
- 110 Pipper J, Inoue M, Ng LF-P, Neuzil P, Zhang Y, Novak L. Catching bird flu in a droplet. *Nature Medicine* 2007; **13**: 1259–1263.
- 111 El-Ali J, Sorger PK, Jensen KF. Cells on chips. *Nature* 2006; **442**: 403–411.
- 112 Streets AM, Huang Y. Chip in a lab: Microfluidics for next generation life science research. *Biomicrofluidics* 2013; **7**: 011302.
- 113 deMello AJ. Microfluidics: DNA amplification moves on. *Nature* 2003; **422**: 28–29.
- 114 Hoshino T, Inagaki F. Molecular quantification of environmental DNA using microfluidics and digital PCR. *Systematic and Applied Microbiology* 2012; **35**: 390–395.
- 115 Kricka LJ, Wilding P. Microchip PCR. *Analytical and Bioanalytical Chemistry* 2003; **377**: 820–825.
- 116 Park S, Zhang Y, Lin S, Wang T-H, Yang S. Advances in microfluidic PCR for point-of-care infectious disease diagnostics. *Biotechnology Advances* 2011; **29**: 830–839.
- 117 Anderson RC, Su X, Bogdan GJ, Fenton J. A miniature integrated device for automated multistep genetic assays. *Nucleic Acids Research* 2000; **28**: e60–e60.
- 118 Liu L, Cao W, Wu J, Wen W, Chang DC, Sheng P. Design and integration of an all-in-one biomicrofluidic chip. *Biomicrofluidics* 2008; **2**: 034103.
- 119 Huebner A, Sharma S, Srisa-Art M, Hollfelder F, Edel JB, deMello AJ. Microdroplets: A sea of applications? *Lab on a Chip* 2008; **8**: 1244.
- 120 Northrup MA. DNA amplification in a microfabricated reaction chamber. Transducer'93. In: *seventh international conference on solid state sensors actuators, Yokohama, Japan*. 1993, pp 924–926.
- 121 Kopp MU, deMello AJ, Manz A. Chemical Amplification: Continuous-Flow PCR on a Chip. *Science* 1998; **280**: 1046–1048.

- 122 Northrup MA, Benett B, Hadley D, Landre P, Lehew S, Richards J *et al.* A miniature analytical instrument for nucleic acids based on micromachined silicon reaction chambers. *Analytical Chemistry* 1998; **70**: 918–922.
- 123 Wilding P, Shoffner MA, Kricka LJ. PCR in a silicon microstructure. *Clinical Chemistry* 1994; **40**: 1815–1818.
- 124 Belgrader P, Benett W, Hadley D, Richards J. PCR detection of bacteria in seven minutes. *Science* 1999; **284**: 449.
- 125 Gulliksen A, Solli L, Karlsen F, Rogne H, Hovig E, Nordstrøm T *et al.* Real-time nucleic acid sequence-based amplification in nanoliter volumes. *Analytical chemistry* 2004; **76**: 9–14.
- 126 Matsubara Y, Kerman K, Kobayashi M, Yamamura S, Morita Y, Takamura Y *et al.* On-Chip Nanoliter-Volume Multiplex TaqMan Polymerase Chain Reaction from A Single Copy Based on Counting Fluorescence Released Microchambers. *Analytical Chemistry* 2004; **76**: 6434–6439.
- 127 Matsubara Y, Kerman K, Kobayashi M, Yamamura S, Morita Y, Tamiya E. Microchamber array based DNA quantification and specific sequence detection from a single copy via PCR in nanoliter volumes. *Biosensors and Bioelectronics* 2005; **20**: 1482–1490.
- 128 Ottesen EA, Hong JW, Quake SR, Leadbetter JR. Microfluidic Digital PCR Enables Multigene Analysis of Individual Environmental Bacteria. *Science* 2006; **314**: 1464–1467.
- 129 Dube S, Qin J, Ramakrishnan R. Mathematical Analysis of Copy Number Variation in a DNA Sample Using Digital PCR on a Nanofluidic Device. *PLoS ONE* 2008; **3**: e2876.
- 130 Baker M. Clever PCR: more genotyping, smaller volumes. *nature methods* 2010; **7**: 351–356.
- 131 Heyries KA, Tropini C, VanInsberghe M, Doolin C, Petriv OI, Singhal A *et al.* Megapixel digital PCR. *Nature Methods* 2011; **8**: 649–651.
- 132 Sundberg SO, Wittwer CT, Gao C, Gale BK. Spinning Disk Platform for Microfluidic Digital Polymerase Chain Reaction. *Analytical Chemistry* 2010; **82**: 1546–1550.
- 133 Shen F, Du W, Kreutz JE, Fok A, Ismagilov RF. Digital PCR on a SlipChip. *Lab on a Chip* 2010; **10**: 2666.
- 134 Shen F, Du W, Davydova EK, Karymov MA, Pandey J, Ismagilov RF. Nanoliter Multiplex PCR Arrays on a SlipChip. *Analytical Chemistry* 2010; **82**: 4606–4612.
- 135 Shen F, Sun B, Kreutz JE, Davydova EK, Du W, Reddy PL *et al.* Multiplexed Quantification of Nucleic Acids with Large Dynamic Range Using Multivolume Digital RT-PCR on a Rotational SlipChip Tested with HIV and Hepatitis C Viral Load. *Journal of the American Chemical Society* 2011; **133**: 17705–17712.

- 136 Beer NR, Hindson BJ, Wheeler EK, Hall SB, Rose KA, Kennedy IM *et al.* On-Chip, Real-Time, Single-Copy Polymerase Chain Reaction in Picoliter Droplets. *Analytical Chemistry* 2007; **79**: 8471–8475.
- 137 Hindson BJ, Ness KD, Masquelier DA, Belgrader P, Heredia NJ, Makarewicz AJ *et al.* High-Throughput Droplet Digital PCR System for Absolute Quantitation of DNA Copy Number. *Analytical Chemistry* 2011; **83**: 8604–8610.
- 138 Williams R, Peisajovich SG, Miller OJ, Magdassi S, Tawfik DS, Griffiths AD. Amplification of complex gene libraries by emulsion PCR. *Nature Methods* 2006; **3**: 545–550.
- 139 Beer NR, Wheeler EK, Lee-Houghton L, Watkins N, Nasarabadi S, Hebert N *et al.* On-Chip Single-Copy Real-Time Reverse-Transcription PCR in Isolated Picoliter Droplets. *Analytical Chemistry* 2008; **80**: 1854–1858.
- 140 Beer NR, Rose KA, Kennedy IM. Monodisperse droplet generation and rapid trapping for single molecule detection and reaction kinetics measurement. *Lab Chip* 2009; **9**: 841–844.
- 141 Beer NR, Rose KA, Kennedy IM. Observed velocity fluctuations in monodisperse droplet generators. *Lab Chip* 2009; **9**: 838–840.
- 142 Hatch AC, Fisher JS, Pentoney SL, Yang DL, Lee AP. Tunable 3D droplet self-assembly for ultra-high-density digital micro-reactor arrays. *Lab on a Chip* 2011; **11**: 2509.
- 143 Hatch AC, Fisher JS, Tovar AR, Hsieh AT, Lin R, Pentoney SL *et al.* 1-Million droplet array with wide-field fluorescence imaging for digital PCR. *Lab on a Chip* 2011; **11**: 3838.
- 144 Leng X, Zhang W, Wang C, Cui L, Yang CJ. Agarose droplet microfluidics for highly parallel and efficient single molecule emulsion PCR. *Lab on a Chip* 2010; **10**: 2841.
- 145 Novak R, Zeng Y, Shuga J, Venugopalan G, Fletcher DA, Smith MT *et al.* Single-Cell Multiplex Gene Detection and Sequencing with Microfluidically Generated Agarose Emulsions. *Angewandte Chemie International Edition* 2011; **50**: 390–395.
- 146 Zhu Y, Fang Q. Analytical detection techniques for droplet microfluidics—A review. *Analytica Chimica Acta* 2013; **787**: 24–35.
- 147 Laurie MT, Bertout JA, Taylor SD, Burton JN, Shendure JA, Bielas JH. Simultaneous digital quantification and fluorescence-based size characterization of massively parallel sequencing libraries. *BioTechniques* 2013; **55**: 61.
- 148 Strain MC, Lada SM, Luong T, Rought SE, Gianella S, Terry VH *et al.* Highly Precise Measurement of HIV DNA by Droplet Digital PCR. *PLoS ONE* 2013; **8**: e55943.
- 149 RainDrop Digital PCR System. <http://raindancetech.com/digital-pcr-tech/raindrop-digital-pcr-system/>.

- 150 Kumaresan P, Yang CJ, Cronier SA, Blazej RG, Mathies RA. High-Throughput Single Copy DNA Amplification and Cell Analysis in Engineered Nanoliter Droplets. *Analytical Chemistry* 2008; **80**: 3522–3529.
- 151 Sun K, Yamaguchi A, Ishida Y, Matsuo S, Misawa H. A heater-integrated transparent microchannel chip for continuous-flow PCR. *Sensors and Actuators B: Chemical* 2002; **84**: 283–289.
- 152 Obeid PJ, Christopoulos TK. Continuous-flow DNA and RNA amplification chip combined with laser-induced fluorescence detection. *Analytica Chimica Acta* 2003; **494**: 1–9.
- 153 Bu M, Melvin T, Ensell G, Wilkinson JS, Evans AG. Design and theoretical evaluation of a novel microfluidic device to be used for PCR. *Journal of Micromechanics and Microengineering* 2003; **13**: S125.
- 154 Crews N, Wittwer C, Gale B. Continuous-flow thermal gradient PCR. *Biomedical microdevices* 2008; **10**: 187–195.
- 155 Schneegaß I, Köhler JM. Flow-through polymerase chain reactions in chip thermocyclers. *Reviews in Molecular Biotechnology* 2001; **82**: 101–121.
- 156 Schneegaß I, Bräutigam R, Köhler JM. Miniaturized flow-through PCR with different template types in a silicon chip thermocycler. *Lab on a Chip* 2001; **1**: 42–49.
- 157 Fukuba T, Yamamoto T, Naganuma T, Fujii T. Microfabricated flow-through device for DNA amplification—towards in situ gene analysis. *Chemical Engineering Journal* 2004; **101**: 151–156.
- 158 Obeid PJ, Christopoulos TK, Crabtree HJ, Backhouse CJ. Microfabricated device for DNA and RNA amplification by continuous-flow polymerase chain reaction and reverse transcription-polymerase chain reaction with cycle number selection. *Analytical chemistry* 2003; **75**: 288–295.
- 159 Li S, Fozdar DY, Ali MF, Li H, Shao D, Vykoukal DM *et al.* A Continuous-Flow Polymerase Chain Reaction Microchip With Regional Velocity Control. *Journal of Microelectromechanical Systems* 2006; **15**: 223–236.
- 160 Zhu Z, Jenkins G, Zhang W, Zhang M, Guan Z, Yang CJ. Single-molecule emulsion PCR in microfluidic droplets. *Analytical and Bioanalytical Chemistry* 2012; **403**: 2127–2143.
- 161 Markey AL, Mohr S, Day PJR. High-throughput droplet PCR. *Methods* 2010; **50**: 277–281.
- 162 Mohr S, Zhang Y-H, Macaskill A, Day PJR, Barber RW, Goddard NJ *et al.* Numerical and experimental study of a droplet-based PCR chip. *Microfluidics and Nanofluidics* 2007; **3**: 611–621.

- 163 Kiss MM, Ortoleva-Donnelly L, Beer NR, Warner J, Bailey CG, Colston BW *et al.* High-Throughput Quantitative Polymerase Chain Reaction in Picoliter Droplets. *Analytical Chemistry* 2008; **80**: 8975–8981.
- 164 Schaerli Y, Wootton RC, Robinson T, Stein V, Dunsby C, Neil MA *et al.* Continuous-flow polymerase chain reaction of single-copy DNA in microfluidic microdroplets. *Analytical chemistry* 2008; **81**: 302–306.
- 165 Teh S-Y, Lin R, Hung L-H, Lee AP. Droplet microfluidics. *Lab on a Chip* 2008; **8**: 198–220.
- 166 Niu X. Building droplet-based microfluidic systems for biological analysis. *Biochemical Society Transactions* 2012; **40**: 615–623.
- 167 Fallah-Araghi A, Baret J-C, Ryckelynck M, Griffiths AD. A completely in vitro ultrahigh-throughput droplet-based microfluidic screening system for protein engineering and directed evolution. *Lab on a Chip* 2012; **12**: 882.
- 168 Guo MT, Rotem A, Heyman JA, Weitz DA. Droplet microfluidics for high-throughput biological assays. *Lab on a Chip* 2012; **12**: 2146.
- 169 Song H, Tice JD, Ismagilov RF. A microfluidic system for controlling reaction networks in time. *Angewandte Chemie* 2003; **115**: 792–796.
- 170 Baroud CN, Robert de Saint Vincent M, Delville J-P. An optical toolbox for total control of droplet microfluidics. *Lab on a Chip* 2007; **7**: 1029.
- 171 Song H, Chen DL, Ismagilov RF. Reactions in droplets in microfluidic channels. *Angewandte chemie international edition* 2006; **45**: 7336–7356.
- 172 Niu X, Gielen F, Edel JB. A microdroplet dilutor for high-throughput screening. *Nature chemistry* 2011; **3**: 437–442.
- 173 Wilhelm TS. Surface-induced droplet fusion in microfluidic devices. *Lab on a Chip* 2007; **7**: 984–986.
- 174 Tan Y-C, Ho YL, Lee AP. Droplet coalescence by geometrically mediated flow in microfluidic channels. *Microfluidics and Nanofluidics* 2007; **3**: 495–499.
- 175 Zagnoni M, Cooper JM. On-chip electrocoalescence of microdroplets as a function of voltage, frequency and droplet size. *Lab on a Chip* 2009; **9**: 2652.
- 176 Tan Y-C, Fisher JS, Lee AI, Cristini V, Lee AP. Design of microfluidic channel geometries for the control of droplet volume, chemical concentration, and sorting. *Lab on a Chip* 2004; **4**: 292–298.
- 177 Tan W-H, Takeuchi S. Timing controllable electrofusion device for aqueous droplet-based microreactors. *Lab on a Chip* 2006; **6**: 757–763.

- 178 Adamson DN, Mustafi D, Zhang JX, Zheng B, Ismagilov RF. Production of arrays of chemically distinct nanolitre plugs via repeated splitting in microfluidic devices. *Lab on a Chip* 2006; **6**: 1178–1186.
- 179 Ménétrier-Deremble L, Tabeling P. Droplet breakup in microfluidic junctions of arbitrary angles. *Physical Review E* 2006; **74**: 035303.
- 180 Link DR, Anna SL, Weitz DA, Stone HA. Geometrically mediated breakup of drops in microfluidic devices. *Physical review letters* 2004; **92**: 054503.
- 181 Huh D, Bahng JH, Ling Y, Wei H-H, Kripfgans OD, Fowlkes JB *et al.* Gravity-driven microfluidic particle sorting device with hydrodynamic separation amplification. *Analytical chemistry* 2007; **79**: 1369–1376.
- 182 Cheng J-Y, Hsieh C-J, Chuang Y-C, Hsieh J-R. Performing microchannel temperature cycling reactions using reciprocating reagent shuttling along a radial temperature gradient. *Analyst* 2005; **130**: 931–940.
- 183 Abgrall P, Gue AM. Lab-on-chip technologies: making a microfluidic network and coupling it into a complete microsystem—a review. *Journal of Micromechanics and Microengineering* 2007; **17**: R15.
- 184 Wise KD, Najafi K. Microfabrication techniques for integrated sensors and microsystems. *Science* 1991; **254**: 1335–1342.
- 185 Haynes WM (ed.). Properties of Semiconductors. In: *CRC Handbook of Chemistry and Physics*. pp 12–80.
- 186 Haynes WM (ed.). Thermal Conductivity of Glasses. In: *CRC Handbook of Chemistry and Physics*. pp 12–216.
- 187 Polymethylmethacrylate (PMMA, Acrylic). <http://www.makeitfrom.com/material-properties/Polymethylmethacrylate-PMMA-Acrylic>.
- 188 Low Expansion Borosilicate Glass (ASTM E438 Type I Class A). <http://www.makeitfrom.com/material-properties/Low-Expansion-Borosilicate-Glass-ASTM-E438-Type-I-Class-A/>.
- 189 Ansys Icepak 12.1 User's Guide. 2009. <http://orange.engr.ucdavis.edu/Documentation12.1/121/ICEPAK/iceug.pdf>.
- 190 Lei KF. Materials and fabrication techniques for nano- and microfluidic devices. In: *Microfluidics in detection science: lab-on-a-chip technologies*. The Royal Society of Chemistry, 2015, pp 1–28.
- 191 Temiz Y, Lovchik RD, Kaigala GV, Delamarche E. Lab-on-a-chip devices: How to close and plug the lab? *Microelectronic Engineering* 2015; **132**: 156–175.

- 192 Quake SR, Scherer A. From micro-to nanofabrication with soft materials. *Science* 2000; **290**: 1536–1540.
- 193 De Mello A. Focus: plastic fantastic? *Lab on a Chip* 2002; **2**: 31N–36N.
- 194 Becker H, Locascio LE. Polymer microfluidic devices. *Talanta* 2002; **56**: 267–287.
- 195 McDonald JC, Whitesides GM. Poly (dimethylsiloxane) as a material for fabricating microfluidic devices. *Accounts of chemical research* 2002; **35**: 491–499.
- 196 Becker H, Gaertner C. Polymer based micro-reactors. *Reviews in Molecular Biotechnology* 2001; **82**: 89–99.
- 197 Lee G-B, Lin C-H, Huang F-C, Liao C-S, Lee C-Y, Chen S-H. Microfluidic chips for DNA amplification, electrophoresis separation and on-line optical detection. In: *Micro Electro Mechanical Systems, 2003. MEMS-03 Kyoto. IEEE The Sixteenth Annual International Conference on. IEEE, 2003*, pp 423–426.
- 198 Zou Q, Miao Y, Chen Y, Sridhar U, Chong CS, Chai T *et al.* Micro-assembled multi-chamber thermal cyler for low-cost reaction chip thermal multiplexing. *Sensors and Actuators A: Physical* 2002; **102**: 114–121.
- 199 Giordano BC, Ferrance J, Swedberg S, Hühmer AFR, Landers JP. Polymerase chain reaction in polymeric microchips: DNA amplification in less than 240 seconds. *Analytical biochemistry* 2001; **291**: 124–132.
- 200 Sethu P, Mastrangelo CH. Cast epoxy-based microfluidic systems and their application in biotechnology. *Sensors and Actuators B: Chemical* 2004; **98**: 337–346.
- 201 El-Ali J, Perch-Nielsen IR, Poulsen CR, Bang DD, Telleman P, Wolff A. Simulation and experimental validation of a SU-8 based PCR thermocycler chip with integrated heaters and temperature sensor. *Sensors and Actuators A: Physical* 2004; **110**: 3–10.
- 202 Haynes WM (ed.). Glass Transition Temperature of Selected Polymers. In: *CRC Handbook of Chemistry and Physics*. pp 13–11.
- 203 Haynes WM (ed.). Physical Properties of Selected Polymers. In: *CRC Handbook of Chemistry and Physics*. pp 13–4.
- 204 Kuo JS, Chiu DT. Disposable microfluidic substrates: transitioning from the research laboratory into the clinic. *Lab on a Chip* 2011; **11**: 2656–2665.
- 205 Neuzil P, Pipper J, Hsieh TM. Disposable real-time microPCR device: lab-on-a-chip at a low cost. *Mol BioSyst* 2006; **2**: 292–298.
- 206 Giordano BC, Copeland ER, Landers JP. Towards dynamic coating of glass microchip chambers for amplifying DNA via the polymerase chain reaction. *Electrophoresis* 2001; **22**: 334–340.

- 207 Shoffner MA, Cheng J, Hvichia GE, Kricka LJ, Wilding P. Chip PCR. I. Surface passivation of microfabricated silicon-glass chips for PCR. *Nucleic Acids Research* 1996; **24**: 375–379.
- 208 Saeki D, Sugiura S, Kanamori T, Sato S, Ichikawa S. Microfluidic preparation of water-in-oil-in-water emulsions with an ultra-thin oil phase layer. *Lab Chip* 2010; **10**: 357–362.
- 209 Technical Data Sheet: Megaposit SPR 220 Series i-Line Photoresits. http://www.microchem.com/PDFs_Dow/SPR%20220%20DATA%20SHEET%20R%26H.pdf.
- 210 Anna SL, Bontoux N, Stone HA. Formation of dispersions using ‘flow focusing’ in microchannels. *Applied physics letters* 2003; **82**: 364–366.
- 211 Thorsen T, Roberts RW, Arnold FH, Quake SR. Dynamic pattern formation in a vesicle-generating microfluidic device. *Physical review letters* 2001; **86**: 4163.
- 212 Iles A, Fortt R, de Mello AJ. Thermal optimisation of the Reimer–Tiemann reaction using thermochromic liquid crystals on a microfluidic reactor. *Lab on a Chip* 2005; **5**: 540.
- 213 Benninger RKP, Koç Y, Hofmann O, Requejo-Isidro J, Neil MAA, French PMW *et al.* Quantitative 3D Mapping of Fluidic Temperatures within Microchannel Networks Using Fluorescence Lifetime Imaging. *Analytical Chemistry* 2006; **78**: 2272–2278.
- 214 Erill I, Campoy S, Erill N, Barbé J, Aguiló J. Biochemical analysis and optimization of inhibition and adsorption phenomena in glass–silicon PCR-chips. *Sensors and Actuators B: Chemical* 2003; **96**: 685–692.
- 215 Kwok DY, Neumann AW. Contact angle measurement and contact angle interpretation. *Advances in colloid and interface science* 1999; **81**: 167–249.
- 216 Srisa-Art M. *Microdroplet Reactors for High-Throughput Chemistry and Biology*. 2010.
- 217 Tice JD, Lyon AD, Ismagilov RF. Effects of viscosity on droplet formation and mixing in microfluidic channels. *Analytica chimica acta* 2004; **507**: 73–77.
- 218 Cho S, Kang D-K, Sim S, Geier F, Kim J-Y, Niu X *et al.* Droplet-based microfluidic platform for high-throughput, multi-parameter screening of photosensitizer activity. *Analytical chemistry* 2013; **85**: 8866–8872.
- 219 Loewe L. Genetic mutation. *Nature Education* 1 (1)(2008).
- 220 Ingram VM. Gene mutations in human haemoglobin: the chemical difference between normal and sickle cell haemoglobin. *Nature* 1957; **180**: 326–328.
- 221 Spence MTZ, Johnson ID. *The molecular probes handbook: a guide to fluorescent probes and labeling technologies*. Life Technologies Corporation: Carlsbad, CA, 2010.

- 222 Marras SA. Selection of fluorophore and quencher pairs for fluorescent nucleic acid hybridization probes. *Fluorescent Energy Transfer Nucleic Acid Probes: Designs and Protocols* 2006; : 3–16.
- 223 Kellogg DE, Rybalkin I, Chen S, Mukhamedova N, Vlasik T, Siebert PD *et al.* TaqStart Antibody: 'hot start' PCR facilitated by a neutralizing monoclonal antibody directed against Taq DNA polymerase. *BioTechniques* 1994; **16**: 1134–1137.
- 224 Protocol for OneTaq hot start DNA polymerase. <http://www.neb.sg/~media/Catalog/All-Products/A15C0267EA124FC98B80BCED782BCB40/Datacards%20or%20Manuals/M0481Datasheet-Lot0051206.pdf>.
- 225 Neuzil P, Zhang C, Pipper J, Oh S, Zhuo L. Ultra fast miniaturized real-time PCR: 40 cycles in less than six minutes. *Nucleic acids research* 2006; **34**: e77–e77.
- 226 Blake RD. Denaturation of DNA. In: *Molecular biology and biotechnology: a comprehensive desk reference*. John Wiley & Sons: New York, 1995, p 207.
- 227 Simple PID Control. <http://forums.ni.com/t5/LabVIEW/Simple-PID-Control/td-p/2171566>.